DAHLGREN DIVISION
NAVAL SURFACE WARFARE CENTER
Dahlgren, Virginia 22448-5100

NSWCDD/TR-97/84

PHASE II DEMONSTRATION TEST OF THE ELECTROMAGNETIC REVERBERATION CHARACTERISTICS OF A LARGE TRANSPORT AIRCRAFT

BY D. MARK JOHNSON MICHAEL O. HATFIELD MICHAEL B. SLOCUM
NSWCDD

CAPTAIN THOMAS A. LOUGHRY
USAF PHILLIPS LABORATORY

ARTHUR R. ONDREJKA ROBERT T. JOHNK
NATIONAL INSTITUTE OF STANDARDS AND TECHNOLOGY

GUSTAV J. FREYER
NORTHEAST CONSORTIUM FOR ENGINEERING EDUCATION

JOINT WARFARE APPLICATIONS DEPARTMENT

SEPTEMBER 1997

REPORT DOCUMENTATION PAGE

Form Approved
OMB No. 0704-0188

1. AGENCY USE ONLY (Leave blank)	2. REPORT DATE	3. REPORT TYPE AND DATES COVERED
	September 1997	Final

4. TITLE AND SUBTITLE

Phase II Demonstration Test of the Electromagnetic Reverberation Characteristics of a Large Transport Aircraft

5. FUNDING NUMBERS

6. AUTHOR(s)

D. Mark Johnson, Michael O. Hatfield, Michael B. Slocum, et al.

7. PERFORMING ORGANIZATION NAME(S) AND ADDRESS(ES)

Commander
Naval Surface Warfare Center
Dahlgren Division (Code J52)
17320 Dahlgren Road
Dahlgren, VA 22448-5100

8. PERFORMING ORGANIZATION REPORT NUMBER

NSWCDD/TR-97/84

9. SPONSORING/MONITORING AGENCY NAME(S) AND ADDRESS(ES)

10. SPONSORING/MONITORING AGENCY REPORT NUMBER

11. SUPPLEMENTARY NOTES

12a. DISTRIBUTION/AVAILABILITY STATEMENT

Approved for public release; distribution is unlimited.

12b. DISTRIBUTION CODE

13. ABSTRACT (Maximum 200 words)

This report describes the second phase of an investigation into the electromagnetic characterization of a typical large commercial aircraft. The test aircraft, the same one used for the Phase I test, was a decommissioned Boeing 707-720B. A major objective was a comparison of data obtained with band-limited white Gaussian noise (BLWGN) excitation and data obtained with continuous wave (CW) excitation and mechanical mode-mixing. Five aircraft areas were instrumented with probes. A common test article (CTA), developed by Naval Surface Warfare Center, Dahlgren Division, was tested in several locations in the cockpit and avionics bay. Test areas were excited from 100 MHz to 6 GHz using discrete or swept-frequency CW signals. Aluminum foil tuners provided mode-mixing. Normalized cavity power density was the ratio of received power to input power. Stirring ratios in several areas were determined and limited cavity-to-cavity coupling was measured. Power received by instrumented boxes and the CTA was measured using discrete and swept-frequency CW. Mode-mixing for the areas excited with BLWGN was in 2-, 10-, and 50-MHz bandwidths; four measurements were obtained for each cavity, frequency span, and bandwidth combination. Pulse decay measurements provided a direct measurement of the cavity quality factor (Q). External excitation from three aspect angles provided external-to-internal shielding effectiveness (SE) measurements. Limited narrow pulsewidth external and internal excitation of two areas was performed. Time domain analysis of received power yielded external-to-internal SE and cavity Q.

14. SUBJECT TERMS	15. NUMBER OF PAGES
electromagnetic environment, high-intensity radiated fields, HIRF, band-limited white Gaussian noise, quality factor, certification-critical functions, certification HIRF environment, power density, fast Fourier transform, FFT, continuous wave excitation, CW	200
	16. PRICE CODE

17. SECURITY CLASSIFICATION OF REPORTS	18. SECURITY CLASSIFICATION OF THIS PAGE	19. SECURITY CLASSIFICATION OF ABSTRACT	20. LIMITATION OF ABSTRACT
UNCLASSIFIED	UNCLASSIFIED	UNCLASSIFIED	UL

FOREWORD

The electromagnetic measurements discussed in this report were obtained by a test team consisting of representatives from the Electromagnetic Effects Division of the United States Air Force Phillips Laboratory, the Electromagnetic Fields Division of the National Institute of Standards and Technology, and the Electromagnetic Effects Branch of the Dahlgren Division of the Naval Surface Warfare Center. The work was funded by the Langley Research Center of the National Aeronautics and Space Administration (NASA), the United States Air Force Phillips Laboratory, and the Naval Surface Warfare Center, Dahlgren Division.

The test was the second in a series of tests to evaluate the electromagnetic characteristics of a transport-sized aircraft. Testing was conducted on the same decommissioned Boeing 707-720B used to conduct Phase I of the test. The aircraft was stored at the Aerospace Maintenance and Regeneration Center, Davis Monthan Air Force Base, Tucson, Arizona.

The aircraft was excited from 100 MHz to 6 GHz using horn and log periodic antennas in multiple locations external to the aircraft and within the avionics bay, cockpit, and cabin. Both continuous wave (CW) and band-limited white Gaussian noise (BLWGN) excitation were used. In addition, time domain measurements were conducted to determine the shielding effectiveness of the airframe and the quality factor, or "Q," of several aircraft cavities.

The test team consisted of Michael O. Hatfield, D. Mark Johnson, and Michael B. Slocum of the Naval Surface Warfare Center, Dahlgren Division; Captain Thomas A. Loughry, SRA David Little, and SRA Chris Van Zandt of the USAF Phillips Laboratory; Arthur R. Ondrejka and Robert Johnk of the National Institute of Standards and Technology; and Gustav J. Freyer of Northeast Consortium for Engineering Education.

This report has been review by William Lucado, Head, Systems Electromagnetic Effects Branch; Leonard Fontenot, Head, Electromagnetic Effects Division; and Dr. Lisle H. Russell, Principal Scientist, Joint Warfare Applications Department.

Approved by:

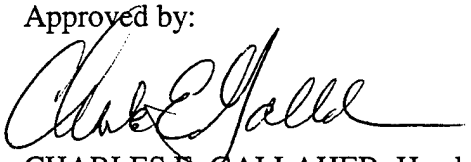

CHARLES E. GALLAHER, Head
Joint Warfare Applications Department

CONTENTS

CONTENTS (Continued)

ILLUSTRATIONS

ILLUSTRATIONS (Continued)

ILLUSTRATIONS (Continued)

ILLUSTRATIONS (Continued)

ILLUSTRATIONS (Continued)

ILLUSTRATIONS (Continued)

ILLUSTRATIONS (Continued)

ILLUSTRATIONS (Continued)

ILLUSTRATIONS (Continued)

ILLUSTRATIONS (Continued)

ILLUSTRATIONS (Continued)

ILLUSTRATIONS (Continued)

ILLUSTRATIONS (Continued)

ILLUSTRATIONS (Continued)

ILLUSTRATIONS (Continued)

TABLES

EXECUTIVE SUMMARY

The second phase of a demonstration test investigating the electromagnetic characterization of a typical large commercial aircraft was conducted on a decommissioned Boeing 707-720B aircraft. The aircraft, located at the Aerospace Maintenance and Regeneration Center, Davis Monthan Air Force Base, Tucson, Arizona, was the same aircraft used for the Phase I test. Some electronic equipment and much of the passenger cabin equipment had been removed since the Phase I test. A major objective of the Phase II test was to compare data obtained with band-limited white Gaussian noise (BLWGN) excitation with data obtained with continuous wave (CW) excitation and mechanical mode-mixing.

Prior to the Phase II test, three instruments from the cockpit instrument panel and two boxes from the avionics bay were instrumented with probes. An additional item, the common test article (CTA) developed by the Naval Surface Warfare Center, Dahlgren Division, was tested in several locations in both the cockpit and the avionics bay.

The cockpit, avionics bay, and passenger cabin were internally excited from 100 MHz to 6 GHz using discrete or swept-frequency CW signals. The transmit antennas were a log periodic from 100 MHz to 1 GHz and a dual-ridged horn from 1 to 6 GHz. Another log periodic and horn antenna pair was used to sample the cavity electromagnetic environment (EME). Aluminum foil tuners in each of the three cavities provided the mode-mixing. The cavity normalized power density was determined from the ratio of received power to input power. Stirring ratios, defined as the ratio of the maximum received signal to the minimum received signal at a discrete frequency as the tuner rotates, were obtained for the cockpit, avionics bay, and passenger cabin. Limited cavity-to-cavity coupling data were obtained by transmitting in one cavity and receiving in another. The power received by the five instrumented boxes and the CTA was measured using both discrete and swept-frequency CW.

The aircraft cavities were also excited using BLWGN. Three noise bandwidths, 2, 10, and 50 MHz, were used for mode-mixing. The same transmit and receive antenna pairs were used as in the CW excitation. In general, four measurements were obtained for each cavity, frequency span, and bandwidth combination. Cavity normalized power density, instrumented box and CTA response, and cavity-to-cavity coupling measurements were performed as in the CW case. Pulse decay measurements provided a direct measurement of the cavity quality factor (Q). In addition, external excitation from three aspect angles provided external to internal shielding effectiveness (SE) measurements.

Limited, narrow-pulse-width external and internal excitations of the cockpit and passenger cabin were performed. Time domain analysis of the received power in the cavities yielded external to internal SE and cavity Q.

1.0 INTRODUCTION

1.1 BACKGROUND

There is significant current interest in the response of aircraft avionics systems to high intensity radiated fields (HIRF). This interest arises from the convergence of three trends:

- The ambient electromagnetic environment (EME) is increasing in density and intensity.
- Electronic systems are replacing mechanical systems for flight-critical functions.
- The use of composite materials may reduce the shielding effectiveness (SE) provided by the aircraft structure.

The Federal Aviation Administration (FAA), along with its European counterpart, the Joint Aviation Authorities (JAA), is proposing revised electromagnetic (EM) certification requirements for commercial aircraft. The new standards will apply to normal, utility, aerobatic, and commuter airplanes (Part 23 of the Federal Aviation Regulations); transport airplanes (Part 25); normal rotorcraft (Part 27); and transport rotorcraft (Part 29). Particularly at frequencies above 400 MHz, the proposed certification levels are substantially higher than previous levels. Table 1-1 shows the proposed certification levels as of January 1995. (Note that all tables and figures in this report can be found at the end of each chapter.)

A current issue for both the FAA and industry is how to perform credible certification tests for the aircraft and avionics systems within reasonable costs and schedules. Reverberation chambers have been suggested as a cost-effective means to demonstrate avionics susceptibility level compliance with the HIRF standards above 100 MHz. Readers unfamiliar with the concept of a reverberation or mode-stirred chamber should review Crawford and Koepke[1].*

Figures 1-1 and 1-2 show proposed routes to certification as documented in the March 15, 1994 draft Advisory Circular. The items marked with an asterisk indicate potential applications of reverberation chambers for testing critical systems. A single asterisk indicates that mode-stirring techniques are permitted for radiated susceptibility testing above 100 MHz. A double asterisk indicates where mode-stirring techniques have potential applications.

When EM energy is introduced into an aircraft cavity, it is expected that field-intensity maxima and minima will be distributed throughout the cavity as a result of the superposition of the

*For the remainder of this report, superscript numbers correspond to the numbered references listed in Section 8.

cavity modes. The field-intensity distribution will be dependent on the frequency, the details of the cavity configuration, and the excitation mechanism. Previous work, particularly the Phase I precursor to this test,[2] has demonstrated the similarity of the EME in internally excited aircraft cavities to the EME in a reverberation chamber.[2,3,4]

Several issues remain to be resolved:

- Whether the tuner size was the cause of the poor agreement with the theoretical EME observed in the Phase I test for frequencies below 800 MHz
- Whether the response of an aircraft system in a reverberation chamber is representative of the system's response in an aircraft cavity with the same power density
- Whether the aircraft cavity EME excited by external sources is equivalent to the EME observed in Phase I for internal excitation
- Whether the avionics-bay-to-cockpit coupling values obtained in Phase I can be repeated and are representative of the values for other aircraft cavity pairs

This test addressed the first issue by increasing the size of the tuner used in the cockpit. The test expanded on Phase I by instrumenting actual aircraft systems in the aircraft. This expanded the system response data base but did not provide definitive answers to the second issue since the aircraft wiring was not totally intact and since the test was run with no power applied to the instruments. The test provided a limited data base directly addressing the third issue.

The avionics-bay-to-cockpit coupling data obtained in this test showed good agreement with the Phase I data. The coupling measurements were extended to show the expected reciprocity for cockpit-to-avionics-bay coupling. The coupling measurements were extended to include coupling from the passenger cabin to the cockpit and avionics bay.

Additionally, the recently developed band-limited white Gaussian noise (BLWGN) technique[5] for cavity mode excitation appears to have HIRF applications. If an aircraft is illuminated with BLWGN, the internal cavity EME will be randomized without resort to mechanical mode-mixing. The avoidance of mechanical tuners could provide at least two benefits for HIRF applications, as described in the following paragraph.

The first benefit is that for densely packed cavities, particularly avionics bays in small aircraft, it is unlikely that it will be possible to use a sufficiently large tuner. Previous data obtained with BLWGN indicate the possibility of characterizing cavity EME without resort to rotating tuners. The second benefit is that the data collection time with BLWGN can be significantly shorter than with mechanical mode-mixed continuous wave (CW) excitation. A BLWGN swept-frequency measurement for a specific configuration requires considerably less time than a swept-frequency measurement with mechanical tuners. However, a potential disadvantage is the difference in effective power spectral density between BLWGN and CW excitation for the same input power. For

BLWGN, the input power is spread uniformly over the noise bandwidth (BW), while for CW excitation, the power is normally within a 1-Hz BW.

Another technique that has been applied to EM characterization of aircraft is time domain analysis of the received signals from short pulse excitation of the aircraft. This technique permits an independent means of determining the shielding effectiveness of the aircraft structure, the cavity-to-cavity coupling, and the cavity quality factor (Q).

Finally, the ambient EME, particularly in the frequency modulation (FM) and television (TV) very-high frequency (VHF) and ultra-high frequency (UHF) bands, provided an additional excitation source for aircraft shielding effectiveness measurements.

1.2 OBJECTIVE

The objectives of this test were to

- Validate the use of BLWGN as an excitation technique for characterizing aircraft cavity EME
- Obtain data on the shielding effectiveness of the aircraft structure
- Further characterize the EME in aircraft cavities representative of large transport aircraft
- Provide additional data on the equivalence of system responses in aircraft cavities and reverberation chambers
- Validate and extend Phase I data on cavity-to-cavity coupling

1.3 TEST AIRCRAFT

Throughout the test planning period the primary aircraft considered for the test was the decommissioned Boeing 707-720B used for the Phase I test. The aircraft was still available at the Aerospace Maintenance and Regeneration Center (AMARC), Davis Monthan Air Force Base, Tucson, Arizona; however, the installed equipment had been reduced and the aircraft's condition had degraded somewhat since the Phase I test.

Several test aircraft alternatives were also considered. These included

- The USAF EMPTAC (B-707) test aircraft at Kirtland Air Force Base, Albuquerque, New Mexico.
- A passenger configured DC-10 recently removed from active airline service at Amarillo International Airport, Texas.

- An operational B-727 at the FAA Technical Center, Atlantic City Airport, New Jersey.
- An operational MD-87 at Yuma International Airport, Arizona.

The USAF EMPTAC aircraft had several advantages including the ability to test in a power-on mode. However, the aircraft was not selected primarily because it had substantial EM shielding modifications. As a test article for electromagnetic pulse (EMP) hardening technology, it had significant differences in its shielding topology from commercial transport aircraft.

The DC-10 was to be modified for resale and a use agreement could not be reached with the airline management.

Unfortunately, it was not possible to coordinate the FAA B-727 and the McDonnell Douglas MD-87 flight utilization schedules with the limited test windows available to the three test organizations. Both of these aircraft options should be reconsidered for any follow-on tests.

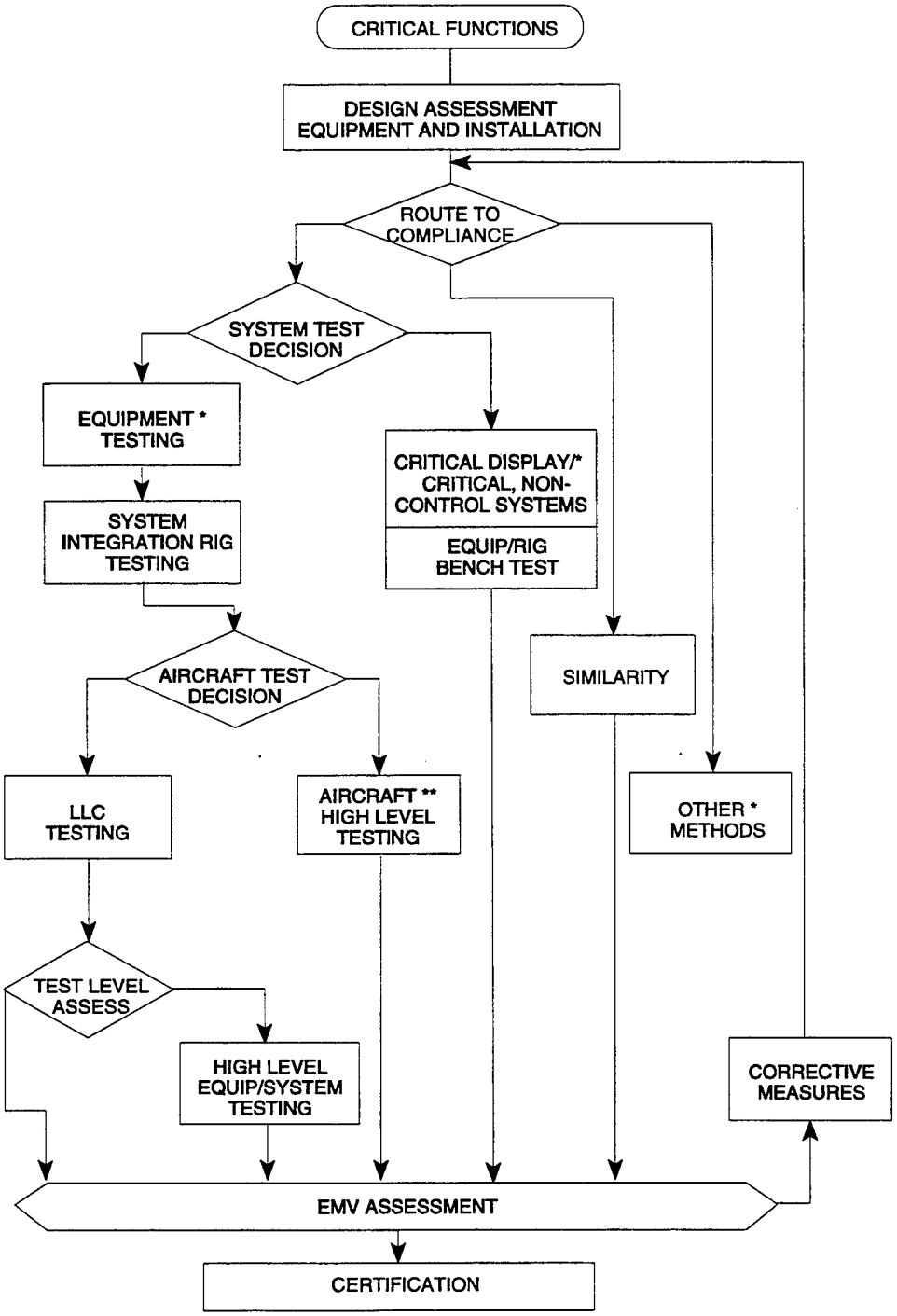

Note:
* Mode-stirring test techniques are permitted.
** Mode-stirring test techniques may be applicable.

FIGURE 1-1. PROPOSED ROUTES TO CERTIFICATION-CRITICAL FUNCTIONS

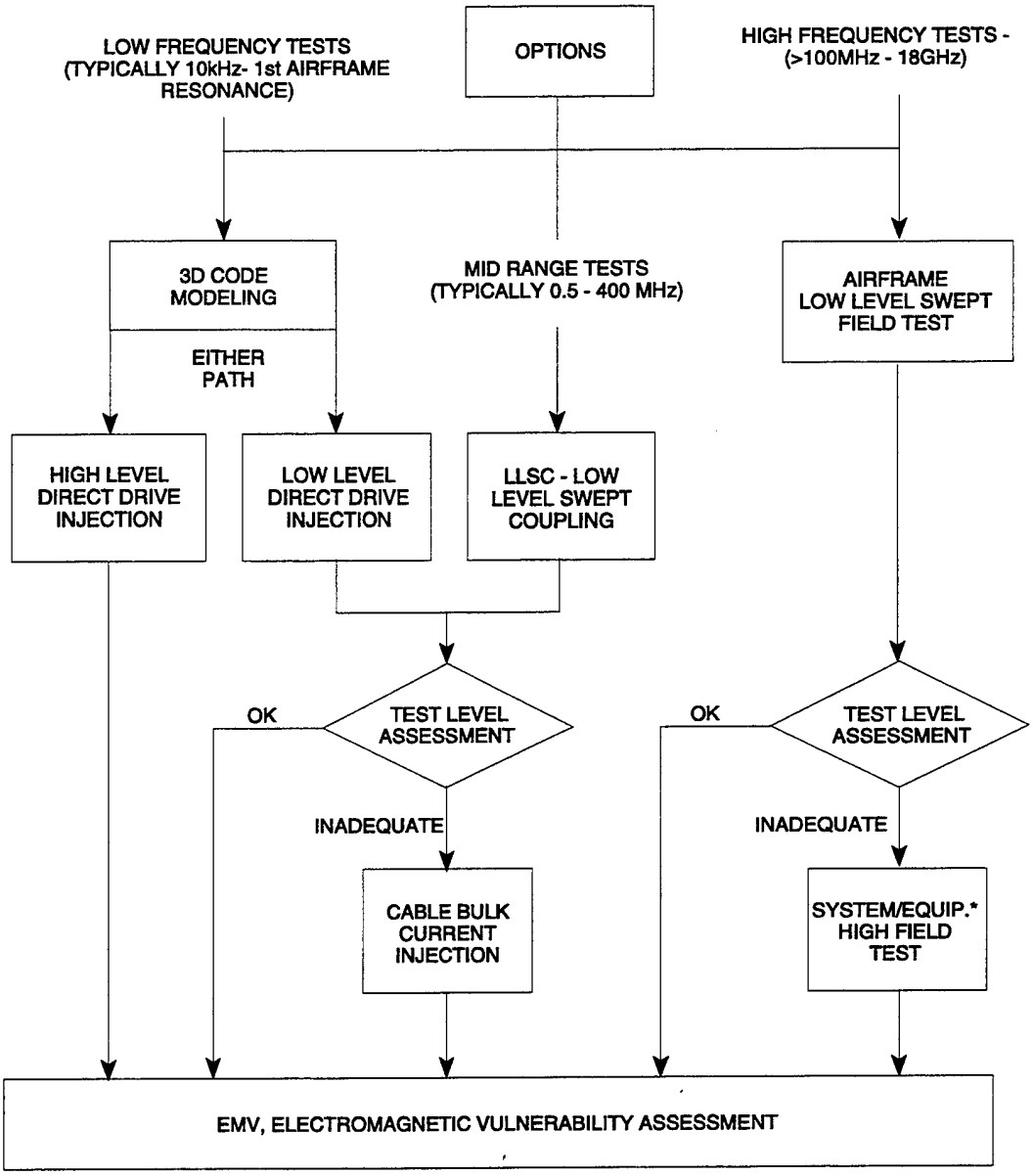

Note: The full frequency range 10 kHz-18 GHz must be covered.
* Mode-stirring test techniques are permitted.

FIGURE 1-2. EXPANDED VIEW OF PROPOSED ROUTES TO CERTIFICATION FOR CRITICAL FUNCTIONS

TABLE 1-1. INTERNATIONAL CERTIFICATION HIRF ENVIRONMENT

Frequency	Field Strength (V/m) (Peak/Average)
10-100 kHz	50/50
100-500 kHz	50/50
500 kHz-2 MHz	40/40
2-30 MHz	100/100
30-70 MHz	20/20
70-100 MHz	20/20
100-200 MHz	50/30
200-400 MHz	70/70
400-700 MHz	1520/750
700 MHz - 1 GHz	950/170
1-2 GHz	2470/180
2-4 GHz	3500/360
4-6 GHz	6800/280
6-8 GHz	1800/330
8-12 GHz	3500/330
12-18 GHz	1700/360

Note: The Certification HIRF Environment above 18 GHz should be used only if the pass/fail criteria are not met in the 12-18 GHz range or if a system that performs a critical function is designed to operate in the 18-40 GHz range. (Current as of January 1995)

2.0 APPROACH

2.1 AIRCRAFT DESCRIPTION

The aircraft used to conduct the Phase II test was the decommissioned Boeing 707-720B that was in storage at AMARC, Davis Monthan Air Force Base, Tucson, Arizona. The aircraft, shown in Figure 2-1, was the same one used to conduct the Phase I test.[2]

The test aircraft was constructed in 1965, had over 50,000 hours of flight time, and was last flown in September 1990. The aircraft had a substantial suite of equipment. The major equipment racks in the avionics bay had over 50 percent of the equipments remaining. With the exception of the center console, which was removed, the cockpit was relatively intact. The passenger compartment, which was essentially intact for the Phase I test, had been stripped of all seats. The structural integrity of the aircraft was good.

Figure 2-2, extracted from the Boeing maintenance manual, shows the profile of the aircraft with the various antenna locations. For emphasis we have highlighted the avionics bay and cockpit with dashed lines.

Figure 2-3 shows a schematic outline of the avionics bay with pertinent EM features. The most significant feature is that the bay is not a closed metallic structure. Note the large area, approximately 5 × 11 ft, directly above the two major equipment racks that has a nonmetallic structure. A phenolic and/or Masonite type material separated the avionics bay from the passenger cabin. The passenger cabin, which had been stripped of all seats and a few of the seat mounting rails, was otherwise intact, including galleys, lavatories, overhead bins, and all wiring bundles. The metal floor between the cockpit and the avionics bay had many penetrations. An access hatch, from the cockpit to the avionics bay, which had a 3/8-inch wire mesh, was closed during all testing. The center console area and the access ports for manual landing gear extension were covered by aluminum foil and conductive tape to reduce coupling between the cockpit and avionics bay.

There were many penetrations of the avionics bay topology including wire bundles, air conditioning ducts, etc. Figure 2-4 shows a schematic of the location of major equipment racks in the avionics bay.

Figure 2-5 shows a schematic outline of the cockpit with features pertinent to EM shielding. For the cockpit, the windows were the major violation of a complete metal enclosure although they had a coating that may have been conductive.

Figure 2-6 shows a schematic of the avionics bay, cockpit, and the front end of the passenger cabin, and shows the location of the tuners, avionics racks, and instrument panels.

2.2 INSTRUMENTED EQUIPMENT

A portion of the Phase II testing included investigation of the radio frequency (RF) coupling characteristics of aircraft and simulated avionics systems. The intent was to measure RF coupling to selected unpowered avionics systems and a simulated avionics system during testing on the aircraft. Subsequently, tests would be performed on the same unpowered systems within the Naval Surface Warfare Center, Dahlgren Division (NSWCDD) reverberation chamber. These measurements were included to verify that the RF coupling to avionics systems over the frequency range 0.1 to 6 GHz measured in a reverberation chamber is a valid description of the RF coupling characteristics of these same systems over the same frequency range when the systems are installed in an aircraft.

The RF coupling to unpowered avionics systems and an unpowered simulated avionics system was measured for the following cases:

- Aircraft avionics systems installed in their appropriate locations within the aircraft and a simulated avionics system positioned within the aircraft similarly to the aircraft avionics systems
- A simulated avionics system positioned in the aircraft in relative isolation from aircraft structure
- Avionics systems and the simulated avionics system tested in several system configurations in the NSWCDD reverberation chamber

The following systems from the cockpit instrument panel and avionics bay were extracted for instrumentation prior to testing

- Radar altimeter (RA)
- Flight director indicator (FDI)
- Directional gyro (DG)
- Automatic pilot computer (AP)
- Automatic direction finder (ADF) receiver

The avionics systems were instrumented to measure the RF energy coupling to

- An interior wire leading to the aircraft wiring harness connector plug (channel 1)

- An interior component lead (channel 2)

An interior circuit component could not be conveniently instrumented in the ADF; therefore, a maintenance test port was instrumented instead.

Furthermore, the FDI's and DG's components were virtually entirely mechanical. Therefore, both instrumentation points on these boxes were for wires leading to the aircraft wiring harness connector plugs.

Instrumentation of the aircraft avionics systems was accomplished by drilling two holes at convenient spots on the front or rear coverplate of each system through which 0.141-in. semi-rigid coaxial cable could be routed with SMA feedthroughs. Appropriate lengths of semi-rigid cable were cut for routing to the point to be instrumented within the box. Approximately 1/4 in. of center conductor was exposed at the instrumented end. SMA feedthroughs were attached at the opposite end. The center conductor was then soldered to the point to be monitored. A grounding strap with a terminal was soldered to the outer conductor of the semi-rigid coax for coax lengths greater than 6 inches. The grounding strap's terminal was fastened to the interior chassis using existing screws. Figures 2-7 and 2-8 show the instrumentation details for the two RA channels. For the RA channel 1, because the semi-rigid cable could not be bent to sufficiently tight radius, a 2.5-in. length of 10-gauge wire was soldered to the center conductor. The wire was shielded using overbraid.

The simulated avionics system was the common test article (CTA) designed by NSWCDD. The CTA is actually a system of three interconnected boxes, only two of which were needed for the Phase II test. The two tested boxes were connected with 3 m of cabling. One box was instrumented to measure the RF coupling to the input pin of a line driver integrated circuit (IC) chip that interfaced with the external connector. A fiberoptic feedthrough on the box was removed and a SMA feedthrough was substituted for a semi-rigid coaxial instrumented line. Figure 2-9 shows the instrumentation details for the CTA.

The results for the RA and the CTA will be reported in this document.

2.3 INSTRUMENTATION

2.3.1 Continuous Wave Excitation

The test setup for continuous wave excitation with mechanical mode-mixing is shown schematically in Figure 2-10.

Dual-ridged horn and log periodic antennas were used to both transmit and receive test signals. A frequency synthesizer was used to generate the test frequencies, which were amplified by an RF amplifier at frequencies above 1.0 GHz. The output power of the amplifier was approximately +20 dBm above 1.0 GHz. Below 1.0 GHz, only the output of the frequency synthesizer was used with its output power set to +15 dBm. Signals were received via two spectrum

analyzers, which were under computer control. The spectrum analyzers collected 601 data points per sweep. All data collected were stored on 3.5-in. disks.

Three aluminum-foil-covered tuners were constructed from Styrofoam and mounted on aluminum shafts. Each tuner was driven by a shielded dc motor. As shown in Figures 2-11, 2-12, and 2-13, the tuners were mounted in the cockpit, avionics bay, and passenger cabin respectively.

The equipments external to the aircraft (e.g., synthesizer, spectrum analyzer, etc.) were mounted in a 16-ft truck. This arrangement maintained the equipment in a fixed position and provided some protection from the sun and the wind. The vehicle remained in a fixed location for the duration of the CW testing. Figure 2-1 shows the vehicle in its location with respect to the aircraft. Figure 2-14 shows the equipment arrangement within the vehicle. The equipment list for all three excitation techniques is shown in Table 2-1.

The required semirigid cables were fabricated on-site to provide cable lengths necessary to reach all points of interest within the aircraft. Calibration was performed for each cavity tested. To calibrate the system, the transmit cable was connected directly to each receive cable. These data were stored on disk and used to correct all test data for cable insertion/connector loss. For verification, the system was recalibrated at the end of each test.

During the Phase I test, five 1/4-in. holes had been drilled through the aircraft pressure hull in the nose landing gear well. These holes were for the purpose of feeding signal into and out of the aircraft and dc power to the tuner motors. For this test, three of the holes were enlarged to accept type "N" feedthroughs. Signals to and from the antennas were fed through the type "N" connectors, while one of the remaining 1/4-in. holes was fitted with an SMA feedthrough for dc power to the tuner. The fifth hole, which was not needed for this test, was covered with conductive tape. Figure 2-15 shows the entry points in the landing gear well. Four holes for type N feedthrough connectors were drilled for access to the cockpit, and an additional four holes were drilled for access to the passenger cabin. These access holes were drilled into the port side of the aircraft. Figure 2-16 shows the entry points into the cockpit.

2.3.2 Band-Limited White Gaussian Noise Excitation

The test setup for BLWGN excitation is shown schematically in Figure 2-17. The control, stimulus, and measurement module contains the computer controller and plotter used to control the test equipment, acquire data, and display data. The sweeper generated the local oscillator signal, which was in the range of 0.2 GHz to 6 GHz for this experiment. The white Gaussian noise (WGN) source generated noise at the proper bandwidth as commanded by the computer. The scaler analyzer was the primary instrument for measuring power received by the various receiver (RX) antennas.

Cavity relaxation-time measurements required the use of a Textronix Digital Signal Analyzer (DSA) Model 602 digitizing oscilloscope and function generator.

The modulator, amplifier, and switching module performed the up-conversion and amplification of the noise to produce the BLWGN signal. Part of the BLWGN signal was sampled

and diode-detected to provide an external-level reference signal for the sweeper in the previous module. The external reference ensured that the power into the aircraft cavity remained relatively constant despite varying amplifier gain and cable losses. The switch controller selected the appropriate modulator and amplifier combination for the frequency being generated. In this test, the 8–18 GHz amplifier was not used.

Finally, the cavity launch and monitoring were accomplished using log periodic antennas (0.2 to 1 GHz) or dual-ridged horn antennas (1 to 6 GHz) as transmitter (TX) antennas. Similar antennas were used to receive the desired internal signals. The TX antenna was placed outside the aircraft during the aircraft SE tests.

The BLWGN measurements used the same aircraft feedthroughs as used for CW excitation.

2.3.3 Short Pulse Excitation

The test setup for short pulse/time-domain measurements is shown in Figure 2-18. The pulse generator produced a baseband, unipolar impulse shown in Figure 2-19. The test signal was a 450-ps, 40-volt impulse with a 50-kHz repetition rate. The useable spectrum of the pulse extends from 50 kHz (the repetition frequency) to approximately 2.5 GHz.

The test signal was radiated by a broadband TEM horn antenna with a flat response from 25 to 1000 MHz. For this test, the antenna response defined the upper measurement frequency. The pulse radiated by the TX antenna was a differentiated version of the generator pulse.

An identical broadband TEM horn antenna measured the desired electromagnetic fields. The TX and RX antennas were specially designed at the National Institute of Standards and Technology (NIST) for maximum pulse fidelity. The RX antenna produced an output signal that was an exact replica of the electromagnetic field on its aperture. The resulting signal was a doublet as shown in Figure 2-20.

Since the system performance was limited by the noise floor of the digital oscilloscope, the RX antenna output was amplified by a very low noise preamplifier before being applied to the scope input. The oscilloscope was a sampling type having a bandwidth extending from dc to 14 GHz, which therefore acted as a wideband receiver for the time domain waveform.

The oscilloscope data was transferred to a computer for processing. The computer was a 486-type PC and communicated with the scope over an IEEE 488 bus.

The computer was capable of recording the time-domain waveform received by the scope, storing it on floppy disk, correcting for system calibration, transforming the information into the frequency domain, and presenting the results as a function of frequency. In this way, one set of time-domain waveforms provided response data at 50 frequencies between 20 MHz and 1000 MHz.

All instrumentation external to the aircraft was set up in, and operated from, a van.

The time domain measurements used the same aircraft feedthroughs as used for CW and BLWGN excitation.

2.4 TEST PROCEDURES

2.4.1 Continuous Wave Excitation

Using the test setup shown in Figure 2-10, the following types of data were collected with CW excitation

- Swept frequency power density (PD) with mode-mixing
- Swept frequency PD without mode-mixing
- Discrete frequency PD with mode-mixing

Each cavity was equipped with a tuner that could be stationary or in continuous rotation at an adjustable rate.

Data were obtained using multiple combinations or "configurations" of TX and RX antenna locations. A configuration is defined as a unique combination of a specific location, orientation, and polarization of the TX and RX antennas and/or tuner combinations. Note that an instrumented avionics system or the CTA may be substituted for the RX antenna on each of the spectrum analyzers. As with all reverberation chamber testing, direct line-of-site between TX and RX antennas was avoided. Further, in some cases, the antennas did not have a direct line-of-site to the tuner.

For swept frequency measurements with mode-mixing, the synthesizer was set to the selected start/stop frequencies, the reference output level, and the sweep time. The spectrum analyzer recorded the maximum received power over the frequency interval for continuous rotation of the tuner. The synthesizer and spectrum analyzer sweep times and the tuner rotation rate were adjustable parameters. These parameters were selected to provide the desired data accuracy in the minimum time. A typical data run required approximately 20 minutes. The spectrum analyzer transmitted the final trace to the computer. The data were recorded on disk after being corrected with the appropriate calibration data. This type of measurement provided the basis for cavity PD, cavity-to-cavity coupling, and instrumented avionics system response determinations.

Swept frequency without mode-mixing measurements used the same procedures as above except that the tuner was stationary and only one sweep was required. These data were compared to the swept frequency data with mode-mixing to evaluate the effectiveness of the tuner.

For discrete frequency with mode-mixing measurements, the synthesizer was set for the desired discrete frequency. The spectrum analyzer sweep time was set to collect data over an interval corresponding to approximately 1.25 revolutions of the tuner. The spectrum analyzer trace

was transmitted to the computer and recorded on disk. In this case, the recorded data was not automatically corrected for the instrument/measurement system calibration data. This type of measurement provided the basis for characterizing the statistical nature of EME in the aircraft cavities.

No cavity relaxation time or SE measurements were performed with CW excitation.

2.4.2 Band-Limited White Gaussian Noise Excitation

Using the test setup shown in Figure 2-17, the following types of data were collected with BLWGN excitation:

- Swept frequency PD
- Discrete frequency cavity relaxation time
- Shielding effectiveness

For the swept frequency PD measurements, the sweeper was configured in the externally leveled sweep mode by the computer with a reference level of −26 dBV. The computer set the selected start/stop frequencies, sweep time, and noise BW. Typically, three noise BWs (2, 10, and 50 MHz) were used for each measurement. The TX antenna injected RF energy into the cavity at the selected reference level. The scaler analyzer recorded the signal measured by the RX antenna and transmitted the trace to the computer. For cavity PD and cavity-to-cavity coupling measurements, four different locations of the RX antenna were used.

For instrumented avionics system and CTA responses, the RX antenna was replaced by the hard-wired connections in the systems, and one measurement per circuit was obtained.

For the discrete-frequency cavity-relaxation-time measurement, the sweeper was configured via the computer to generate an externally pulse-modulated, fixed-frequency signal. Internal leveling of the sweeper was set to −5 dBm for testing at the lower frequencies and was increased to +5 dBm at the higher frequencies to improve the measurements. The function generator provided a 1-kHz, 50-percent duty cycle, square wave to the external pulse modulation input of the sweeper. The pulse-modulated signal was mixed with noise from the WGN source and amplified for launch into the cavity via the TX antenna. The WGN source was commanded by the computer to insert the 25-MHz low pass filter on the output so that the BLWGN signal had a 50-MHz bandwidth. The TX and RX antennas were placed in the same cavity and positioned so as to produce minimal direct coupling between them. The signal returned by the RX antenna was diode-detected and displayed on the DSA 602 digitizing oscilloscope. The DSA 602 was triggered directly by the function generator so that a large number of time-correlated pulses could be collected and averaged to provide an ensemble average that could then be analyzed. The DSA 602's voltage range was set to 5 mV per division and the variable attenuator was adjusted so that the signal just fit in the display. This ensured that the diode was being operated in the square law region so that the output voltage was

proportional to input power. The DSA 602 reported the 0.9 to 0.1 (amplitude drop from 90 percent to 10 percent of initial value) fall time of the received signal. This procedure was repeated for each frequency of interest and for each of the three cavities.

Aircraft SE measurements were performed as described for the PD measurements except that the TX antenna was outside the aircraft. Measurements were obtained with the TX antenna 100 ft from the aircraft at a height of 152 in. above the ground at three aspect angles. One aspect angle had the TX antenna aligned with the aircraft axis and pointed at the nose. The other two aspect angles were with the TX antenna at 45° and 90° right of the angle. The aim point for the 45° and 90° locations was the forward cabin door. Data were obtained for both vertical and horizontal polarizations of the TX antenna at each of the three locations. A reference measurement was performed with the TX and RX antennas positioned 100 ft apart at 152 in. above the open field where the aircraft was located. The reference measurement used the same cables and instrumentation as used in the SE measurements.

2.4.3 Short Pulse Excitation

Using the test setup shown in Figure 2-18, the following types of data were collected with short pulse excitation

- Cavity relaxation time
- Shielding effectiveness

For cavity relaxation time measurements, both the TX and RX antennas were placed in the same cavity. The SE measurements were performed for the same TX locations and polarizations as described in Section 2.4.2 for BLWGN excitation. The tuners fabricated for mechanical mode-mixing with CW excitation were used to provide a limited number of different cavity configurations during the measurements. As with BLWGN, a reference measurement was performed over the same ground conditions. The reference measurement used all the cables and components used in the SE measurements. Thus the reference signal contains all the information about the measurement system without the aircraft. This reference signal was used to calibrate the aircraft data to obtain the SE.

No PD or cavity-to-cavity coupling measurements were performed with short pulse excitation.

2.4.4 Ambient EME Excitation

Using the receive portion of the test setup shown in Figure 2-10 for CW excitation, cockpit SE data were collected with ambient EME excitation.

For ambient EME excitation, the RX antenna, either a monopole or a log periodic, was placed in several locations in the cockpit. Both horizontal and vertical polarizations were used. Data were obtained with and without the tuner operating. The SE references were measurements obtained in an open field away from the aircraft at the same height as the cockpit.

FIGURE 2-1. BOEING 707 TEST AIRCRAFT AT AEROSPACE MAINTENANCE AND REGENERATION CENTER, DAVIS MONTHAN AFB, TUCSON, AZ

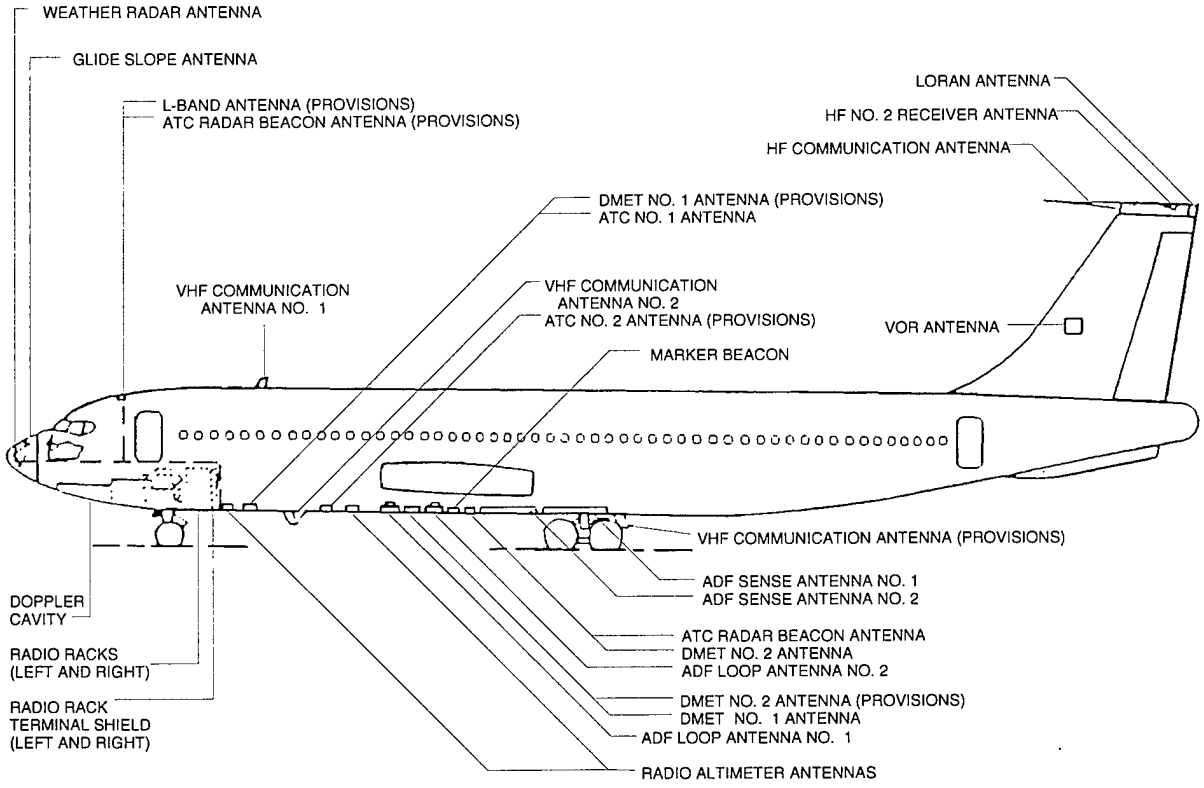

FIGURE 2-2. PROFILE OF BOEING 707 AIRCRAFT

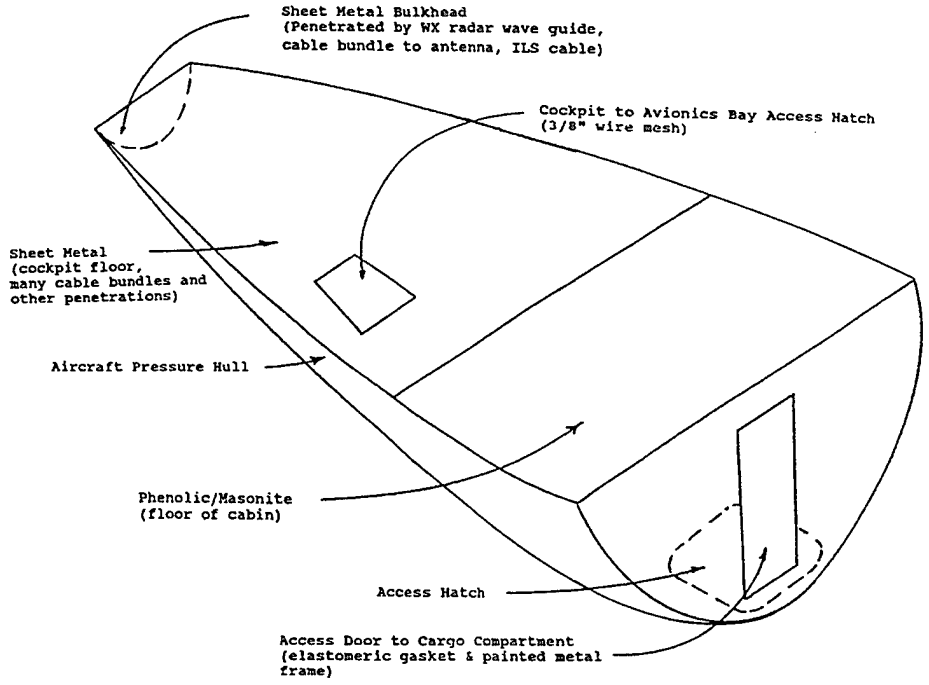

FIGURE 2-3. SCHEMATIC OF AVIONICS BAY ELECTROMAGNETIC TOPOLOGY FOR BOEING 707

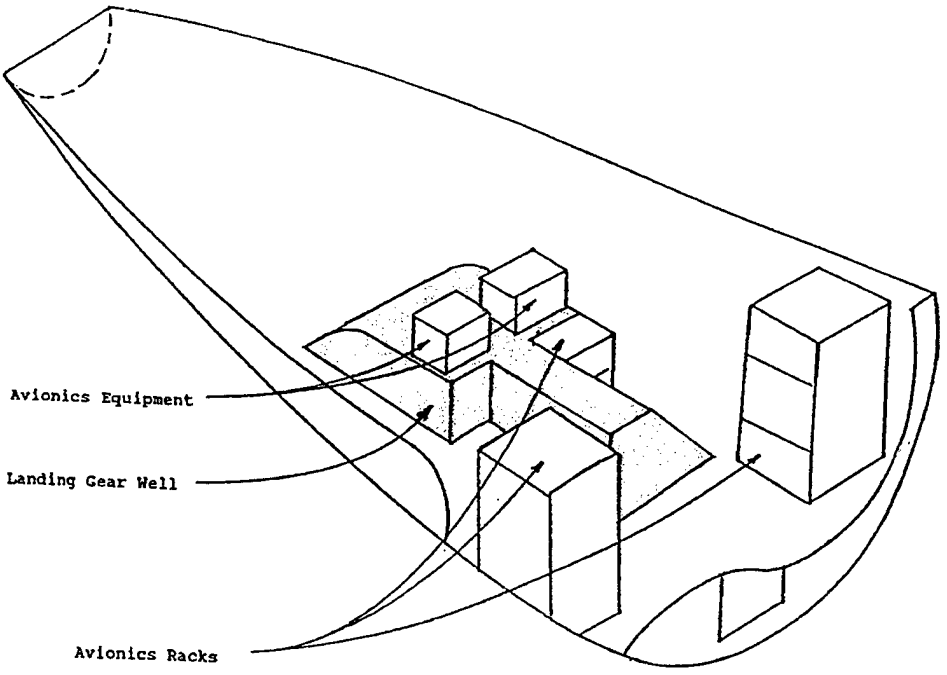

FIGURE 2-4. LOCATION OF MAJOR EQUIPMENT RACKS IN BOEING 707 AVIONICS BAY

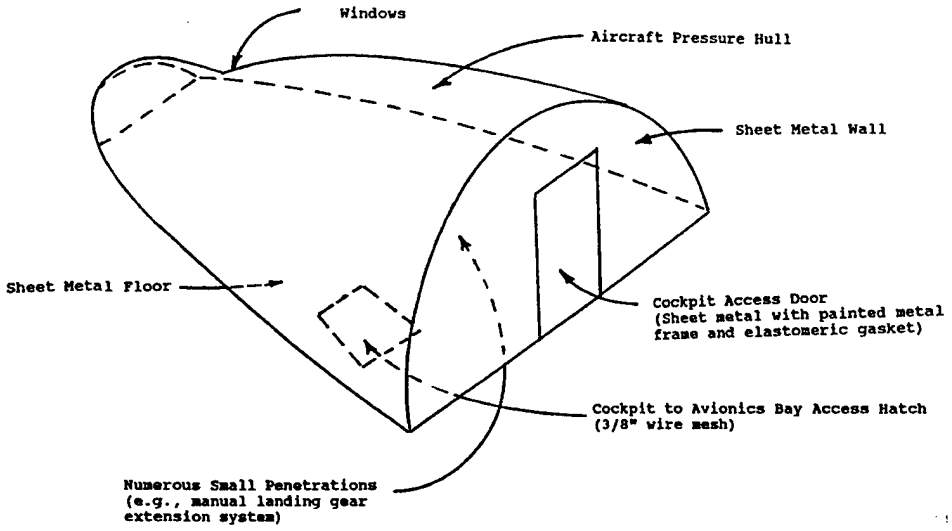

FIGURE 2-5. SCHEMATIC OF COCKPIT ELECTROMAGNETIC TOPOLOGY FOR BOEING 707

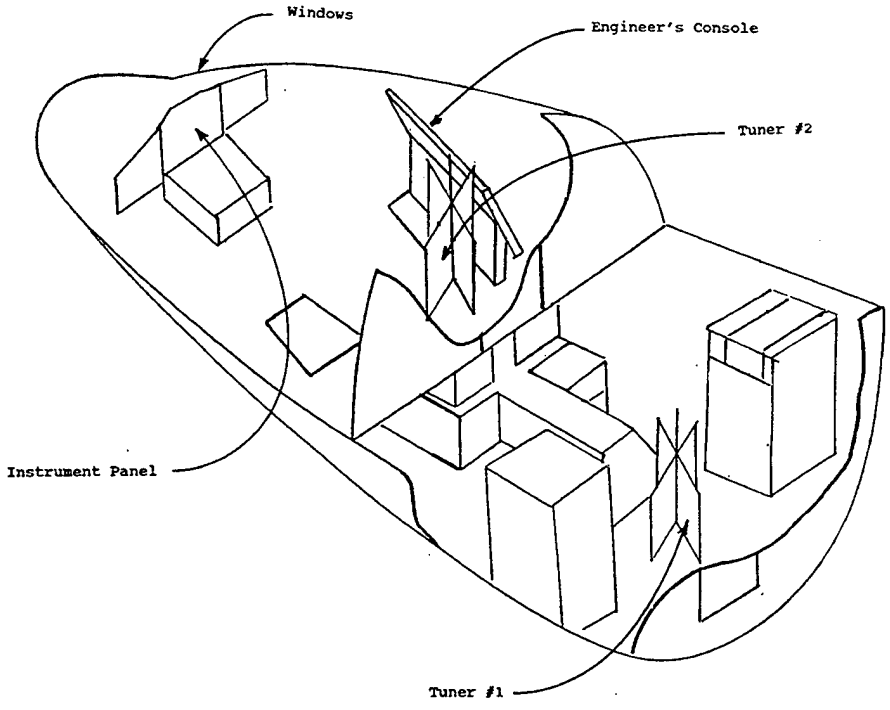

FIGURE 2-6. LOCATION OF TUNERS IN BOEING 707 COCKPIT AND AVIONICS BAY

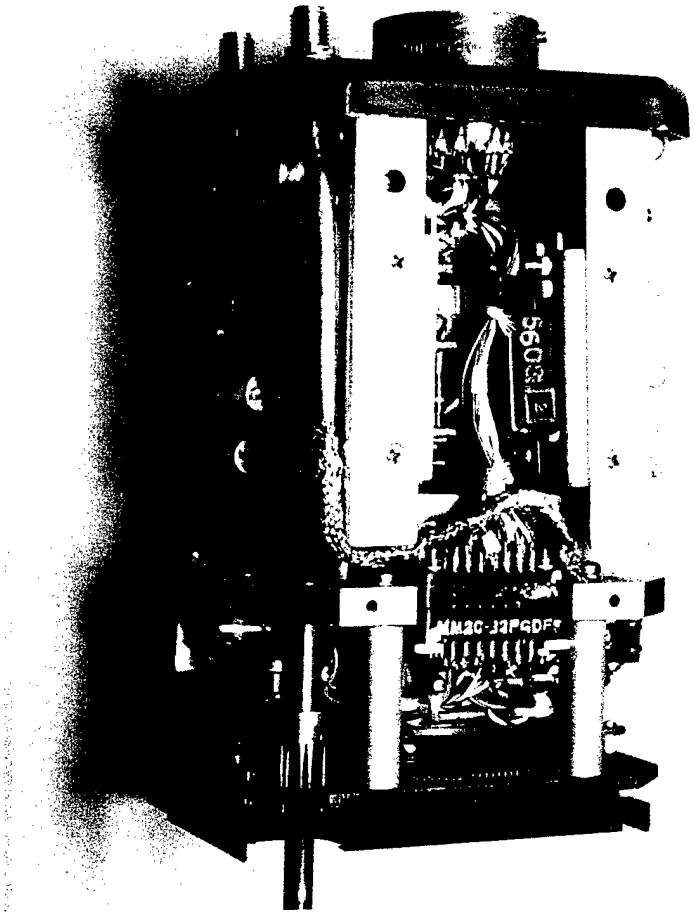

FIGURE 2-7. INSTRUMENTATION OF RADAR ALTIMETER INDICATOR INTERIOR WIRE LEADING TO AIRCRAFT WIRING HARNESS CONNECTOR PLUG (CHANNEL 1)

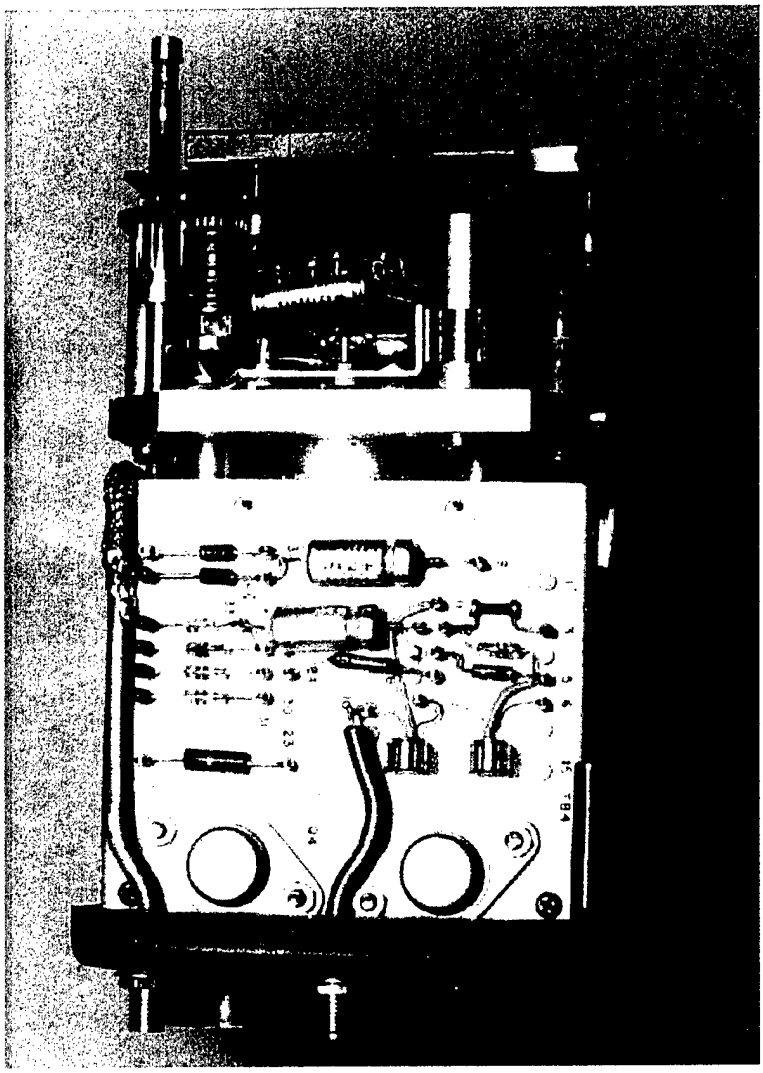

FIGURE 2-8. INSTRUMENTATION OF TRANSISTOR INSIDE RADAR ALTIMETER INDICATOR (CHANNEL 2)

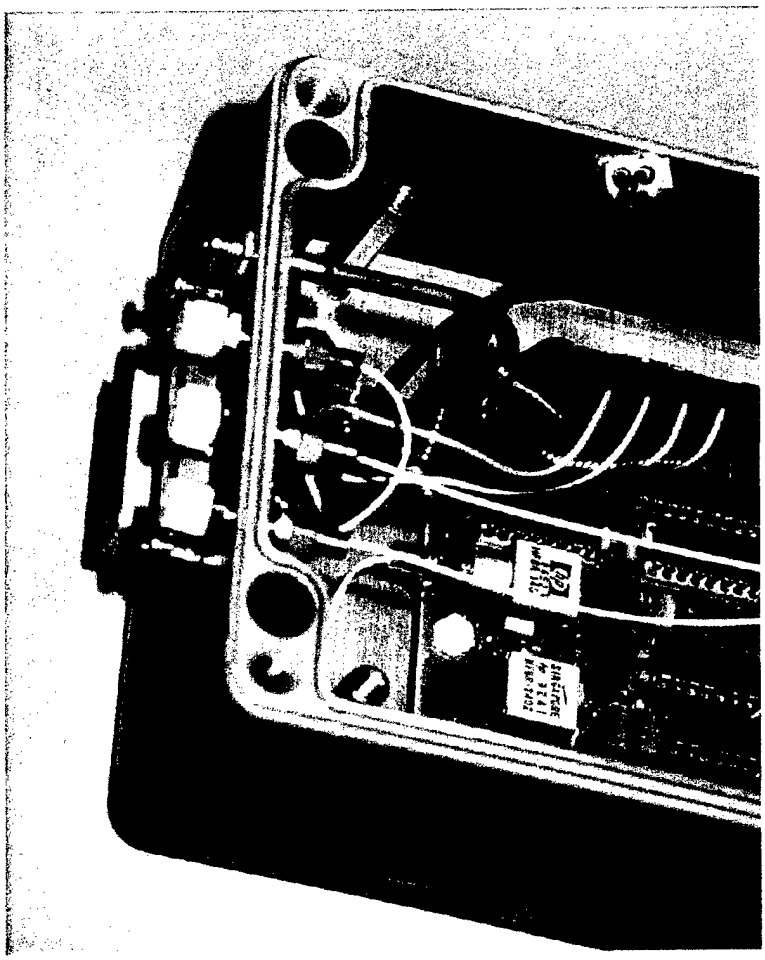

FIGURE 2-9. INSTRUMENTATION OF LINE DRIVER INTEGRATED CIRCUIT INPUT PIN IN CTA

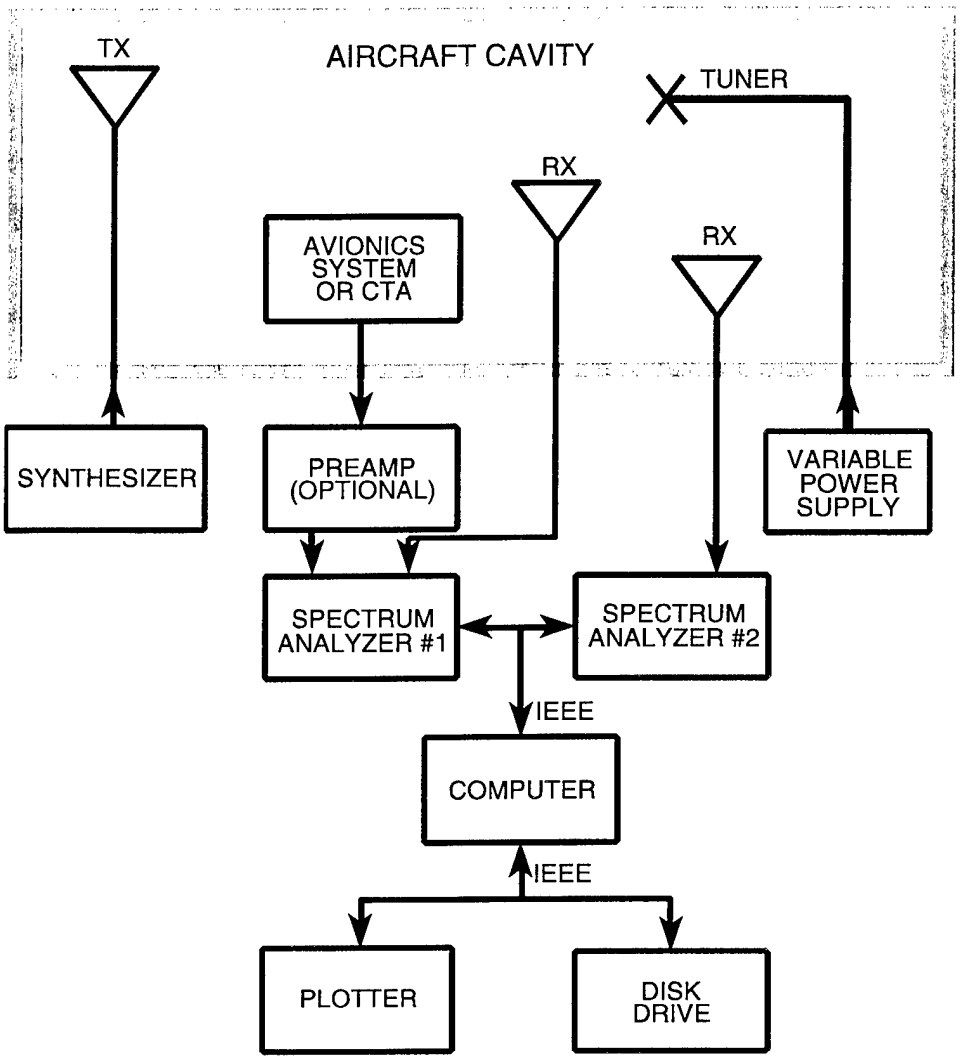

FIGURE 2-10. SCHEMATIC OF TEST SETUP FOR CW EXCITATION

FIGURE 2-11. PHOTO OF COCKPIT TUNER

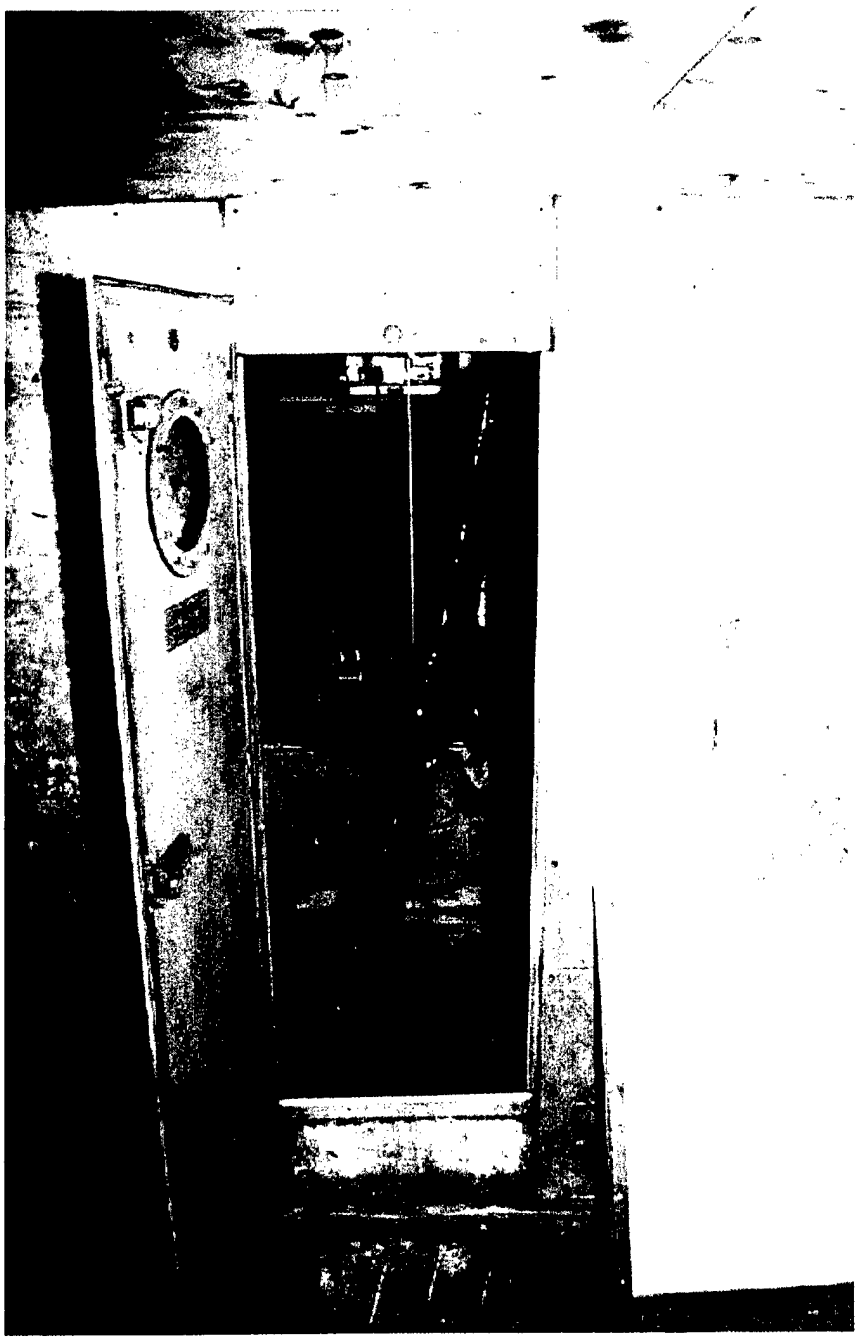

FIGURE 2-12. PHOTO OF AVIONICS BAY TUNER

FIGURE 2-13. PHOTO OF PASSENGER CABIN TUNER

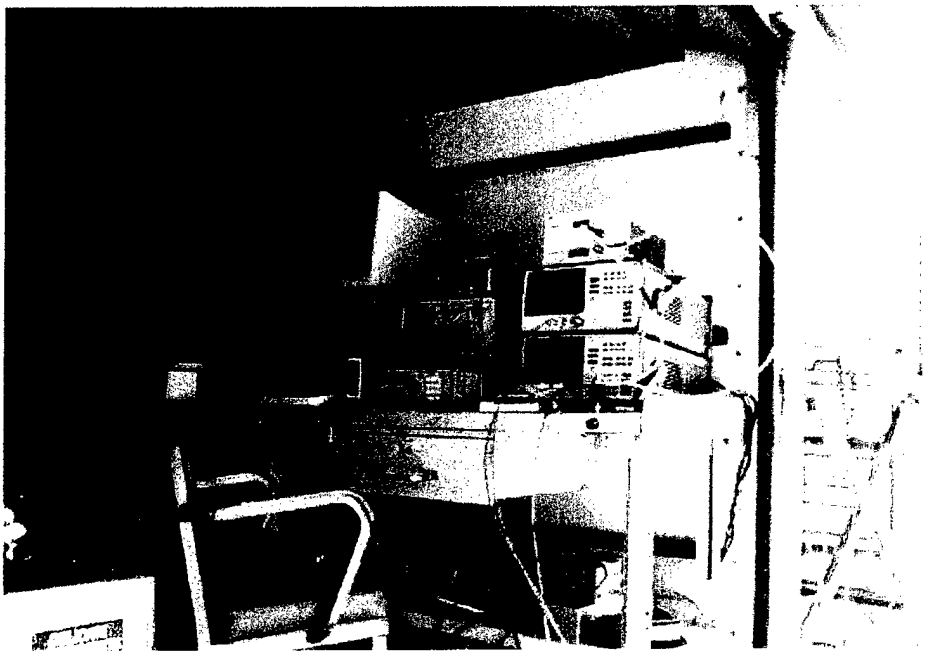

FIGURE 2-14. TEST EQUIPMENT SETUP IN SUPPORT VEHICLE

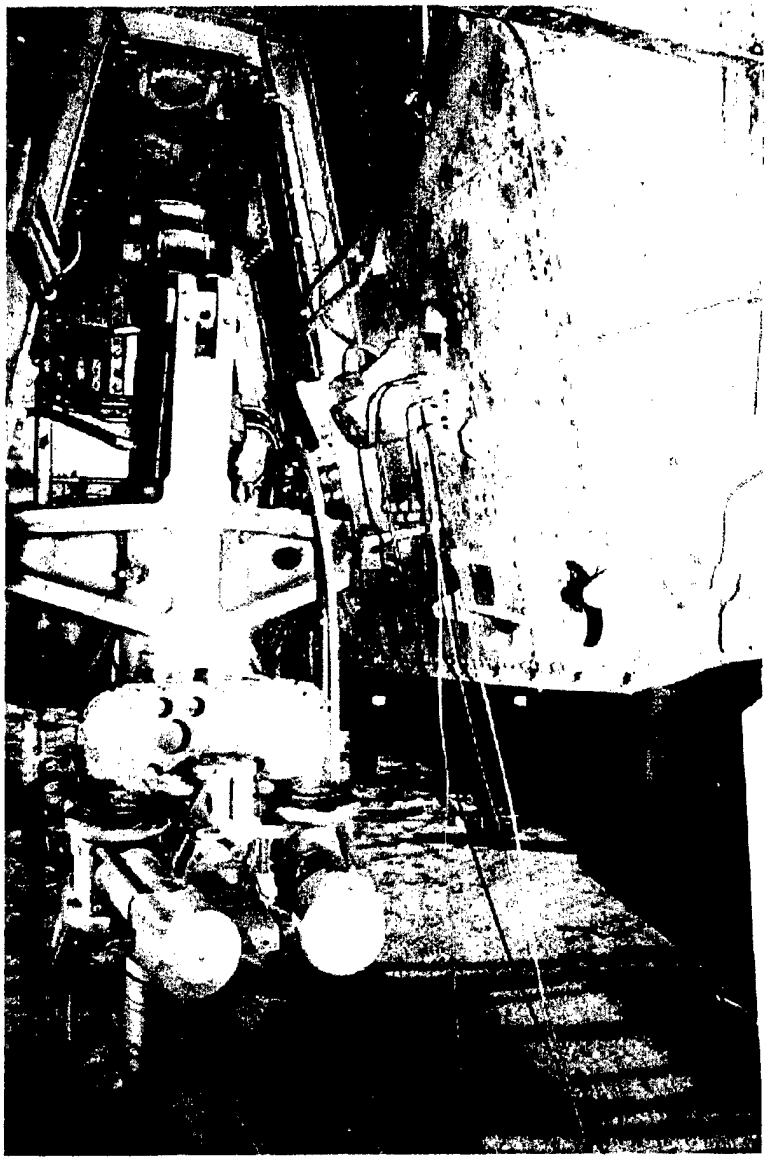

FIGURE 2-15. AVIONICS BAY INSTRUMENTATION CABLE PENETRATIONS OF AIRCRAFT PRESSURE HULL IN LANDING GEAR WELL

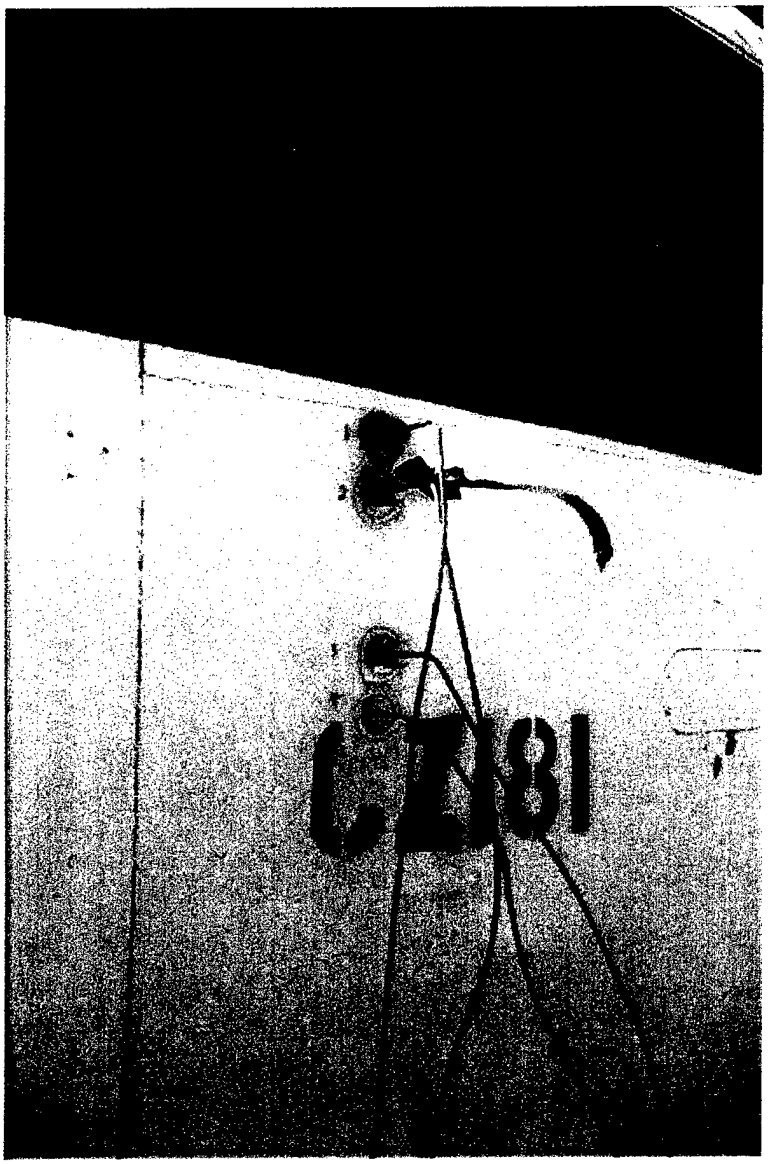

FIGURE 2-16. COCKPIT INSTRUMENTATION CABLE PENETRATION OF AIRCRAFT PRESSURE HULL

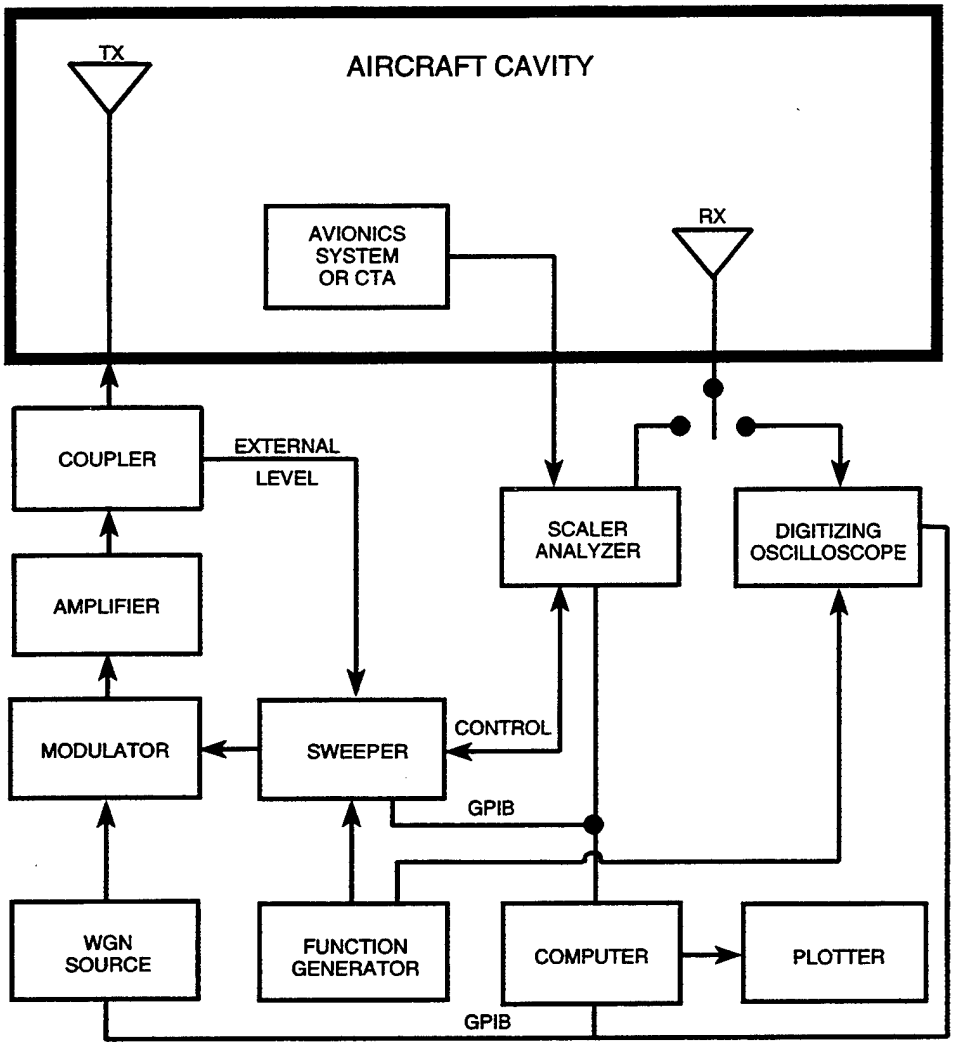

FIGURE 2-17. SCHEMATIC OF TEST SETUP FOR BLWGN EXCITATION

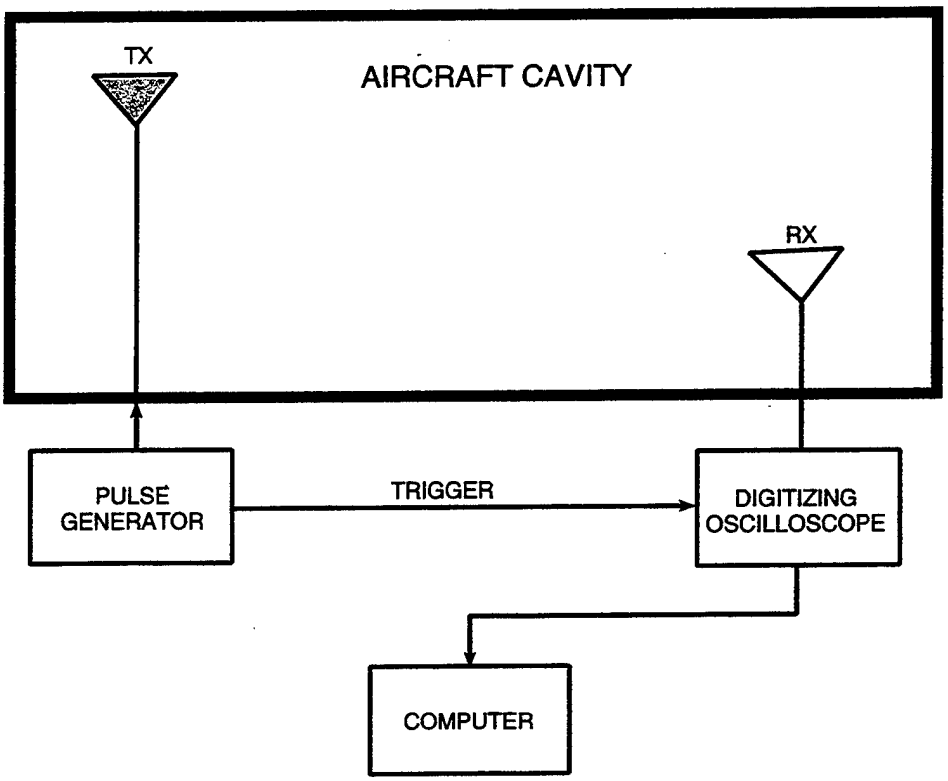

FIGURE 2-18. SCHEMATIC OF TEST SETUP FOR SHORT PULSE EXCITATION

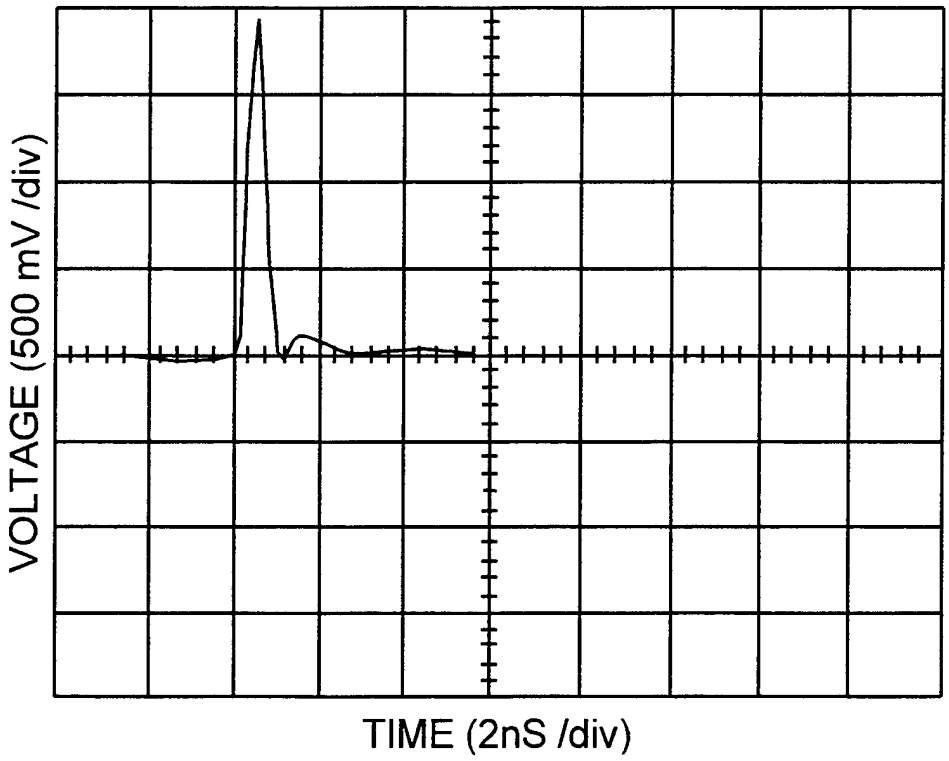

FIGURE 2-19. PULSE PRODUCED BY PULSE GENERATOR

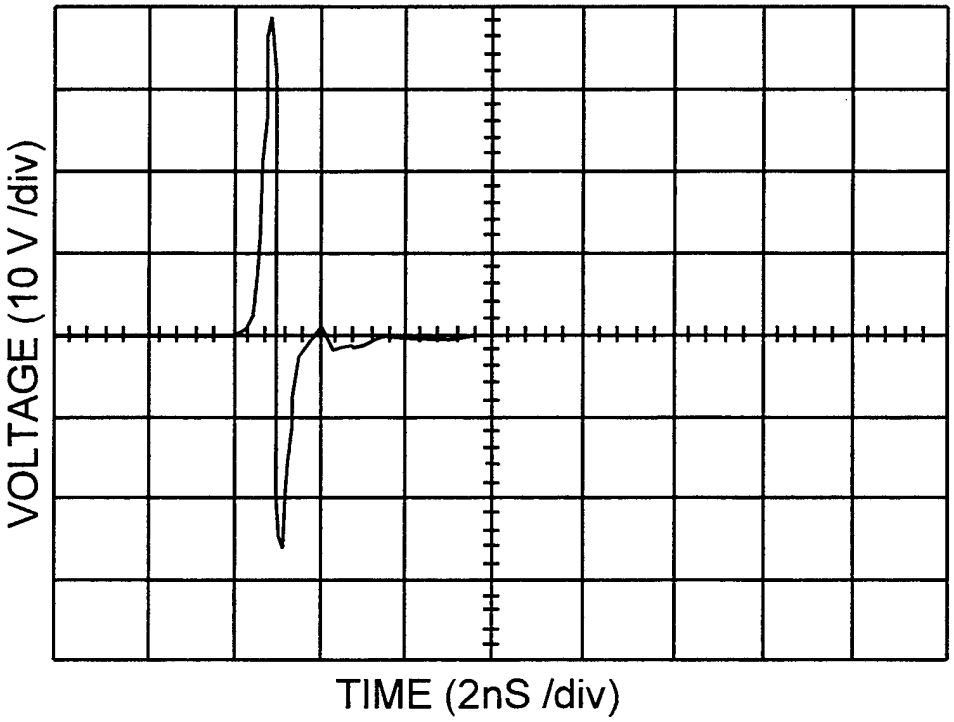

FIGURE 2-20. DOUBLET WAVEFORM OUTPUT OF RECEIVE ANTENNA

TABLE 2-1. EQUIPMENT LIST

HP8341 (83620) Sweep Frequency Synthesizer
Gigatronics 7300 Sweep Frequency Synthesizer
HP3314A Function Generator
Picosecond Pulse Labs Model 1000 Impulse Generator
Mixers
Picosecond Pulse Labs Model 5810 Impulse Amplifier
Amplifiers
NoiseCom 7907 Noise Source
Log Periodic Antennas (2)
EMCO 1 - 18 GHz Dual Ridged Horn Antenna
Eaton 1 - 18 GHz Dual Ridged Horn Antenna
NIST 25 - 1000 MHz Resistively Loaded TEM Horns (2)
Antenna Support Stands
HP85025A AC/DC Detectors
HP423B Crystal Detectors
B&H AC260 83H20 Preamplifier
HP8349B 2-20 GHz Preamplifier
HP8562A Spectrum Analyzer
HP8757C Scaler Network Analyzer
HP Power Meters
Tektronix DSA 602 Digitizing Signal Analyzer
Tektronix DSO 7854 (14 GHz) Digitizing Sampling Oscilloscope
Computer and Associated Peripherals
Miscellaneous Cable, Couplers, Attenuators, etc.

3.0 SUMMARY OF DATA OBTAINED

This chapter identifies the specific types of data obtained during the test. Table 3-1 shows the details of the types of data collected versus the excitation source. In most cases, there is more than one excitation source for each EME parameter investigated.

During this test, data were collected for many configurations. Data from these multiple configurations can be averaged to obtain nominal cavity and system responses. The multiple configurations also provide increased confidence that response bounds will be observed.

This chapter covers calibration data (Section 3.1), mode-mixing effectiveness data (Section 3.2), cavity PD data (Section 3.3), cavity decay time data (Section 3.4), avionics systems/CTA responses (Section 3.5), cavity-to-cavity coupling data (Section 3.6), and SE data (Section 3.7). For each type of data, sample traces are presented, the extent of the data base is discussed, and the type of excitation is identified.

3.1 CALIBRATION DATA

Appropriate calibrations were performed as required for each type of measurement as described below.

For mode-mixing effectiveness with CW excitation (e.g., stirring ratio (SR) data), no calibrations were required since the data of interest are relative measurements. If absolute measurements are required, the calibration runs from PD measurements (described below) are available.

For cavity PD, instrumented avionics system responses, and cavity-to-cavity coupling measurements for both CW and BLWGN excitations, calibration data were obtained by connecting the TX cable directly to the RX cable. The measured cable/connector-loss data were used to correct all measurements.

For cavity decay-time measurements, no specific calibrations were required for either the BLWGN or short-pulse measurements.

Ambient EME SE results were derived from simultaneous, relative measurements between two identical antennas, one outside and one inside the aircraft. The cabling was considerably different for the two RX antennas. Each cable run was calibrated by connecting the antenna end of the cable directly to the frequency synthesizer. The synthesizer output was set to 0 dBm and a frequency sweep performed. These data were stored as a calibration data file.

For BLWGN and time domain SE measurements, in addition to the cable/connector loss calibrations, a reference measurement was obtained with the RX antenna placed at the same distance and height as the aim point on the aircraft. The RX antenna was in an open area away from the aircraft. The difference in the terrain path for the reference and the actual aircraft measurements should be minimal since they were both accomplished over the same open field.

3.2 MODE-MIXING EFFECTIVENESS

The effectiveness of mode-mixing depends on the cavity mode density and the mode-mixing technique. For mechanical mode-mixing the rotating tuner changes the modal structure by changing the cavity boundary conditions. The mode-mixing effectiveness can be determined from discrete frequency data. As an example of discrete frequency data, Figure 3-1 shows the power density as a function of tuner rotation obtained at 700 MHz with a log periodic antenna in the cockpit. As described in Section 2.4.1, data were collected over approximately 1.25 rotations of the tuner. Pattern repetition can be seen by comparing the data trace for times greater than approximately 5.7 seconds (the rotation period) with the start of the trace. These data yield the SR, which can be compared to the accepted guideline discussed in Crawford and Koepke.[1] The data can also be compared to a theoretical statistical distribution function. The Phase I test collected extensive discrete frequency data to address a specific test objective. In this Phase II test, only limited discrete frequency data were collected for the three aircraft cavities.

3.3 NORMALIZED CAVITY POWER DENSITY

Normalized cavity PD, that is, the ratio of the measured cavity PD to an input power of 1 mW (0 dBm), is the most common measurement available in this test.

For CW excitation, the PD was obtained with mechanical mode-mixing using a tuner. The data were collected in the mode-stirring mode of operation, that is, with the tuner in continuous rotation. The rotating tuner changes the cavity boundary conditions, and hence, the modal structure.

In the Phase II test matrix, the typical data collection time allocated for a swept frequency, CW PD measurement was approximately 25 minutes. The time allocated was a trade-off between long collection times for best statistics and short collection times for more instrument and cavity characterizations. The tuner rotation speed, the signal generator sweep time, and the spectrum analyzer sweep time were adjusted to optimize the data collected.

Figure 3-2 shows swept-frequency, CW PD data with mechanical mode-mixing for the cockpit. The frequency span is 0.1 to 1 GHz. The TX and RX antennas were both log periodic.

With approximately 25 minutes allocated to each swept frequency measurement for each of the three frequency bands covering the test range of 0.1 to 6 GHz, time constraints limited the number of test configurations that could be investigated. One swept frequency PD measurement was obtained with CW excitation and mechanical mode-mixing for each of the three aircraft cavities.

For the BLWGN technique, existing cavity modes are excited by a level input power over the noise BW. The modal structure varies with frequency and with cavity configuration. The BLWGN measurement yields an average PD over the BW. The measured PD will depend on the noise BW and on the fine structure in the cavity modes. Three noise BWs, 2, 10, and 50 MHz, were investigated in this test.

Figure 3-3 shows swept frequency, BLWGN PD data for a single run in the cockpit. The frequency span was 0.2 – 1 GHz, the BW was 50 MHz, and the TX and RX antennas were both log periodic.

The data collection time for a swept frequency, BLWGN PD measurement was approximately one-half minute. Therefore, it was possible to obtain data for several test configurations for each cavity, frequency band, and BW. Power density data obtained with BLWGN excitation are available over the frequency interval 0.2 – 6 GHz for noise bandwidths of 2, 10, and 50 MHz. In most cases, four PD measurements were obtained in each cavity by moving the TX and/or RX antenna locations.

3.4 CAVITY DECAY TIME

The cavity decay or relaxation time provides the data for a direct computation of the cavity Q.

For BLWGN excitation, the decay time was measured with the DSA 602, which sampled the received power as a function of time after input power cutoff for a large number of pulse repetitions. The DSA 602 provided a direct numerical readout of the 0.9 – 0.1 decay time. A typical measurement averaged enough samples to obtain a stable readout in the third significant figure. The measured decay time data for the cockpit, avionics bay, and passenger cabin are shown in Table 3-2.

Decay time is a derived parameter using short pulse excitation. A typical time domain data trace used for determining decay time is shown in Figure 3-4. Derived decay time values for the cockpit and passenger cabin are shown in Table 3-3.

3.5 AVIONICS SYSTEMS/COMMON TEST ARTICLE RESPONSES

As stated in Section 2.2, the RA and the CTA were instrumented with voltage probes. The RA had two response monitoring points. These were connected to ports on the system enclosure, which were in turn connected to the spectrum analyzer.

The monitoring points within the RA were the source of the received signals. A typical response for CW excitation is shown in Figure 3-5. These data are for the two ports of the RA display located in the cockpit instrument panel. One swept CW run is available for the RA and several locations of the CTA. Figure 3-6 shows a typical data trace for the RA with 50-MHz BLWGN. One BLWGN run is available for each frequency band and noise BW for both channels of the RA and the single monitor point of the CTA.

Follow-on testing of the RA was conducted in the NSWCDD reverberation chamber. Figures 3-7 and 3-8 show the response of the RA display when tested on a dielectric block in the center of the reverberation chamber.

Comparable data are available for the CTA. The CTA, which had only one monitoring point, was deployed in several locations in both the cockpit and the avionics bay.

3.6 CAVITY-TO-CAVITY COUPLING

Two types of measurements support the determination of the cavity-to-cavity coupling. The first is PD measurements whose availability was discussed in Section 3.3 and summarized in Table 3-1. The second is the measurement of the PD in one cavity for power input into another cavity.

Figure 3-9 shows the PD in the cockpit for swept frequency, CW excitation of the passenger cabin with the tuners in operation in both cavities. The frequency span is 0.1 to 1 GHz. The TX and RX antennas were both log periodic. These data would be combined with PD data described in Section 3.3 to determine cavity-to-cavity coupling. Data like that in Figure 3-9 are available for CW excitation of all aircraft cavity pairs for the frequency span 0.1 to 6 GHz.

Figure 3-10 shows the received power in the cockpit for swept frequency, 50-MHz BW, BLWGN excitation in the passenger cabin. The frequency span is 0.2 to 1 GHz. The TX and RX antennas were both log periodic. These data would be combined with PD data described in Section 3.3 to determine cavity-to-cavity coupling. Data like that in Figure 3-10 are available for BLWGN excitation for all cavity pairs, the frequency span 0.2 to 6 GHz, and the three noise BWs.

3.7 SHIELDING EFFECTIVENESS

The ambient EME provided one source of aircraft excitation for SE measurements. Useable signals were available in the FM (88 to 108 MHz) and VHF/UHF (0.1 to 1 GHz) bands. Typical ambient EMEs external to the aircraft for the FM and VHF/UHF bands are shown in Figures 3-11 and 3-12, respectively. The reference for the ambient SE was obtained from an RX antenna located 100 ft from the nose of the aircraft at cockpit height. Both horizontal and vertical polarizations were obtained for the reference measurements. Data were collected using a pair of monopole antennas and a pair of log periodic antennas.

Typical measurements of the received power in these same bands in the cockpit are shown in Figures 3-13 and 3-14. Data were collected with an antenna located in several locations within the cockpit. Data were obtained with and without mechanical mode-mixing.

Figure 3-15 shows a typical configuration of the external log periodic RX antenna with respect to the aircraft. Note the mountains near the right edge of the photo. Most of the FM and TV transmitters are located on the mountains about 10 miles from the aircraft. The aircraft is oriented approximately 135° to these transmitter locations. Data were collected for only one orientation of

the aircraft because of both test time constraints and intermittent wet ground conditions, which would have permitted aircraft movement only at specific times during the test.

The aircraft was externally excited with both horizontal and vertical polarizations from three positions—0°, 45°, and 90° off the nose on the copilot's side—using both BLWGN and repetitive short pulse excitation.

Figure 3-16 shows a data trace for the cockpit response to vertical-polarization, 0°, BLWGN excitation from 0.2 to 1 GHz at 50-MHz BW. The data in Figure 3-16 are the ratio of the received power in the cockpit to the reference received power external to the aircraft. Thus these data show the inverse of the SE. For each of the three external positions and two polarizations, the received power at four positions in each cavity was monitored. The available SE data are summarized in Table 3-1.

Figure 3-17 shows a data trace for the passenger cabin response to horizontal-polarization, 90°, short pulse excitation. To obtain the aircraft SE, these data require correction for the reference signal and a transform to frequency domain. For this TX antenna configuration, the internal passenger cabin response was measured for seven positions of the mechanical tuner to determine the response variation. For all other TX antenna configurations, only one cavity response was measured. Shielding effectiveness data from short pulse excitation are available for the cockpit and passenger cabin for three external antenna positions and two polarizations.

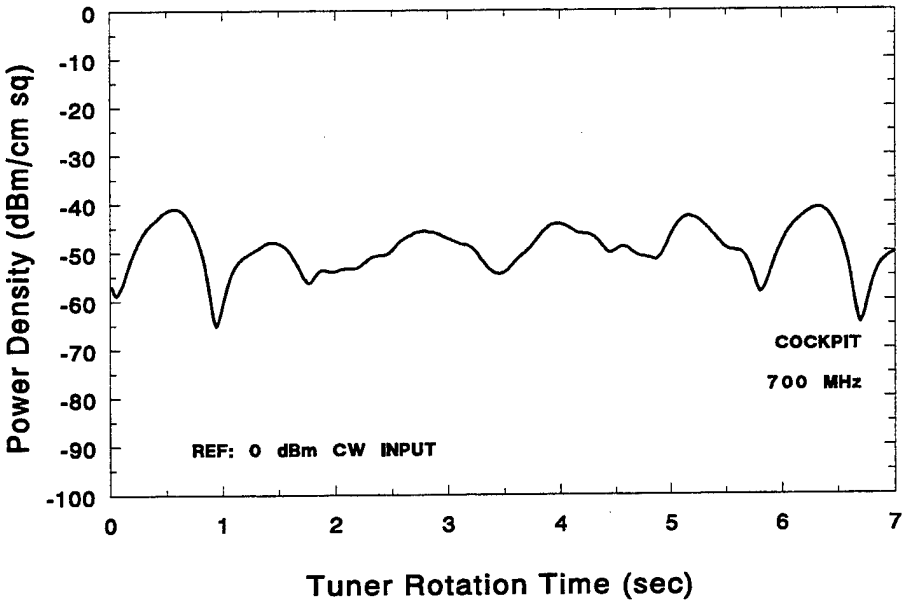

FIGURE 3-1. RECEIVED POWER IN COCKPIT AT DISCRETE FREQUENCY OF 700 MHz

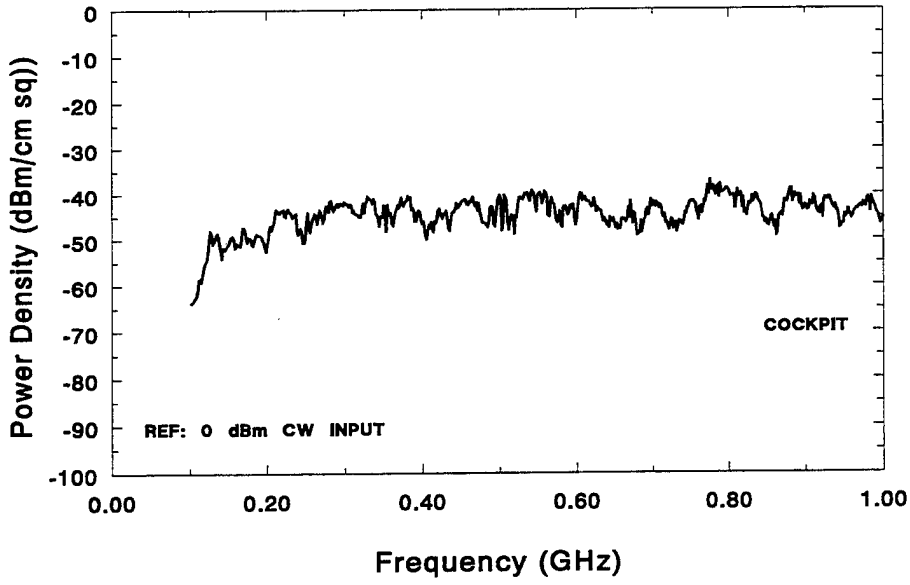

FIGURE 3-2. POWER DENSITY IN COCKPIT OVER 0.1 – 1 GHz FOR CW EXCITATION

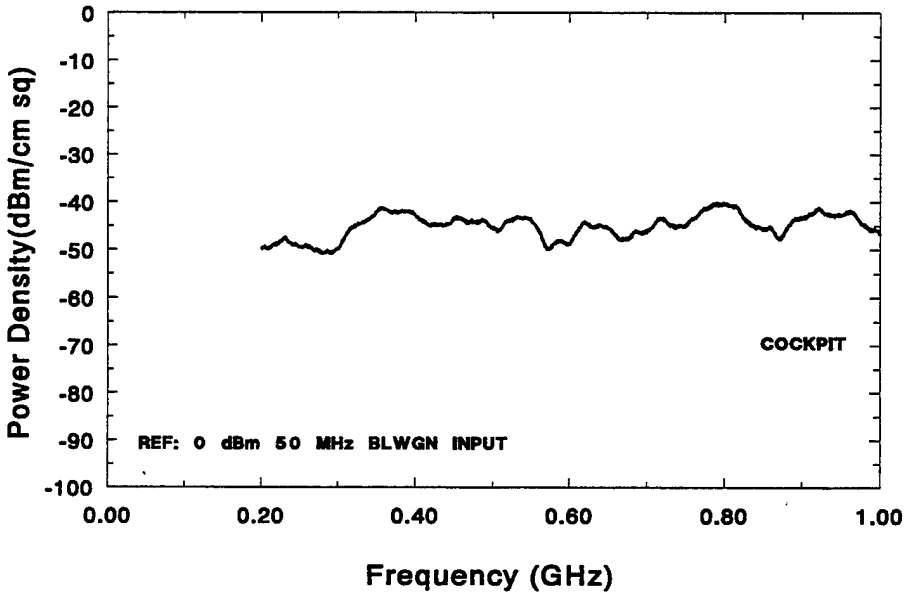

FIGURE 3-3. POWER DENSITY IN COCKPIT OVER 0.1 – 1 GHz FOR 50-MHz BW BLWGN EXCITATION

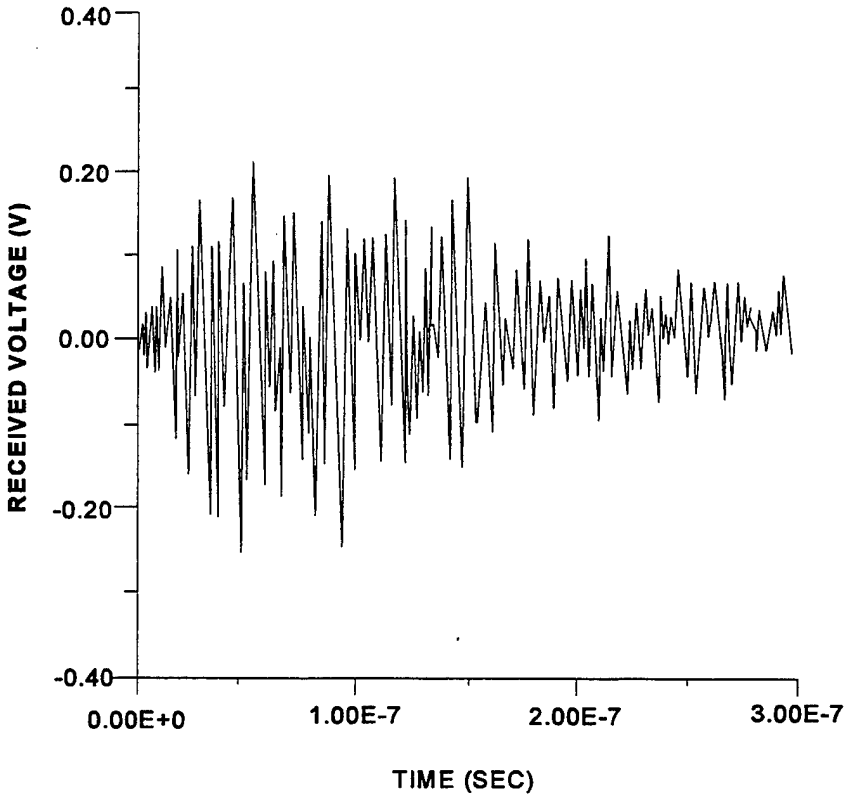

FIGURE 3-4. TIME DOMAIN PULSE DECAY RESPONSE IN PASSENGER CABIN

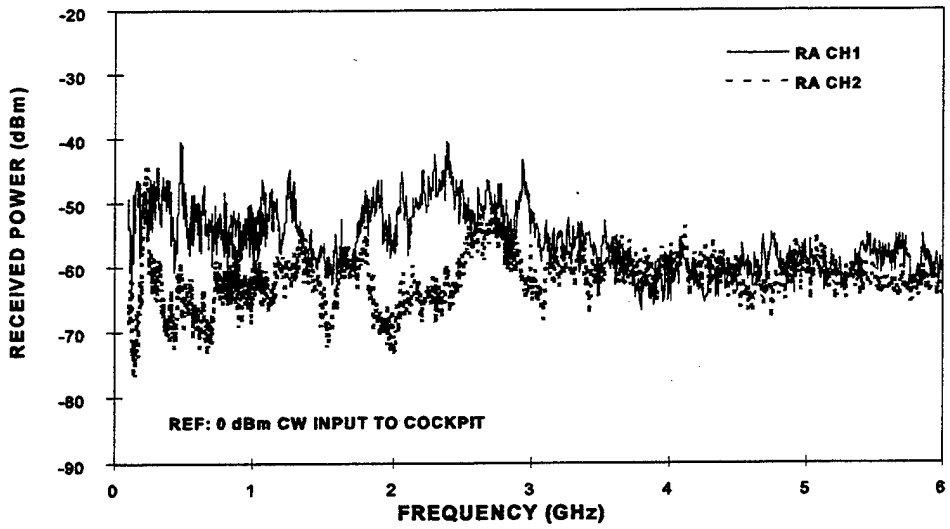

FIGURE 3-5. RESPONSE OF RADAR ALTIMETER FOR CW EXCITATION IN COCKPIT

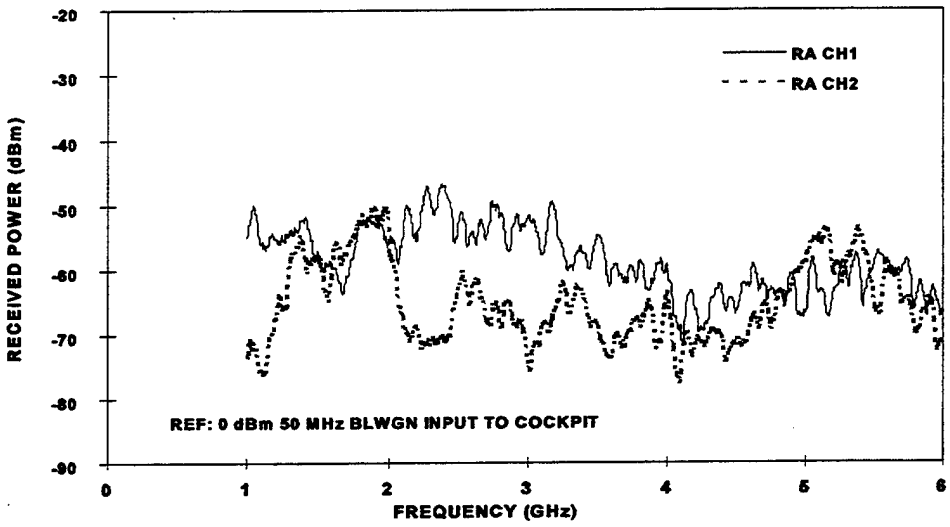

FIGURE 3-6. RESPONSE OF RADAR ALTIMETER FOR 50-MHz BW BLWGN EXCITATION IN COCKPIT

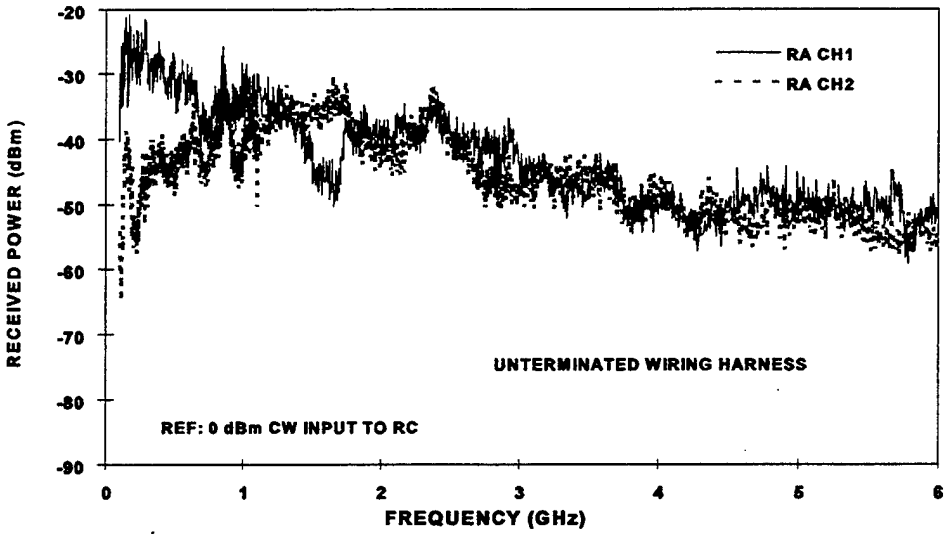

FIGURE 3-7. RESPONSE OF RADAR ALTIMETER FOR CW EXCITATION IN NSWCDD REVERBERATION CHAMBER

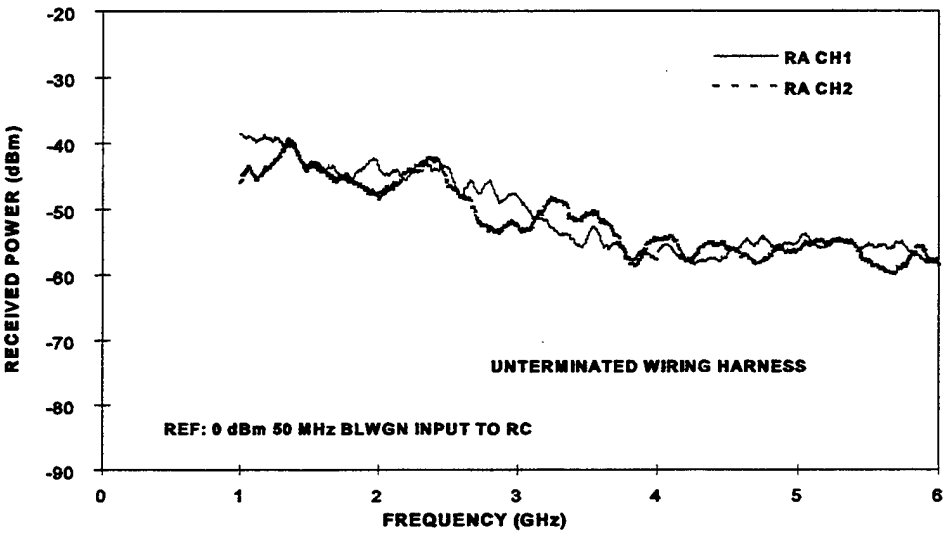

FIGURE 3-8. RESPONSE OF RADAR ALTIMETER FOR BLWGN EXCITATION IN NSWCDD REVERBERATION CHAMBER

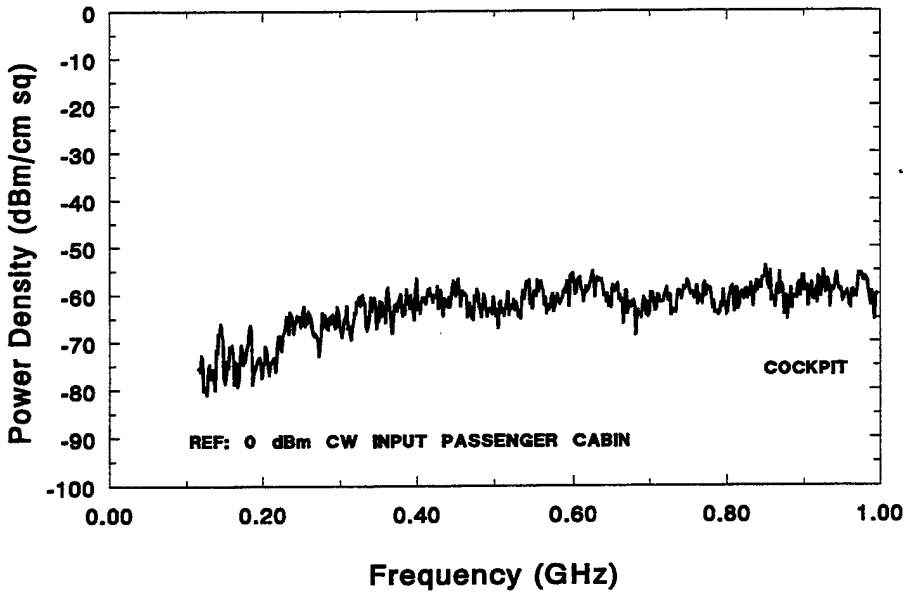

FIGURE 3-9. POWER DENSITY IN COCKPIT OVER 0.1 – 1 GHz FOR CW EXCITATION OF PASSENGER CABIN

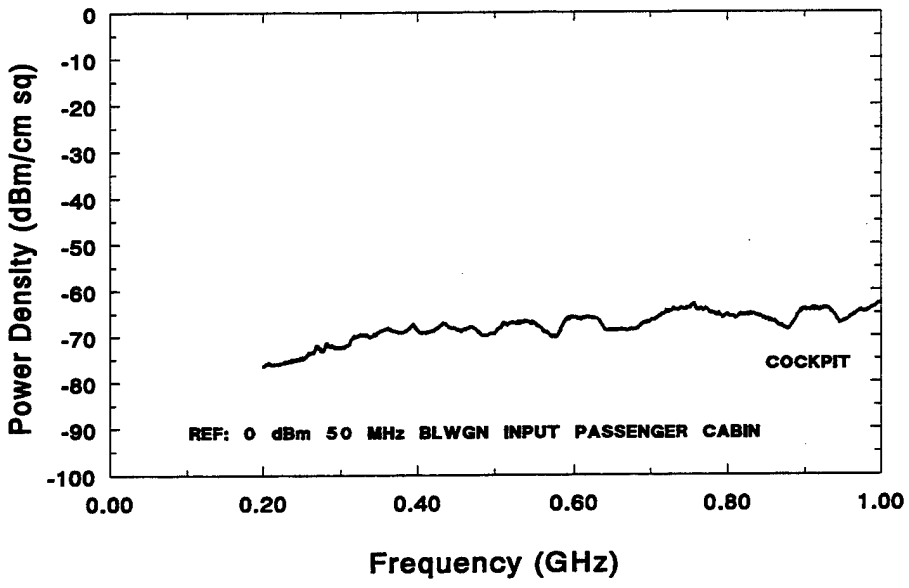

FIGURE 3-10. POWER DENSITY IN COCKPIT OVER 0.2 – 1 GHz FOR 50-MHz BW BLWGN EXCITATION OF PASSENGER CABIN

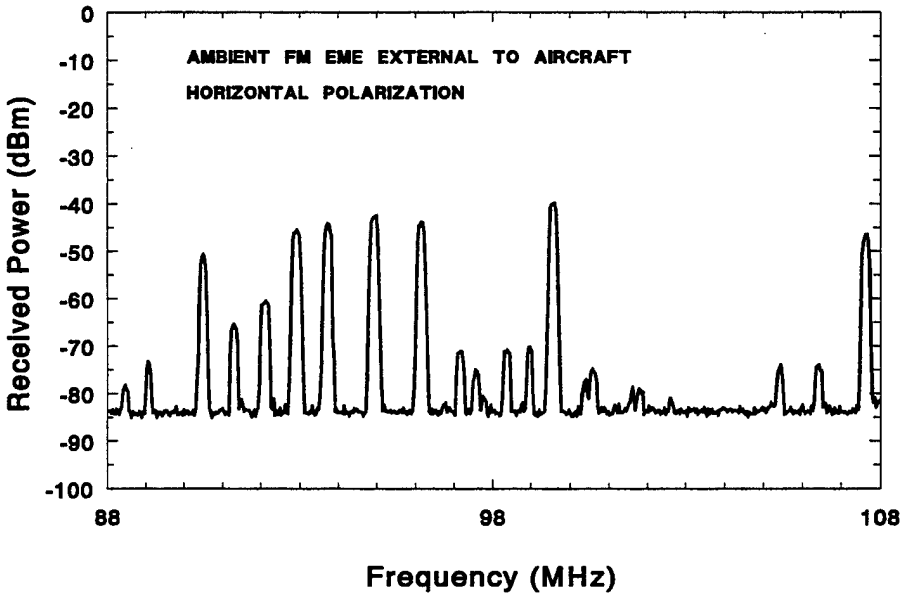

FIGURE 3-11. TYPICAL HORIZONTALLY POLARIZED AMBIENT FM BAND ELECTROMAGNETIC ENVIRONMENT EXTERNAL TO AIRCRAFT

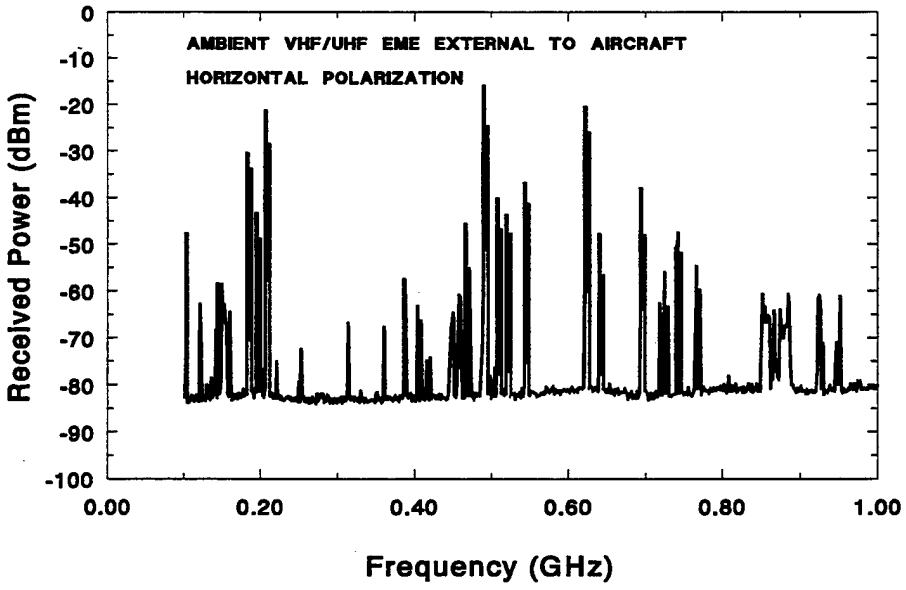

FIGURE 3-12. TYPICAL HORIZONTALLY POLARIZED AMBIENT VHF/UHF BAND ELECTROMAGNETIC ENVIRONMENT EXTERNAL TO AIRCRAFT

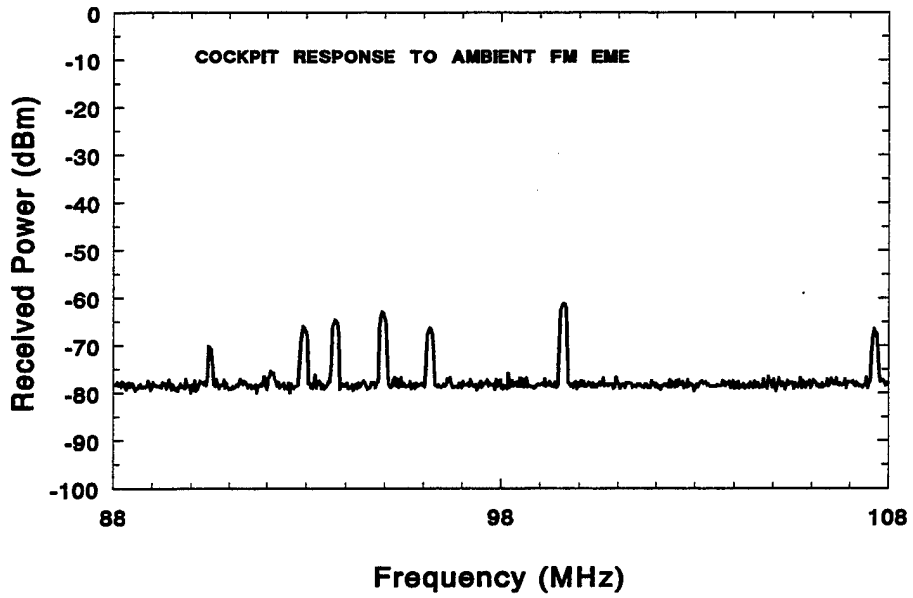

FIGURE 3-13. TYPICAL COCKPIT ELECTROMAGNETIC ENVIRONMENT FOR AMBIENT FM BAND

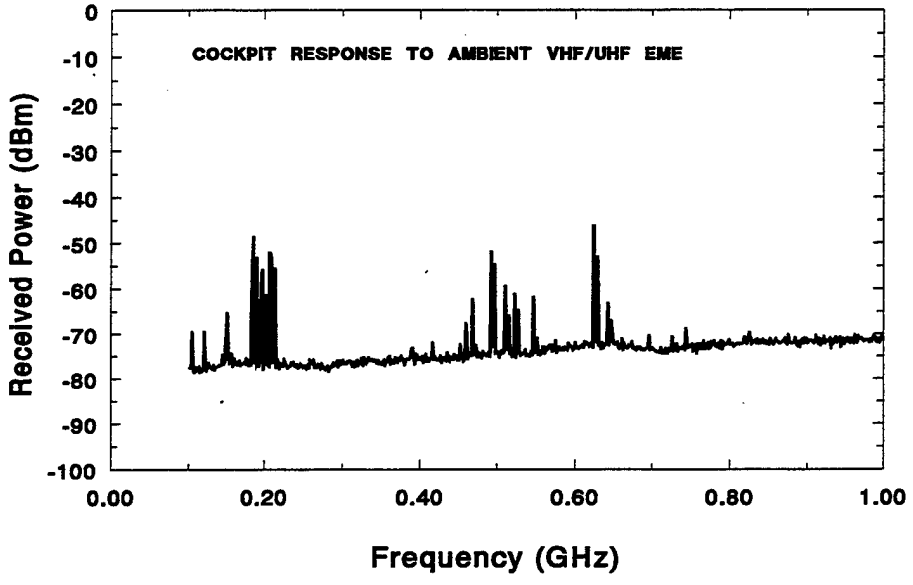

FIGURE 3-14. TYPICAL COCKPIT ELECTROMAGNETIC ENVIRONMENT FOR AMBIENT VHF/UHF BAND

FIGURE 3-15. LOCATION OF REFERENCE ANTENNA FOR AMBIENT ELECTROMAGNETIC ENVIRONMENT MEASUREMENTS

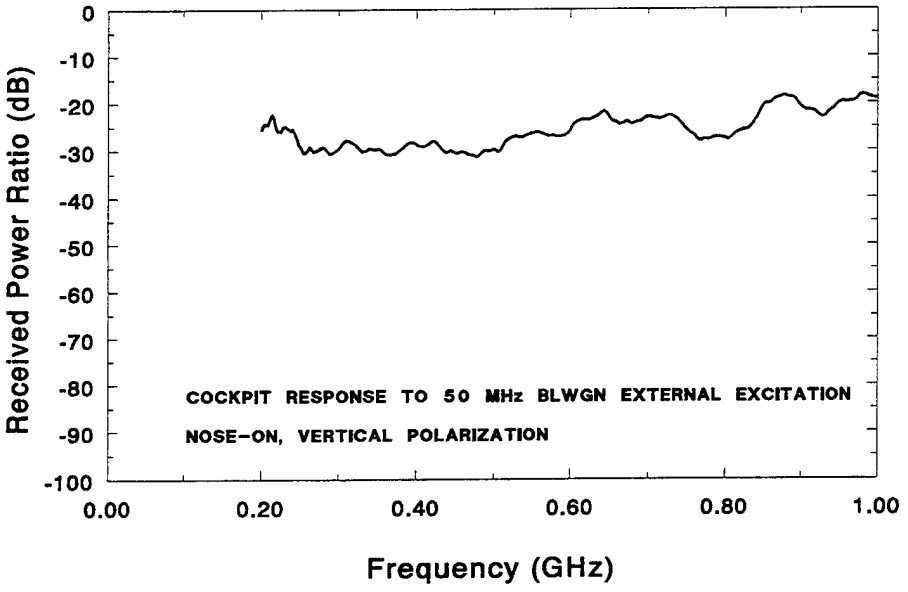

FIGURE 3-16. TYPICAL COCKPIT ELECTROMAGNETIC ENVIRONMENT FOR NOSE-ON, VERTICALLY POLARIZED 50-MHz BW BLWGN EXCITATION

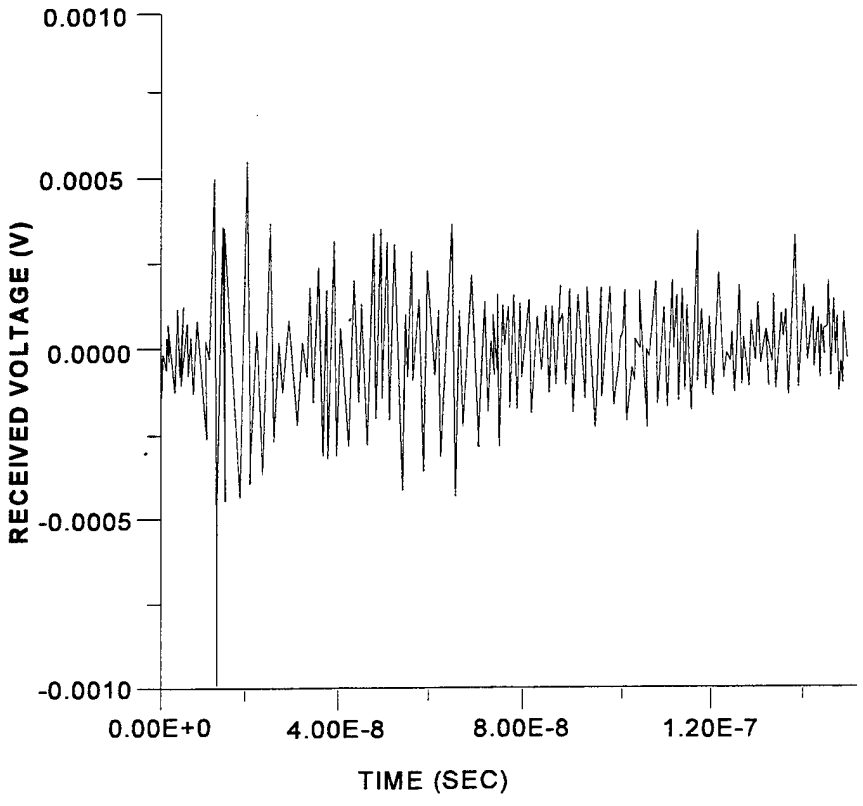

FIGURE 3-17. TIME DOMAIN RESPONSE IN PASSENGER CABIN FOR 90°, HORIZONTALLY POLARIZED, EXTERNAL SHORT PULSE EXCITATION

TABLE 3-1. TYPES OF DATA AVAILABLE

	EXCITATION TECHNIQUE				
DATA TYPE	AMBIENT EME	CW	BLWGN	TIME DOMAIN	REV. CHAMBER
MODE-MIXING EFFECTIVENESS					
COCKPIT		X			
AVIONICS BAY		X			
PASSENGER CABIN		X			
CAVITY POWER DENSITY					
COCKPIT		X	X		
AVIONICS BAY		X	X		
PASSENGER CABIN		X	X		
CAVITY DECAY TIME					
COCKPIT			X	X	
AVIONICS BAY			X		
PASSENGER CABIN			X	X	
AVIONICS/CTA RESPONSES					
RADAR ALTIMETER		X	X		X
FLIGHT DIRECTOR		X	X		X
DIRECTIONAL GYRO		X	X		X
AUTOPILOT		X	X		X
AUTOMATIC DIRECTION FINDER		X	X		X
CTA		X	X		X
CAVITY-TO-CAVITY COUPLING					
COCKPIT TO AVIONICS BAY		X	X		
COCKPIT TO PASSENGER CABIN			X		
AVIONICS BAY TO COCKPIT		X	X		
AVIONICS BAY TO PASSENGER CABIN			X		
PASSENGER CABIN TO COCKPIT		X	X		
PASSENGER CABIN TO AVIONICS BAY		X	X		
SHIELDING EFFECTIVENESS					
COCKPIT	X		V/H[1]	V/H	
AVIONICS BAY			V/H		
PASSENGER CABIN			V/H	V/H	

[1] NOTE: V/H Indicates Vertical and Horizontal Polarization

TABLE 3-2. CAVITY DECAY TIMES MEASURED USING BLWGN EXCITATION

FREQUENCY(GHz)	COCKPIT DECAY TIME (ns)	AVIONICS BAY DECAY TIME (ns)	PASSENGER CABIN DECAY TIME (ns)
0.2	87	60	113
0.4	52	22	164
0.6	30	37	104
0.8	32	65	115
1.0	40	53	130
1.2	38	44	139
1.4	53	64	118
1.6	36	35	148
1.8	35	51	162
2.0	19	46	109
2.2	41	59	133
2.4	49	75	110
2.6	51	66	141
2.8	52	64	116
3.0	54	56	91
3.2	37	33	137
3.4	35	59	130
3.6	76	64	91
3.8	60	44	130
4.0	32	74	113
4.2	65	63	100
4.4	63	79	96
4.6	38	55	126
4.8	36	60	100
5.0	49	64	125
5.2	57	67	119
5.4	67	58	69
5.6	47	34	101
5.8	60	49	119
6.0	58	65	136

TABLE 3-3. CAVITY DECAY TIMES MEASURED USING SHORT PULSE EXCITATION

FREQUENCY (GHz)	COCKPIT DECAY TIME (ns)	PASSENGER CABIN DECAY TIME (ns)
0.10	21.17	77.02
0.12	21.79	73.74
0.14	21.6	76.84
0.16	20.69	76.97
0.18	20.23	75.96
0.20	14.78	69.38
0.22	19.87	76.87
0.24	20.32	67.08
0.26	20.23	68.33
0.28	22.4	70.66
0.30	23.83	71.53
0.32	25.59	58.69
0.34	24.8	57.28
0.36	24.43	54.04
0.38	23.47	54.65
0.40	23.18	53.35
0.42	21.82	55.41
0.44	21.81	51.51
0.46	23.32	48.45
0.48	22.18	46.24
0.50	20.12	48.06
0.52	20.93	50.15
0.54	23.42	53.82
0.56	22.62	62.0
0.58	23.08	62.3
0.60	23.78	59.7
0.62	23.32	50.76
0.64	20.04	56.65
0.66	21.1	56.42
0.68	21.59	55.1

TABLE 3-3. CAVITY DECAY TIMES MEASURED USING SHORT PULSE EXCITATION (Continued)

FREQUENCY (GHz)	COCKPIT DECAY TIME (ns)	PASSENGER CABIN DECAY TIME (ns)
0.70	20.4	53.44
0.72	21.43	49.5
0.74	22.95	50.56
0.76	19.73	51.68
0.78	19.99	52.15
0.80	20.62	56.18
0.82	20.74	57.67
0.84	20.47	58.6
0.86	23.42	56.26
0.88	21.91	55.95
0.90	24.13	57.95
0.92	23.76	59.92
0.94	24.0	58.06
0.96	22.94	58.59
1.00	20.56	58.25

4.0 ANALYSIS OF DATA

For each parameter investigated, this chapter describes the analysis procedure for the pertinent data and discusses the results.

Section 4.1 covers the cavity characteristics, which depend strongly on the mode density and the effectiveness of the mode-mixing technique employed. An estimate of the theoretical mode density is given along with a calculation of the "effective" mode density. The effectiveness of mechanical mode-mixing in the three cavities is discussed. The analysis techniques and the power density and Q are presented for the aircraft cavities as measured by the three excitation techniques. The uniformity of the cavity EME is the final cavity characteristic covered.

Section 4.2 covers cavity-to-cavity coupling as determined by CW and BLWGN excitation. Section 4.3 discusses the analysis techniques for the responses of the RA and the CTA as obtained with both CW and BLWGN excitations. The section also covers the responses of these same systems in the NSWCDD reverberation chamber. Section 4.4 presents the aircraft shielding effectiveness, as measured using the ambient EME in the FM and VHF/UHF bands, and direct excitation with BLWGN and short-pulse, time domain techniques.

4.1 CAVITY CHARACTERISTICS

The EME in an aircraft cavity depends on many variables. The first consideration is the method of excitation. For external excitation, the internal cavity EME will depend on the external field strength, the aspect angle, the polarization, and whether the source provides plane wave or spot illumination. For internal excitation, the cavity EME will depend on the field strength, emitter location, orientation, and polarization. For both excitation possibilities, the EME will also vary with location within the cavity.

A second consideration is the character of the cavity itself. Most aircraft cavities are complex, and above some minimum frequency, will have a modal structure that depends on the cavity geometry. These factors indicate that intrinsically, above some frequency, an aircraft cavity EME must be described in terms of statistical rather than discrete parameters.

Section 4.1.1 discusses the cavity mode structure, which plays an important role in determining the characteristics of the cavity EME. For sufficient mode density and mode-mixing, theory predicts a specific statistical distribution for the cavity EME. Theory also predicts that all complex cavities with sufficient mode density and adequate mode-mixing are statistically equivalent.

Section 4.1.2 covers the effectiveness of the mechanical mode-mixing. The distribution of the measured cavity EME using mechanical mode-mixing is compared to the theoretical distribution.

Aircraft cavities will be lossy depending on the absorbers present within the cavity and the leakage out of the cavity. Section 4.1.3 covers measurements that indicate the power density in a cavity referenced to 1 mW (0 dBm) of input power.

Section 4.1.4 covers the cavity Q as determined by several techniques. The uniformity of the cavity EME also depends on the mode density and the effectiveness of mode-mixing. Section 4.1.5 describes the field uniformity measured in the aircraft cavities.

4.1.1 Mode Density

The statistical behavior of the aircraft cavity EME at a particular frequency depends on the effective mode density and the adequacy of the mode-mixing technique. Several expressions are available to estimate the number of modes in a cavity.[1] For the purposes of this analysis, the theoretical number of modes can be estimated from

$$N(f) \approx (8\pi/3c^3)\, V\, f^3 \tag{4.1}$$

where c = the speed of light
V = the cavity volume
f = the frequency

The volumes of the aircraft cavities are difficult to determine because of the internal metallic structures as well as the curvature of the cavity exteriors. However, an estimate of the B-707 cavities can be made based on the exterior dimensions of the cockpit, avionics bay, and passenger cabin. Figure 4-1 shows the estimated number of modes in the B-707 cavities. Previous work[1] indicated that for effective mode-mixing using mechanical techniques in a high Q reverberation chamber, a minimum of 60 modes are required. Using this guideline, the smallest cavity, the cockpit, would have a sufficient number of modes above 300 MHz.

Perhaps of more interest is the mode density, which indicates the number of modes accessible by the BW characteristics of the mode-mixing technique used. The greater the number of effective modes that can be excited, the closer the EME should be to the theoretical distribution and the better the field uniformity should be within the cavity. The theoretical mode density can be estimated by the differential of Equation (4.1), or

$$MD_t(f) = dN(f) \approx (8\pi/c^3)\, V\, f^2\, df \tag{4.2}$$

where df is the bandwidth attributed to the mode-mixing technique. The estimated mode density for the B-707 cockpit is shown in Figure 4-2 for several mode-mixing bandwidths.

As a reference, at the lowest suggested operating frequency for the NIST reverberation chamber, the theoretical mode density for a 1-MHz BW is less than ten. Using the theoretical mode

density from Figure 4-2, the NIST data suggest that a noise BW of 50 MHz should provide adequate mode-mixing over the entire frequency range tested, and that a 1-MHz BW should be adequate above 1 GHz for all the aircraft cavities. However, in practice, each resonant mode of the aircraft cavities has a bandwidth, BW_Q, associated with it that is related to the cavity Q and its center frequency, f:

$$BW_Q = f/Q \tag{4.3}$$

If BW_Q becomes as large as, or larger than, the spacing between the resonant modes, the modes will overlap, causing more than one mode to be excited by a single frequency. Thus, to excite a completely independent set of modes, the frequency must be changed by at least one BW_Q. This has the overall effect of reducing the total number of modes available in a given mode-mixing BW. Hence, the total number, N_Q, of independent modes in a given bandwidth, BW, is:

$$N_Q = MD_Q * BW = BW/BW_Q \tag{4.4}$$

Thus, the **effective** cavity mode density, MD_{eff}, can be defined as

$$MD_{eff} = \min(MD_Q, MD_t) \tag{4.5}$$

The BW_Q can be calculated for select frequencies from the Q data derived from BLWGN measurements to be presented in Section 4.1.4.3 for each cavity. Table 4-1 shows the calculated BW_Q for the three cavities.

Table 4-1 indicates no values of BW_Q less than 2 MHz. This implies that 2 MHz of noise BW for BLWGN excitation will not provide effective mode-mixing in the aircraft cavities at any frequency. The mode density, MD_Q, calculated from Equation (4.3) and the data in Table 4-1 is shown in Table 4-2. A zero indicates that the noise bandwidth is less than the BW_Q. As can be seen in Table 4-2, the effective mode densities in the aircraft cavities are not very high even at 50 MHz of noise BW.

4.1.2 Mode-mixing Effectiveness

A qualitative measure of the effectiveness of the randomization of the EME in a cavity due to mechanical mode-mixing is the observed stirring ratio. The SR is defined as the maximum received power to the minimum received power (or the noise floor, whichever is highest) for discrete frequency measurements over a complete rotation of the tuner.

Although many factors will influence the SR, substantial contributors are the enclosure Q, the number of available cavity modes, and the tuner effectiveness. A SR of a least 20 dB is an empirical guideline,[1] which implies sufficient mode-mixing to assure that the field spatial uniformity and peak-to-average values are consistent with the expected characteristics of a high-Q reverberation chamber.

Substantial data were collected in Phase I to characterize the randomization of the EME in low-Q aircraft cavities. A general observation from that data was that mode-mixing, based on the 20-dB guideline, was limited below about 800 MHz for both the cockpit and the avionics bay. Since for both cavities, there are sufficient modes at much lower frequencies, the Phase I report suggested that tuner size and symmetry may have contributed to the 800-MHz limitation on the effectiveness of mode-mixing. In Phase II, the maximum dimension and the total area of the cockpit tuner was two and three times that of the respective parameters of the Phase I tuner. In addition, the Phase II tuner was oriented such that all cavity surfaces could contribute to the mode-mixing.

Figure 4-3 shows a 17-dB SR at 100 MHz in the cockpit. While these data show the improved performance of the tuner, the data also suggest that there are insufficient cavity modes for proper EME randomization at 100 MHz. Equation (4.1) indicates only two modes available in the cockpit at 100 MHz.

As shown in Figure 4-1, by 300 MHz, the number of modes in a rectangular cavity of the same volume as the cockpit exceeds the guideline of a minimum of 60 modes[1] for the proper operation of a high-Q reverberation chamber. Figure 4-4 shows the discrete frequency data for 400 MHz in the cockpit. The SR is 21 dB. Figure 4-5 shows a summary of the cockpit SR data from both the Phase I and Phase II tests. The Phase II data show that the lower limit on consistent SRs above 20 dB is 400 MHz.

A more robust evaluation of the effectiveness of mode-mixing is to compare the observed distribution of the power density with the theoretical distribution for a complex cavity with sufficient mode density and adequate mode-mixing.[6] The expected distribution for the power density is chi-square with 6-degrees-of-freedom distribution. This distribution represents an isotropic, randomly polarized cavity EME. The distribution is characterized by the mean.

The experimental data were obtained by sampling the aircraft cavity with directional, polarized antennas. For frequencies of 1 GHz and below, in-band log periodic antennas were used. For frequencies of 1 GHz and above, wide-band, dual-ridged horn antennas were used. These antennas sample two of the six random field variables. As a result, the experimental data should be distributed as a chi-square with 2-degrees-of-freedom distribution.

Figure 4-6 shows the cumulative distribution of the 400 MHz, received power cockpit data from Figure 4-4. Also plotted in Figure 4-6 is a chi-square distribution with 2 degrees of freedom. The data are not a good match to the theoretical distribution.

Additional cockpit SR data were analyzed to determine the minimum frequency at which the measured cavity EME essentially matched the expected distribution. Figure 4-7 shows the cumulative distribution for the cockpit at 700 MHz. In this case, the agreement between the measured data and theory appears reasonable. In summary, while the SR exceeded the 20 dB guideline above 400 MHz, the more rigorous comparison indicates that the cockpit EME does not closely approximate an isotropic, randomly polarized EME until about 700 MHz. With the Phase I tuner, the lowest frequency for which the experimental results were a reasonable match to the theoretical distribution was about 1 GHz for the cockpit. These data indicate the impact of tuner effectiveness on the observed cavity EME.

The Phase II mode-mixing effectiveness in the avionics bay did not show the improvement noted in the cockpit. The Phase II tuner was somewhat larger than the Phase I tuner but was limited by the space available for rotation. Being larger, the Phase II tuner was closer to metallic structures than the recommended distance of one wavelength at the lowest useable frequency.

Another potential problem was the size of the log periodic TX and RX antennas used for Phase II measurements below 1 GHz. It was difficult to find locations for the TX and RX antennas that provided adequate separation from metal surfaces while avoiding line-of-sight between the antennas. While measurements were performed with log periodic antennas in the avionics bay, these data require additional detailed analysis and interpretation and will not be covered in this report. In Phase I, short-wire antennas were used for measurements below 1 GHz with considerably less positioning problems.

The available data for the avionics bay show SRs greater than 20 dB above 900 MHz. Figure 4-8 shows the cumulative distribution for the avionics bay at 1 GHz. The agreement between the measured and theoretical distributions is not as good as in the cockpit. This disparity indicates that the avionics bay tuner provided less effective mode-mixing than the other tuners. However, note that the theoretical distribution bounds the measured data for PDs greater than the mean. This is common for the data analyzed.

Only limited SR data were collected for the passenger cabin in Phase II, and no SR data were collected in the cabin during Phase I. Figure 4-9 shows a SR of 30 dB at 500 MHz for the passenger cabin. As shown in Figure 4-10, cabin SRs are consistently greater than 20 dB above 500 MHz for the limited data set.

The 500 MHz data does not show good agreement with the desired cavity EME power density distribution. However, Figure 4-11 shows that at 1 GHz, the passenger cabin EME is in excellent agreement with the theoretical distribution.

In summary, if a sufficiently large tuner can be used in aircraft cavities, mode-mixing can be achieved that will result in an isotropic and randomly polarized cavity EME. Further, at values above the mean, the theoretical distribution function bounds the normalized power density that can be achieved at a given spatial location in the cavity as the excitation conditions vary.

4.1.3 Normalized Power Density

The aircraft cavity losses are characterized by the normalized PD as defined in Section 3.3.

4.1.3.1 Power Density From Swept Frequency Continuous Wave Excitation. Figure 4-12 shows the PD for the cockpit for CW excitation and mechanical mode-mixing. If a sufficiently large sample of boundary conditions (e.g., tuner positions) were obtained at each frequency, the swept frequency CW measurement would yield the peak PD of the EME distribution discussed in Section 4.1.2. In this test, the allocated time for swept frequency measurements was less than that necessary to assure the peak of the distribution was sampled. Therefore, the swept frequency PD should be between the mean and the peak of the distribution. Discrete frequency data yield a good estimate

of the peak value of the distribution. Figure 4-13 shows discrete frequency and swept frequency PD data for the same TX/RX antenna configurations and instrumentation for the frequency interval 0.1 to 6 GHz. In every case, the swept frequency data are equal to or less than the discrete frequency data. Fifteen discrete frequency data points are available to correlate with the swept frequency data. The swept frequency data are within 1 dB of the discrete frequency data for six of the samples. A maximum difference of about 3 dB was observed for four samples. The data suggest that within a few decibels, the swept frequency data approximate the peak values of the EME distribution.

For comparison with the data from Figure 4-12, the cockpit PD measured with horn antennas in the Phase I test is shown in Figure 4-14 for the frequency range 1 to 2.9 GHz. There is good agreement between these PD measurements made two years apart. These data demonstrate the repeatability of aircraft cavity EME measurements using this technique.

The normalized PD in the cockpit is essentially independent of frequency over the frequency interval 0.5 to 6 GHz and has an average value of about - 45 dBm/cm^2 (reference 0 dBm input). The magnitude of the normalized PD is bounded by - 40 dBm/cm^2.

Figure 4-15 shows the PD for the avionics bay. The normalized PD in the avionics bay is essentially independent of frequency over the frequency interval 1 to 6 GHz, with an average value of about -50 dBm/cm^2 and a bounding magnitude of about -45 dBm/cm^2. The avionics bay normalized PD is about 5 dB less than the cockpit PD, which is consistent with the Phase I results.

Figure 4-16 shows the PD for the passenger cabin. Note that for the passenger cabin, only data from 0.1 to 2.9 GHz are available for CW excitation. The passenger cabin showed an offset of about 5 dB in the data above and below 1 GHz as the TX/RX antennas were changed. The placement constraints associated with the avionics bay were not present in the passenger cabin. There are insufficient CW data available to resolve whether this is a measurement artifact or an actual cavity characteristic.

The average PD in the passenger cabin is about -52 dBm/cm^2 with a bounding value of -45 dBm/cm^2. The average loss in the passenger cabin is a few decibels more than in the avionics bay above 1 GHz. No passenger cabin data are available from Phase I.

The passenger cabin shows an increased loss at about 1.8 GHz. The large number of windows in the passenger cabin (98) would suggest a significant loss mechanism, which would have a frequency dependence. However, their 10 × 13 in. dimension does not appear to correlate with any structure in the power density trace of Figure 4-16.

In summary, it is interesting to note two characteristics of the aircraft cavity EME. The first is the frequency-dependent, fine structure with variations up to 10 dB common to all of the data. Data samples were obtained for frequency steps of 1.5, 3.5, and 5.5 MHz for the frequency bands 0.1 to 1, 0.8 to 2.9, and 2.75 to 6 GHz, respectively. The second observation is that the average PD, and hence the cavity losses for the three cavities, vary by only about 5 dB over the frequency interval 1 to 6 GHz.

4.1.3.2 Power Density From Band-Limited White Gaussian Noise Excitation. Three noise BWs, 2, 10, and 50 MHz, were investigated in this test. Figures 4-17, 4-18, and 4-19 show data traces for the PD in the cockpit for 2, 10, and 50 MHz noise BWs for the frequency band 0.2 to 1 GHz. Note the significant structure in the 2-MHz BW data. The structure is less at 10 MHz and is a minimum at 50-MHz BW. These results are expected based on the discussion of the effective mode density in Section 4.1.1. As is evident from the data in Table 4-2, the 2- and 10-MHz BWs do not provide adequate mode excitation in the cockpit.

As noted in Section 3.3, in most cases, BLWGN data were obtained for four different RX antenna configurations for a given TX location. Figure 4-20 shows the averages of the four measurements for each of the three BWs for 0.2 to 1 GHz in the cockpit. Except for the structure in the 2- and 10-MHz data, all three average values track within a decibel.

In most cases, only 50-MHz BW data will be considered in the remainder of this report.

The four-run average PD using 50-MHz BW for each of the three aircraft cavities is shown in Figures 4-21, 4-22, and 4-23. The average normalized PD in the cockpit varies by less than 5 dB over the frequency interval 0.2 to 6 GHz. The magnitude of the PD is bounded by -40 dBm/cm^2.

The average normalized PD in the avionics bay has a value of about -55 dBm/cm^2 and is essentially constant over the frequency interval 1 to 6 GHz. The PD is bounded by -52 dBm/cm^2.

In Figure 4-23, note the approximately 7 dB discontinuity at the 1 GHz band change. No explanation for this discontinuity has been identified. The average PD in the passenger cabin is about -60 dBm/cm^2 and changes by less than 5 dB over the frequency interval 1 to 6 GHz. The passenger cabin PD is bounded by -55 dBm/cm^2.

4.1.3.3 Comparison of Power Density Measurements. Prior to making direct comparisons of the PD data collected with CW and BLWGN excitation, it should be noted, as discussed in Section 3.3, that the measurements are intrinsically different. A single CW PD measurement resulted from exciting the cavity with a narrowband signal for a large number of different cavity configurations (e.g., different boundary conditions generated by the tuner). The CW PD approximates the peak PD in the cavity for a large number of possible configurations. A single BLWGN measurement resulted from randomly exciting the existing modes over the selected noise BW for a specific cavity configuration. Multiple BLWGN measurements involve different cavity configurations as well as different locations/orientations/polarizations of the RX antenna. The difference in the swept frequency PD data will be determined by the interplay of the cavity modal structure, the effectiveness of the mechanical mode-mixing, the sampling effectiveness of the swept CW measurement, the BLWGN BW, the uniformity of the cavity EME, and the peak and average characteristics of the two measurements. For most situations, the measurements from the two techniques are expected to agree over sufficiently large BWs within an uncertainty somewhat greater than the cavity uniformity.

The CW data generally show more frequency-dependent structure than the BLWGN data. An exception is the 2-MHz BW BLWGN data, which has structure comparable to the CW data. The cavity Q BWs shown in Table 4-1 indicate that even narrowband CW will excite modes over a BW comparable to the 2-MHz BW BLWGN.

To investigate the relationship between the CW data and the 50-MHz BW BLWGN data, a 50 MHz running average of the cockpit CW PD over the frequency band 0.1 to 1 GHz was calculated. The results are shown in Figure 4-24 coplotted with the BLWGN data from Figure 4-18. Above 0.3 GHz, the traces are within 3 dB.

The PD data from CW excitation with mechanical mode-mixing are shown in Figures 4-12, 4-15, and 4-16 for the cockpit, avionics bay, and passenger cabin, respectively. Power density data for the average of four BLWGN data runs with 50-MHz BW are shown in Figures 4-21, 4-22, and 4-23.

The cockpit power density measured by the two techniques is the same within the measurement uncertainty of the two techniques.

For the avionics bay, the CW data (Figure 4-15) from a single measurement is approximately 7 dB greater than the four-measurement average of 50-MHz BW BLWGN data (Figure 4-22). The CW measurement lies outside the measurement uncertainty predicted for the BLWGN measurements. Since only a single swept CW measurement was available, no uncertainty bounds could be established for the swept CW Phase II data. However, data from three Phase I swept CW measurements were compared to the Phase II data. The Phase II data were 2 to 5 dB higher than the average of the three Phase I measurements. Since the standard deviation of the Phase I measurements was about 2 dB, the Phase II data were marginally within the measurement uncertainty. The Phase I average tends to be 1 to 3 dB higher than the BLWGN data, which is within the combined measurement uncertainties.

In summary, the analysis indicated that the Phase II CW and BLWGN PDs for the avionics bay are marginally within the uncertainties of the two measurement techniques when both Phase I and Phase II CW data are considered. In Section 4.4, there is a further discussion of the differences in avionics bay CW and BLWGN PD measurements.

For the passenger cabin, both techniques indicate a few-decibel offset between bands 1 and 2 (hereinafter referred to as "band 1/2"). Furthermore, this offset for both techniques is in the same direction. As indicated in Section 4.1.3.1, there was no difficulty locating the log periodic antennas away from metal structure in the passenger cabin. No explanation for this discontinuity has been identified.

The passenger cabin PD from the CW measurement is about 10 dB greater than the four-measurement average of 50-MHz BW BLWGN excitation data. This difference is outside the expected measurement uncertainty. No Phase I data are available for comparison.

Except for the 1.8-GHz structure in the passenger cabin data with CW excitation, above 1 GHz, the frequency dependence of the PD for each of the three cavities is essentially the same for the two methods of excitation.

4.1.4 Quality Factor

Another important cavity characteristic is how lossy the cavity is. This is typically described by the cavity quality factor, Q. The cavity Q is defined as:

$$Q = 2\pi(\text{time averaged energy stored at a resonant frequency})/(\text{the energy dissipated in one period of this frequency}) \quad (4.6)$$

Based on this definition, a Q_{decay} can be determined from a measurement of the 1/e decay time, τ, of the energy stored in a cavity[7]

$$Q_{decay} = 2\pi f \tau \quad (4.7)$$

As discussed in Section 3, the decay time was measured directly using a fast digital oscilloscope with BLWGN excitation. The Q_{decay} can also be calculated from decay time values derived from short pulse excitation.

A steady state cavity Q_{ss}, also derived from the definition, Equation (4.6), can be determined from[1]

$$Q_{ss} = (16\pi^2/c^3)\, V\, f^3\, (P_{rec}/P_{in}) \quad (4.8)$$

where V = cavity volume,
c = speed of light,
f = frequency, and
P_{rec}/P_{in} = ratio of the received power to the input power.

In terms of the normalized PD discussed in Section 4.1.3,

$$Q_{ss} = (2\pi/c)\, V\, f\, (PD/P_{in}) \quad (4.9)$$

The Q values obtained using these three techniques will be discussed below.

4.1.4.1 Decay-Time Quality Factor From Band-Limited White Gaussian Noise Excitation.

With BLWGN excitation of the cavity, the decay time was the measured 0.9 to 0.1 fall time of the ensemble average of a pulse. The ensemble average was obtained by averaging over a large number of individual pulse decay times. The decay times measured with 50-MHz BLWGN were given in Table 3-2 for the cockpit, avionics bay, and passenger cabin. The Q_{decay} values obtained from these data using Equation (4.7) are shown in Figure 4-25. Note the general frequency-dependence in the data. Note also the variability in the data points. The variability between data points and the general frequency-dependent trend is approximately 25 percent (~ 1 dB).

The cockpit Q increases from less than 50 at 0.2 GHz to approximately 1000 at 6 GHz. The avionics bay Q values have the same frequency-dependence as the cockpit Q and are slightly higher in magnitude.

The Q for the passenger cabin varies from about 100 at 0.2 GHz to about 2000 at 6 GHz. The passenger cabin Q relative to the other two cavities is surprisingly high, based on the many potential loss mechanisms in the cabin. These include 98 windows, four large doors without EM seals, a quantity of absorbing material, and the leakage access to the cargo compartment and the avionics bay. The volume of the cabin is much greater than either of the other two cavities and appears to be the dominant factor in determining the Q. To verify this proposition, the volume normalized Q is shown in Figure 4-26. These data imply larger loss mechanisms in the cabin than in the other two cavities.

4.1.4.2 Decay-Time Quality Factor From Short Pulse Excitation. Time decay measurements were obtained in the cockpit and passenger cabin using the setup and techniques described in Section 2.3.3. A typical time response for the cockpit is shown in Figure 4-27 and the passenger cabin in Figure 4-28. Note the similarity of the two waveforms. These waveforms were captured in 50-ns windows, progressing from the first response of the cabin at time t = 0, until t = 500 ns. The gradual decrease in the signal strength is apparent in the figures.

The received voltage waveform in each time window of the time-domain waveform was first transformed into the frequency domain using a standard fast Fourier transform (FFT) and then converted to power. If data were taken at various tuner positions, the data from each tuner position were averaged within each time window and at each frequency between 20 MHz and 1000 MHz.

Since the time window is 50 ns, the FFT calculates spectral data that is in reality an average over the minimum bandwidth of the FFT, which is 1/50 ns or 20 M. A decision can be made at this point whether to average several different frequency data or not. Averaging three adjoining frequency data points increases the bandwidth to 60 MHz; five data points result in averaging over 100 MHz. The wider the bandwidth, the smoother the change in power as a function of time, and therefore, the easier to determine a decay time for the energy. The analysis used three frequency data points, and therefore the Q values are an average over a 60-MHz BW.

At this point, there was one data point at each frequency in each time window. An exponential curve-fitting routine was applied to the data to determine the decay time, τ, according to the equation,

$$\text{Power}(t) = \text{Power}(\text{initial})\, e^{-t/\tau} \qquad (4.10)$$

All of the time windows were used to determine the decay time, so that there was additional averaging due to the curve-fitting algorithm. The resulting decay times were presented in Table 3-3.

Once the decay time was determined, the Q factor was calculated using Equation (4.7). Figure 4-29 shows the Q values for the cockpit and passenger cabin over the frequency range 0.1 to 1 GHz. Note the general frequency-dependence in the data. The variability between data points and the general frequency-dependent trend is about 20 percent.

In the cockpit, the Q values vary from a minimum of 13 at 0.1 GHz to a maximum of 142 at 0.94 GHz. In the passenger cabin, the Q values range from 48 at 0.1 GHz to a maximum of 366 at 1 GHz.

4.1.4.3 Steady-State Quality Factor From Continuous Wave Excitation. The PD data from CW excitation using mechanical mode-mixing for the cockpit, avionics bay, and passenger cabin, shown in Figures 4-12, 4-15, and 4-16 respectively, were used in Equation (4.9) to obtain the cavity Q_{ss}.

As mentioned in Section 3.3, a CW measurement approximates the peak PD for a large number of EM configurations of the aircraft cavities. Since Q values are typically based on average power measurements at steady state, the CW PD measurements should be adjusted to reflect average PD. The peak-to-average ratio for a specific frequency is available from mode-mixing data, as shown in Figure 4-4. However, measured values are not available for the swept frequency PD data of Figures 4-12, 4-15, and 4-16. The adjustment factor must therefore be an estimate of the actual peak-to-average ratio for each frequency. Based on the expected distribution of PD in mode-mixed data (see Section 4.1.2), nominal peak-to-average ratios are in the range of 6 to 8 dB.[1,4] For the Q calculations, a value of 7.5 dB was used to adjust the CW PD measurements.

The results are shown in Figures 4-30, 4-31, and 4-32. Note the frequency-dependence in the cavity Q_{ss} derived from the CW PD data.

The average cockpit Q_{ss} derived from CW excitation varies from less than 10 at 0.1 GHz to about 70 near 6 GHz. The average avionics bay Q_{ss} varies from less than 10 at 1 GHz to about 50 near 6 GHz. The average passenger cabin Q_{ss} varies from less than 10 to a high of about 200 over the frequency interval 0.1 to 2.9 GHz.

4.1.4.4 Steady-State Quality Factor From Band-Limited White Gaussian Noise Excitation. The PD data from 50-MHz BW BLWGN, shown in Figures 4-21, 4-22, and 4-23 for the cockpit, avionics bay, and passenger cabin respectively, were used in Equation (4.9) to obtain an estimate of the cavity Q_{ss}. The results are shown in Figures 4-33, 4-34, and 4-35. Note the relatively flat frequency-dependence above about 3 GHz for all the cavities.

The average cockpit Q_{ss} derived from the 50-MHz BW BLWGN excitation varies from about 30 at 0.2 GHz to about 220 at 6 GHz. The average Q_{ss} for the avionics bay varies from less than 10 at 0.2 GHz to about 45 at 6 GHz. The average passenger cabin Q_{ss} varies from less than 10 at 0.2 GHz to a high of about 175 near 6 GHz.

4.1.4.5 Comparison of Quality Factor Results. Comparisons of all the data are shown in Figures 4-36, 4-37, and 4-38 for the cockpit, avionics bay, and passenger cabin respectively. No short pulse data were collected in the avionics bay. The CW data in the passenger cabin were limited to 2.9 GHz.

The magnitude and general frequency-dependence of Q_{decay} from the two time-decay techniques are in good agreement.

In the cockpit, the Q_{ss} results for the two excitation techniques do not agree within the expected measurement uncertainties. For the avionics bay and passenger cabin, there is reasonably good agreement in Q_{ss} for CW and BLWGN excitation.

It is clear that Q_{ss} is quite different from Q_{decay}. Although the volumes of the cavities required in Equation (4.9) are not known with precision, they would have to be in error by considerably more than a factor of two to explain the difference in Q_{ss} and Q_{decay} magnitudes. An error of this magnitude is unlikely. As a check, using values of one standard deviation for the τ and PD measurements at 1 GHz for the cockpit, the required magnitude of the cockpit volume was derived. This value was not within the expected uncertainty based on the detailed measurements of the cockpit dimensions.

Further, the data indicate that no frequency-independent factor, such as the volume, could bring Q_{ss} into agreement with Q_{decay}. The frequency-dependence of the Q determined from the two techniques is substantially different. The discrepancy between Q_{decay} and Q_{ss} needs to be investigated further.

It should be noted that Q_{decay} assumes that a single parameter, exponential decay, adequately describes the cavity energy loss. Also note that neither technique requires any knowledge of the actual cavity loss mechanisms.

4.1.5 Field Uniformity

The field uniformity in an aircraft cavity is a function of the effective mode density, the adequacy of the mode-mixing, the effect of localized absorbers, and the proximity to apertures and metal structures. As discussed in Section 4.1.2, at a discrete frequency, the EME in a complex cavity with adequate mode-mixing is a random variable described by a chi-square distribution function. Since this distribution is characterized by its mean, the field uniformity at a discrete frequency in a cavity can be estimated by comparing the mean power density measured with the same instrumentation at several locations within the cavity.

For the aircraft cavities, the data available to estimate the uniformity are multiple, swept frequency PD measurements with the same input power. Using these data, there are several possible ways to characterize the aircraft cavity uniformity. One approach is to consider the spread between the maximum and minimum PD at each frequency for the multiple TX/RX antenna configurations.

A second approach is to characterize the uniformity by the standard deviation about the mean. This approach has the advantage of yielding a confidence level to the uniformity band. Data for CW and BLWGN excitation will be presented using both of these approaches.

4.1.5.1 Swept Frequency Continuous Wave Excitation. In Phase II, only one swept frequency CW insertion loss measurement was obtained in each cavity because of the long data acquisition time. However, during Phase I, several measurements were obtained with combinations of horn and wire TX and RX antennas in the cockpit and avionics bay. One of these is shown in Figure 4-14. Three Phase I measurements in the cockpit using dual-ridged horns for the TX and RX

antennas were combined with the single measurement from Phase II to obtain a four-measurement set for uniformity analysis. The useful overlap range for the Phase I and Phase II measurements is 1.0 to 2.9 GHz.

Figure 4-39 shows the maximum and minimum values of the four data traces available from Phases I and II. The difference between the maximum and minimum values is shown in Figure 4-40. The maximum difference is about 12 dB with an average difference of about 6 dB at 1 GHz decreasing to about 4 dB at 2.9 GHz.

Figure 4-41 shows the average power density and the standard deviation for these measurements. A representative value for the standard deviation over the frequency interval of 1 to 2.9 GHz is 3 dB.

4.1.5.2 Band-Limited White Gaussian Noise Excitation. Four measurements were obtained for each cavity and each BW using BLWGN excitation. These measurements were accomplished with different configurations of the RX antenna for the same TX antenna configuration.

Figure 4-42 shows the maximum and minimum values of four data runs from 0.2 to 1 GHz in the cockpit for 2-MHz BW BLWGN excitation. Figure 4-43 shows the difference between the maxima and minima of the four data runs. The maximum difference exceeds 30 dB, with an average difference of about 12 dB. As can be seen from the figures, the 2-MHz BLWGN data show very poor field uniformity. Primarily, this poor field uniformity is due to the low number of equivalent modes available for mode-mixing at this bandwidth as noted in Table 4-2.

Figures 4-44 and 4-45 show the same data for 10-MHz BW excitation. The maximum difference exceeds 20 dB with an average difference of about 9 dB. The 10-MHz BW data show an improvement over the 2-MHz data, but still yield relatively poor uniformity.

Figure 4-46 and 4-47 show the same data for 50-MHz BW excitation. The maximum difference is less than 15 dB with an average of about 7 dB. The 50-MHz BW BLWGN data show significantly better uniformity based on the increased number of modes available for excitation in the greater BW.

These data validate the expectation that the apparent uniformity of the aircraft cavity EME when excited by BLWGN will improve with BW. However, fine structure in the normalized power density data will be lost as the BW increases.

Based on the above observations, only the 50-MHz data will be considered for the remainder of this analysis.

Figure 4-48 shows the cockpit maxima and minima for both data collection bands covering the full test frequency range 0.2 to 6 GHz for the 50-MHz BW BLWGN excitation. Figure 4-49 shows a maximum and average difference of 14 and 7 dB respectively between the cockpit maximum and minimum measurements. Figure 4-50 shows the average power density and a representative value, 3 dB, of the standard deviation over the range 0.2 to 6 GHz. The few data

points in Figure 4-49 that exceed the 2σ-envelope about the average values in Figure 4-50 are consistent with the expectation of a 95 percent confidence interval.

Figure 4-51 shows the maxima and minima in the measured PD in the avionics bay for 50-MHz BW BLWGN excitation. Figure 4-52 shows a maximum and average difference of 12 and 6 dB, respectively, for the avionics bay. Figure 4-53 shows the average power density and a representative standard deviation of 3 dB for the avionics bay uniformity.

Figure 4-54 shows the maxima and minima in the measured power density in the passenger cabin for 50-MHz BW BLWGN excitation. Figure 4-55 shows a maximum and average difference of 14 and 5 dB respectively for the passenger cabin. Figure 4-56 shows the average power density and a representative standard deviation of 3 dB for the passenger cabin uniformity.

4.1.5.3 Comparison of Field Uniformity Results. A comparison of the CW excitation data in Figures 4-39 through 4-41 with the BLWGN excitation data in Figures 4-48 through 4-50 show good agreement. While the maximum variation for BLWGN is a few decibels greater than for CW excitation, representative values for the standard deviations are the same. These data indicate that it is important to take several measurements to determine the average cavity PD within reasonable limits.

As discussed earlier, the CW power density measurement yields the maximum power density, which is a random variable. The average value, which characterizes the distribution function, should have less variation than the maximum value. Therefore, the available data suggest that a comparison of the average power density for both CW and BLWGN excitation would yield a slightly better uniformity for CW excitation.

Also, it should be noted that the data runs with CW excitation were taken two years apart in Phase I and II with different instrumentation, tuners, and TX/RX antenna configurations. These data indicate the excellent repeatability of aircraft cavity power density measurements obtained with mode-mixing techniques.

A representative value for the standard deviation of the power density data was 3 dB for all the aircraft cavities using 50-MHz BW BLWGN. These results indicate that for frequencies where there is adequate mode density and mode-mixing, the field uniformity in low Q aircraft cavities is comparable to that of laboratory test facilities.

4.2 CAVITY-TO-CAVITY COUPLING/ISOLATION

One of the EM characteristics of interest for large transport aircraft is the potential for coupling energy from one cavity to another. A typical concern is the fraction of energy emitted in the cabin from electronic devices operated by passengers, which can be coupled to the cockpit or avionics bay.

In Phase II, the cavity-to-cavity coupling data shown in Table 3-1 were collected.

There at least two ways to describe the coupling/isolation of the aircraft cavities. The first is coupling efficiency (CE), which is the dimensionless ratio of the power density in the receive cavity to the power density in the transmit cavity or

$$CE_{tr} = PD_r/PD_t \tag{4.11}$$

This parameter quantifies the fraction of the energy introduced into one cavity that will couple into a second cavity.

The second way to describe the coupling/isolation of aircraft cavities is a coupling coefficient (CC), or transfer function, with dimensions of area that describe the power coupled into the receive cavity for a given power density in the transmit cavity.

Both of these parameters will be investigated in Section 4.2.

4.2.1 Cavity-to-Cavity Coupling Efficiency

This section covers the CE for the three cavity-to-cavity interactions of most interest: cockpit to avionics bay, passenger cabin to cockpit, and passenger cabin to avionics bay.

4.2.1.1. Coupling Efficiency From Continuous Wave Excitation. For mechanical mode-mixing, the tuner operations included operations in the TX cavity, in the RX cavity, and in both cavities. Operation of both tuners yielded a bounding condition for the energy measured in the receive cavity.

Figure 4-57 shows the PD measurement obtained with CW excitation in the cockpit and the RX antenna in the avionics bay. Tuners were operating in both cavities. These data are normalized to 0 dBm input in the cockpit. The CE shown in Figure 4-58 is the ratio of the data in Figure 4-57 to that of the cockpit PD shown in Figure 4-12. Because of the previously mentioned problems with avionics bay data obtained with log periodic antenna, only data above 1 GHz obtained with a dual-ridged horn antenna will be presented. Above 1 GHz, the average value of the CE is about −12 dB. A bounding envelope on the CE curve indicates that over the frequency interval 1 to 6 GHz, the maximum coupling efficiency varies from about −6 to −4 dB or 25 to 40 percent. In the Phase I report, CE was not specifically considered. However, data from Figures 4-5 and 4-8 of the Phase I report[2] yield the results shown in Figure 4-59. The Phase I measurement was obtained with monopole TX and RX antennas over the continuous frequency band 0.1 to 2.9 GHz. Above 1 GHz, the average value of CE from the Phase I measurements is about −15 dB. The agreement between the cockpit-to-avionics-bay CE obtained with CW excitation in the Phase I and Phase II tests is within measurement uncertainty.

Figure 4-60 shows the passenger-cabin-to-cockpit PD obtained with both the cockpit and passenger cabin tuners operating. These data are normalized to 0 dBm input in the passenger cabin. The structure at about 1.8 GHz reflects the decreased PD in the passenger cabin as measured with CW excitation and as noted in Figure 4-16.

The CE shown in Figure 4-61 is the ratio of the data in Figure 4-60 to that of the passenger cabin PD shown in Figure 4-16. The offset at 1 GHz results from the previously discussed antenna change at 1 GHz in the data of Figure 4-16.

The average CE is about −5 dB up to 1 GHz and about −7 dB above 1 GHz. The CE data show peak values close to 0 dB for frequencies of a few hundred megahertz. Above 1 GHz, a value of about −3 dB envelopes the data.

Figure 4-62 shows the passenger-cabin-to-avionics-bay PD obtained with both the avionics bay and passenger cabin tuners operating. These data are normalized to 0 dBm input in the passenger cabin.

The CE shown in Figure 4-63 is the ratio of the data in Figure 4-62 to that of the passenger cabin PD shown in Figure 4-16. The passenger-cabin-to-avionics-bay CE data obtained with CW excitation show an average value of a few decibels of gain. Substantial coupling between the two cavities is not unexpected. As shown in Figure 2-3 and discussed in Section 2.1, there is a large common boundary between the two cavities. The structural aluminum ribs and a large number of cable bundles provide the only conducting material separating the two cavities.

4.2.1.2. Coupling Efficiency From Band-Limited White Gaussian Noise Excitation. Figure 4-64 shows the PD measurement obtained from a four-run average using 50-MHz BW BLWGN excitation in the cockpit and the RX antenna in the avionics bay. These data are normalized to 0 dBm input in the cockpit.

The CE shown in Figure 4-65 is the ratio of the data in Figure 4-64 to that of the cockpit PD shown in Figure 4-21. Above 1 GHz, the data is bounded by −13 dB and has an average value of about −17 dB.

Figure 4-66 shows the PD measurement obtained from a four-run average using 50 MHz BW BLWGN excitation in the passenger cabin and the RX antenna in the cockpit. These data are normalized to 0 dBm input in the passenger cabin. The CE shown in Figure 4-67 is the ratio of the data in Figure 4-66 to that of the passenger cabin PD shown in Figure 4-23. The approximately 7 dB offset in the CE at the 1-GHz band change reflects the previously discussed offset in the passenger cabin PD shown in Figure 4-23.

The average CE is about −3 dB up to 1 GHz and about −7 dB above 1 GHz. The data show peak values close to 0 dB for frequencies of a few hundred megahertz. Above 1 GHz, a value of about −3 dB envelopes the data.

Figure 4-68 shows the PD measurement obtained from a four-run average using 50-MHz BW BLWGN excitation in the passenger cabin and the RX antenna in the avionics bay. These data are normalized to 0 dBm input in the passenger cabin.

The CE shown in Figure 4-69 is the ratio of the data in Figure 4-68 to that of the passenger cabin PD shown in Figure 4-23. Above 1 GHz, the average CE is about −13 dB with a bounding envelope of −9 dB.

These data imply about 10 dB less energy coupled to the avionics bay than to the cockpit. This is counter to expectations based on the completeness of the EM topology of the two cavities. A check of the 2- and 10-MHz BW data was not productive since none of these data sets were useable. Since no further verification of these data is possible, caution is advised in drawing conclusions from Figures 4-68 and 4-69.

4.2.1.3 Comparison of Coupling Efficiency Results. For cockpit-to-avionics-bay CE data, shown in Figures 4-58 and 4-65, the frequency dependencies are similar. Above 1 GHz the average CE determined from CW is about 5 dB greater than that from BLWGN. This difference is marginally within the combined uncertainty for the averages of the two measurements. Further discussion of these data can be found in Section 4.2.2.3.

The passenger-cabin-to-cockpit CE data from Figures 4-61 and 4-67 for CW and BLWGN excitation, respectively, are combined in Figure 4-70 for direct comparison. The agreement between the two data sets, including frequency dependencies and magnitudes as well as discontinuity at 1 GHz, is quite good.

The passenger-cabin-to-avionics-bay data from Figures 4-63 and 4-69 for CW and BLWGN excitation results do not agree. There are insufficient data available to resolve the discrepancy. Section 4.2.2.3 has further discussion of this issue. The EM topology between the passenger cabin and the avionics bay favors the CE results obtained with CW excitation.

The CEs for the three cavity pairs investigated are summarized in Table 4-3.

4.2.2 Cavity-to-Cavity Coupling Coefficient

This section covers the CC for the same three cavity interactions discussed in Section 4.2.1. The CC, with dimensions of area, describes the power coupled into the receive cavity for a given power density in the transmit cavity. The coupling coefficients can be evaluated by performing an energy balance analysis based on

$$(\text{Power In})_{\text{cavity}} = (\text{Power Out})_{\text{cavity}} \tag{4.12}$$

As shown in Figure 4-71, the energy balance in cavity 1 when cavity 1 is internally excited by the TX antennas can be described by

$$P_{in/1} + \sigma_{21} * PD_{2/1} = P_{rec/1} + L_1 * PD_1 + \sigma_{12} * PD_1 \tag{4.13}$$

where $P_{in/1}$ = power injected into cavity 1 by the TX antenna
σ_{21} = CC from cavity 2 to cavity 1
$PD_{2/1}$ = power density in cavity 2 due to coupling from cavity 1
$P_{rec/1}$ = power extracted from cavity 1 by RX antennas in cavity 1
L_1 = loss coefficient in cavity 1, which includes all power losses from cavity 1 other than that coupled to cavity 2 or extracted by the RX antenna

PD_1 = power density in cavity 1
σ_{12} = CC from cavity 1 to cavity 2

The energy balance in cavity 2 can be described by a similar expression

$$P_{in/2} + \sigma_{12}*PD_{1/2} = P_{rec/2} + L_2*PD_2 + \sigma_{21}*PD_2 \quad (4.14)$$

where the terms are equivalent to those previously defined in Equation (4.13).

The energy balance in cavity 2 due to excitation in cavity 1 can be described by

$$\sigma_{12}*PD_1 = P_{rec/2/1} + L_2*PD_{2/1} + \sigma_{21}*PD_{2/1} \quad (4.15)$$

Finally, the energy balance in cavity 1 due to excitation in cavity 2 can be written as

$$\sigma_{21}*PD_2 = P_{rec/1/2} + L_1*PD_{1/2} + \sigma_{12}*PD_{1/2} \quad (4.16)$$

The power density can be expressed in terms of the measured received power

$$P_{rec} = A_{eff}*\eta*PD \quad (4.17)$$

where A_{eff} is the effective area of the antenna (which is $\lambda^2/8\pi$ for a directional, polarized antenna with Gain = 1), and η is the antenna efficiency.

Using Equation (4.17) to express $P_{rec2/1}$ in terms of $PD_{2/1}$, Equation (4.15) yields L_2 in terms of σ_{12} and σ_{21}. Similarly, L_1 can be expressed in terms of σ_{21} and σ_{12} using Equations (4.16) and (4.17).

With these values for L_1 and L_2, Equations (4.13) and (4.14) can be solved simultaneously for σ_{12} and σ_{21} yielding

$$\sigma_{12} = (P_{in/2}/PD_2)(CE_{12}/(1 - CE_{12}*CE_{21})) \quad (4.18)$$

$$\sigma_{21} = (P_{in/1}/PD_1)(CE_{21}/(1 - CE_{12}*CE_{21})) \quad (4.19)$$

Note that the difference between the CE and the CC (σ), is the normalized PD in the receive cavity. Since the CC accounts for the intrinsic losses in both cavities, the CCs between a pair of cavities should be the same.

In Phase I, the cavity-to-cavity coupling data were limited. The only available data were from the cockpit to the avionics bay. In order to approximate the CC, an assumption was made in the analysis. The terms $\sigma_{21}*PD_{2/1}$ in Equation (4.13) and $\sigma_{12}*PD_{1/2}$ in Equation (4.14) were considered second-order effects and were neglected. If, in fact, the coupling is small, Equations (4.18) and (4.19) above reduce to Equation (4.6) in the Phase I report.[2] However, in the case of passenger-cabin-to-avionics-bay coupling, the Phase I assumption would be marginal. In any case, the Phase I analysis should yield a lower bound on the CC.

4.2.2.1. Coupling Coefficient From Continuous Wave Excitation. The data from Figures 4-15 and 4-58, along with the data for the CE from avionics-bay-to-cockpit, were used in Equation (4.18) to calculate the CC from cockpit-to-avionics-bay. The results are shown in Figure 4-72. The CC is slightly less than 1 m^2.

Data from Figure 4-10 of the Phase I report[2] is overlaid as the bold trace on the Phase II data from Figure 4-73. The agreement is generally better than 3 dB.

Using the same data as above plus the cockpit PD from Equation (4.12), Equation (4.19) was used to calculate the CC for avionics-bay-to-cockpit, which is shown in Figure 4-74.

As discussed above, the CCs from two interacting cavities should be the same. In Figure 4-75, an evaluation of the difference in the two CCs shows an average difference of zero, with a ±3 dB measurement uncertainty in the fine structure.

As noted in Table 3-1, no CW measurements are available for cockpit-to-passenger-cabin. However, a lower bound on the passenger-cabin-to-cockpit CC can be obtained by neglecting the product $CE_{pc/c}$* $CE_{c/pc}$ in the denominator of Equation (4.18). This is equivalent to the Phase I assumption. The results are shown in Figure 4-76. Over the common frequency interval, 1 to 2.9 GHz, the CC from passenger-cabin-to-cockpit is about the same as for cockpit-to-avionics-bay. This is expected from the EM topology between the two cavities.

As in the case of the passenger-cabin-to-cockpit CC, the available data limits the analysis to an approximation of the CC from the passenger-cabin-to-avionics bay. The results are shown in Figure 4-77. Over the frequency interval 1 to 2.9 GHz, the average CC is about 10 m^2. The significantly larger CC for the passenger-cabin-to-avionics-bay is consistent with the EM topology between the two cavities.

4.2.2.2 Coupling Coefficient from Band-Limited White Gaussian Noise Excitation. The data from Figures 4-27 and 4-65, along with the data for the CE from avionics-bay-to-cockpit, were used in Equation (4.18) to calculate the CC from cockpit-to-avionics-bay. The results are shown in Figure 4-78. The CC averages 1 to 2 dB less than 1 m^2.

The data from Figures 4-21 and 4-67, along with the data for the CE from cockpit-to-passenger-cabin, were used in Equation (4.18) to calculate the CC from passenger-cabin-to-cockpit. The results are shown in Figure 4-79. The CC averages 1 dB less than 1 m^2.

The data from Figures 4-23 and 4-69, along with the data for the CE from avionics-bay-to-passenger-cabin, were used in Equation (4.18) to calculate the CC from passenger-cabin-to-avionics-bay. The results are shown in Figure 4-80. The CC averages 3 dB more than 1 m^2.

4.2.2.3 Comparison of Coupling Coefficient Results. For cockpit-to-avionics-bay CC data shown in Figures 4-73 and 4-78, the two mode excitation techniques yield average CC values within about 2 dB. Underlying this apparent agreement is an offset between all CW and BLWGN measurements in the avionics bay. The minimum offset, first noted in Section 4.1.3.3, which compares PD measurements in the cockpit and avionics bay, is at least 2σ of the expected

uniformity. In one case, the offset exceeds 6σ. Equation (4.18) requires the ratio of two avionics bay measurements. In this case, both BLWGN measurements are offset approximately 6 dB from the CW measurement. As a result, the offset does not affect the ratio in the CC calculation and the agreement is fortuitous.

The CCs for passenger-cabin-to-cockpit for CW and BLWGN are shown in Figures 4-76 and 4-79, respectively. In the overlap interval, 1 to 2.9 GHz, the agreement is good.

The passenger-cabin-to-avionics-bay CCs for CW and BLWGN are shown is Figures 4-77 and 4-80, respectively. In the overlap interval, 1 to 2.9 GHz, the CC measured by CW is almost 10 dB greater than the CC from BLWGN. Based on the EM topology, the set of CW data more closely matches expectations than does the BLWGN data. The PD measurements in the avionics bay for excitation in the passenger cabin, shown in Figures 4-62 and 4-68, have a large discrepancy between CW and BLWGN. A detailed analysis of CW and BLWGN data for specific configurations, as well as a comparison to Phase I CW measurements, indicated a consistent offset in avionics bay BLWGN data. While no explanation for this offset in avionics bay data is available, the offset does explain a number of observations discussed in this and earlier sections.

4.3 RADAR ALTIMETER/COMMON TEST ARTICLE RESPONSES

This section covers the results of the instrumented RA and CTA testing described in Sections 2.2 and 3.5.

In general, the coupling transfer function of a given system will vary with frequency, polarization, and angle of incidence of the EME. The power received by a given system is related mathematically to the coupling transfer function by the expression:

$$P_{rec}(f,\varphi,\theta,\phi) = PD(f,\varphi,\theta,\phi) * \sigma_{sys}(f,\varphi,\theta,\phi) \qquad (4.20)$$

where P_{rec} = received power, in mW, coupled to a system
PD = power density, in mW/cm^2, to which the system is exposed
σ_{sys} = coupling transfer function, in cm^2, of the system
f = frequency of the incident energy
φ = polarization of the incident energy
θ = azimuth angle of the incident energy
ϕ = elevation angle of the incident energy

Theory predicts, and reverberation measurements support, that when a sufficient number of independent modes have been excited in an arbitrary complex cavity, and an adequate mode-mixing technique is used, the EME is isotropic and randomly polarized. For an isotropic and randomly polarized EME, the factors in Equation (4.20) are dependent only on frequency:

$$P_{rec}(f) = PD(f) * \sigma_{sys}(f) \qquad (4.21)$$

The transfer functions for the instrumented systems are not known analytically. They can be obtained empirically when the PD inside the complex cavity of interest is known. The analytic coupling transfer function of an in-band receive antenna, such as those used for the normalized PD measurements in the aircraft cavities and the reverberation chamber, is known and is equivalent to the antenna's effective area times the antenna efficiency.[1] Using the received power values of each channel of the instrumented systems and the PD in the aircraft cavities or in the NSWCDD reverberation chamber, the RF coupling transfer function (in $dBcm^2$) can be computed as follows:

$$\sigma_{sys}(f)\ [dBcm^2] = 10 * Log(P_{rec}(f)/PD(f)) \qquad (4.22)$$

where P_{rec} and PD are as defined for Equation (4.20).

Prior to testing, the RA was positioned in its normal location in the instrument panel and connected to its wiring bundles.

Figure 4-81 shows the instrumented RA positioned in the cockpit instrument panel. The CTA was tested in both the cockpit and avionics bay, but was not able to be connected to an aircraft wiring harness. For the CTA, during the CW and BLWGN excitation in the cockpit, the pilot's and copilot's instrument panels were unfastened and folded face down, as would occur during maintenance of the instrument panel. One of the CTA's boxes was positioned on top of the pilot's instrument panel; the other was placed on top of the copilot's instrument panel. The CTA's 3-m interconnecting cable was routed behind the center cockpit console, similar to the wiring bundles of the aircraft instruments. Figure 4-82 shows the CTA as configured for mechanical and BLWGN testing in the cockpit. For mechanical and BLWGN measurements on the CTA in the avionics bay, the CTA boxes were placed on separate levels of the equipment rack on the copilot's side of the avionics bay, as shown in Figure 4-83. Also visible in Figure 4-83 is how the CTA's 3-m interconnecting cable was routed behind the rack, similar to aircraft wiring bundles. During BLWGN testing in the avionics bay, RF-coupling measurements were also made with the CTA positioned such that it was suspended with nonconductive string from the avionics bay ceiling in relative isolation from aircraft cavity structure.

RF coupling transfer functions in the aircraft were computed from measurements obtained from the following sequence:

- An aircraft cavity was excited using either CW or BLWGN
- Cavity PD was measured using an in-band monitor antenna
- Power received by the RA or CTA was measured

During cavity CW PD measurements and RF coupling measurements, only one transmit antenna location was used for a given configuration, as described in Table 3-1. During BLWGN PD measurements, the transmit antenna was positioned in four distinct locations for each measurement configuration; the PD measurements at the four locations were then arithmetically averaged. However, during BLWGN RF coupling measurements, only one location of the transmit antenna was used for each measurement configuration.

The RA was tested in the NSWCDD reverberation chamber in the following configuration variations:

- Positioned on a dielectric block:
  - Wiring harness not connected
  - Unterminated wiring harness connected
  - Wiring harness connected and terminated in a short
  - Wiring harness connected and terminated in a 50-ohm dummy load
- Positioned on a ground plane grounded to the reverberation chamber's interior:
  - Wiring harness not connected
  - Unterminated wiring harness connected
  - Wiring harness connected and terminated in a short
  - Wiring harness connected and terminated in a 50-ohm dummy load

The CTA with its 3-m interconnecting wiring was tested on the dielectric block and on the ground plane.

Testing with the RA and CTA on the ground plane was performed with a setup as specified in DO-160C. That is, the ground plane was grounded to the chamber as per the specification, and 5-cm-thick dielectric material was used to support avionics wiring harness and interconnecting CTA wiring.

Figures 4-84 through 4-86 are representative of the setups used. Wherever possible, all RF hardware and equipment, and computer hardware and software used in the aircraft tests were also used in the reverberation chamber tests. For example, the semi-rigid cables used on the aircraft test were marked as to their function and position (e.g., "TX signal from equipment van to cockpit"). For testing in the reverberation chamber, the cables were used for the same function (e.g., "TX signal from ante-room to chamber"). Not all the equipment used during aircraft testing was available for the reverberation chamber tests, however. Only one of the log periodic antennas was available. A log spiral antenna was substituted for the RX log periodic antenna. Furthermore, no small DC motors were used in the reverberation chamber CW measurements. Instead, the chamber's large computer-controlled stepper-motors and paddle wheel tuners were used. All the BLWGN equipment was different from that used on the aircraft.

Continuous wave RF coupling measurements were performed using the same procedures and equipment settings as during the CW measurements in the aircraft. BLWGN measurements were made using the same noise bandwidths as those used during the aircraft tests; other settings such as

sweep times, although consistent throughout aircraft testing, were unrecorded during the aircraft tests. Therefore, engineering judgement was used to select reasonable settings on the BLWGN equipment for the reverberation chamber tests. All settings used during BLWGN measurements taken in the NSWCDD reverberation chamber were recorded and remained consistent.

During reverberation chamber PD and RF coupling measurements using mechanical mode-mixing, only one transmit antenna location was used for a given configuration, as described in Table 3-1. During BLWGN PD measurements, the transmit antenna was positioned in four distinct locations for each measurement configuration; the received power measurements at the four locations were then arithmetically averaged. However, during BLWGN RF coupling measurements, only one location of the transmit antenna was used for each measurement configuration.

4.3.1 Responses Obtained from Continuous Wave Excitation in Aircraft

4.3.1.1 Radar Altimeter Indicator Continuous Wave Response. Figure 3-5 shows the received power in channels 1 and 2 of the RA for CW excitation in the cockpit. Figures 4-87 and 4-88 show the RF coupling transfer functions for channels 1 and 2 respectively, computed using Equation (4.22) and the data from Figures 3-5 and 4-12.

The transfer functions show the fine structure typical of CW measurements. The transfer function for channel 1 bounds that of channel 2 over the entire frequency range. Above about 3.5 GHz, the transfer functions are approximately equivalent within measurement uncertainty.

4.3.1.2 Common Test Article Continuous Wave Response. Figure 4-89 shows the RF coupling transfer function of the CTA positioned in the cockpit instrument panels. The magnitude of the coupling transfer function for the CTA in the cockpit instrument panel is generally within 10 dB of RA channel 1.

Figure 4-90 shows the RF coupling transfer function of the CTA positioned on the equipment rack on the copilot's side of the avionics bay. The magnitudes of the CTA transfer functions in the cockpit instrument panel and in the avionics bay rack obtained with CW excitation are in general agreement over the frequency range 1 to 6 GHz. The average variation is less than 10 dB. This suggests that the details of the metal topology may not have a major effect on the coupling to an avionics system.

4.3.2 Responses Obtained from Band-Limited White Gaussian Noise Excitation in Aircraft

4.3.2.1 Radar Altimeter Indicator Band-Limited White Gaussian Noise Response. Figure 3-6 shows the received power in channels 1 and 2 of the RA for 50-MHz BLWGN excitation in the cockpit. Figures 4-91 and 4-92 show the coupling transfer functions for RA channels 1 and 2 respectively, computed using Equation (4.22) and the data from Figures 3-6 and 4-21. Note the reduced structure in the data typical of BLWGN excitation. Except for a few small frequency intervals, the transfer function for channel 1 bounds that of channel 2. The maximum variations between the two transfer functions are on the order of 25 dB.

4.3.2.2 Common Test Article Band-Limited White Gaussian Noise Response. Figure 4-93 shows the RF-coupling transfer function of the CTA positioned in the cockpit instrument panels. The magnitude of the coupling transfer function for the CTA in the cockpit instrument panel is generally within 10 dB of RA channel 1.

Figure 4-94 shows the RF coupling transfer function of the CTA positioned on the avionics bay equipment rack on the copilot's side, as shown in Figure 4-83.

The magnitudes of the CTA transfer functions in the cockpit instrument panel and in the avionics bay rack obtained with BLWGN are in general agreement. Over a small frequency interval, the average transfer function in the avionics bay is less than 10 dB smaller than the cockpit data.

Figure 4-95 shows the transfer function obtained when the CTA was positioned in relative isolation from other metal structures in the avionics bay. The transfer function generally bounds the cockpit instrument panel and avionics bay rack configurations. In fact, the response averages about 5 dB greater than when the CTA was in closer proximity to metal structures. This result is expected based on the nature of the cavity fields near metal surfaces compared to a third of a wavelength or more from the surfaces.

4.3.3 Comparison of Responses Obtained from Continuous Wave and Band-Limited White Gaussian Noise Excitation in Aircraft

In the Phase II test, the agreement between results obtained with CW and BLWGN excitation of the aircraft and its cavities is of interest. In this section, comparison will be made between the results obtained on the aircraft for the two types of excitation.

4.3.3.1 Comparison of Radar Altimeter Indicator Responses Obtained in Aircraft. Figures 4-96 and 4-97 compare the CW and BLWGN responses for RA channels 1 and 2, respectively. Comparison of the channel 1 results shows that the coupling transfer functions for the two techniques are in good agreement up to 4 GHz. Above 4 GHz, except for a few small frequency intervals, the responses from the two techniques are within measurement uncertainty. For channel 2, the responses show considerably less agreement; however, the CW transfer function typically bounds the BLWGN transfer function. The frequency structure and the magnitude of the transfer functions show significant variations.

4.3.3.2 Comparison of Common Test Article Responses Obtained in Aircraft. Figures 4-98 and 4-99 compare the CW and BLWGN responses for the CTA in the cockpit instrument panel and the avionics bay equipment rack, respectively. Except for a few small frequency intervals over the range 1 to 6 GHz, the two excitation techniques are within measurement uncertainty for both test configurations.

4.3.4 Responses Obtained from Continuous Wave Excitation in NSWCDD Reverberation Chamber

4.3.4.1 Radar Altimeter Indicator Continuous Wave Response. Figure 3-7 shows the received power of RA channels 1 and 2 for CW excitation in the reverberation chamber. This figure is representative of the coupling data obtained during reverberation chamber tests. Figures 4-100 and 4-101 show the RF coupling transfer functions for channels 1 and 2, respectively, when the RA was positioned on a Styrofoam block in the reverberation chamber for the different configurations discussed in Section 4.3. Note that for all the configuration variations tested with the RA positioned on the dielectric block, the most significant change in the RF coupling transfer function occurs when the wiring harness is connected. As could be expected, this effect is observed primarily below 1 GHz. Also note that in general, the RF coupling transfer function of both channels is relatively unaffected by changes in termination of the wiring harness.

Figures 4-102 and 4-103 show the RF coupling transfer function for channels 1 and 2 when the RA was positioned on the ground plane for the configuration variations discussed in Section 4.3. Note that for all the configuration variations tested with the RA positioned on the ground plane, the most significant change in the RF coupling transfer function occurs when the wiring harness is connected. As noted above, this effect is observed primarily below 1 GHz and the RF-coupling transfer function of both channels is relatively unaffected by changes in termination of the wiring harness.

Comparison of Figures 4-100 through 4-103 shows that the coupling transfer functions obtained with the RA positioned on a dielectric block and positioned on a ground plane are in good agreement across most of the frequency bands.

4.3.4.2 Common Test Article Continuous Wave Response. Figures 4-104 and 4-105 show the RF coupling transfer function for the CTA positioned on the dielectric block and the ground plane, respectively. Comparison of Figures 4-104 and 4-105 shows that the coupling transfer function obtained with the CTA positioned on a dielectric block and positioned on a ground plane are in good agreement across most of the frequency interval tested.

4.3.5 Responses Obtained from Band-Limited White Gaussian Noise Excitation in NSWCDD Reverberation Chamber

4.3.5.1 Radar Altimeter Indicator Band-Limited White Gaussian Noise Response. Figures 4-106 and 4-107 show the RF coupling transfer function of each RA channel when the RA was positioned on a styrofoam block in the reverberation chamber for the different configurations discussed in Section 4.3. Note that, similarly to the CW results, the most significant change in the RF coupling transfer function occurs when the wiring harness is connected. Also, as was found for the CW results, in general, the RF coupling transfer function of both channels is relatively unaffected by changes in termination of the wiring harness.

Figures 4-108 and 4-109 show the RF coupling transfer function for channels 1 and 2 when the RA was positioned on the ground plane for the configuration variations discussed in Section 4.3.

For all the configuration variations tested with the RA positioned on the ground plane, the most significant change in the RF coupling transfer function occurs when the wiring harness is connected. In general, the RF coupling transfer function of both channels is relatively unaffected by changes in termination of the wiring harness.

Comparison of Figures 4-106 through 4-109 shows that the coupling transfer functions obtained with the RA positioned on a dielectric block and positioned on a ground plane are in good agreement across most of the frequency bands.

4.3.5.2 Common Test Article Band-Limited White Gaussian Noise Response. Figures 4-110 and 4-111 show the RF coupling transfer function of the CTA positioned on a Styrofoam block and the ground plane, respectively. Comparison of the responses in these figures shows that the coupling transfer function obtained with the CTA positioned on a dielectric block and positioned on a ground plane are in good agreement across most of the frequency bands.

4.3.6 Comparison of Responses Obtained from Continuous Wave and Band-Limited White Gaussian Noise Excitation in NSWCDD Reverberation Chamber

The most common configuration for an avionics system test in a reverberation chamber would be on a dielectric block with its wire harness terminated in the appropriate loads. Continuous wave and BLWGN responses for this configuration will be compared in Sections 4.3.6.1 and 4.3.6.2.

4.3.6.1 Comparison of Radar Altimeter Indicator Responses Obtained in NSWCDD Reverberation Chamber. Figures 4-112 and 4-113 compare the coupling transfer function for CW and BLWGN excitation for RA channels 1 and 2. The transfer functions are generally within measurement uncertainty over the entire frequency range 1 to 6 GHz. The CW response bounds the BLWGN response with only a few exceptions at small frequency ranges.

4.3.6.2 Comparison of Common Test Article Responses Obtained in NSWCDD Reverberation Chamber. Figure 4-114 compares the coupling transfer function for CW and BLWGN excitation of the CTA. The CW response generally bounds the BLWGN response. The two responses are within measurement uncertainty over most of the frequency range 1 to 6 GHz.

4.3.7 Comparison of Responses Obtained in Aircraft and NSWCDD Reverberation Chamber

As discussed above, CW responses tend to bound the BLWGN responses. Further, responses from a reverberation chamber test with the system configured with its wire harness terminated in an appropriate load and tested on a dielectric block tend to bound other configurations. The large data base on RA and CTA reverberation chamber responses will be represented by these test conditions.

As noted earlier, the estimated standard deviation of the measured insertion loss is 4 dB in the aircraft and 2 dB in the reverberation chamber. Recall that the insertion loss data and the power received by the instrumented points in the avionics and CTA are used in the computation of the RF coupling transfer functions. No standard deviation estimate is available for the instrumented avionics

or CTA received power data. Therefore, as a first approximation to the uncertainty of the transfer functions, the estimated standard deviation for the insertion loss will be used.

The transfer functions obtained in the aircraft and reverberation chamber with standard deviations applied will be compared for overlap as an indication of the agreement.

4.3.7.1 Comparison of Radar Altimeter Indicator Responses. Figures 4-115 and 4-116 compare the responses of RA channels 1 and 2 in the aircraft and the reverberation chamber. Except for limited fine structure, all the responses for channel 1 are within a 1σ interval. Figure 4-116 shows that the channel 2 RF coupling transfer functions obtained in the aircraft are bounded by those obtained in the reverberation chamber, at frequencies up to approximately 5 GHz. At frequencies below approximately 5 GHz, except for limited fine structure, the responses for channel 2 are typically within a 2σ interval. At frequencies above 5 GHz, except for limited fine structure, the responses for channel 2 are within a 1σ interval.

4.3.7.2 Comparison of Common Test Article Responses. Figures 4-117 and 4-118 compare the CTA responses in the aircraft and in the reverberation chamber. Again, except for fine structure over limited frequency intervals, the responses in the aircraft and the reverberation chamber are typically within a 1σ interval.

As discussed in Section 4.3, only BLWGN data are available for the CTA in the isolated configuration in the avionics bay. Figure 4-119 compares the CTA response when excited by 50-MHz noise in the avionics bay and in the reverberation chamber. The reverberation chamber BLWGN data are generally less than the aircraft data, but within measurement uncertainty. However, unlike almost all of the other data analyzed, the CTA BLWGN response on the dielectric block in the reverberation chamber does not approximate a bound to the aircraft BLWGN data. When reverberation chamber CW data are compared to the BLWGN aircraft data, except for limited frequency intervals, the results are generally within measurement uncertainty.

4.4 SHIELDING EFFECTIVENESS MEASUREMENTS

This section covers the aircraft SE data obtained with the three excitation sources described in Section 3.7. The SE is defined as the ratio of the external EME to the internal EME.

4.4.1 Ambient FM/VHF/UHF Band Measurements

The external ambient EME and the cockpit EME were measured in the FM and VHF/UHF bands with both monopole and log periodic RX antennas. The log periodic antennas were used out-of-band for FM measurements. However, since identical antennas were used, the reduced collection efficiency in the FM band will cancel in the SE calculations.

The external log periodic antenna was directed toward the mountain assumed to be the location of the majority of the FM and TV emitters covering the frequency intervals 88 to 108 MHz (FM band), 174 to 216 MHz (channels 7 through 13) and 470 to 810 MHz (channels 14 through 69).

For these emitters, the analysis included a 6 dB antenna directivity factor applied to the external measurements. For other frequency intervals, the emitter locations were unknown, and recognizing the uncertainties involved, the analysis used the measured received power as the reference for the SE calculations. No directivity factor was applied to the internal measurements since the cockpit cavity washes out the directivity effects.

The external measurements included both horizontal and vertical polarizations. Figures 3-11 and 3-12 show typical traces for the external EME in the two bands.

The cockpit EME data were obtained with the RX antenna in two different orientations. Data from more than one RX antenna position was desired since over most of the frequency range of interest for the SE analysis, the tuner was not totally effective. The external and internal measurements were performed simultaneously over an interval of several minutes.

In the FM band, a few discrete frequencies showed temporal variations of 4 dB or less. The polarization difference in the external EME was less than 6 dB with the horizontally polarized EME typically being greater.

Figure 3-13 shows a typical trace of the cockpit EME in the FM band. The maximum cockpit discrete frequency variations were 3 dB as the RX antenna location/orientation was varied. Figure 4-120 shows the minimum composite SE data for the cockpit in the FM band. Minimum SE data with the bold markers were derived from simultaneous external and internal measurements with a constraint that both signals had to be at least 5 dB above the noise level. The light markers indicate data points where the internal signal was less than 5 dB above the noise level. No polarization effects were noted in these data. The minimum SE over the FM band is in the 5- to 15-dB range.

As indicated in Figure 3-12, there are many discrete frequency emitters available in the interval 0.1 to 1 GHz. The analysis of SE in this frequency interval required care since some strong emitters were intermittent as well as mobile. Although a large number of the emitters were TV stations located in a relatively small region on a mountain top, other emitters were probably distributed over all azimuths. For a given polarization, below 450 MHz, run-to-run variations as large as 6 dB were observed. Above 450 MHz, the variations were less than 3 dB.

Polarization effects changed with frequency and could be as large as 15 dB. Over the frequency intervals 100 to 150 MHz, 220 to 450 MHz, and 810 to 950 MHz, vertical polarization dominated the ambient EME. Figure 4-121 shows typical polarization effects in the ambient EME.

The internal measurements were obtained for two orientations of the RX antenna. The SE analysis used data from simultaneous external and internal measurements. The minimum cockpit SE values derived from the ambient VHF/UHF EME are plotted in Figure 4-122. As for the FM band, data with signal-to-noise (S/N) ratios greater than and less than 5 dB are shown in bold and light markers, respectively. The SE results derived from data with greater than 5 dB S/N ratios should have a higher level of confidence than those derived from data with less than 5 dB S/N ratios. The error bars reflect a number of uncertainties, including ambient signal variability, polarization effects, the effective gain of the external antenna for a particular emitter, and the cockpit antenna positional effects. The data in Figure 4-122 imply that the cockpit SE over the frequency interval 0.1 to 1 GHz

can be as low as a few decibels, which is in agreement with data obtained in the Phase I test. The data also indicate the probability of a significant fine structure in the aircraft SE.

4.4.2 Band-Limited White Gaussian Noise Excitation

The aircraft was excited using BLWGN as described in Section 3.7. The TX antennas were located at 0°, 45°, and 90° from the aircraft's longitudinal axis. Data were collected for horizontal and vertical polarizations for these three positions for each of the aircraft cavities. Data from four RX antenna positions in the cockpit and avionics bay are available. A limited set of data is available for the passenger cabin.

Figure 4-123 shows the maximum and minimum SE variation in the cockpit for horizontally polarized, 0° illumination of the aircraft. These data give an indication of the measurement variability that can be expected using these procedures. The maximum variation is 20 dB, while the standard deviation is about 3 dB. Most of the variability can probably be attributed to the uniformity of the cockpit EME.

Figure 4-124 shows the average SE for the cockpit for horizontally polarized, 0° illumination. As described in Section 2.4.2, the internal SE measurements were corrected with a reference measurement obtained with the same TX/RX antennas, but without the aircraft present. This technique introduces a bias at frequencies where destructive interference occurs between the direct path and the ground-reflected path. At these frequencies, the reference signal is small. Typically, the "reference-corrected" measurements will have maximum values where the reference signal is small. Figure 4-124 has markers along the top axis indicating the frequencies where destructive interference should be expected for a single, ideal ground-reflected path. The markers imply that a significant fraction of the structure observed in Figure 4-124 (and subsequent figures) is due to the referencing technique. In practice, the frequency and magnitude of the minimum values will depend on the multiple scattering paths possible over rough ground.

Average SE data will be used throughout the rest of this section.

Figures 4-124 to 4-126 show the aspect-angle dependence of the average SE for horizontally polarized illumination of the cockpit. The data show that the SE generally increases a few decibels with aspect angle. At 45°, the average increase in SE is about 4 dB. This increase is the expected result since the maximum cockpit window area is exposed at 0° angle of illumination.

Figures 4-127 to 4-129 show the cockpit SE for vertically polarized illumination for the three aspect angles. The aspect-angle dependence is about the same as for horizontal polarization. The data of Figures 4-124 and 4-127 indicate that the cockpit SE for vertical polarization is generally equal to or a few decibels less than for horizontal polarization.

The underlying measurement uncertainty in the average values shown in the figures is about ± 3 dB. For some applications, the parameter of interest is the minimum SE that can be expected. For the cockpit, the all-aspect angle, both-polarization, minimum SE increases from about 15 dB at low frequencies to about 20 dB at 6 GHz.

Figures 4-130 to 4-132 show the SE for the avionics bay for horizontally polarized illumination from 0°, 45°, and 90°, respectively. The data in these figures show an interesting aspect-angle dependence. At low frequencies, the 90° aspect angle data show a higher SE than the 0° data. However at higher frequencies, the reverse is true. The 90° data is unique in that it does not exhibit the general trend toward increasing SE with increasing frequency observed in all other BLWGN data.

Figures 4-133 to 4-135 show the SE for the avionics bay for vertically polarized illumination. These data show a slight aspect-angle dependence, with the SE for 90° illumination being a few decibels less than for 0°.

The SE of the avionics bay is a few decibels less for horizontal polarization than for vertical polarization.

The data suggest that at 0° illumination, the avionics bay EME, and hence the SE may be dominated by cavity-to-cavity coupling effects from the cockpit. At 90° illumination, direct coupling to the avionics bay apertures may be more important as a result of the increased cockpit SE and, therefore, lower cockpit EME.

The minimum SE for the avionics bay is about 25 dB at low frequencies, increasing to about 30 dB at 6 GHz.

Figures 4-136 to 4-138 show the SE for the passenger cabin for horizontally polarized excitation from 0°, 45°, and 90°. Note that for the passenger cabin, the data base is limited in frequency span, and generally only two RX antenna locations are available. The available data show essentially no aspect-angle dependence. This result is somewhat unexpected since the collection area for 90° illumination is considerably greater than for 0°. Also at 90°, the penetration through the passenger cabin windows should be considerably greater than for other aspect angles. Again, a possible explanation is that for the 0° illumination, the energy is coupled into the cockpit and then by cavity-to-cavity coupling to the passenger cabin.

Figures 4-139 to 4-141 show the SE for the passenger cabin for vertically polarized illumination from 0°, 45°, and 90°. The 45° data imply about 5 dB greater SE for vertical polarization. The data for 90° illumination show the unexpected result that there is essentially no difference between the two polarizations. The match of a horizontally polarized, external EME to the major aircraft dimension would suggest greater energy coupling and therefore a lower SE than for a vertically polarized EME.

The data indicate an increase in minimum SE from about 18 dB at low frequencies to about 25 dB at 6 GHz.

The limited data set suggests caution in drawing conclusions about the aspect-angle dependence of the passenger cabin SE.

4.4.3 Short Pulse Excitation

For the short pulse excitation, the SE is defined as the ratio of the total energy in the reference signal at any given frequency to the total energy inside the aircraft at that same frequency. The reference waveform is shown in Figure 4-142. For the reference measurement, the antennas were separated by the same 100 ft used in the actual measurement, and were positioned the same 11 ft above the ground. This "reference" signal contains all the information about the measurement system without the aircraft and is used to normalize the internal EME data to obtain the shielding effectiveness.

The waveform contains two doublets barely 2 ns apart. This is due to the multipath transmission of the direct path and the ground-reflection path. The distance required for the energy to propagate by way of the ground-reflected path is approximately two feet more than the direct path, resulting in a 2-ns delay at the RX antenna. The ground-reflected signal is phase coherent with the direct path signal and therefore produces a spectrum that contains an interference pattern with deep nulls, as shown in Figure 4-143. During the normalization process for determining the SE, the signal measured inside the aircraft is deconvolved using this reference. If the internal signal were also composed of these same two signals, it would also have the same nulls in the spectrum, and during normalization, the nulls would cancel out. However, the spectrum of the signal within the aircraft does not display the deep nulls. The signal received inside the aircraft is a composite of signals from many apertures and involves many multiple reflections. This process destroys the phase coherence between the internal and external fields. Thus as noted in Section 4.4.2, a normalization process using the reference of Figure 4-143 would result in a structure of peaks and nulls that are not representative of the actual SE for plane wave excitation. However, in the time domain analysis, the second doublet can be easily removed by windowing, yielding the simpler waveform shown in Figure 4-144. The doublet is no longer symmetric above and below the zero volt line because of the frequency-dependent losses in the longer coaxial cable that was used for the actual measurements. The single doublet has a smoother spectrum, as shown in Figure 4-145. The spectrum shown in Figure 4-145 is the modified reference used to normalize the data measured inside the aircraft.

The ability to time-gate out the ground bounce is one of the unique advantages of the time-domain measurement technique.

The aircraft SE was calculated in the frequency domain after applying the FFT to the voltage waveform shown in Figure 3-17. Since the electromagnetic pulse that illuminates the aircraft is very short in duration (less than 1 ns), the entire pulse is captured in one 50-ns window of the oscilloscope sweep. The FFT of that time window yields the total energy in the pulse. However, the time response of the energy inside the aircraft continues for a much longer time (more than 500 ns) because of the Q enhancement effect. It requires a particularly complex measurement system to capture the complete waveform in one continuous piece. For optimum processing, the waveform digitizer should be capable of digitizing and storing an 8000-sample sequence with a bandwidth of 2 GHz. The computer should be capable of performing 8000-point FFTs. The equipment available for this test did not have these optimum capabilities. As a result, data were obtained by taking a series of separate time windows, each delayed from the previous by one time-window duration. An FFT was performed on each window. The spectral components of all the windows were added to get a total.

It could require twenty or more time windows to capture the total energy. This process would consume too much time for any practical measurement cycle. Instead, the total energy inside the aircraft was estimated by using the initial energy, P_o, in the first significant time window, and the value of τ from the Q factor measurements. These parameters were fit to Equation (4.10) for the energy as a function of time, and the equation integrated to obtain the total energy. If P(t) were a continuous function, the total energy would be

$$P_{total} = P_o * \tau \tag{4.23}$$

Since the data are not a continuous function but discrete points, it is better to consider an infinite sum to calculate the total energy. The result of this process is given by

$$P_{total} = P_o / (1 - e^{W/\tau}), \tag{4.24}$$

where τ is the decay time as defined previously, and W is the duration of one time window, 50 ns for this analysis.

These results were used to calculate the penetration or shielding effectiveness of the aircraft by dividing the total reference energy by the total internal energy.

To justify this procedure, it was necessary to demonstrate that the sum of the energy in each of the windows was equal to the energy in the total waveform. If the waveforms have some phase coherence from one time window to the next, the phase is an important part of the signal and each window must be added to the next using vector addition. If there is no phase coherence, then the energy can be added directly.

4.4.3.1 Effect of Phase Coherence on the Sum of Energy. The analysis covered three possible types of phase coherence that could affect the data processing of the aircraft SE data. The first can be characterized by the response of a lumped constant network. In this case, there would be only one impulsive input, and the entire system response belongs to that pulse only. Theoretically, the same steady state response can be calculated from any part of the time-domain response, even the first 10 percent, since the response is determined by the circuit and only one input pulse.

A spectrum indicating the total energy in the circuit at any given frequency can be obtained from an FFT of the impulse response. If the impulse response is divided into a sequence of smaller time windows and the FFT performed on each, the voltage in each of the windows could be added. In this case, the square of the sum of the windows would be equal to the total energy in the whole signal. This is true because the phase of each spectral component remains constant with time. This condition is called total phase coherence.

If there are two inputs to a particular circuit that can be delayed with respect to each other, or if there are delay circuits within the circuit under test (a distributed system), the later response may not be in phase with the earlier. It would be unusual if it were. The second response could subtract from the first, rather than add. In this case, it is necessary to combine the spectral components vectorially. This condition is called partial coherence.

The third condition is one in which there are very many inputs, all with different delays. Since there are so many signals present, the decay of one or the beginning of a new one will not significantly change either the amplitude or the phase of the ensemble. In this case, the phase of the ensemble can be assumed not to change significantly with time, and the energy in the total waveform will be equal to the sum of each partial window. This is referred to as total incoherence and has been shown to be approximately true in the aircraft measurements.

The aircraft response to the external short-pulse excitation is too complex to be totally coherent and not complex enough to be totally incoherent. It is at best partially coherent. The question remains whether it is close enough to incoherence to permit the use of that assumption in the calculations. The simple test described in the next section was developed to evaluate this condition.

4.4.3.2 Test for Coherency in the Data. The recorded time-domain waveforms used time windows of 50 ns duration. The delay to the next time window took advantage of a convenient delay control on the oscilloscope. This control does not have the accuracy needed to do precise phase matching between windows. Consequently, it was not possible to measure the phase coherency between one window and the next. Instead, the FFT of a single window was calculated as well as the FFT on the two half-windows. The spectral energy in each half-window at some chosen frequencies was added both vectorially and algebraically. The vector sum agreed with the whole waveform FFT and was used as a check that the separation into two windows was done correctly. Then the result of the sum of the two energies was compared to the whole waveform energy to see if the error between them was acceptable. This was repeated at several different frequencies. In most cases, errors between 1 and 15 dB indicated there must be some partial coherence. Some additional processing was necessary to reduce the coherence in the data.

4.4.3.3 Artificial Reduction of Partial Coherence. The most common means for reducing coherence is the use of mechanical mode stirrers. These are large reflecting surfaces within the aircraft that can be moved to significantly shift the phases of the signals being measured. If the phase of all frequency components can be shifted by at least ±180°, good stirring will render the signal phases incoherent. In this case, algebraic addition of the window energies should produce little error.

A second method for reducing the partial coherency requires increasing the averaging bandwidth of the measurement. In simple terms, the energy calculated for various frequencies was summed. The coherency decreases as the bandwidth increases. The disadvantage of this method is that it tends to wash out the characteristic modal responses at specific frequencies.

Both methods were somewhat unsatisfactory for calculating the passenger cabin SE. Finally, applying Parseval's Theorem lead to increasing the bandwidth to 1.2 GHz, that is, using all the frequencies that were available. All the frequency components were summed and the whole window spectrum compared to the sum of the two halves. Under these conditions, total incoherence prevailed within an error of 0.04 dB. This validated the method of increasing the bandwidth, or, frequency averaging.

4.4.3.4 Analysis of the Cockpit Shielding Effectiveness Data. One set of cockpit SE data was tested for tuner effectiveness. The results are shown in Table 4-4. The data in Table 4-4 indicate that the worst error due to combining time windows occurs in the earliest window. Errors seem to get smaller in the later windows. However, the signal is much stronger in the first window and will contribute most toward the total energy. Table 4-5 shows the sum of the three windows as an estimate of the total energy.

This analysis shows that the separate time windows do not combine well at all frequencies. There is a particularly serious problem at 400 and 600 MHz. This is probably the result of inadequate mode-mixing. However, whatever its cause, the SE measurements at these frequencies may have larger than desirable errors. The results are better at 700 MHz and above. These results indicate that the error bounds for the cockpit shielding effectiveness measurements should be +2 dB and −4 dB.

4.4.3.5 Analysis of the Passenger Cabin Shielding Effectiveness Data. One set of main cabin data was tested for coherence and the results presented in Table 4-6.

In eight cases, the energy in the whole waveform is less than the sum of the energy in the two half-windows. The range of this difference is −0.4 dB to −8.6 dB. The seven cases where the energy in the whole waveform is greater than the sum of half-windows show a much smaller variation, +0.3 dB to +2.8 dB. This is in keeping with the variation caused by phase problems in the whole waveform. As the phase varies from 0° to 180°, the amplitude can vary from twice the voltage to none at all, or +6 dB to *−infinity* dB. There are no frequencies at which the difference is consistently less than 1.0 dB. Furthermore, the error remains about the same for the later windows as for the first one. This implies that the effectiveness of the tuner in the main cabin was not adequate for time domain data processing and implies limited confidence in results using this technique.

In order to assess the limits of error for these measurements, the above readings were combined to estimate the total energy in the interior of the aircraft. The results are shown in Table 4-7.

The data in Table 4-7 show a gradual improvement with increasing frequency. However, the error at 200 MHz is unacceptable and indicates that the data at this frequency will have to be summed as vector voltages. Given this one change, the limits of error can be expressed as +2 dB, −3 dB.

4.4.3.6 Shielding Effectiveness Results. The short pulse excitation SE data spans the frequency interval 0.1 to 1 GHz with ten data points that yield the SE averaged over an 80-MHz BW. The data are available for three aspect angles for the cockpit and passenger cabin.

Figures 4-146 and 4-147 show the aspect angle dependence of the SE for the cockpit for horizontally and vertically polarized illumination. The uncertainty in the cockpit data is +2 and −4 dB. The SE for horizontal polarization averages about 23 dB for 0° illumination. The aspect angle dependence is a few decibels. Within measurement uncertainty, the cockpit SE for vertical illumination has essentially the same magnitude, frequency-dependence, and aspect-angle dependence as for horizontal polarization.

The all-aspect-angle, both-polarization, minimum SE for the cockpit is about 18 dB.

Figures 4-148 and 4-149 show the SE for the passenger cabin. In this case, there is about a 5-dB aspect-angle dependence. As expected, due to effectiveness of window coupling and total aircraft body coupling, the passenger cabin SE is a minimum at 90° for horizontal polarization. The average SE for horizontal polarization is about 21 dB for 90° illumination. The SE for vertically polarized illumination is about 5 dB greater than for horizontal illumination, which is expected from the polarization mismatch to the largest aircraft dimension.

The all-aspect-angle, both-polarization, minimum SE for the passenger cabin is about 15 dB. The uncertainty in the passenger cabin data is +2 and −3 dB.

4.4.4 Comparison of Shielding Effectiveness Results

There are limited data sets where the ambient SE data and that obtained with direct illumination using BLWGN and short pulses overlap. For the cockpit, over the frequency interval 0.2 to 1 GHz, SE data obtained using all three techniques are available. For the passenger cabin, no ambient measurements were obtained and the BLWGN data set is incomplete in terms of aspect angle and polarization.

4.4.4.1 Comparison of Results for the Cockpit. Figure 4-150 shows cockpit SE data from all three excitation techniques. The curve is the minimum of the response averages of four RX antenna positions in the cockpit for each of six excitation conditions (three aspect angles and two polarizations) using 50-MHz BW BLWGN. The uncertainty of the average values is essentially independent of frequency and is approximately ±3 dB, as shown in the figure at 0.38 GHz.

The triangular markers show the minimum SE for short pulse excitation from three aspect angles and both polarizations. Based on the time domain analysis procedures, the estimated uncertainties are +2 dB and −4 dB. These values are also essentially independent of frequency. A representative error bar is shown at 0.7 GHz. The SE data derived from these two techniques agree within the uncertainty bounds.

The ambient measurements are shown by the + markers with typical error bars that are frequency-dependent. Only data from Figure 4-122 with a S/N ratio of >5 dB are shown. The SE values derived from the ambient EME have significantly greater scatter and generally larger uncertainty bounds than the other two techniques.

There are several possible explanations for the greater scatter in the ambient EME measurements. One is based on the measurement itself. For example, for some of the ambient emitters, there is an ambiguity in location and hence in the actual power density measured with a fixed, directional antenna. If the emitter were located out of the main beam of the log periodic antenna, the received power, and hence the reference for the SE calculation, would have an undetermined error.

However, the four data points between 0.62 and 0.645 GHz are deduced from TV emitters. These emitters have a high probability of being located within the beamwidth of the external log periodic antenna. Therefore, the correction factors and uncertainties of these measurements should be approximately the same. However, these measurements show a difference of almost 20 dB, which is outside the expected uncertainty bound. This difference suggests two possibilities: a fine structure in the cockpit SE or the effects of modal structure on the internal measurement.

The BLWGN was averaged over a 50-MHz BW, while the time domain analysis was averaged over a 80-MHz BW. The ambient measurement technique provides data over a 1.5-MHz BW, the frequency step size of the spectrum analyzers for the experimental setup. Thus the fine structure in the ambient data would not be expected in the data from the other two techniques.

A detailed investigation using an emitter-rich ambient EME with individual emitter locations characterized could help resolve this issue. A fourth technique, CW excitation with internal mechanical stirring could also provide fine structure SE data. In this case, ground-reflection problems in the reference signal would have to be addressed.

For the cockpit, BLWGN and short pulse excitation indicate the that cockpit SE is a minimum for 0° excitation. Excitation from 45° and 90° aspect angles result in a few decibels higher SE. These techniques yield approximately the same minimum SE for both horizontally and vertically polarized excitation.

For the cockpit, there is good agreement in the minimum SE values obtained with the three techniques. In most cases, the measurements from all three techniques lie within the uncertainty bounds. The BLWGN and short pulse excitation technique that yield average SE values show a relatively constant, minimum SE of 15 ± 5 dB over the frequency range 0.2 to 1 GHz. The ambient EME data suggest the possibility of fine structure in the cockpit SE. In several windows, the SE could be as low as a few decibels.

4.4.4.2 Comparison of Results for the Passenger Cabin. Figure 4-151 shows data for both BLWGN and short pulse excitation of the passenger cabin. The curve is the minimum of the averages of all the available BLWGN data. The square markers show the minimum of all the short pulse data. These data agree within the estimated uncertainty bounds.

Both excitation techniques yield a slightly greater SE for vertically polarized illumination.

A nominal range for the minimum passenger cabin SE over the frequency range 0.1 to 1 GHz is 18 to 20 dB with a ±5 dB uncertainty.

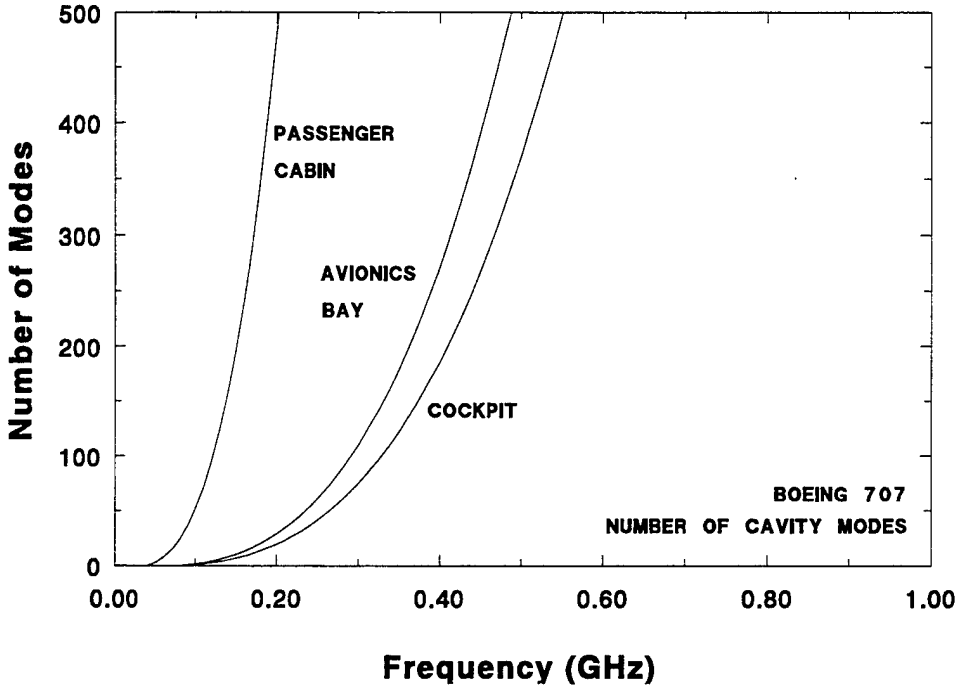

FIGURE 4-1. ESTIMATED NUMBER OF MODES IN B-707 CAVITIES

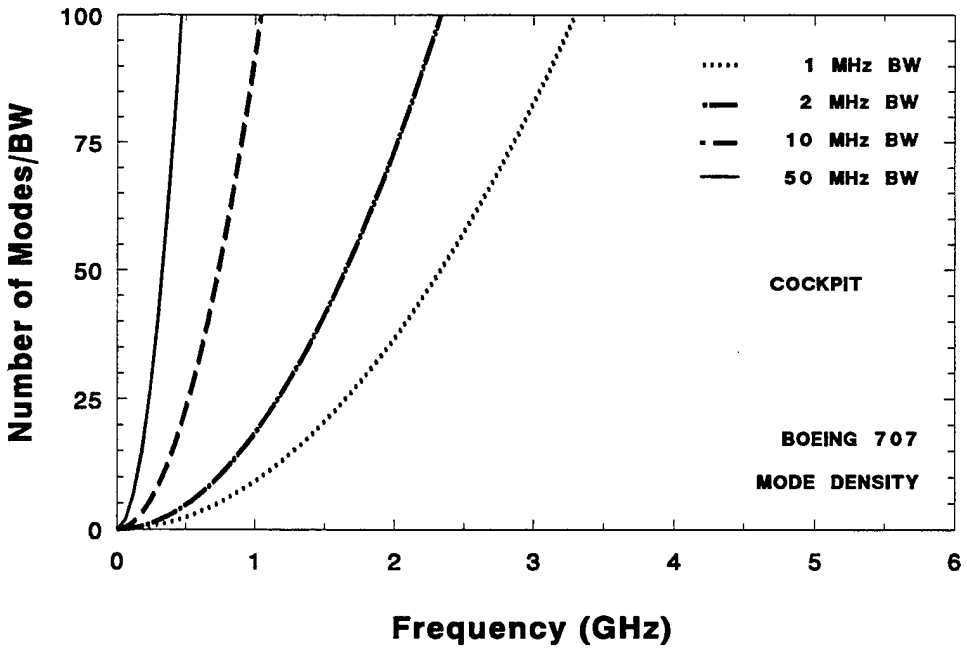

FIGURE 4-2. ESTIMATED MODE DENSITY IN B-707 COCKPIT FOR SEVERAL BANDWIDTHS

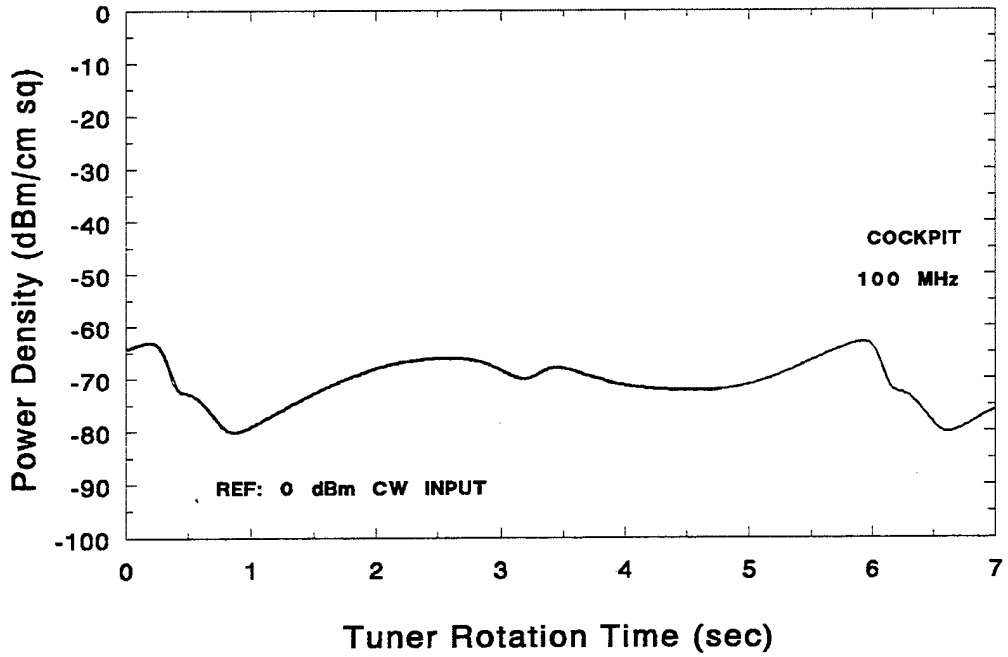

FIGURE 4-3. COCKPIT DISCRETE FREQUENCY DATA AT 100 MHz

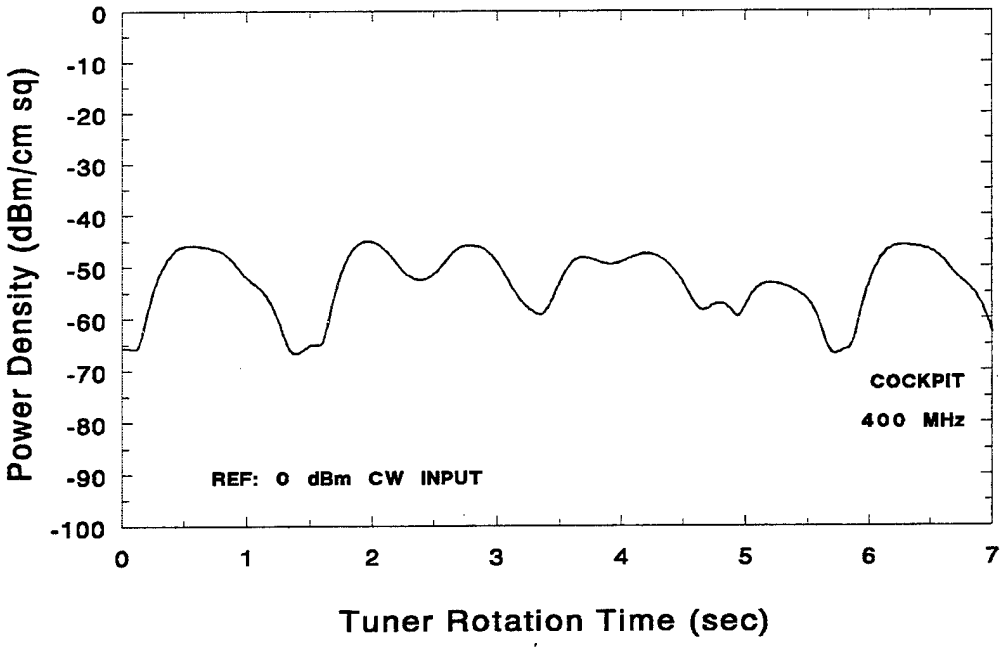

FIGURE 4-4. COCKPIT DISCRETE FREQUENCY DATA AT 400 MHz

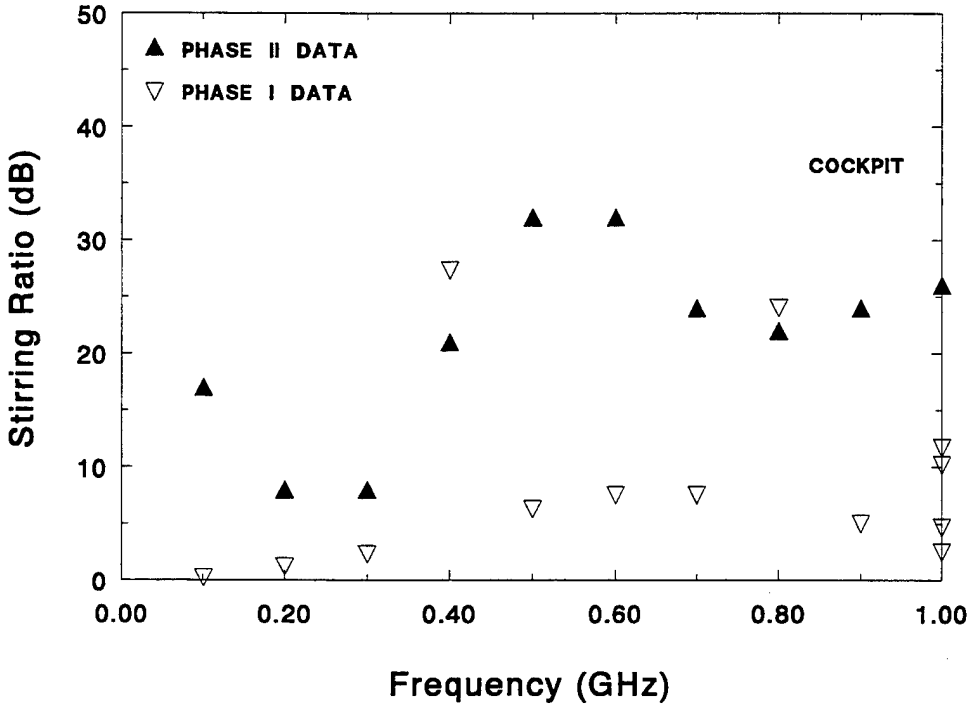

FIGURE 4-5. PHASE I/II COCKPIT STIRRING RATIO DATA

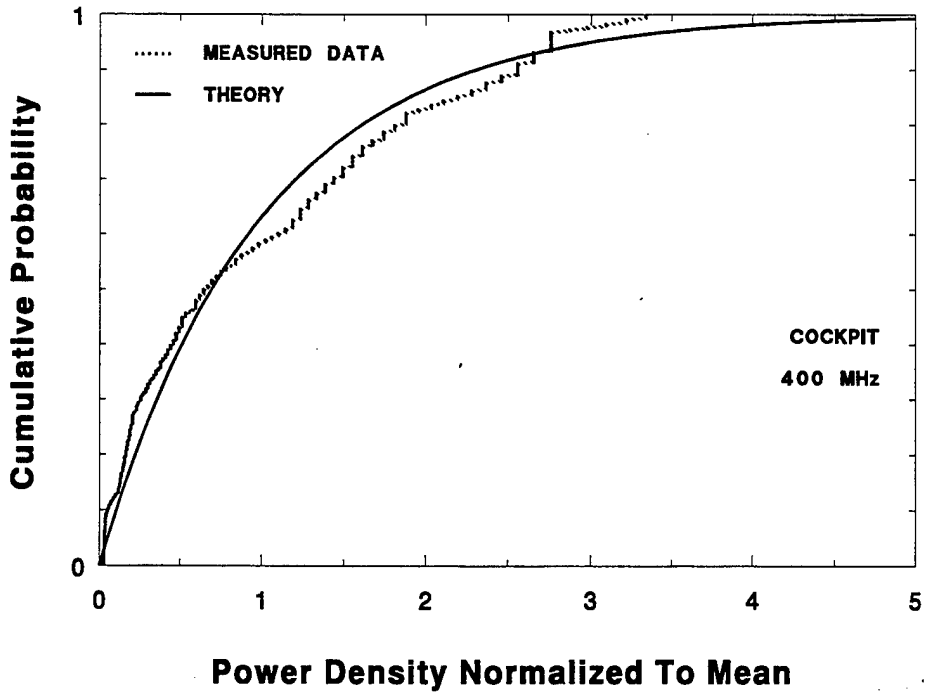

FIGURE 4-6. MEASURED AND THEORETICAL DISTRIBUTION FUNCTIONS IN COCKPIT AT 400 MHz

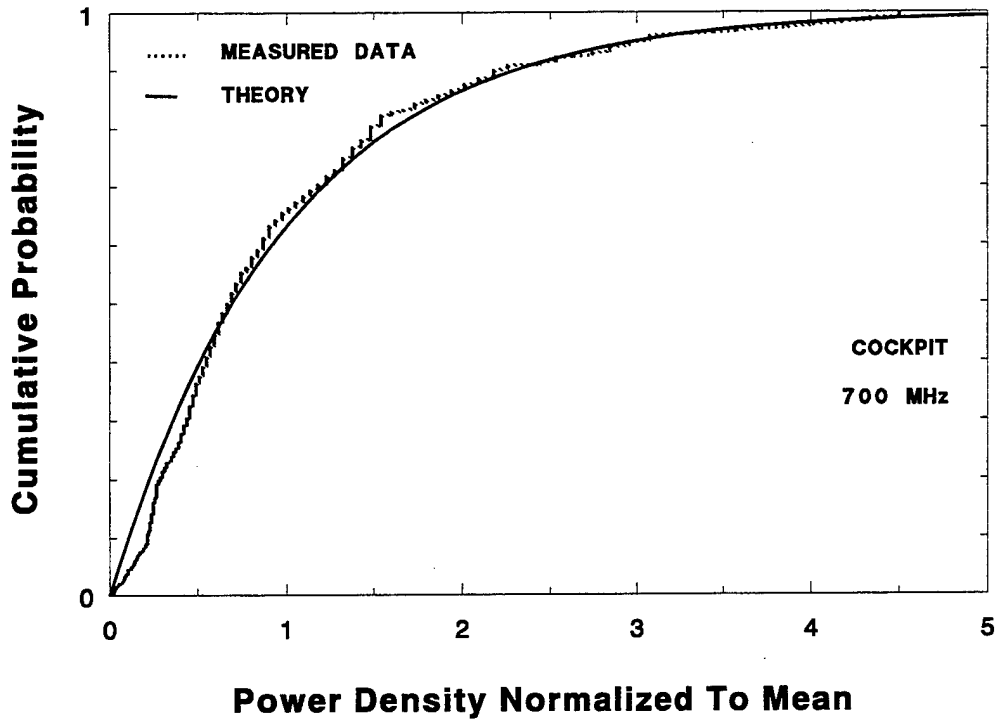

FIGURE 4-7. MEASURED AND THEORETICAL DISTRIBUTION FUNCTIONS IN COCKPIT AT 700 MHz

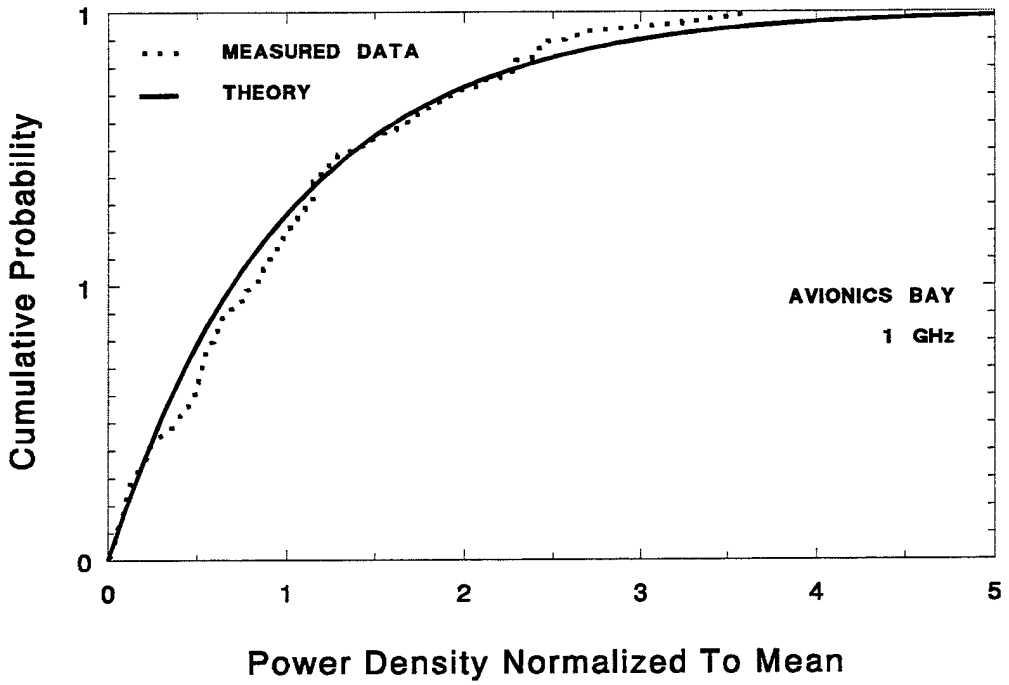

FIGURE 4-8. MEASURED AND THEORETICAL DISTRIBUTION FUNCTIONS IN AVIONICS BAY AT 1 GHz

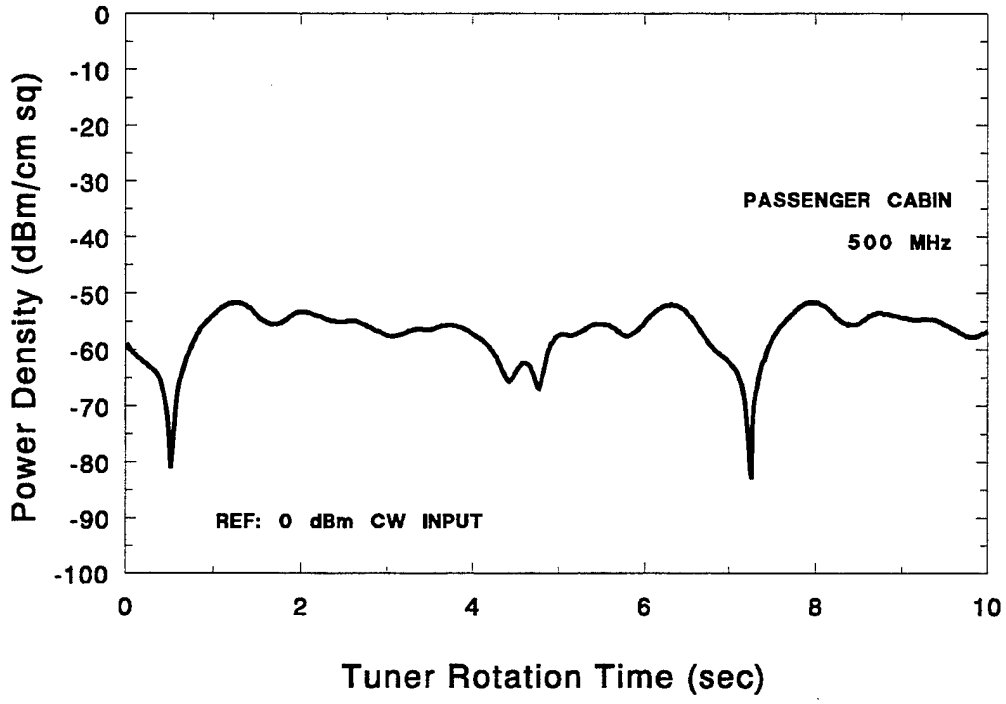

FIGURE 4-9. PASSENGER CABIN DISCRETE FREQUENCY DATA AT 500 MHz

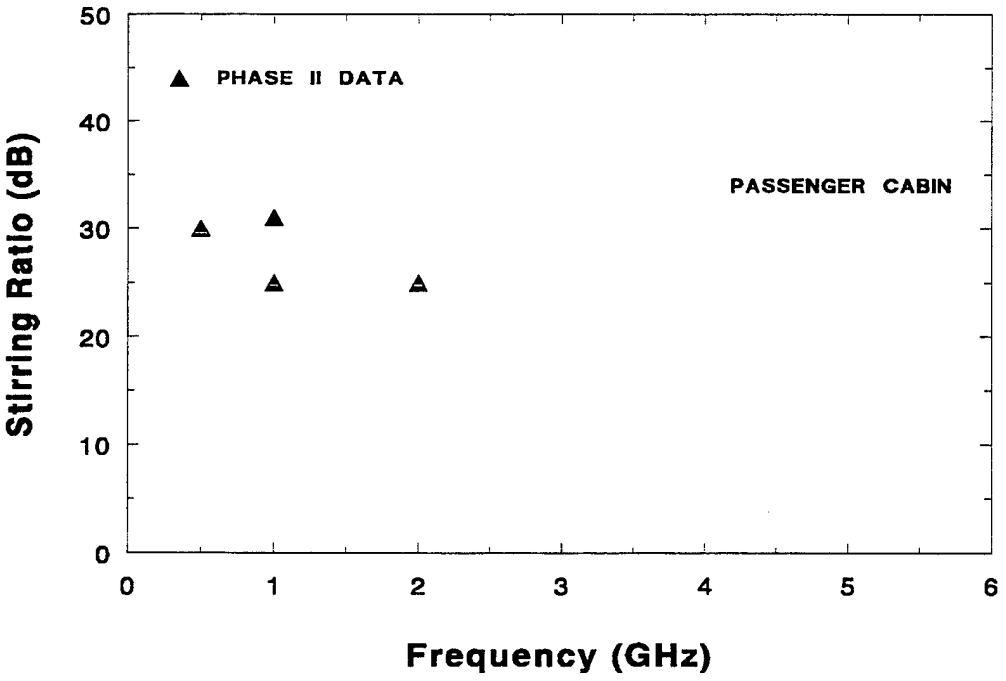

FIGURE 4-10. PASSENGER CABIN STIRRING RATIO DATA

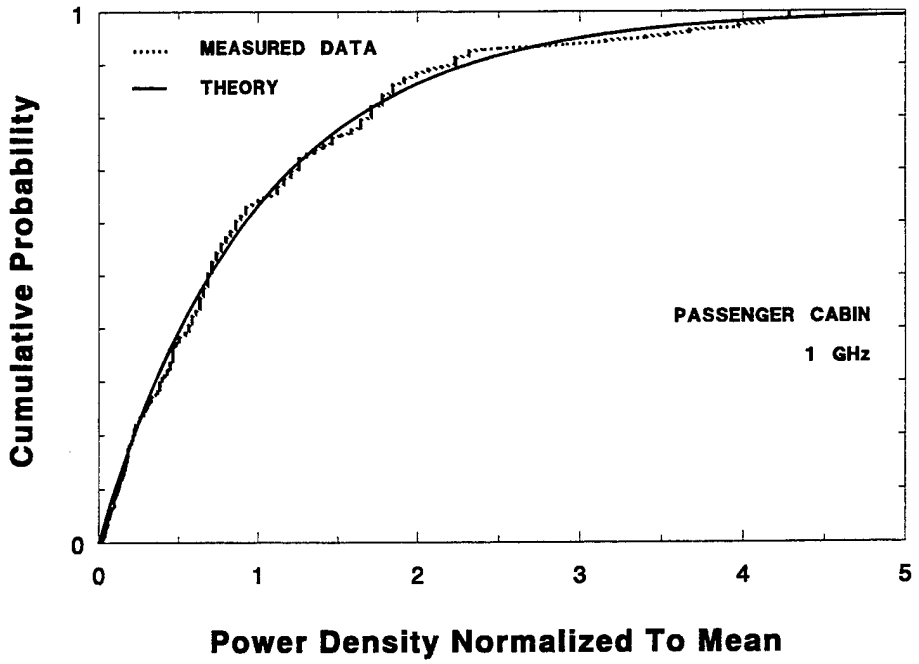

FIGURE 4-11. MEASURED AND THEORETICAL DISTRIBUTION FUNCTIONS IN PASSENGER CABIN AT 1 GHz

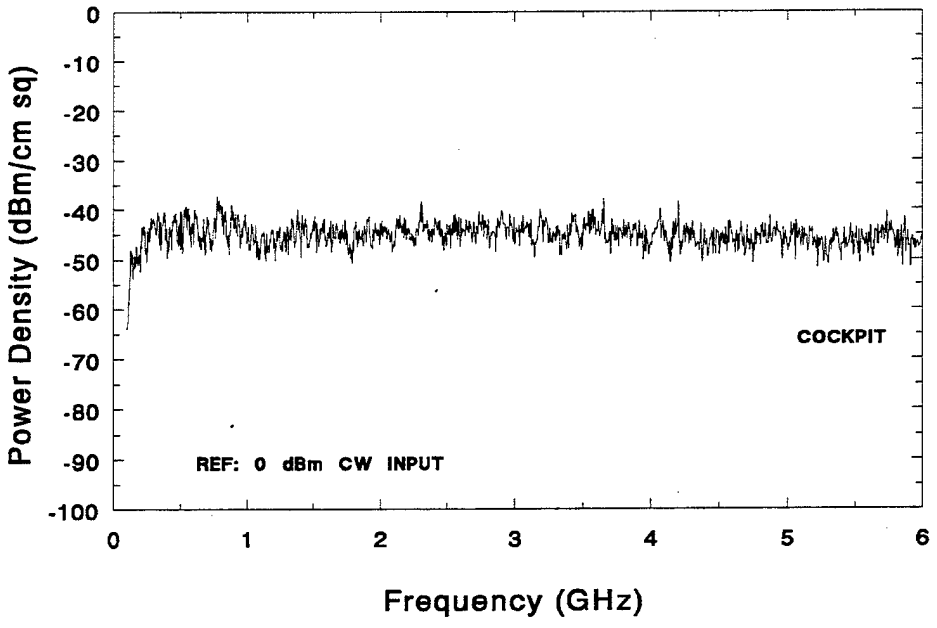

FIGURE 4-12. COCKPIT 0.1 – 6 GHz POWER DENSITY FOR CW EXCITATION

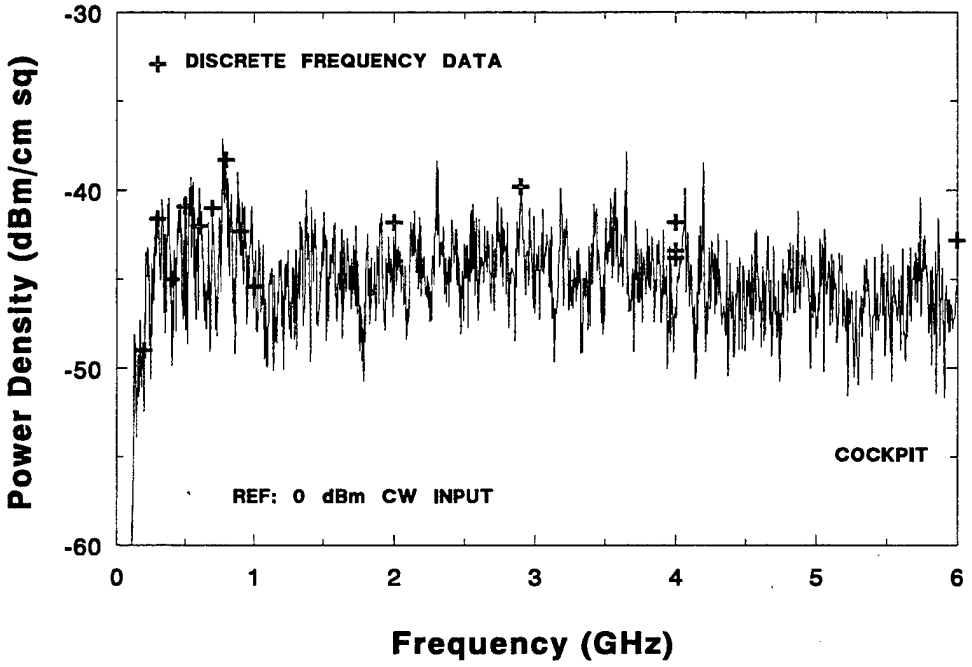

FIGURE 4-13. COMPARISON OF COCKPIT DISCRETE AND SWEPT FREQUENCY POWER DENSITY FOR CW EXCITATION

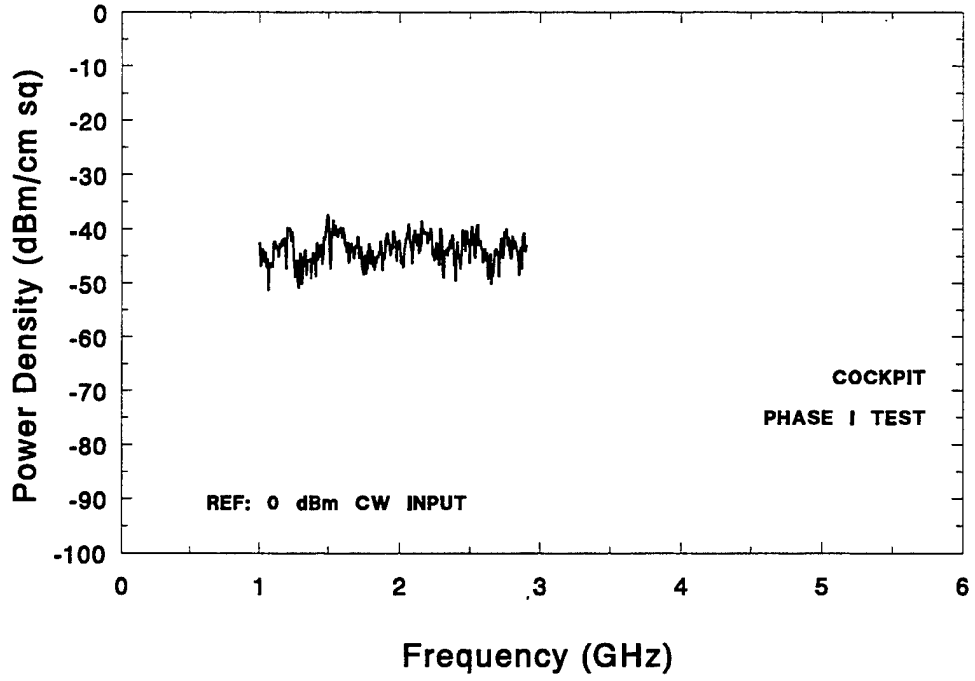

FIGURE 4-14. COCKPIT PHASE I POWER DENSITY FOR CW EXCITATION

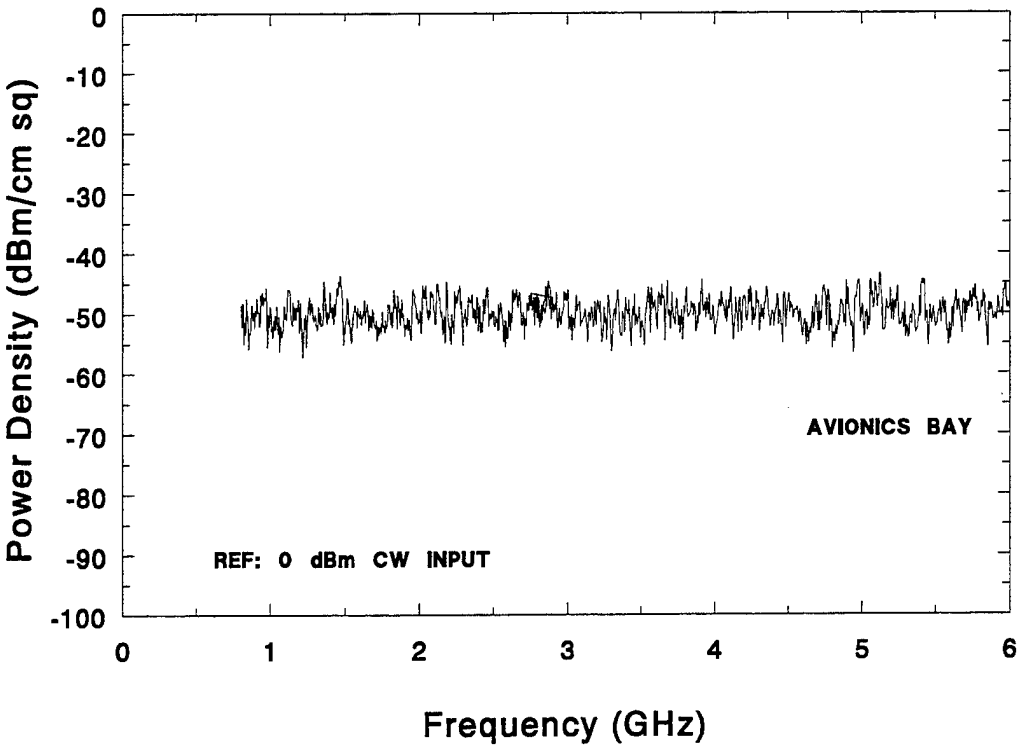

FIGURE 4-15. AVIONICS BAY 1 – 6 GHz POWER DENSITY FOR CW EXCITATION

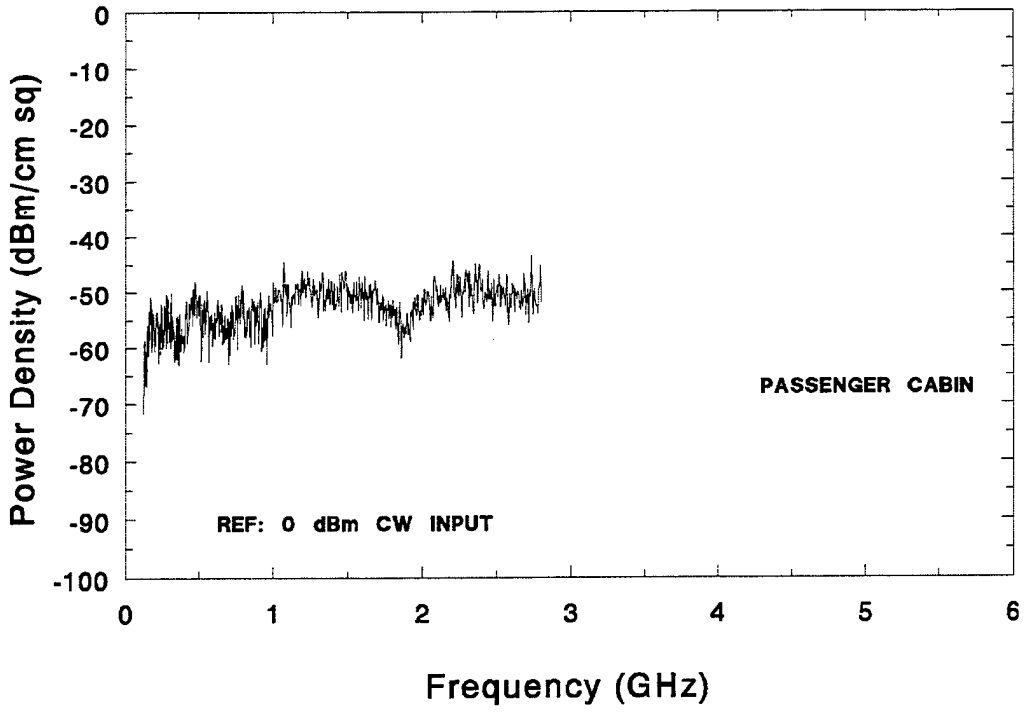

FIGURE 4-16. PASSENGER CABIN 0.1 – 2.9 GHz POWER DENSITY FOR CW EXCITATION

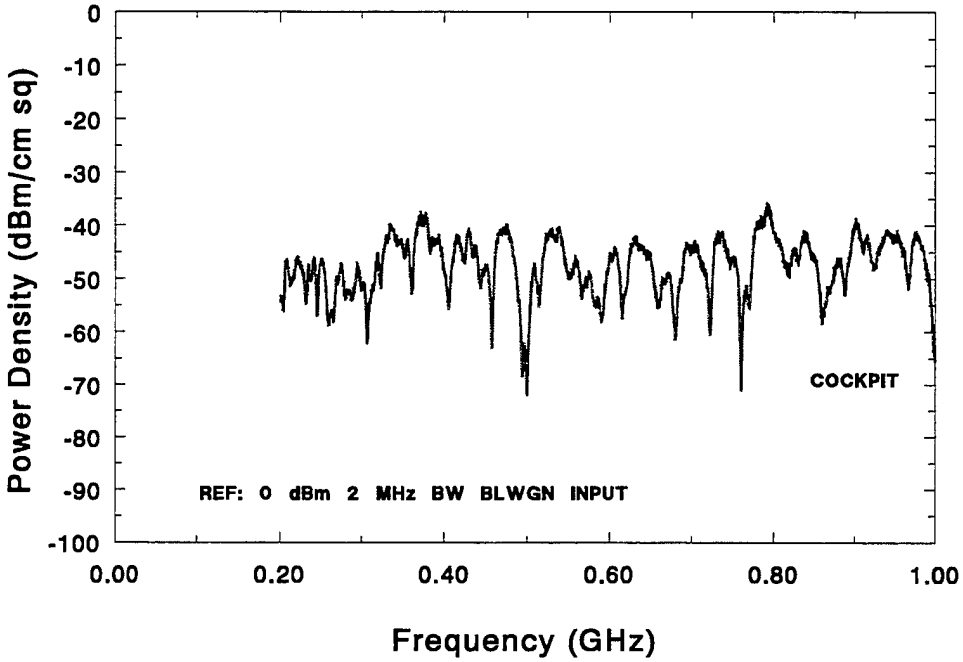

FIGURE 4-17. COCKPIT 0.2 – 1 GHz POWER DENSITY FOR 2-MHz BW BLWGN EXCITATION

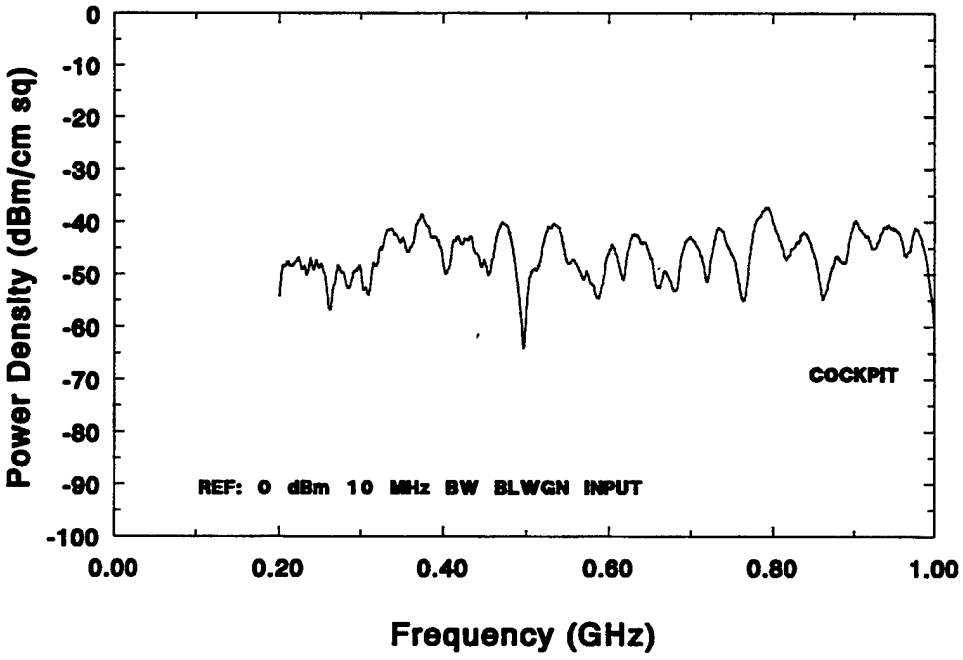

FIGURE 4-18. COCKPIT 0.2 – 1 GHz POWER DENSITY FOR 10-MHz BW BLWGN EXCITATION

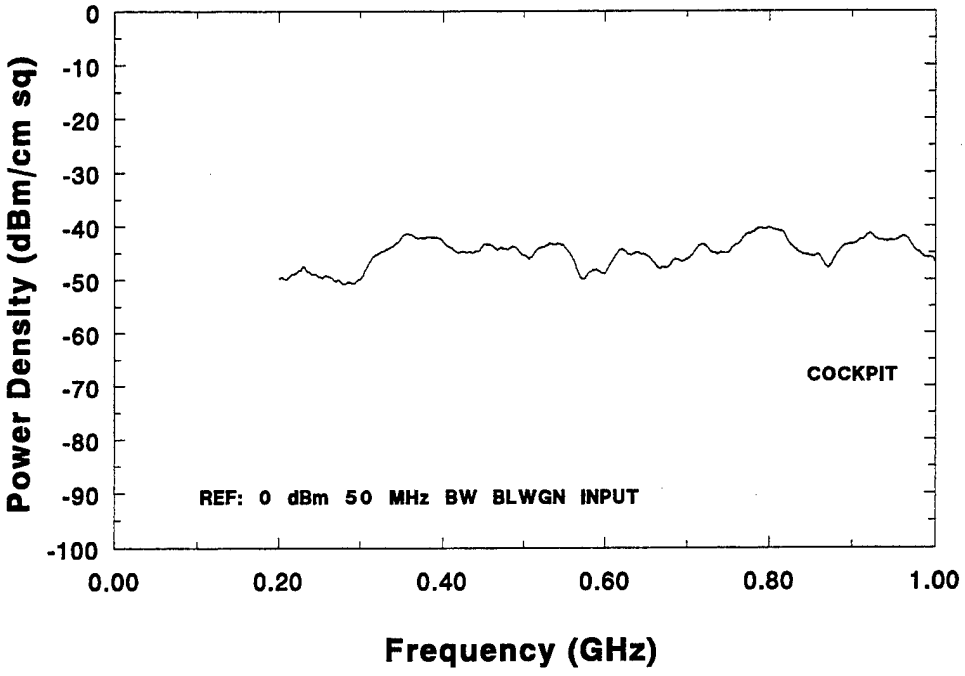

FIGURE 4-19. COCKPIT 0.2 – 1 GHz POWER DENSITY FOR 50-MHz BW BLWGN EXCITATION

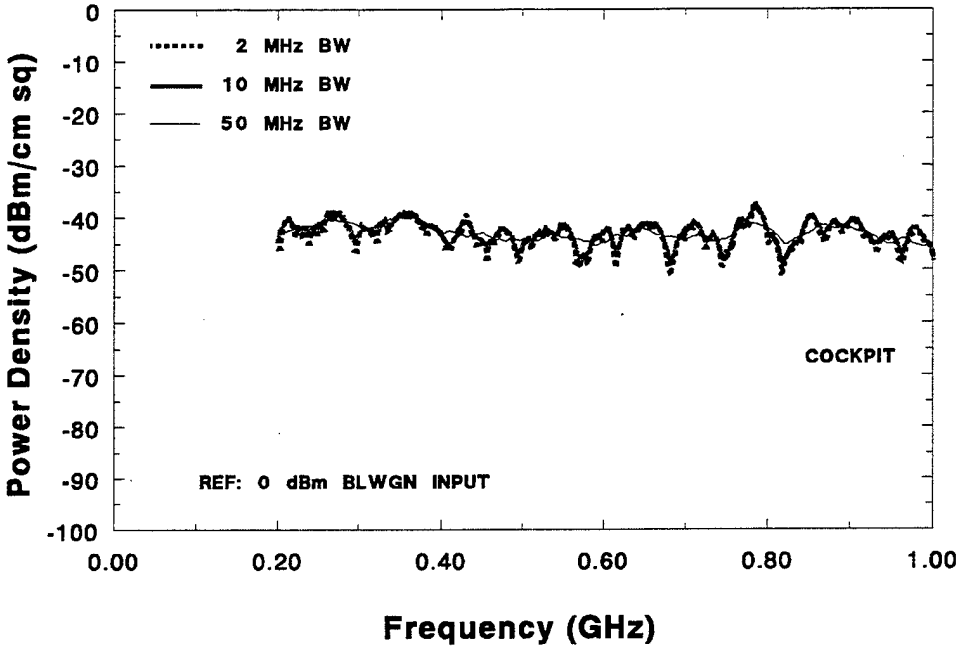

FIGURE 4-20. FOUR POSITION AVERAGE COCKPIT POWER DENSITIES FOR 2-, 10-, AND 50-MHz BWs BLWGN EXCITATION OVER 0.2 – 1 GHz

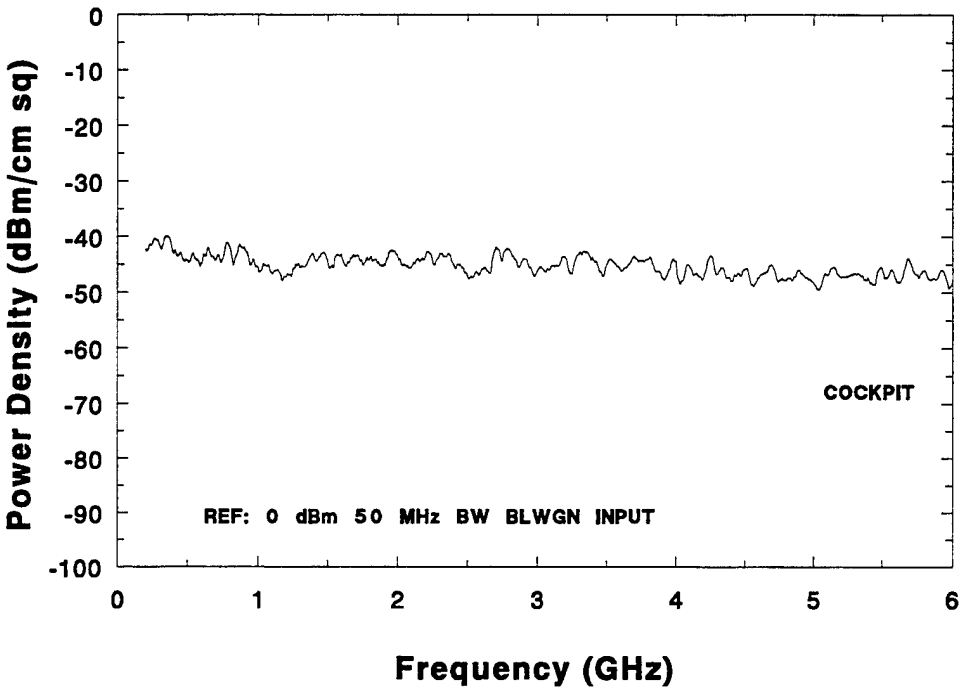

FIGURE 4-21. COCKPIT 0.2 – 6 GHz POWER DENSITY FOR 50-MHz BLWGN EXCITATION

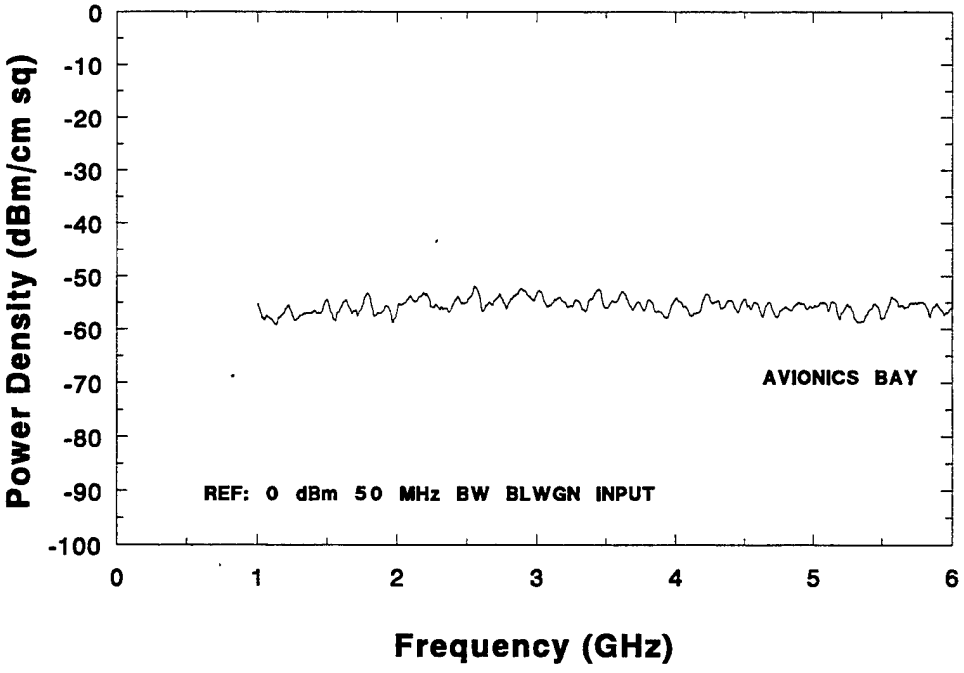

FIGURE 4-22. AVIONICS BAY 1 – 6 GHz POWER DENSITY FOR 50-MHz BLWGN EXCITATION

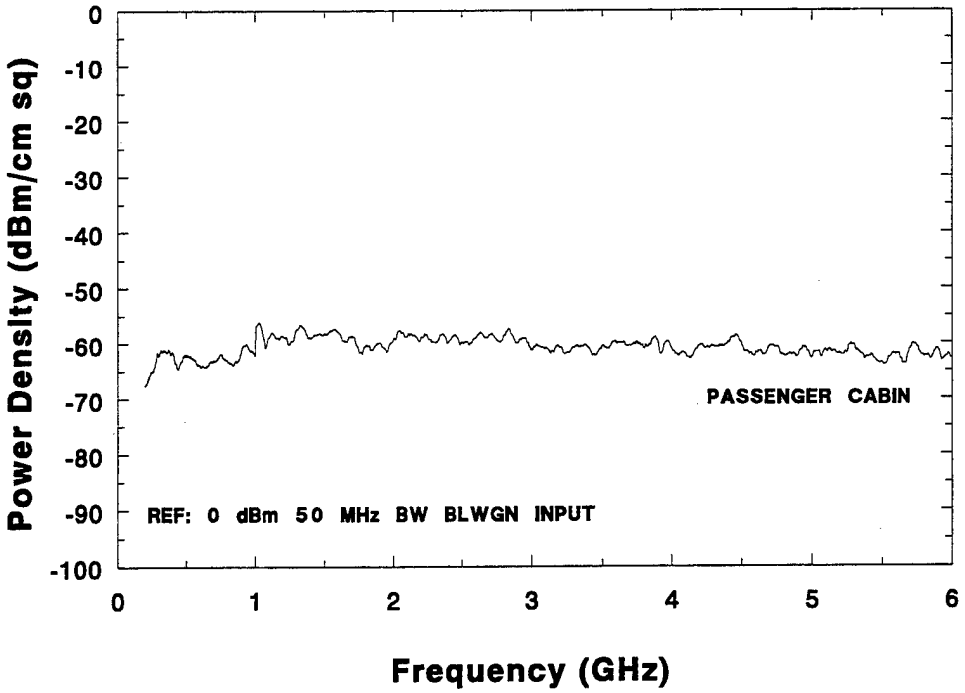

FIGURE 4-23. PASSENGER CABIN 0.2 – 6 GHz POWER DENSITY FOR 50-MHz BLWGN EXCITATION

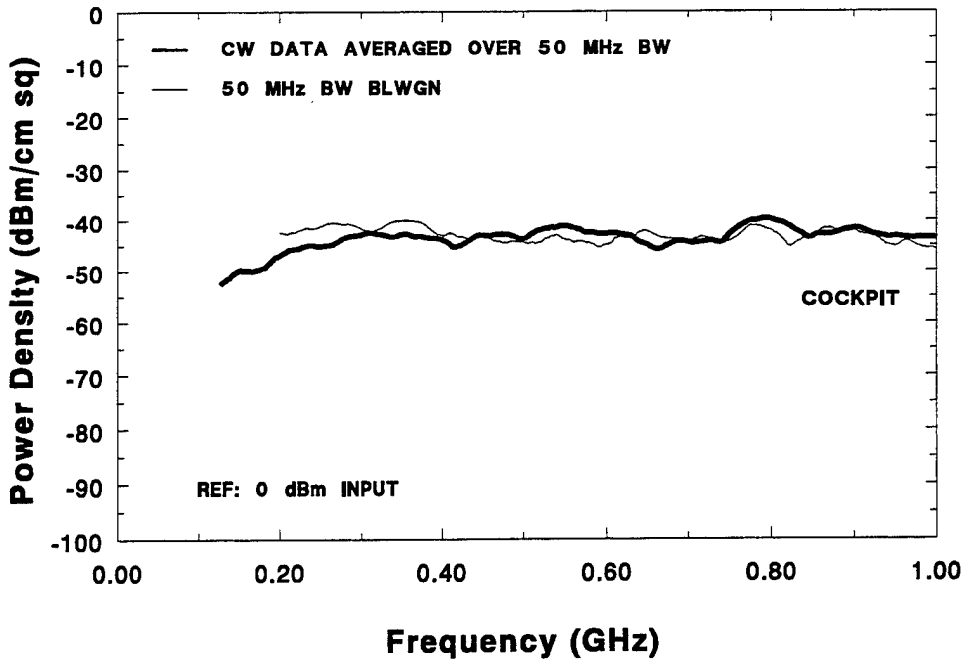

FIGURE 4-24. COMPARISON OF 50-MHz BW AVERAGED CW AND BLWGN POWER DENSITIES

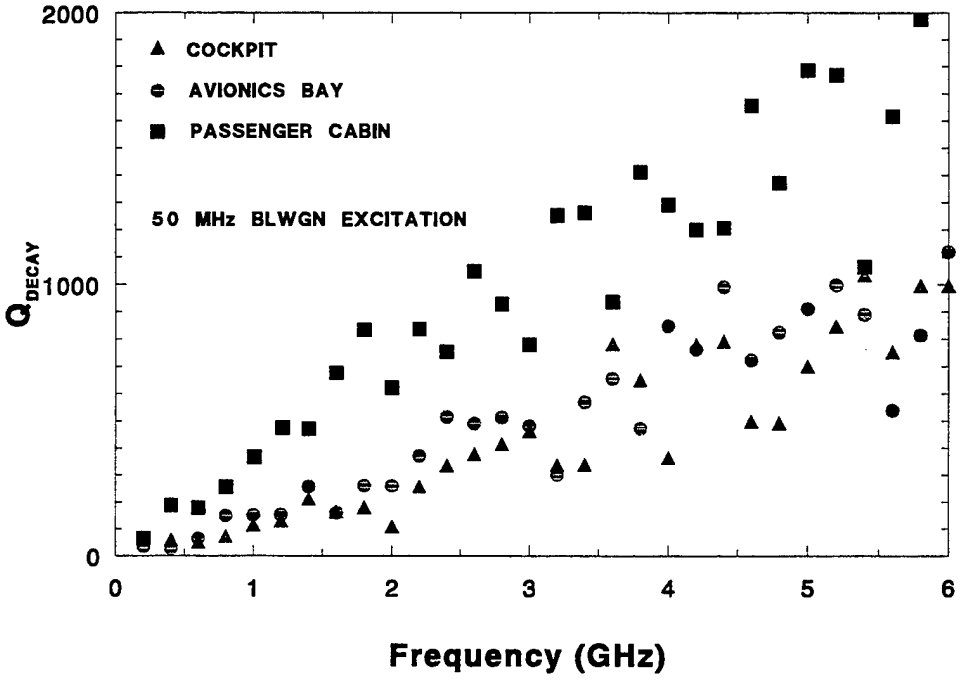

FIGURE 4-25. DECAY TIME QUALITY FACTOR FROM BLWGN EXCITATION

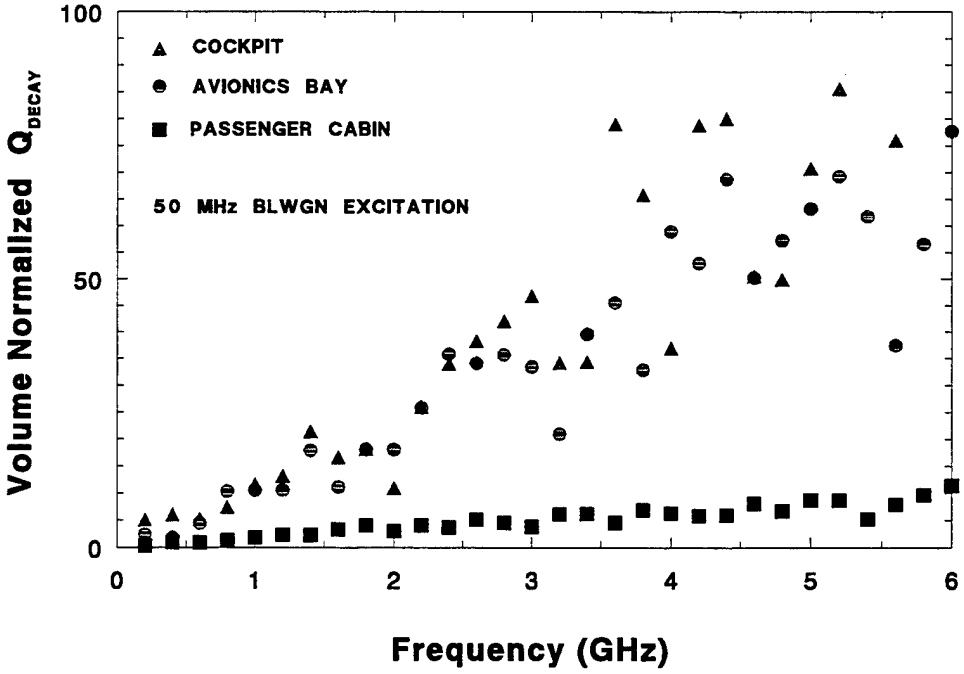

FIGURE 4-26. VOLUME NORMALIZED DECAY TIME QUALITY FACTOR FROM BLWGN EXCITATION

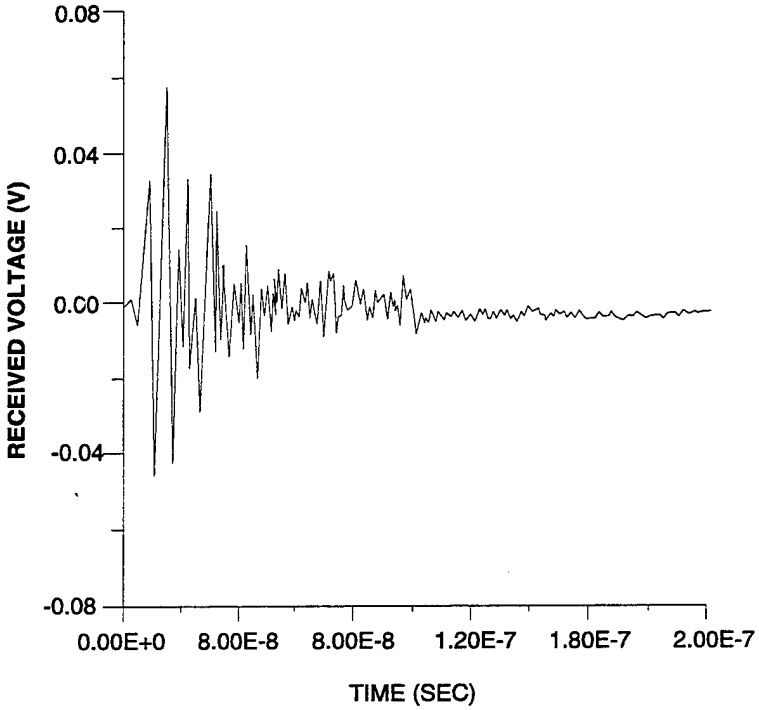

FIGURE 4-27. COCKPIT TIME DOMAIN RESPONSE FROM SHORT PULSE EXCITATION

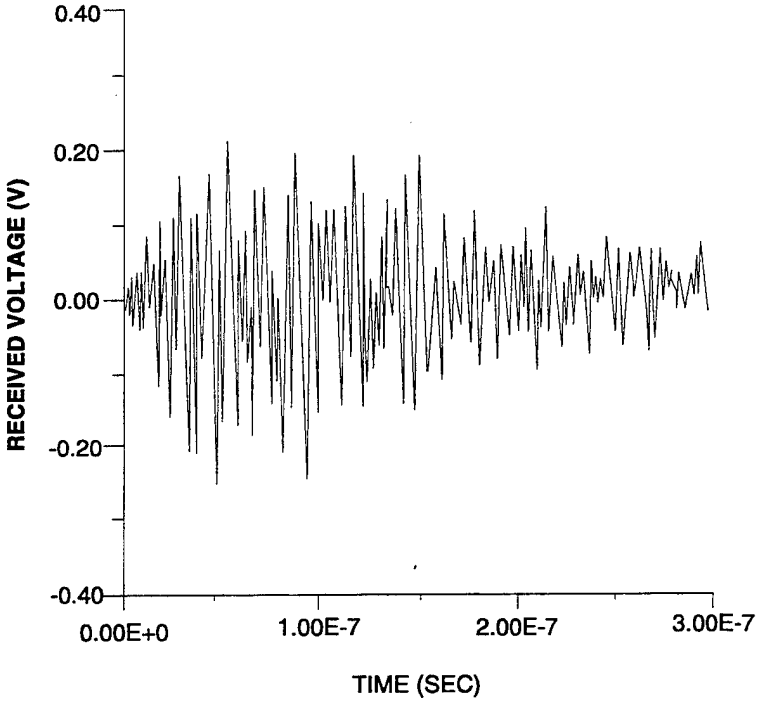

FIGURE 4-28. PASSENGER CABIN TIME DOMAIN RESPONSE FROM SHORT PULSE EXCITATION

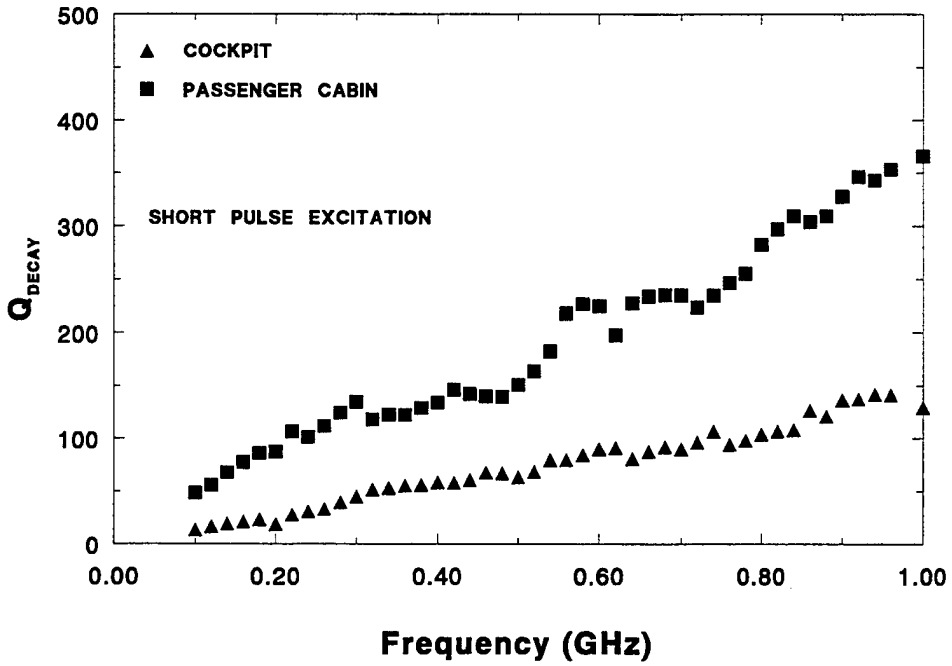

FIGURE 4-29. DECAY TIME QUALITY FACTOR FROM SHORT PULSE EXCITATION

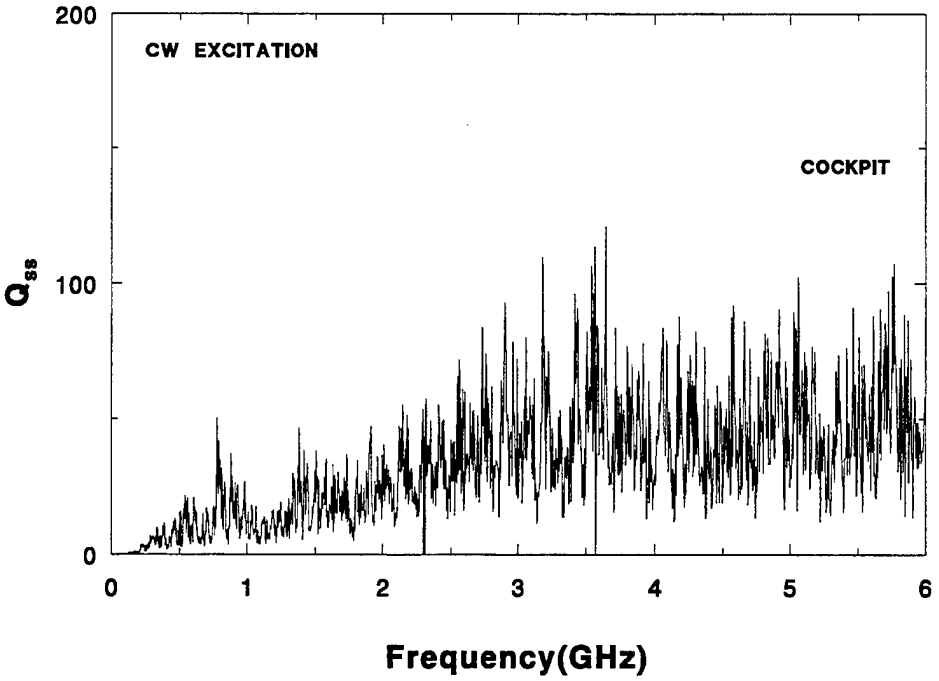

FIGURE 4-30. COCKPIT STEADY STATE QUALITY FACTOR FROM CW EXCITATION

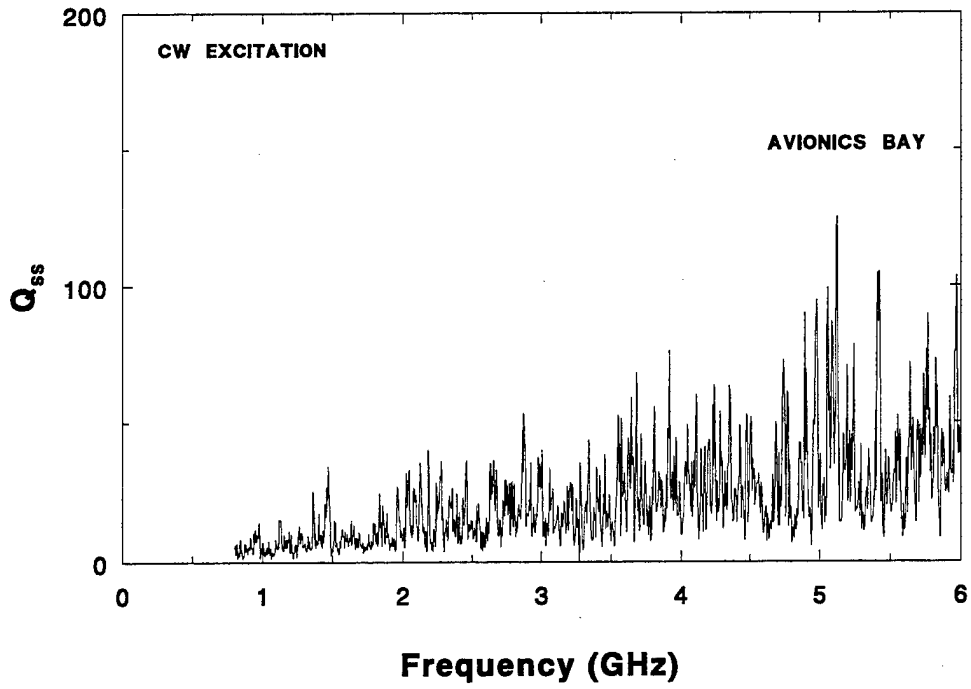

FIGURE 4-31. AVIONICS BAY STEADY STATE QUALITY FACTOR FROM CW EXCITATION

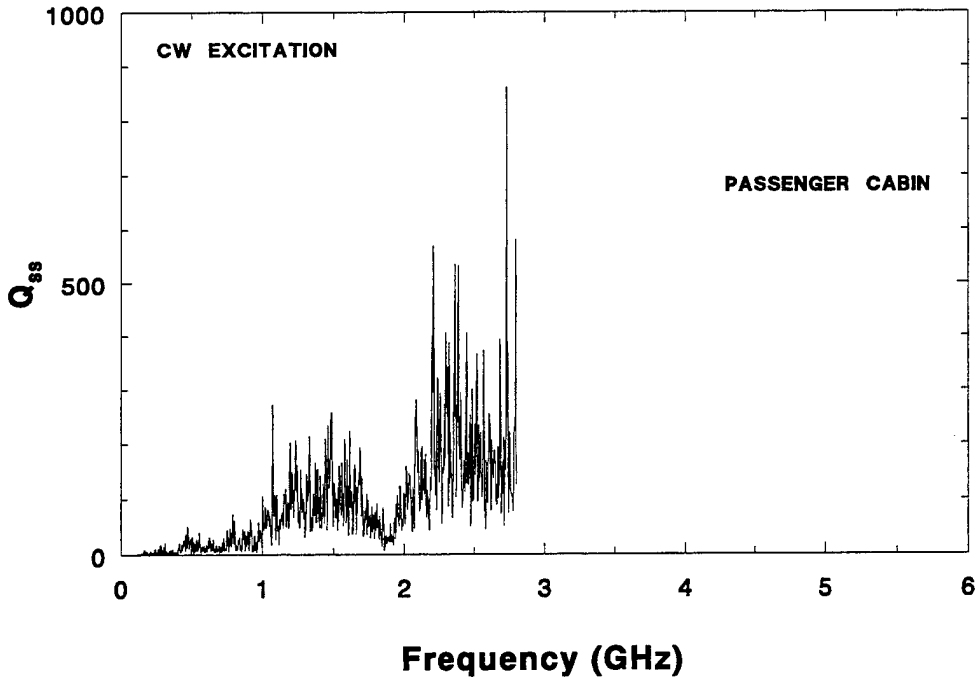

FIGURE 4-32. PASSENGER CABIN STEADY STATE QUALITY FACTOR FROM CW EXCITATION

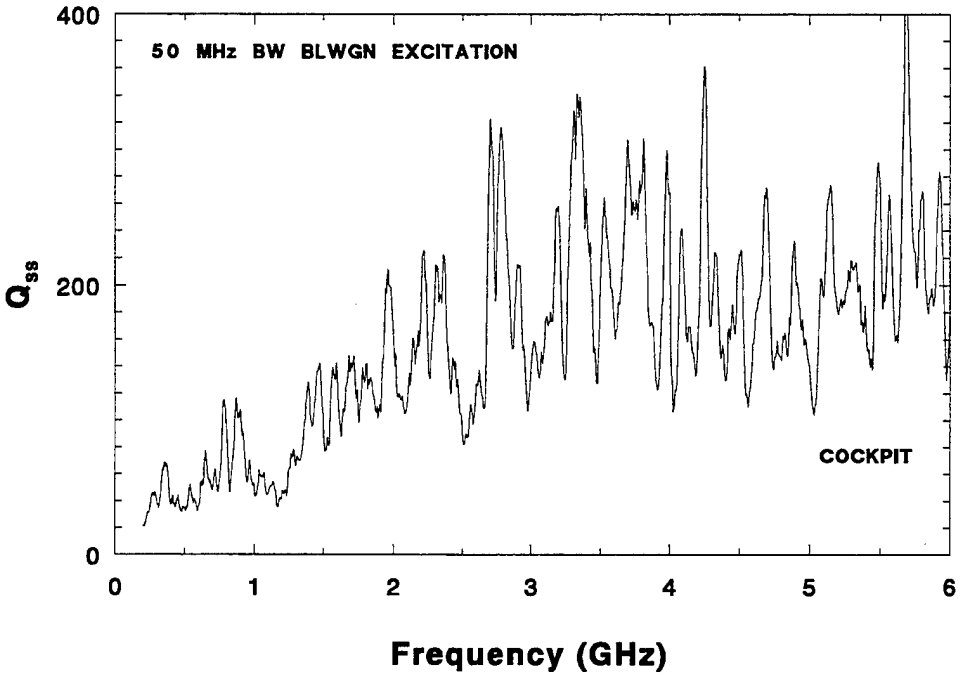

FIGURE 4-33. COCKPIT STEADY STATE QUALITY FACTOR FROM 50-MHz BW BLWGN EXCITATION

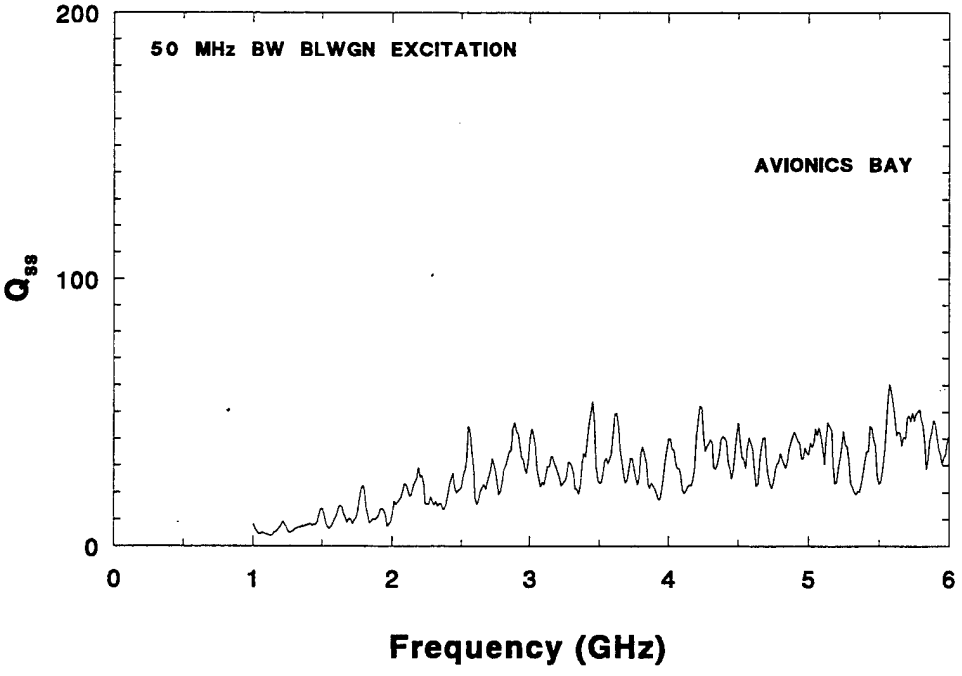

FIGURE 4-34. AVIONICS BAY STEADY STATE QUALITY FACTOR FROM 50-MHz BW BLWGN EXCITATION

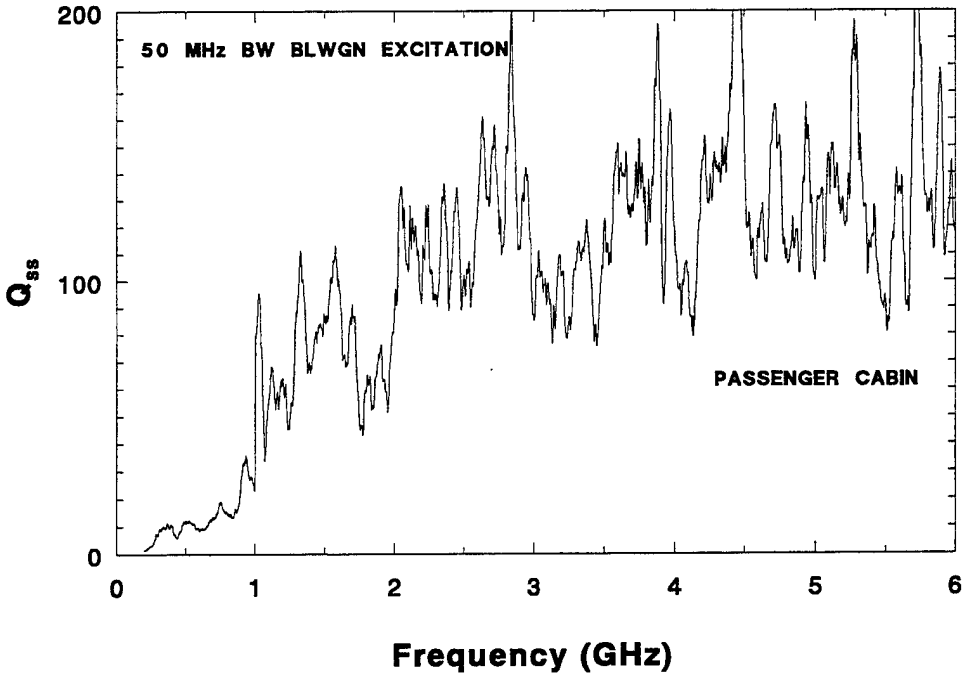

FIGURE 4-35. PASSENGER CABIN STEADY STATE QUALITY FACTOR FROM 50-MHz BW BLWGN EXCITATION

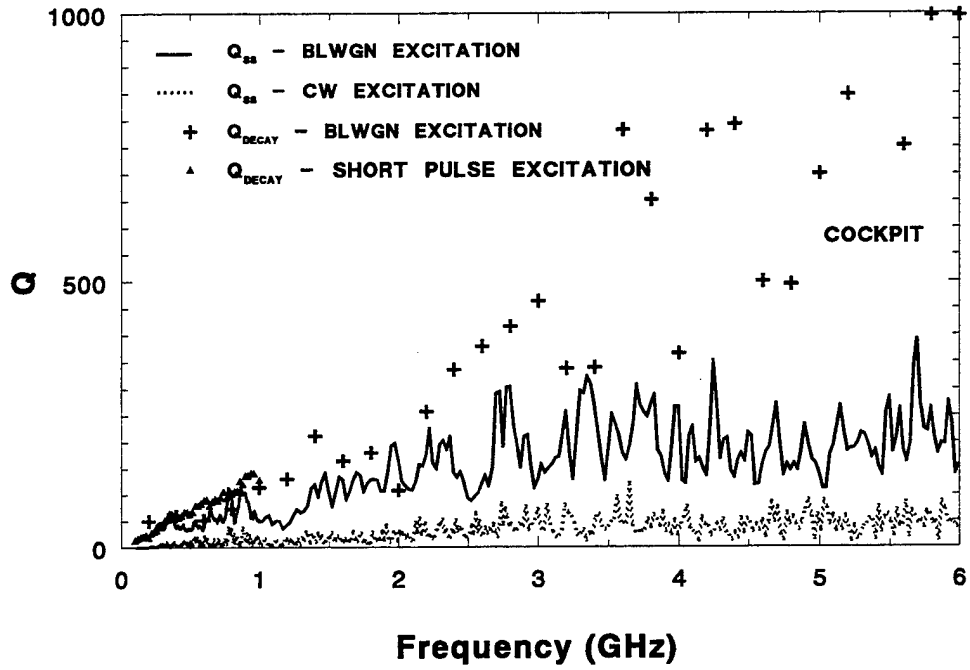

FIGURE 4-36. COCKPIT QUALITY FACTOR COMPARISONS

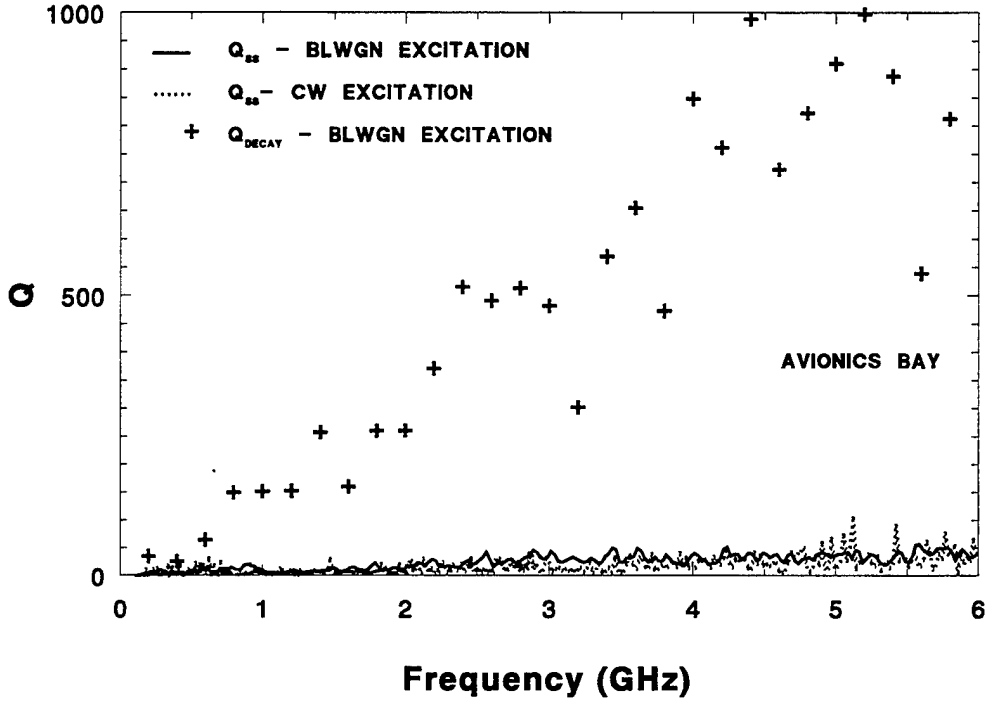

FIGURE 4-37. AVIONICS BAY QUALITY FACTOR COMPARISONS

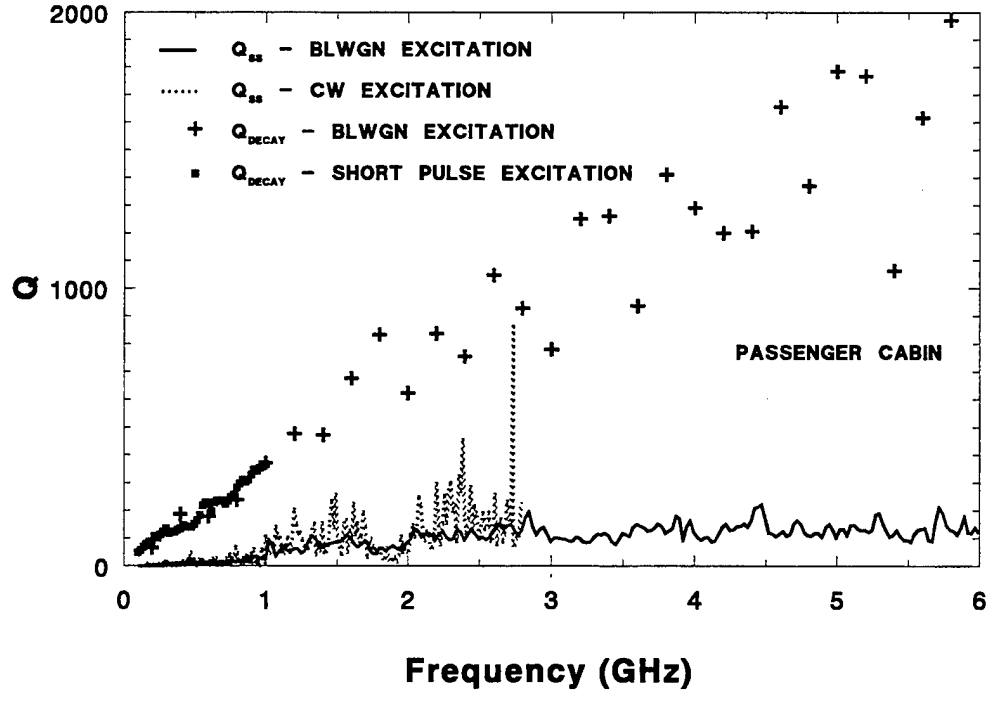

FIGURE 4-38. PASSENGER CABIN QUALITY FACTOR COMPARISONS

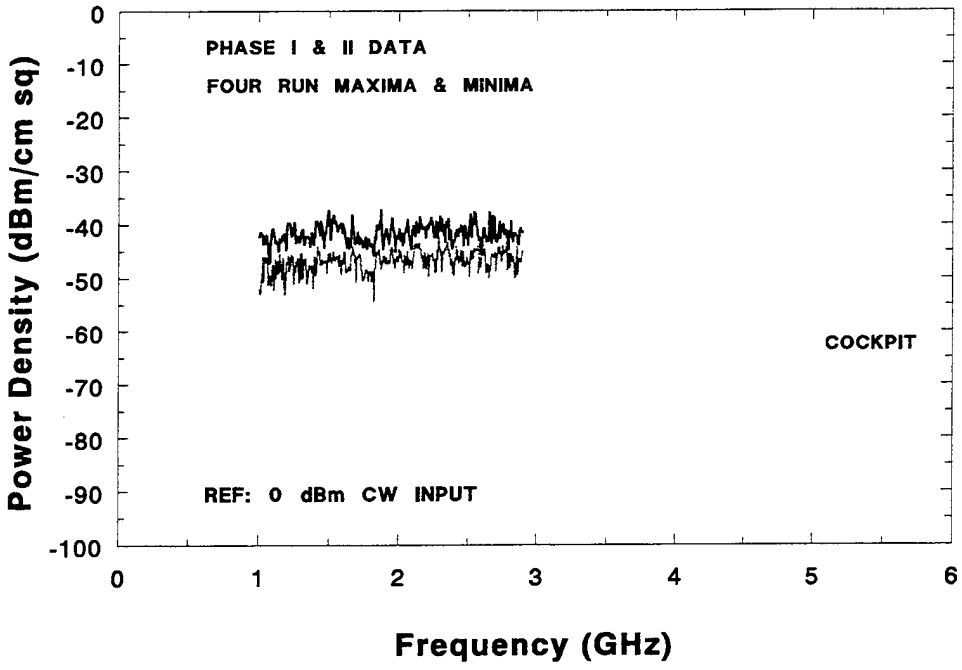

FIGURE 4-39. MAXIMUM AND MINIMUM POWER DENSITY VARIATIONS IN COCKPIT FOR CW EXCITATION

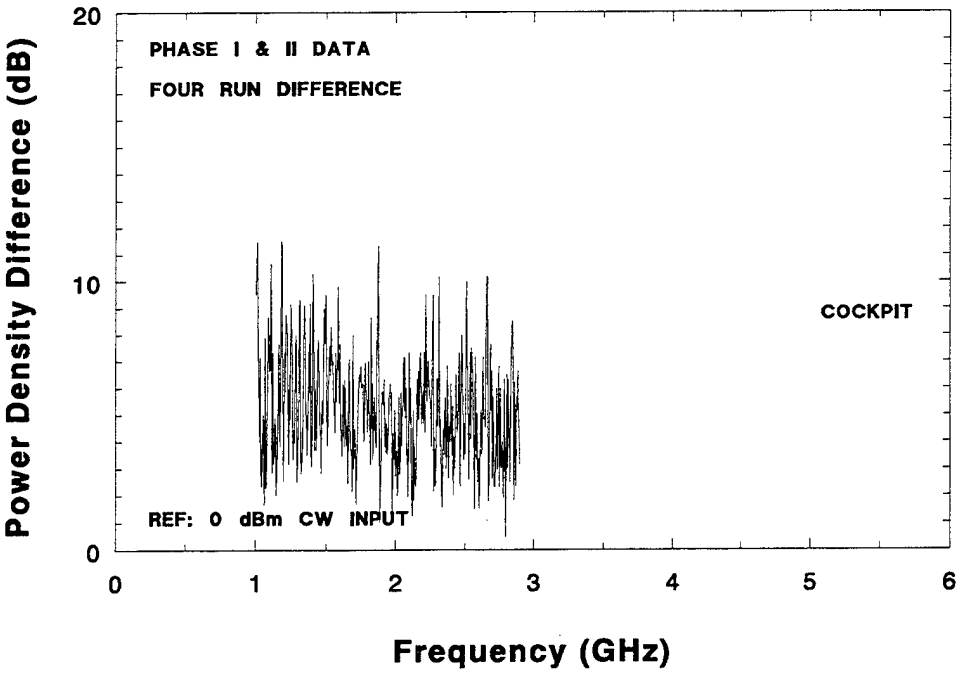

FIGURE 4-40. POWER DENSITY DIFFERENCES IN COCKPIT FOR CW EXCITATION

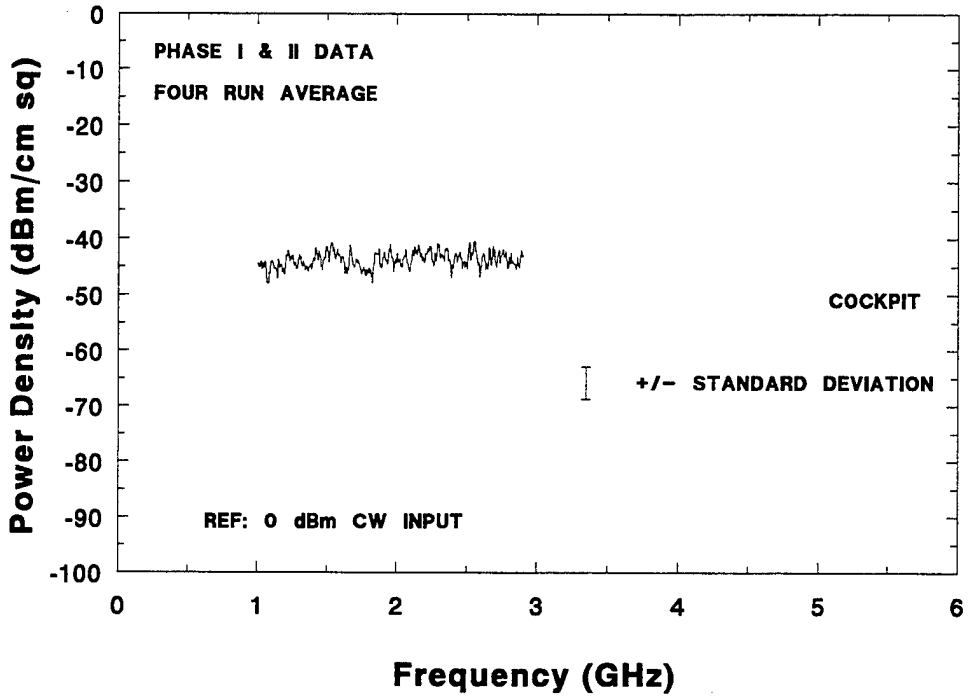

FIGURE 4-41. AVERAGE POWER DENSITY AND STANDARD DEVIATION IN COCKPIT FOR CW EXCITATION

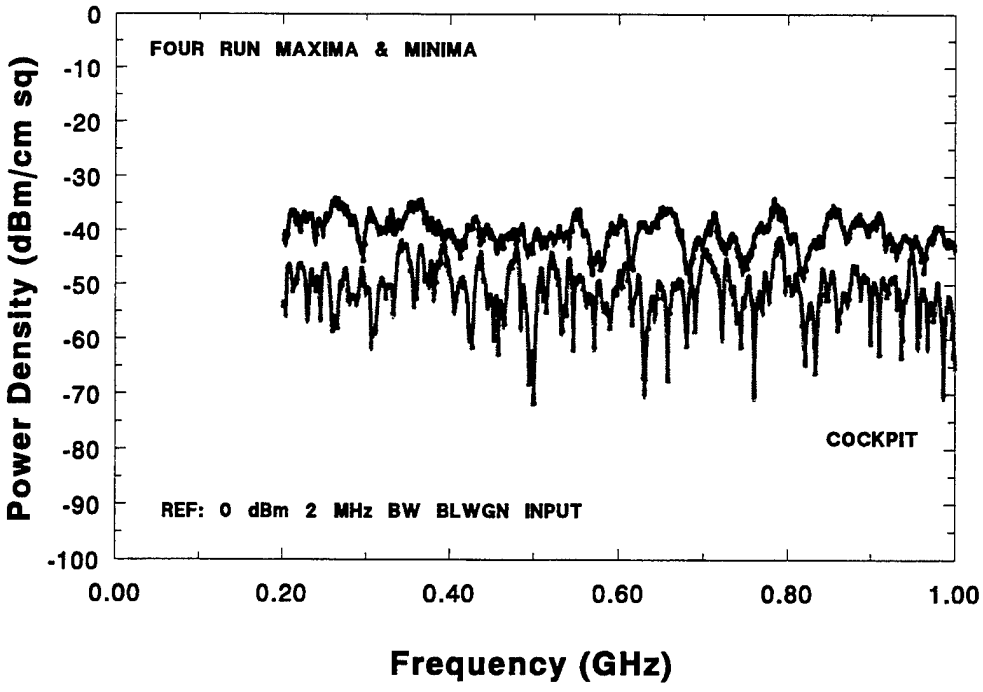

FIGURE 4-42. MAXIMUM AND MINIMUM POWER DENSITY VARIATIONS IN COCKPIT FOR 2-MHz BW BLWGN EXCITATION OVER 0.2 – 1 GHz

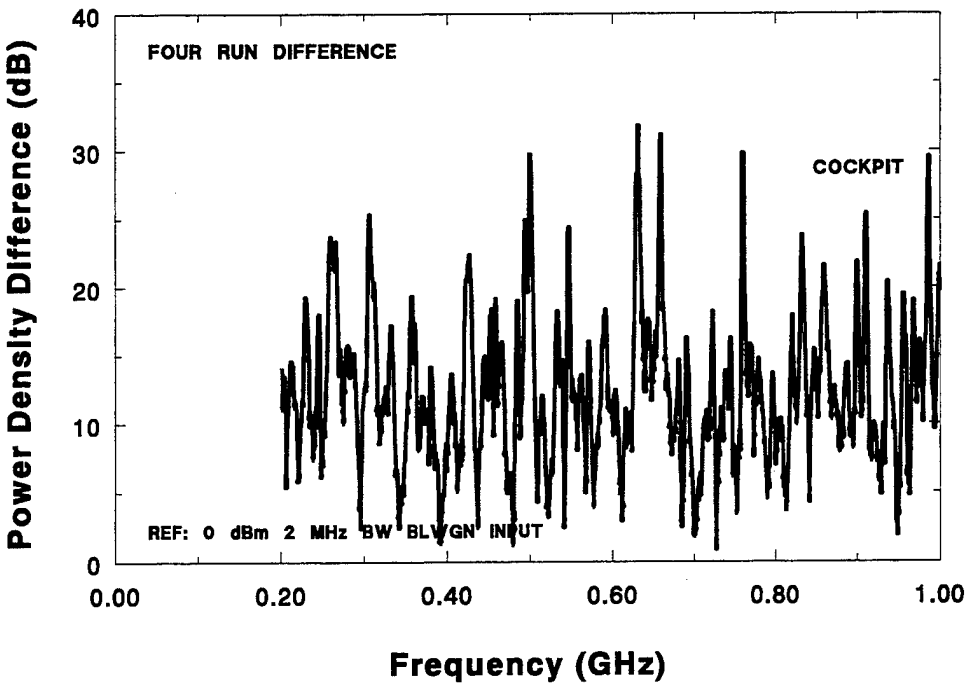

FIGURE 4-43. POWER DENSITY DIFFERENCES IN COCKPIT FOR 2-MHz BW BLWGN EXCITATION OVER 0.2 – 1 GHz

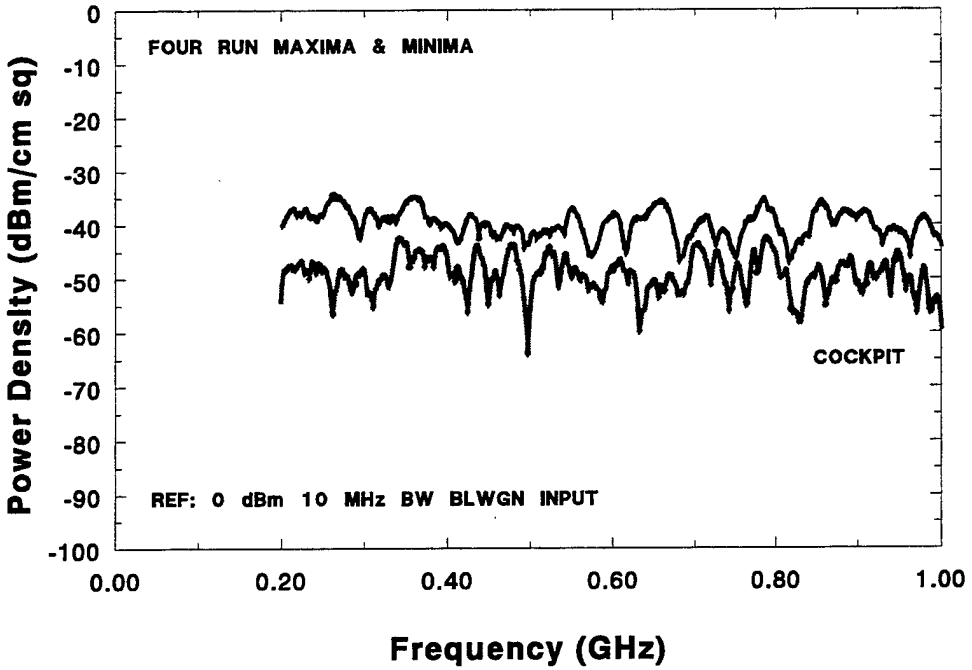

FIGURE 4-44. MAXIMUM AND MINIMUM POWER DENSITY VARIATIONS IN COCKPIT FOR 10-MHz BW BLWGN EXCITATION OVER 0.2 – 1 GHz

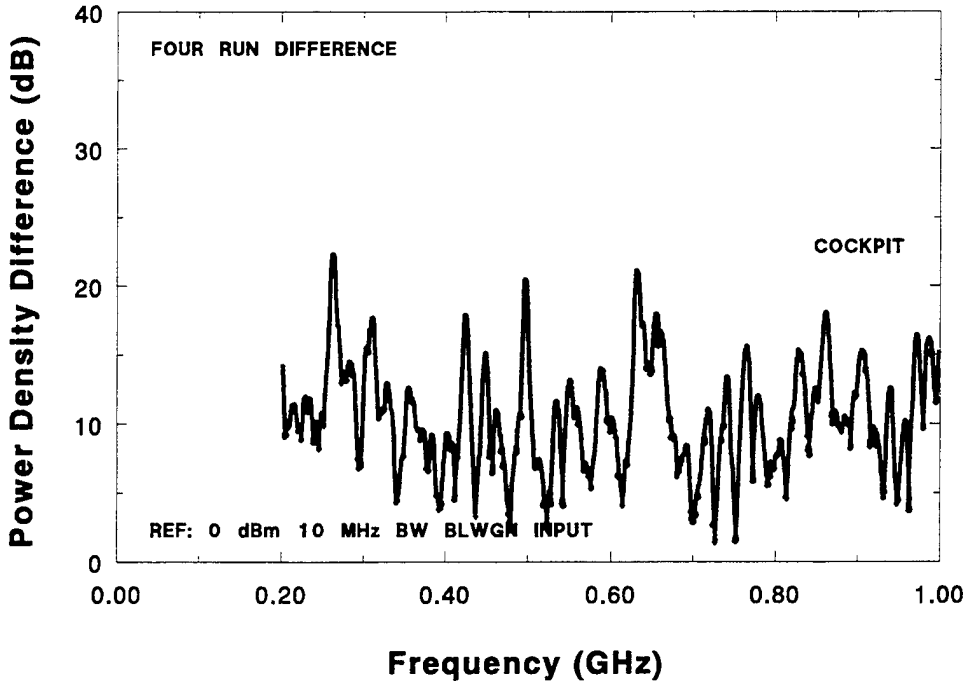

FIGURE 4-45. POWER DENSITY DIFFERENCES IN COCKPIT FOR 10-MHz BW BLWGN EXCITATION OVER 0.2 – 1 GHz

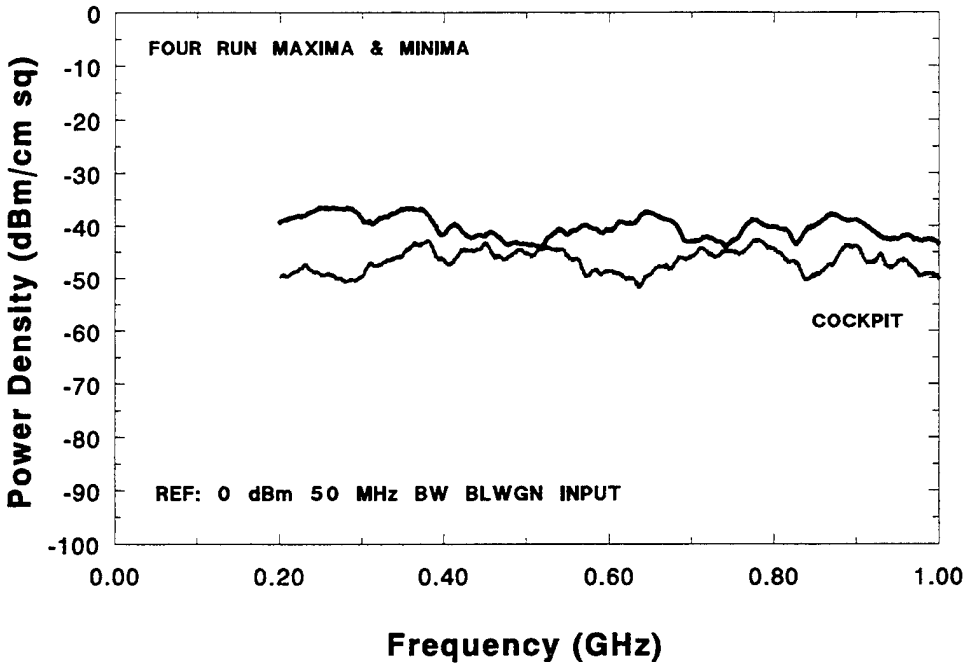

FIGURE 4-46. MAXIMUM AND MINIMUM POWER DENSITY VARIATIONS IN COCKPIT FOR 50-MHz BW BLWGN EXCITATION OVER 0.2 – 1 GHz

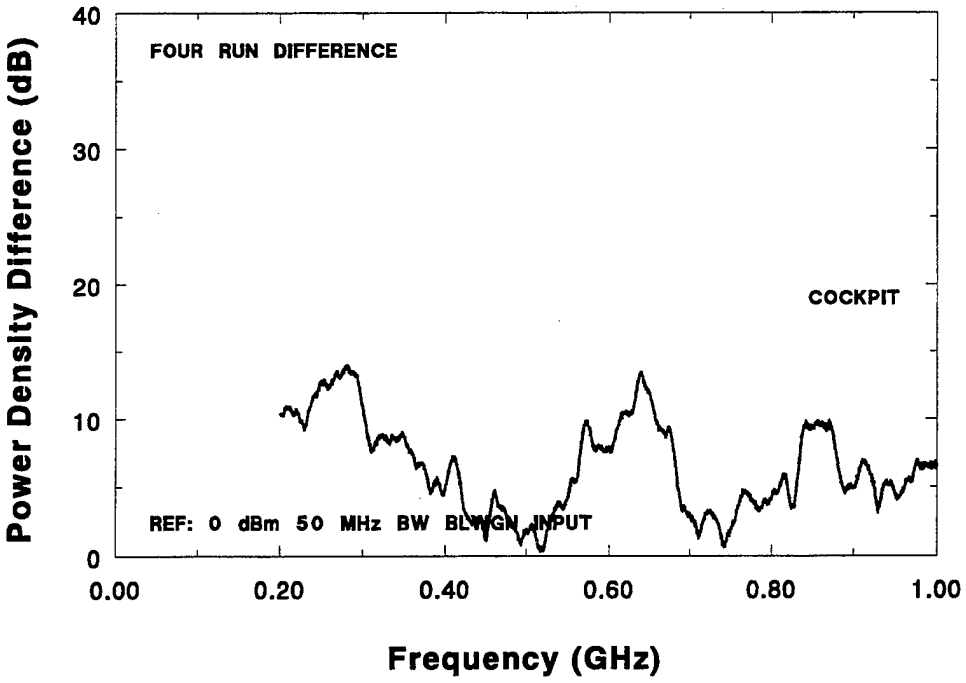

FIGURE 4-47. POWER DENSITY DIFFERENCES IN COCKPIT FOR 50-MHz BW BLWGN EXCITATION OVER 0.2 – 1 GHz

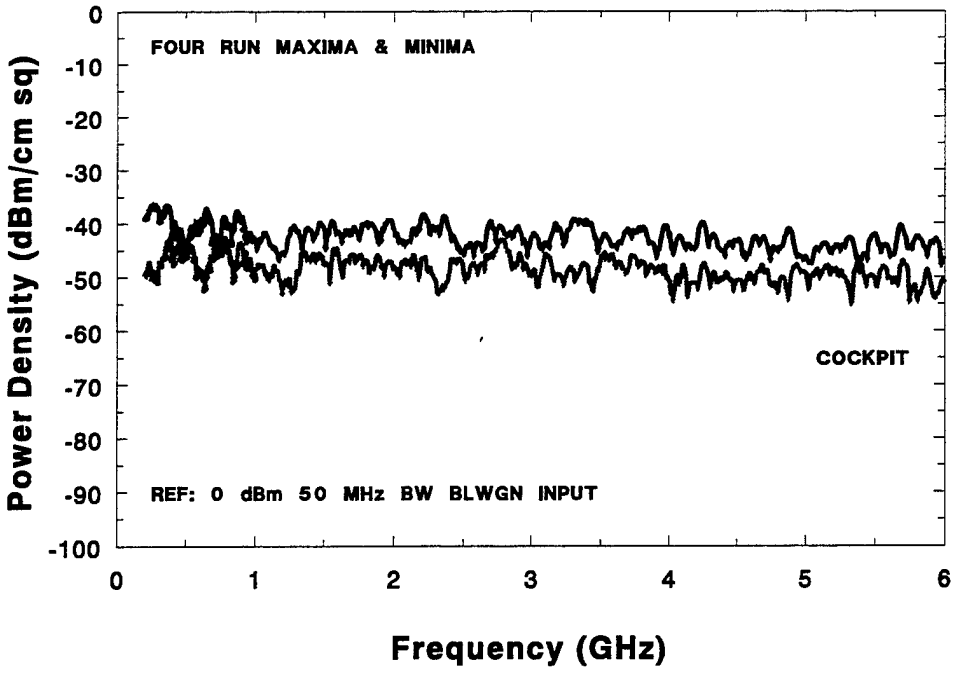

FIGURE 4-48. MAXIMUM AND MINIMUM POWER DENSITY VARIATIONS IN COCKPIT FOR 50-MHz BW BLWGN EXCITATION OVER 0.2 – 6 GHz

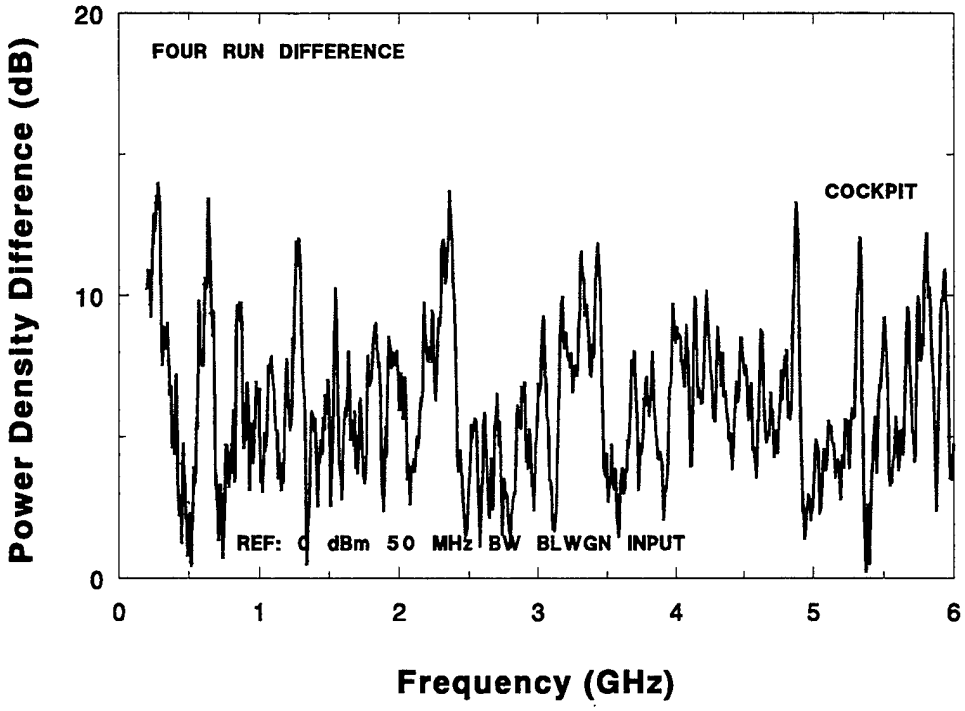

FIGURE 4-49. POWER DENSITY DIFFERENCES IN COCKPIT FOR 50-MHz BW BLWGN EXCITATION OVER 0.2 – 6 GHz

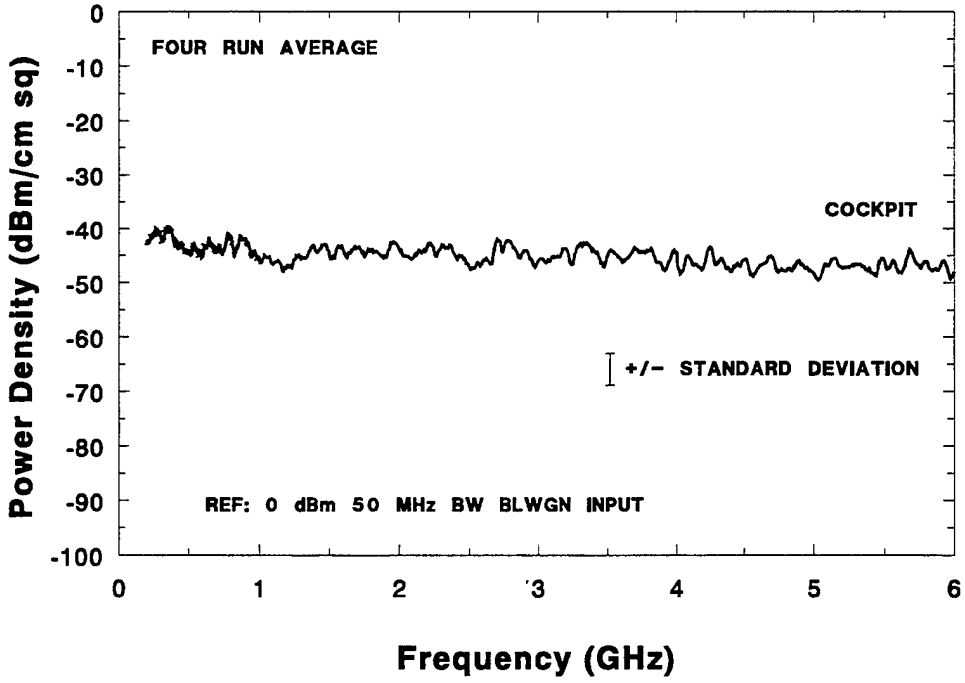

FIGURE 4-50. AVERAGE POWER DENSITY AND STANDARD DEVIATION IN COCKPIT FOR 50-MHz BW BLWGN EXCITATION OVER 0.2 – 6 GHz

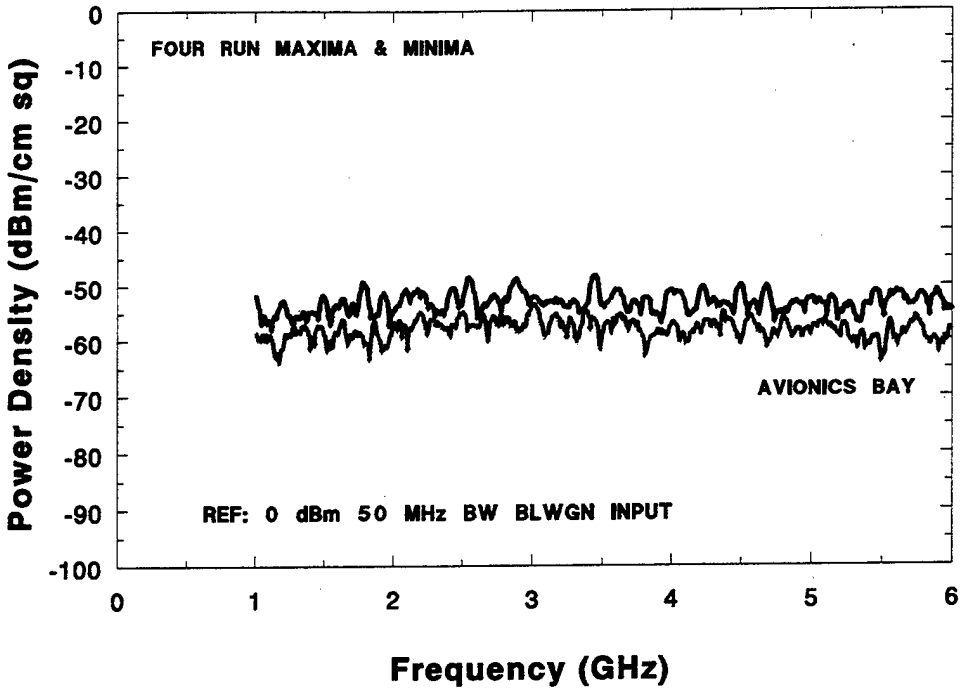

FIGURE 4-51. MAXIMUM AND MINIMUM POWER DENSITY VARIATIONS IN AVIONICS BAY FOR 50-MHz BW BLWGN EXCITATION OVER 0.2 – 6 GHz

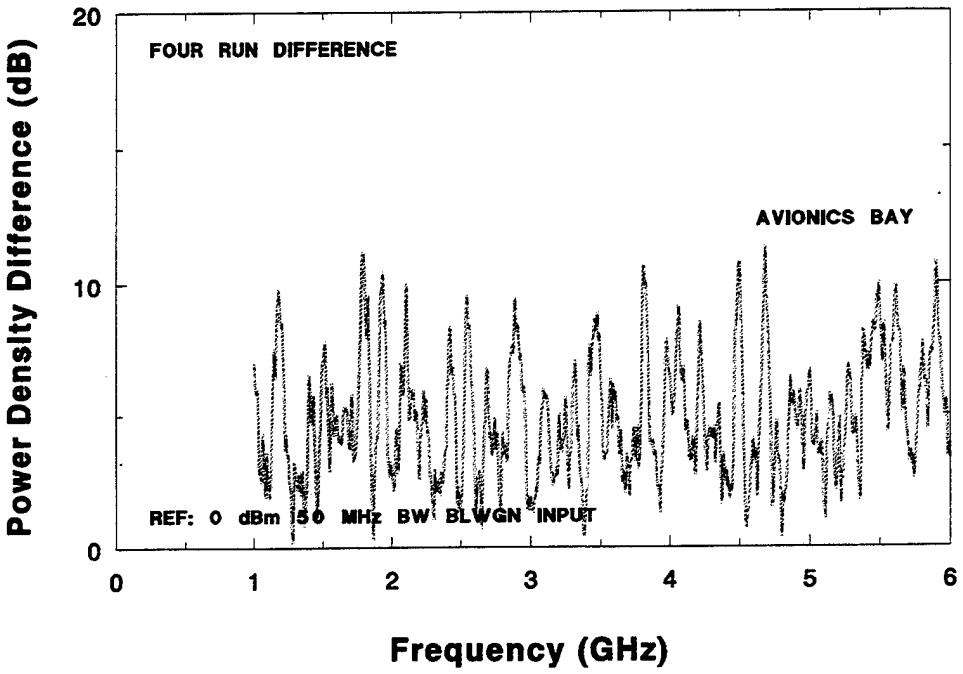

FIGURE 4-52. POWER DENSITY DIFFERENCES IN AVIONICS BAY FOR 50-MHz BW BLWGN EXCITATION OVER 0.2 – 6 GHz

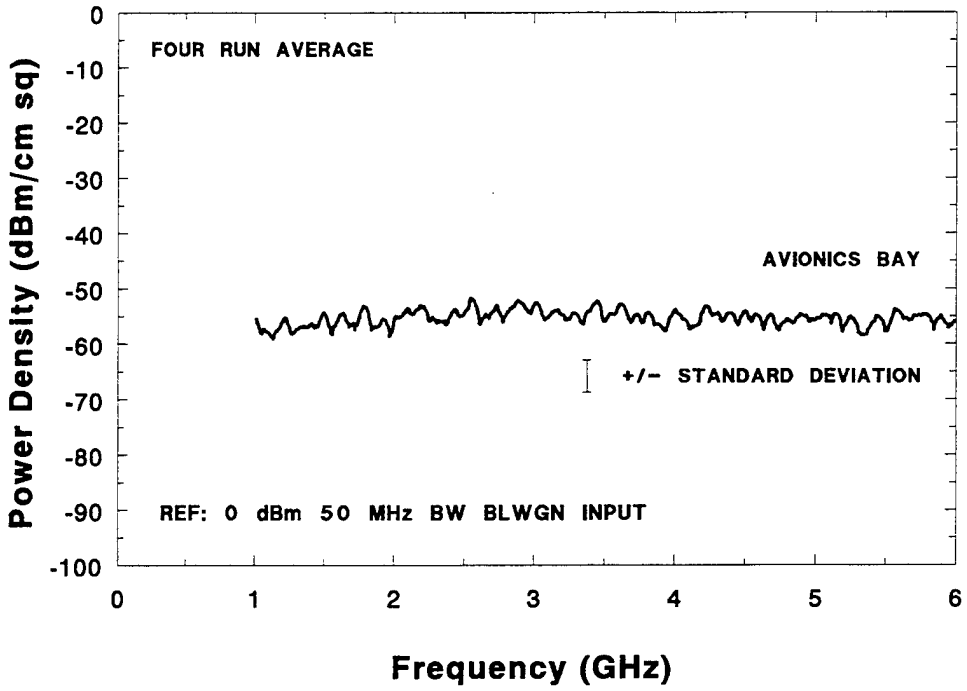

FIGURE 4-53. AVERAGE POWER DENSITY AND STANDARD DEVIATION IN AVIONICS BAY FOR 50-MHz BW BLWGN EXCITATION OVER 0.2 – 6 GHz

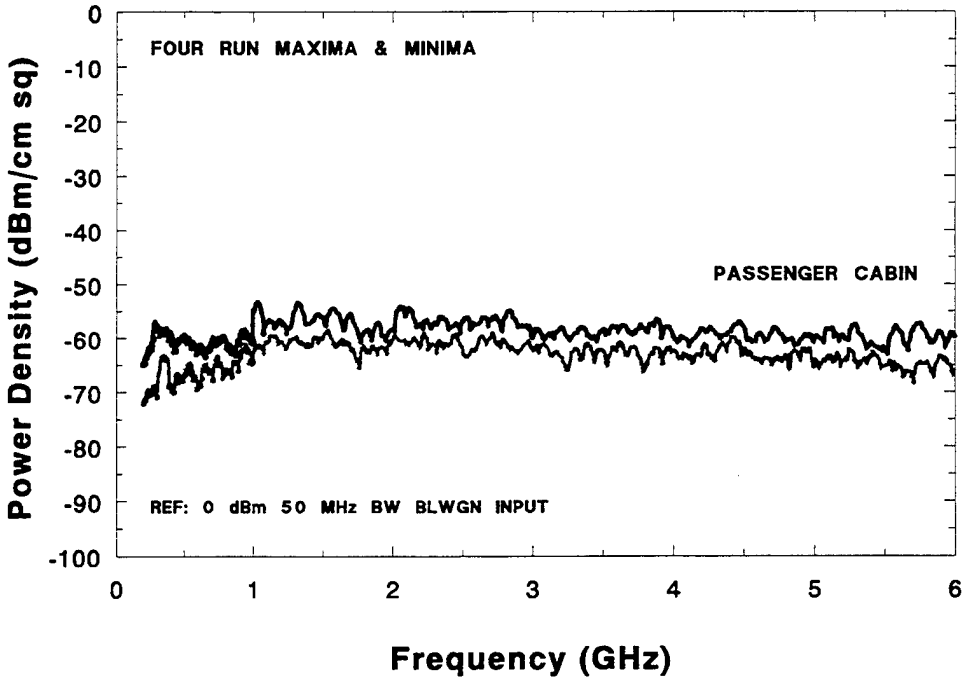

FIGURE 4-54. MAXIMUM AND MINIMUM POWER DENSITY VARIATIONS IN PASSENGER CABIN FOR 50-MHz BW BLWGN EXCITATION OVER 0.2 – 6 GHz

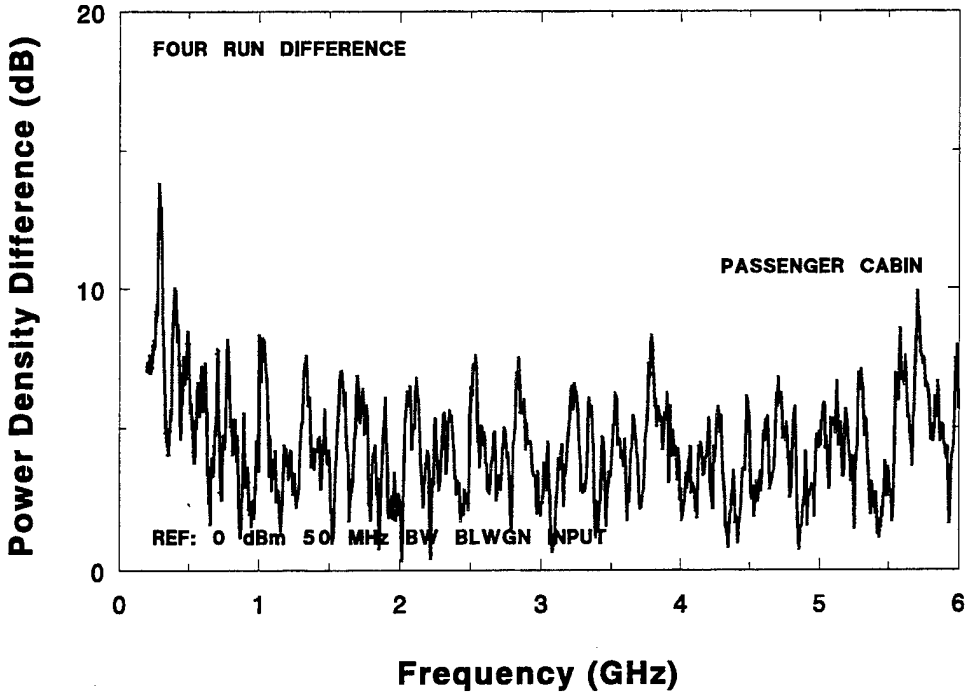

FIGURE 4-55. POWER DENSITY DIFFERENCES IN PASSENGER CABIN FOR 50-MHz BW BLWGN EXCITATION OVER 0.2 – 6 GHz

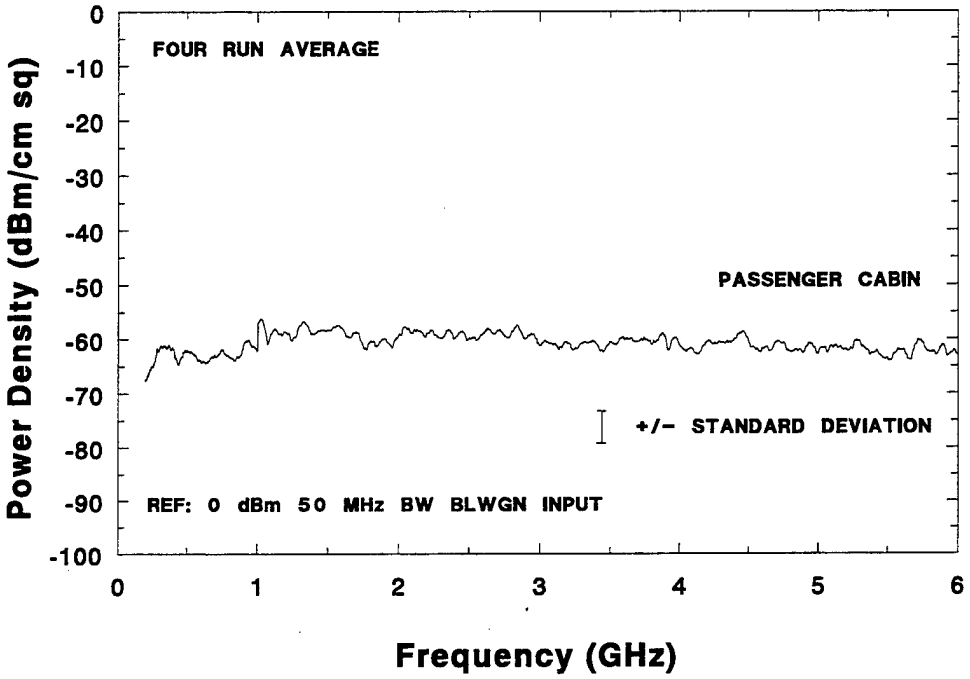

FIGURE 4-56. AVERAGE POWER DENSITY AND STANDARD DEVIATION IN PASSENGER CABIN FOR 50-MHz BW BLWGN EXCITATION OVER 0.2 – 6 GHz

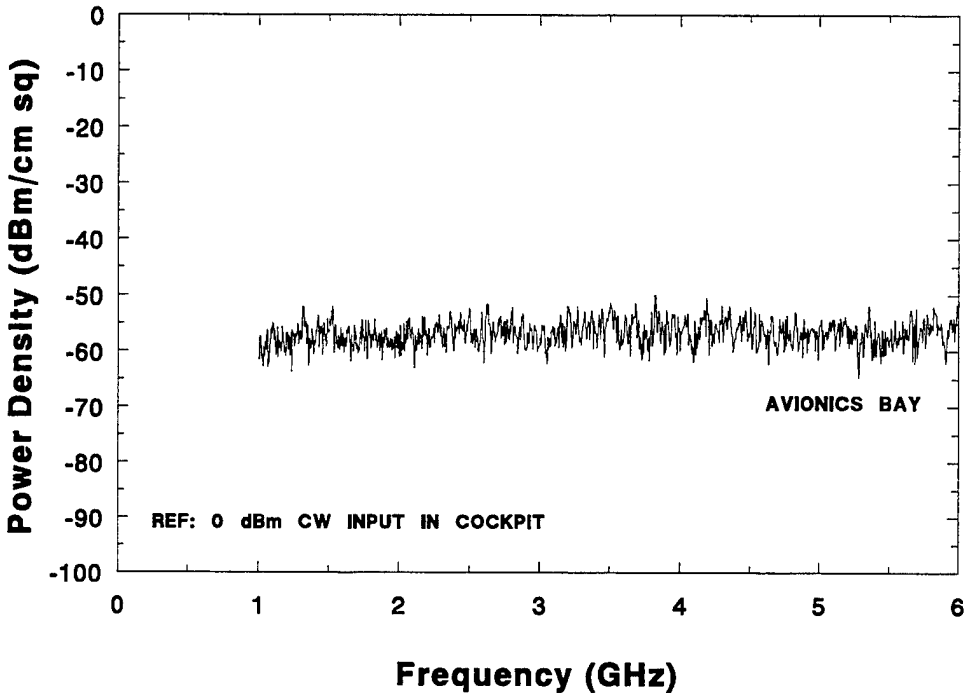

FIGURE 4-57. AVIONICS BAY 1–6 GHz POWER DENSITY FOR CW EXCITATION IN COCKPIT

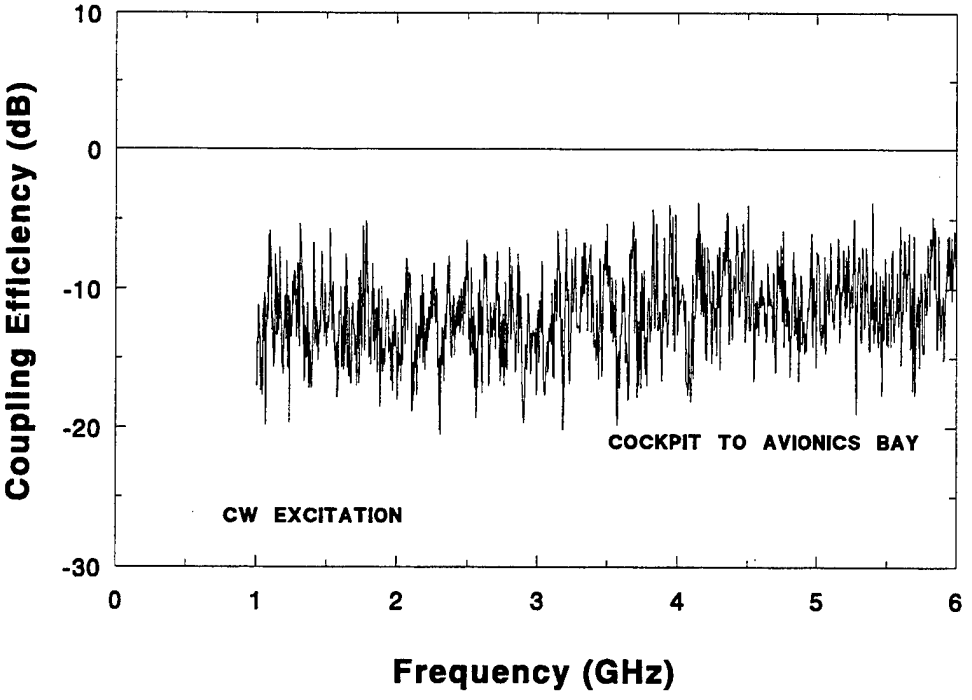

FIGURE 4-58. COCKPIT TO AVIONICS BAY COUPLING EFFICIENCY FOR CW EXCITATION

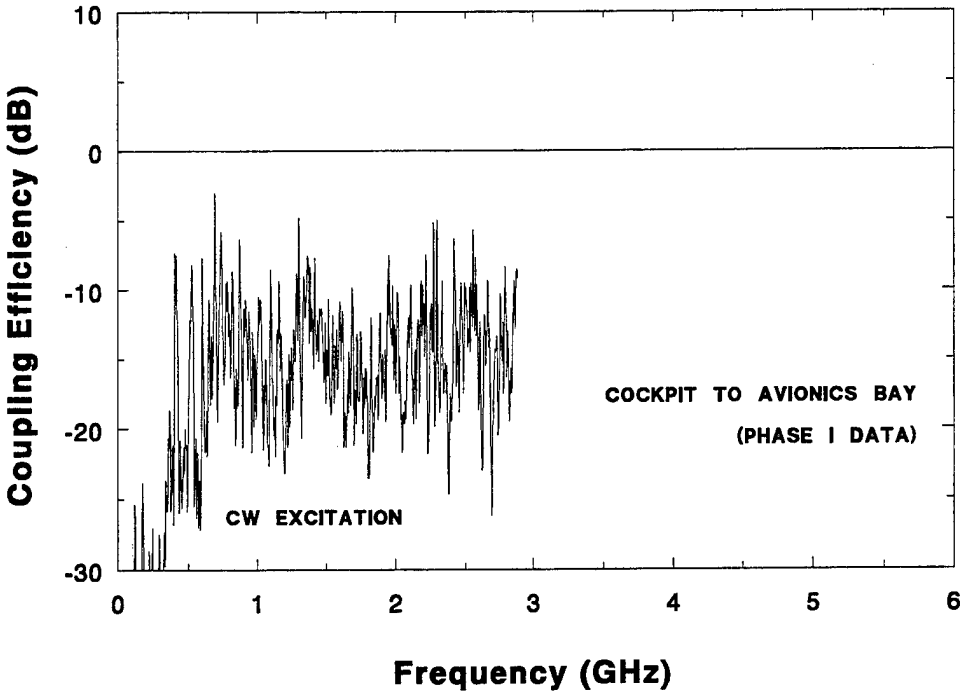

FIGURE 4-59. COCKPIT TO AVIONICS BAY COUPLING EFFICIENCY FOR CW EXCITATION FROM PHASE I

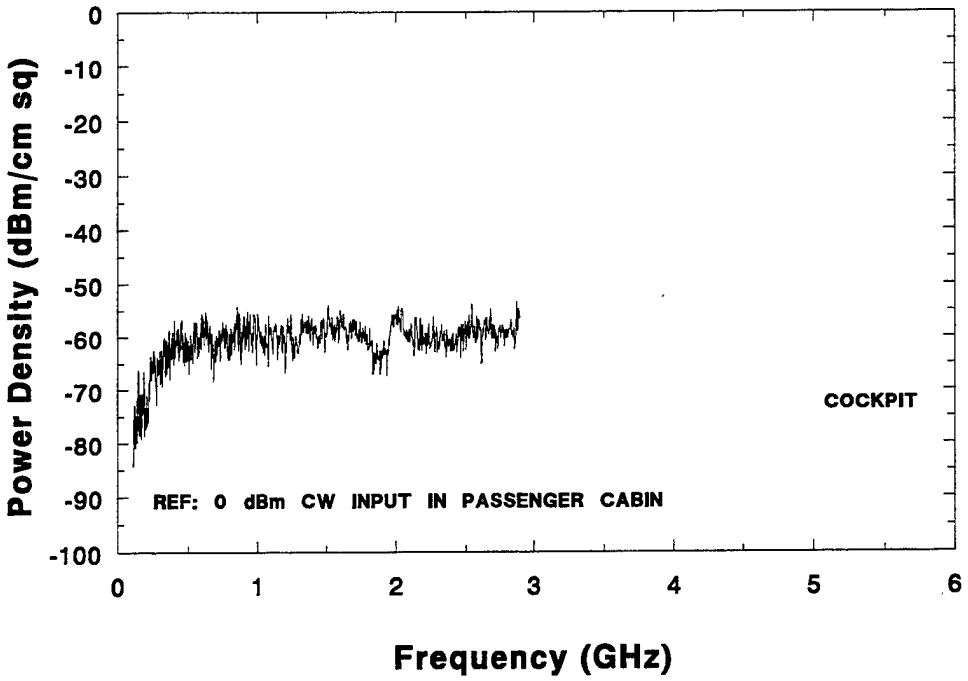

FIGURE 4-60. COCKPIT 0.1–2.9 GHz POWER DENSITY FOR CW EXCITATION IN PASSENGER CABIN

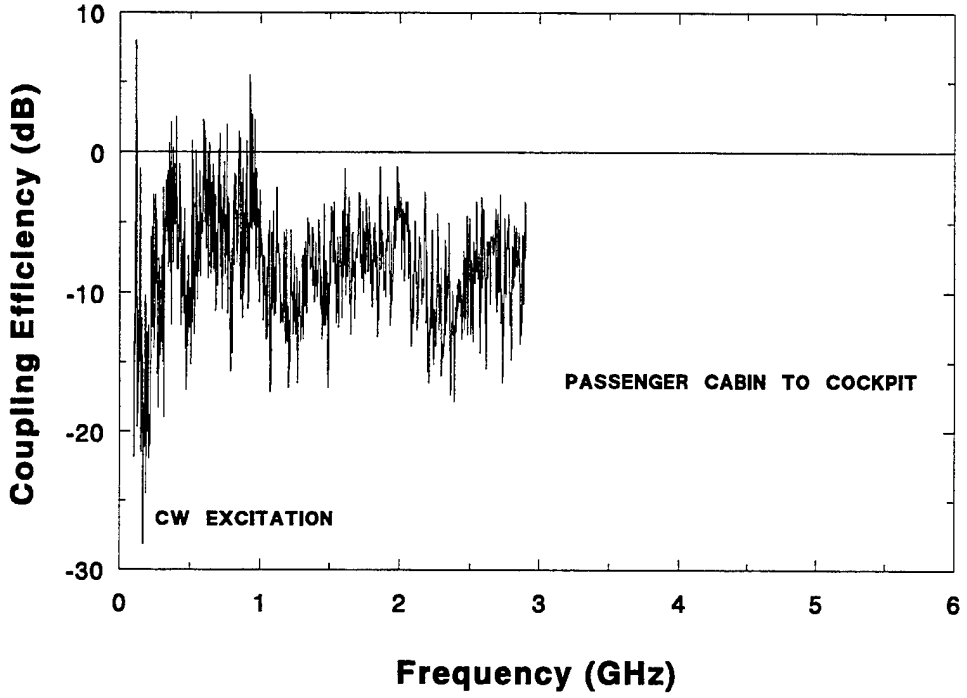

FIGURE 4-61. PASSENGER CABIN TO COCKPIT COUPLING EFFICIENCY FOR CW EXCITATION

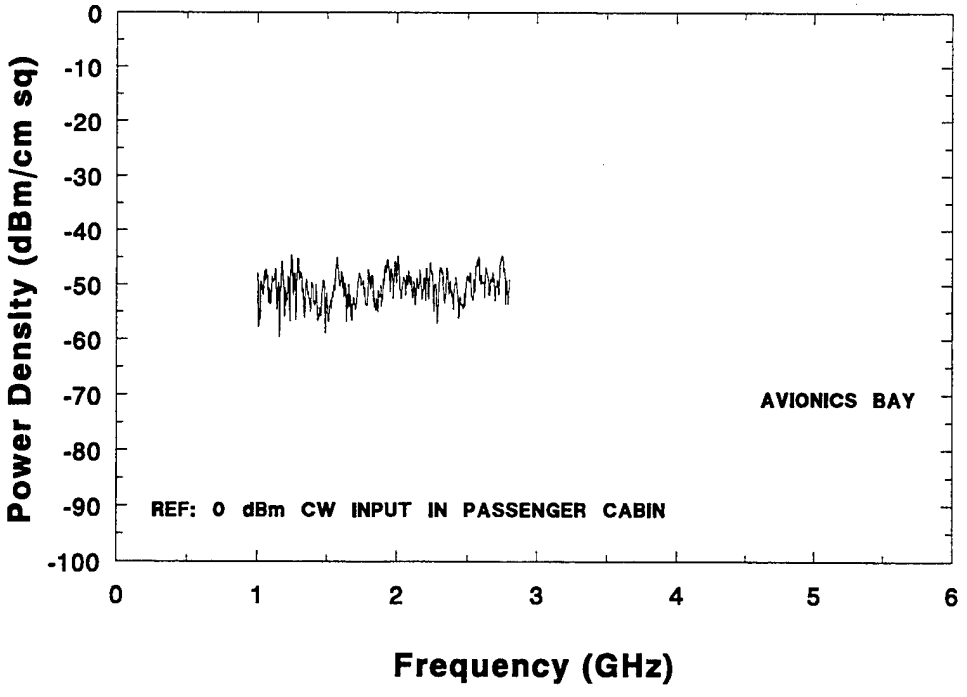

FIGURE 4-62. AVIONICS BAY 1–2.9 GHz POWER DENSITY FOR CW EXCITATION IN PASSENGER CABIN

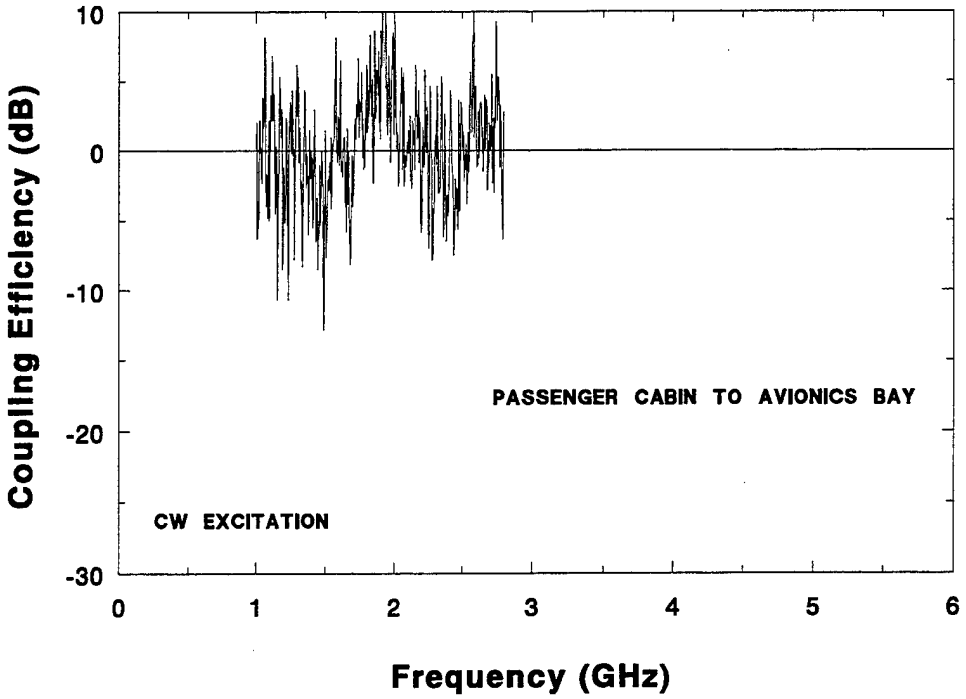

FIGURE 4-63. PASSENGER CABIN TO AVIONICS BAY COUPLING EFFICIENCY FOR CW EXCITATION

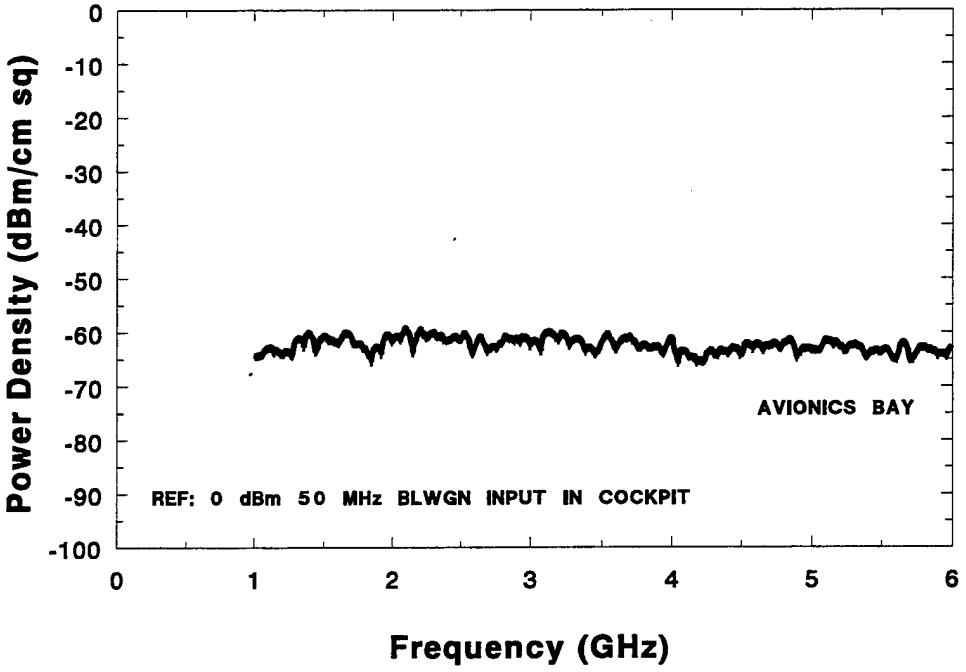

FIGURE 4-64. AVIONICS BAY 1–6 GHz POWER DENSITY FOR BLWGN EXCITATION IN COCKPIT

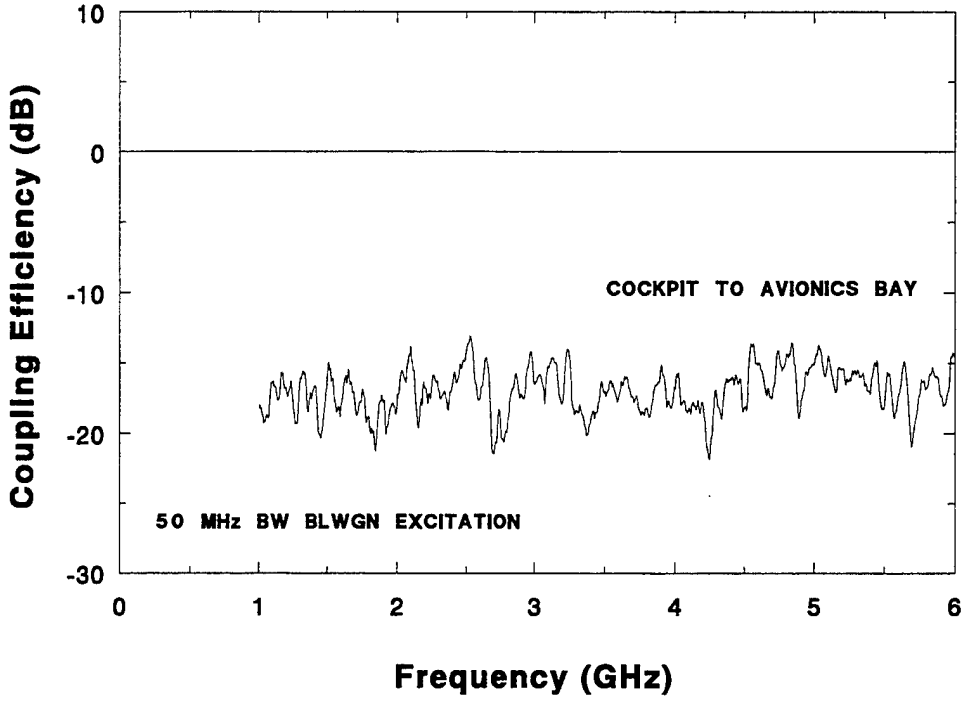

FIGURE 4-65. COCKPIT TO AVIONICS BAY COUPLING EFFICIENCY FOR BLWGN EXCITATION

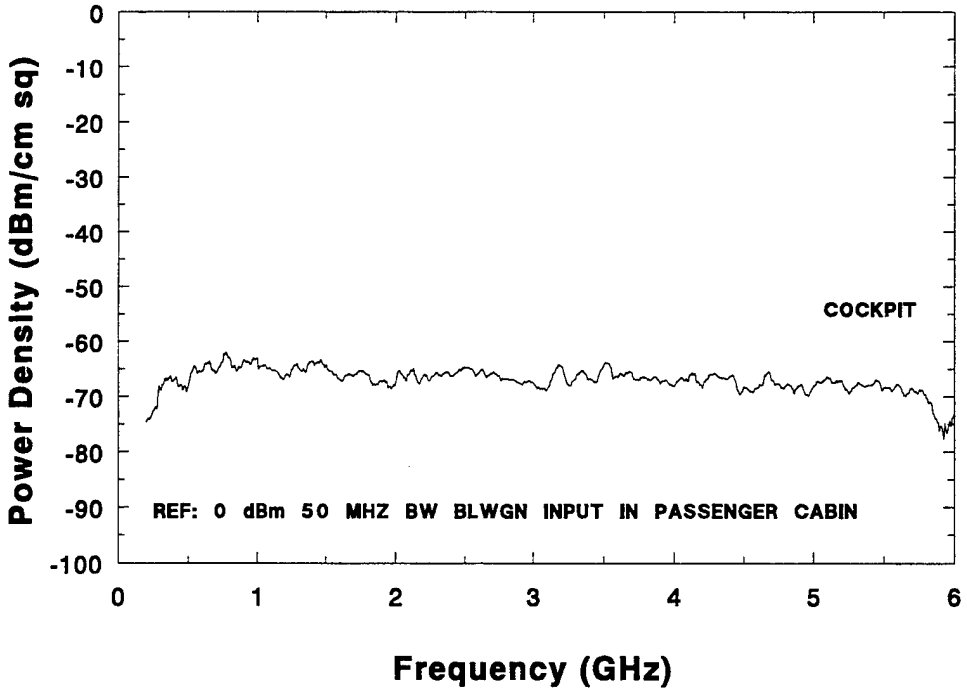

FIGURE 4-66. COCKPIT 1–6 GHz POWER DENSITY FOR BLWGN EXCITATION IN PASSENGER CABIN

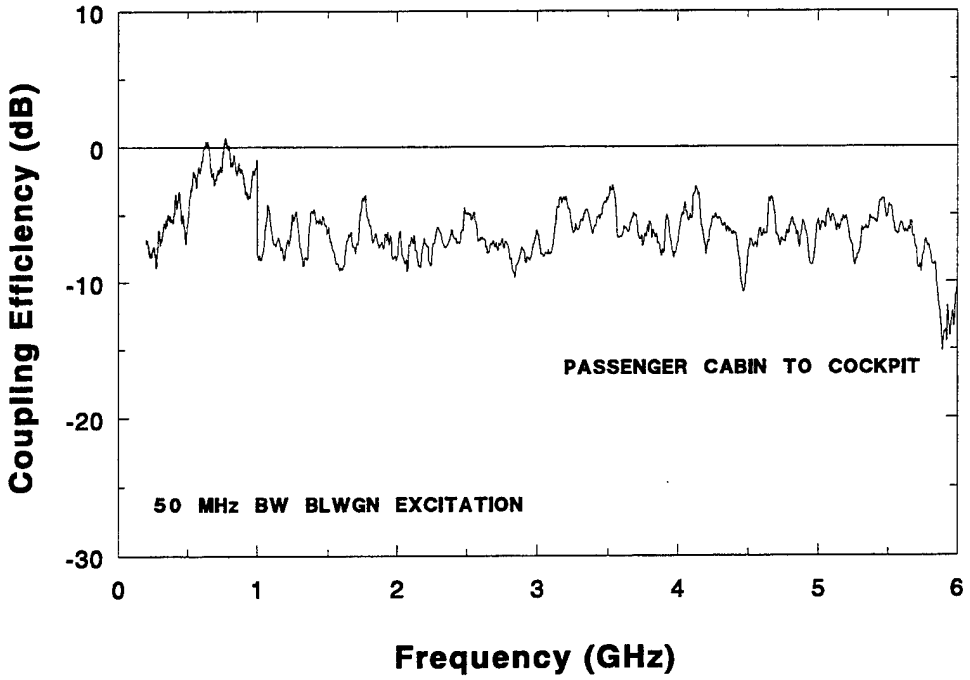

FIGURE 4-67. PASSENGER CABIN TO COCKPIT COUPLING EFFICIENCY FOR BLWGN EXCITATION

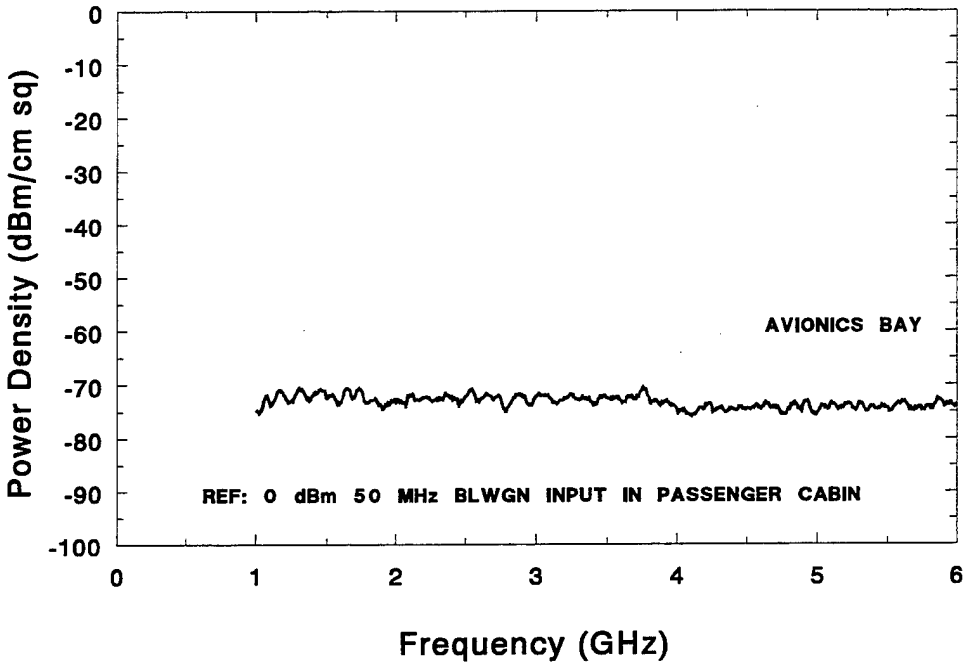

FIGURE 4-68. AVIONICS BAY 1–6 GHz POWER DENSITY FOR BLWGN EXCITATION IN PASSENGER CABIN

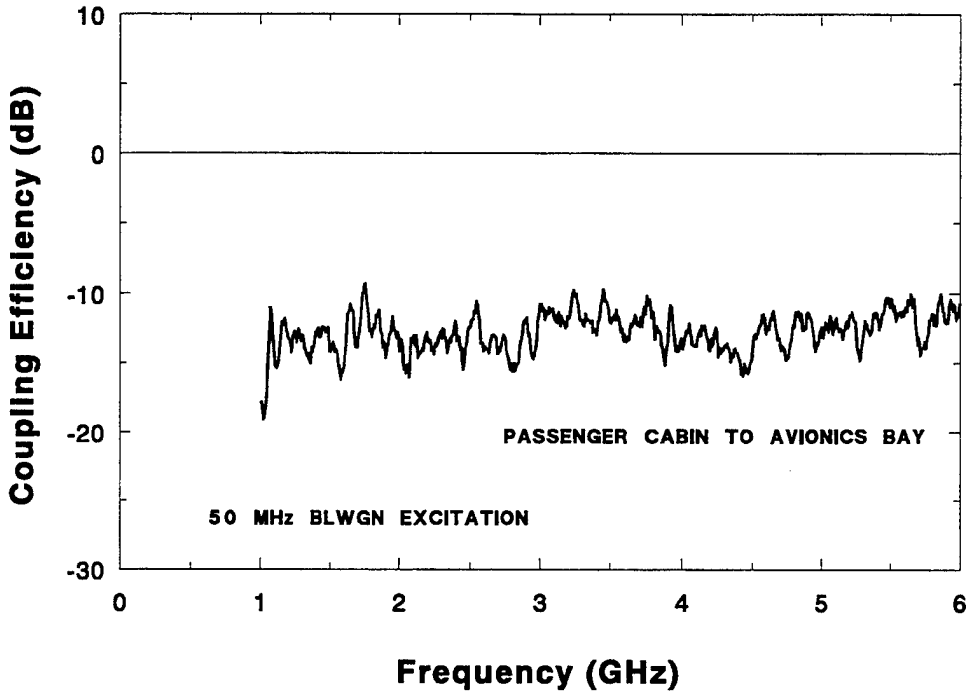

FIGURE 4-69. PASSENGER-CABIN-TO-AVIONICS-BAY COUPLING EFFICIENCY FOR BLWGN EXCITATION

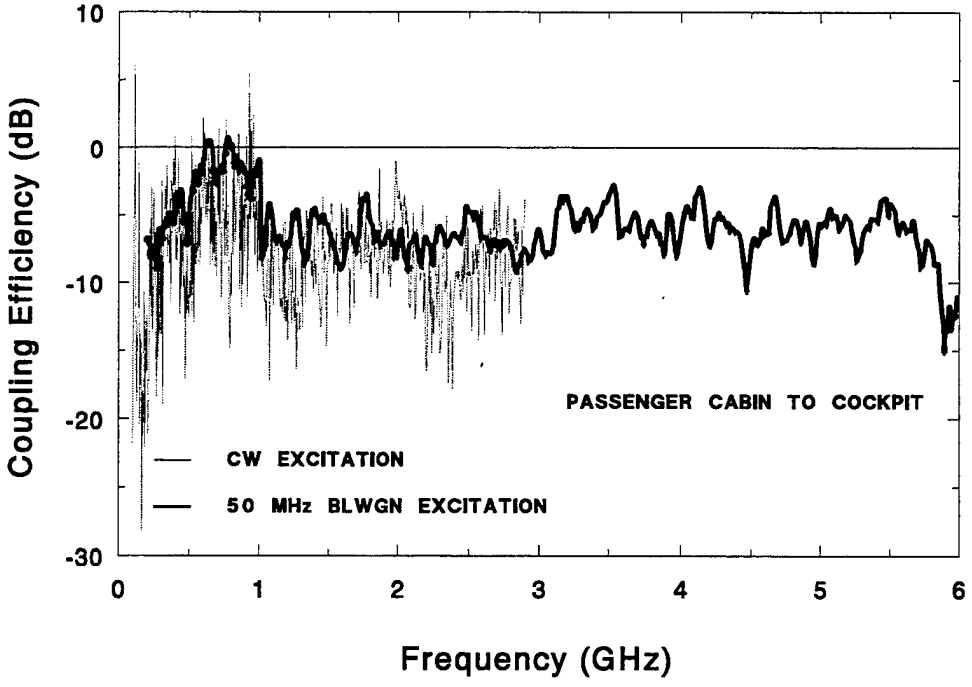

FIGURE 4-70. COMPARISON OF PASSENGER-CABIN-TO-COCKPIT COUPLING EFFICIENCY FOR CW AND BLWGN EXCITATION

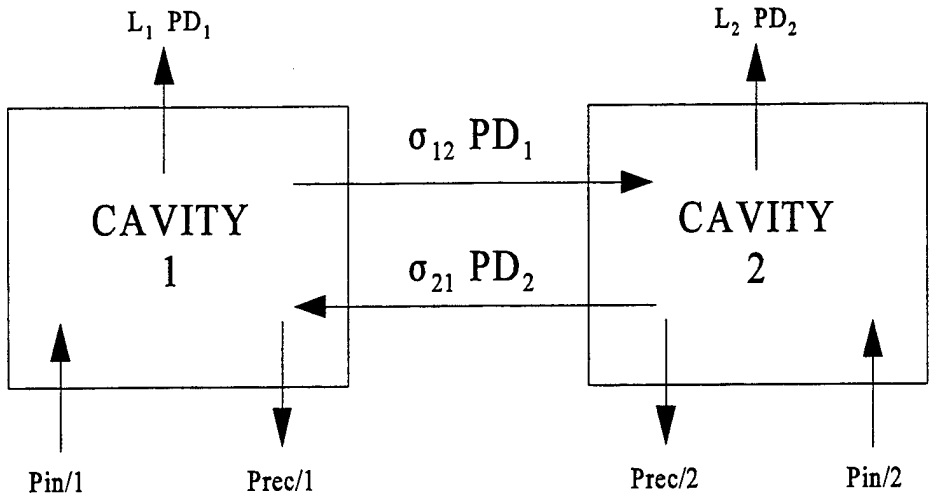

FIGURE 4-71. ENERGY BALANCE BETWEEN TWO CAVITIES

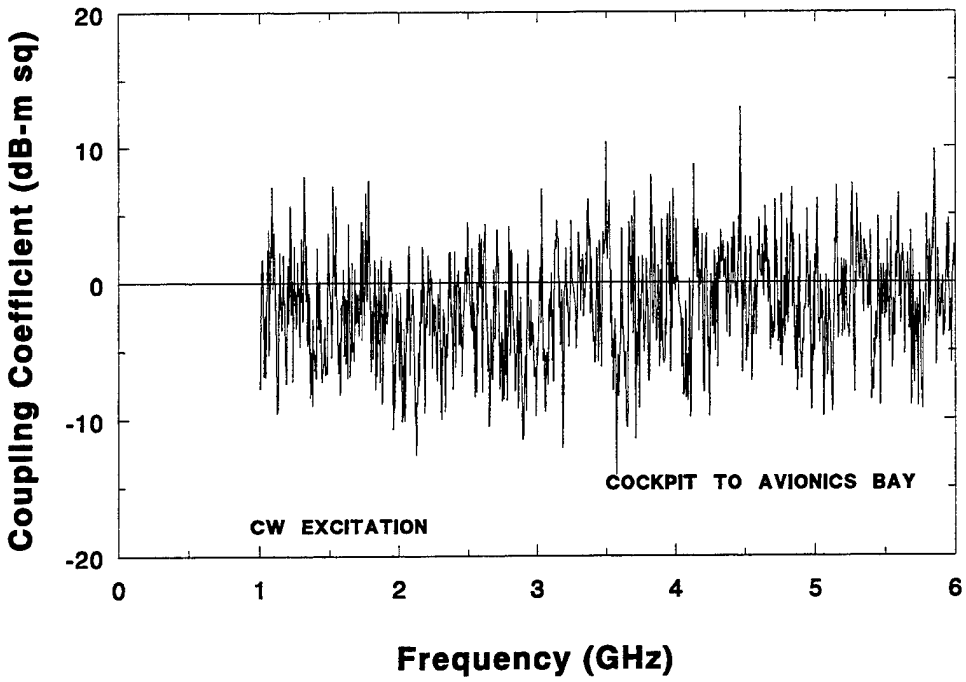

FIGURE 4-72. COCKPIT-TO-AVIONICS-BAY COUPLING COEFFICIENT FOR CW EXCITATION

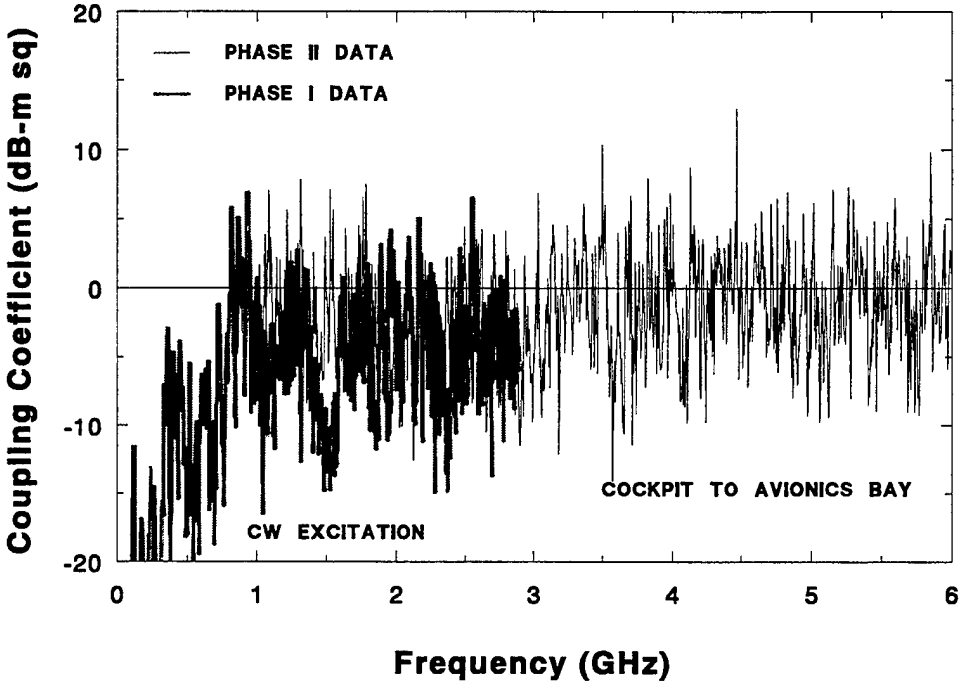

FIGURE 4-73. COMPARISON OF PHASE I AND II COCKPIT-TO-AVIONICS-BAY COUPLING COEFFICIENT FOR CW EXCITATION

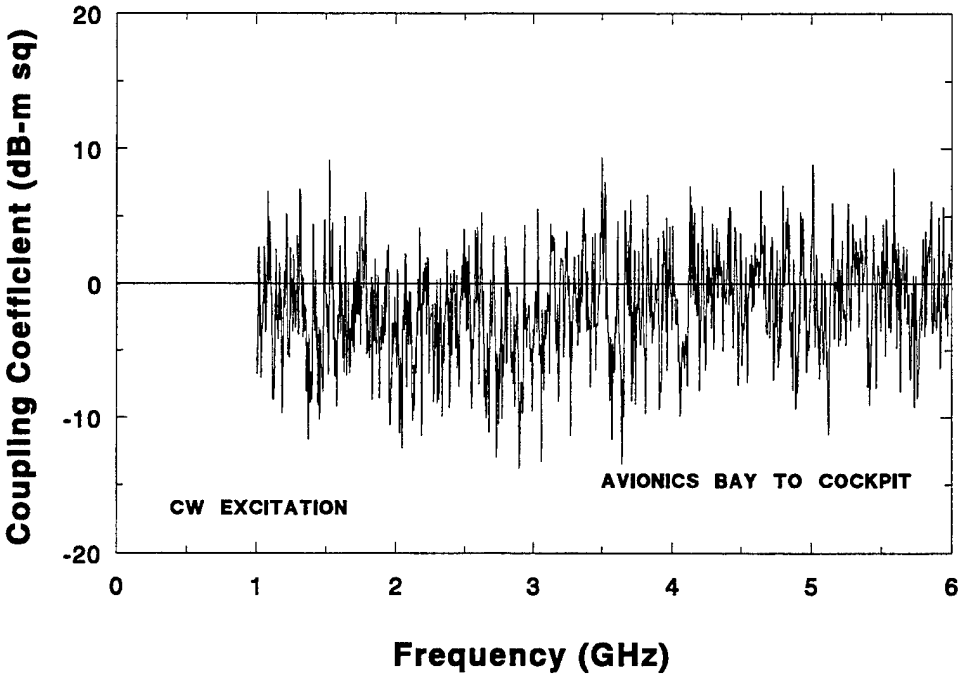

FIGURE 4-74 . AVIONICS-BAY-TO-COCKPIT COUPLING COEFFICIENT FOR CW EXCITATION

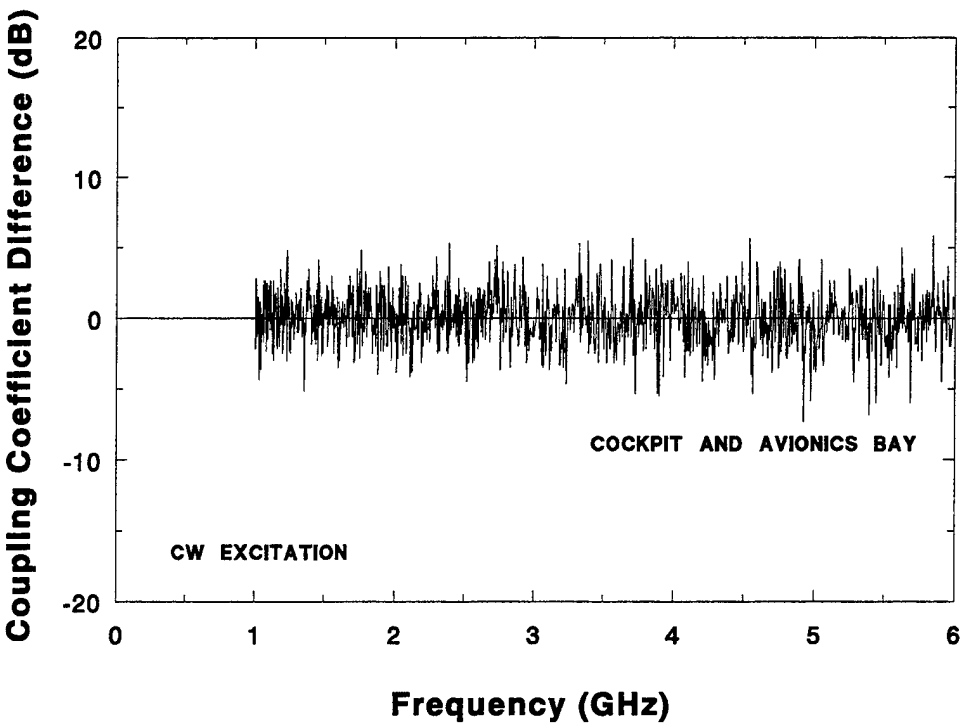

FIGURE 4-75. DIFFERENCE IN COCKPIT-TO-AVIONICS-BAY COUPLING COEFFICIENT AND AVIONICS-BAY-TO-COCKPIT COUPLING COEFFICIENT

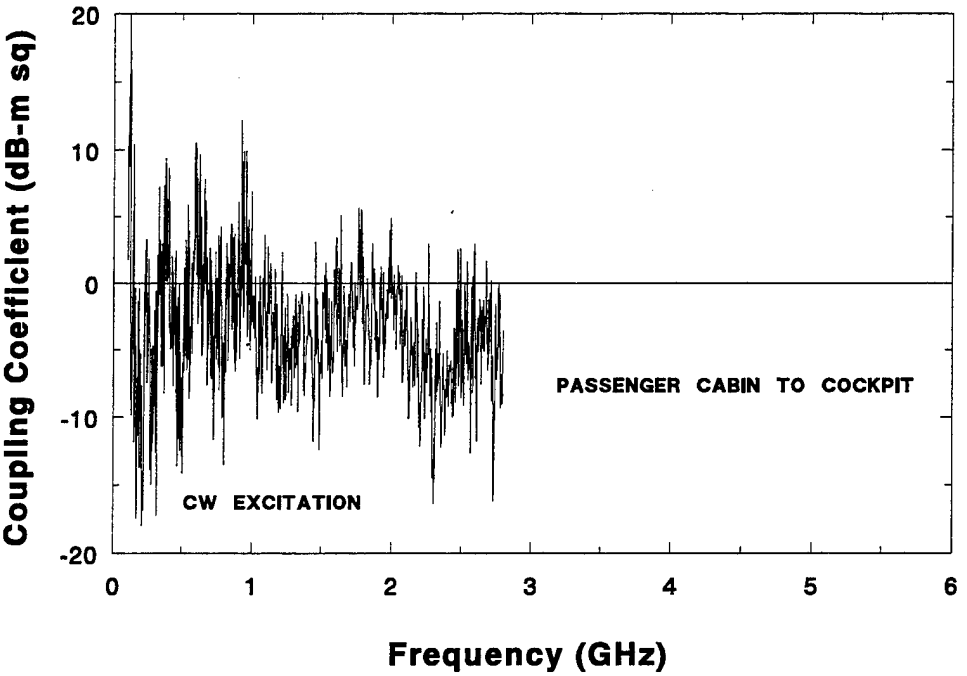

FIGURE 4-76. PASSENGER-CABIN-TO-COCKPIT COUPLING COEFFICIENT FOR CW EXCITATION

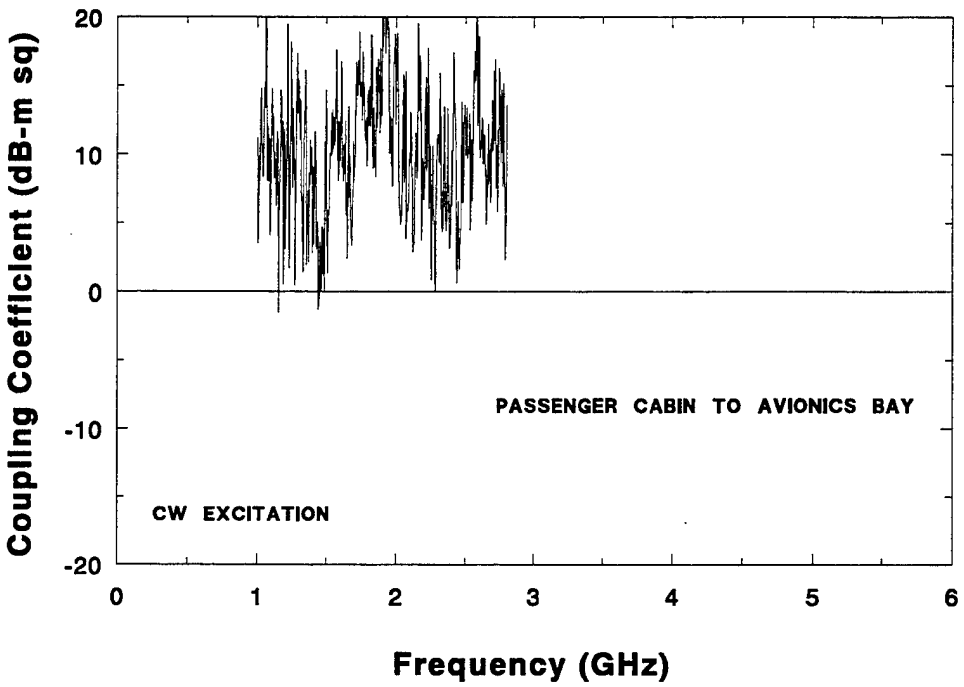

FIGURE 4-77. PASSENGER-CABIN-TO-AVIONICS-BAY COUPLING COEFFICIENT FOR CW EXCITATION

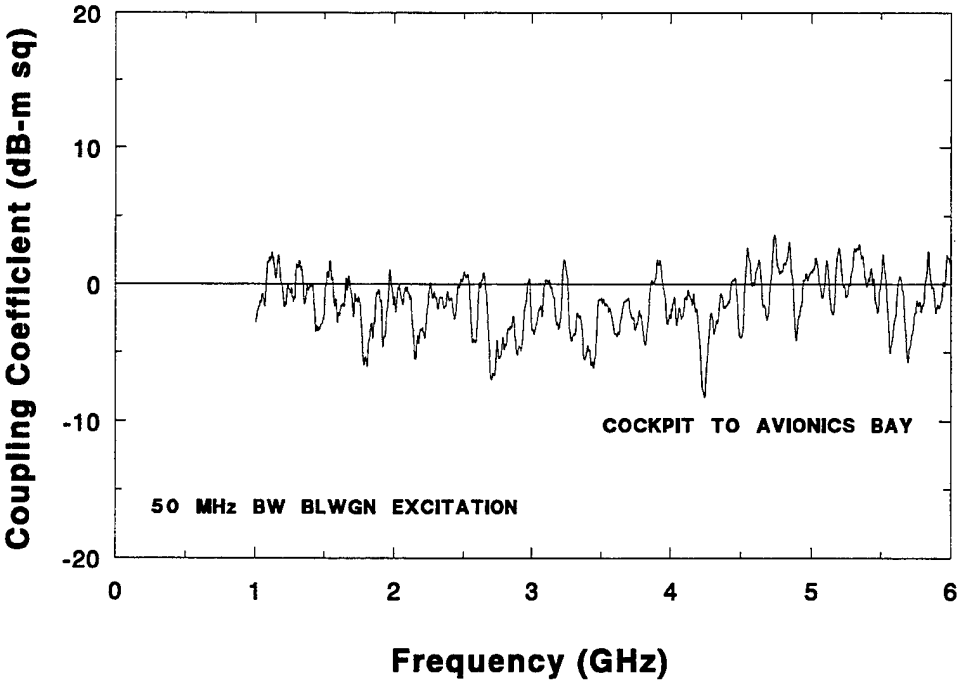

FIGURE 4-78. COCKPIT-TO-AVIONICS-BAY COUPLING COEFFICIENT FOR BLWGN EXCITATION

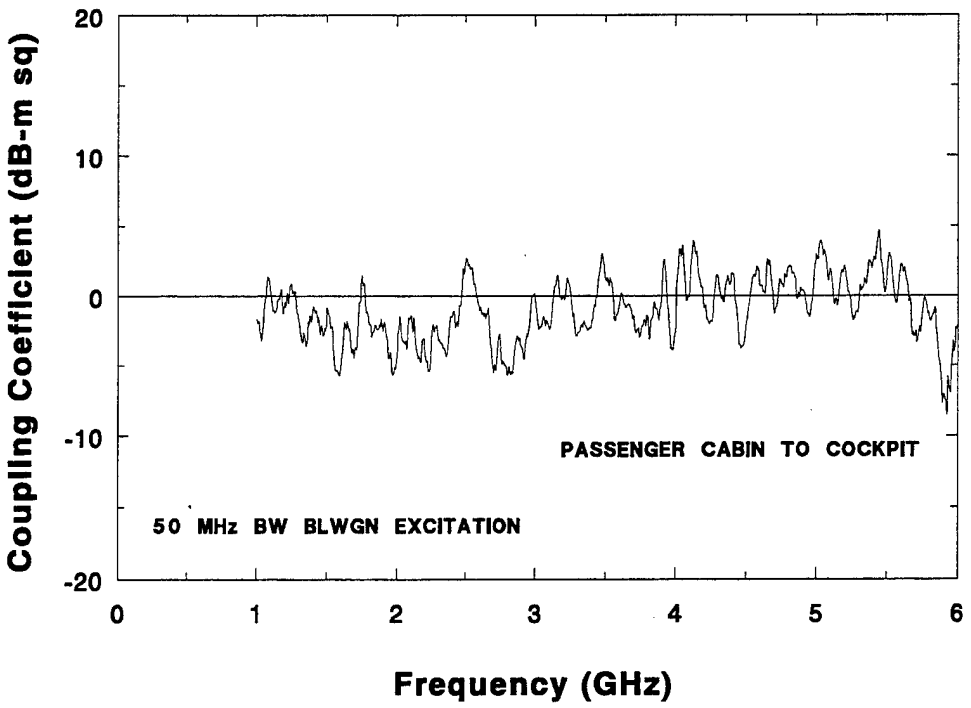

FIGURE 4-79. PASSENGER-CABIN-TO-COCKPIT COUPLING COEFFICIENT FOR BLWGN EXCITATION

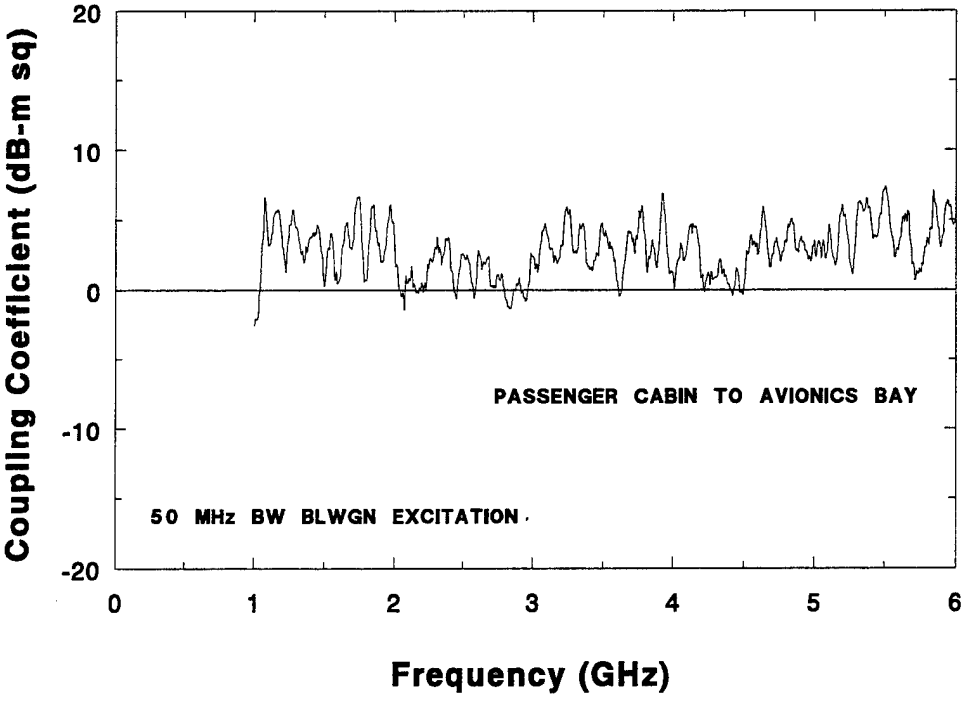

FIGURE 4-80. PASSENGER-CABIN-TO-AVIONICS-BAY COUPLING COEFFICIENT FOR BLWGN EXCITATION

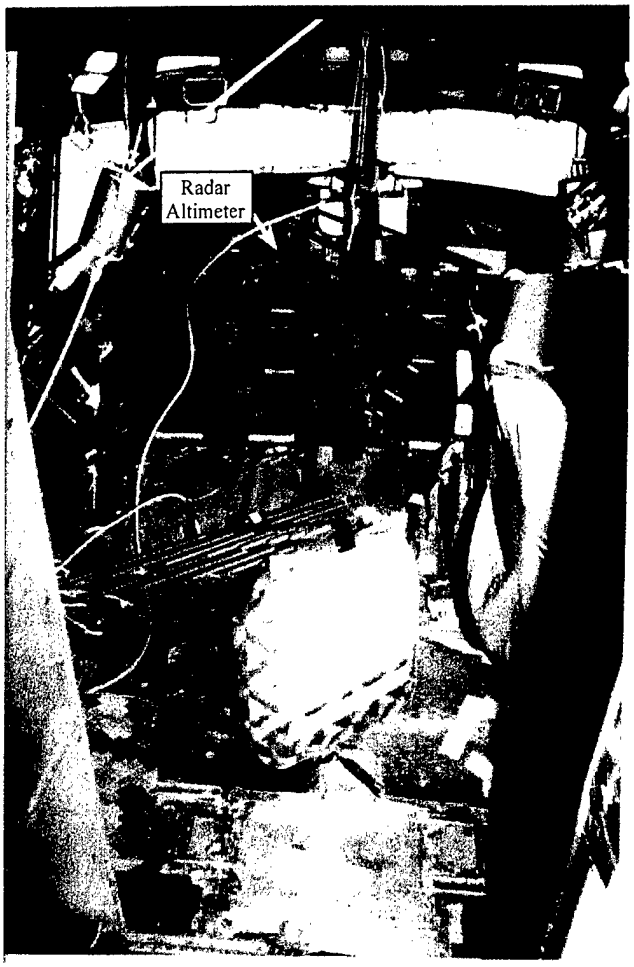

FIGURE 4-81. RADAR ALTIMETER IN COCKPIT INSTRUMENT PANEL

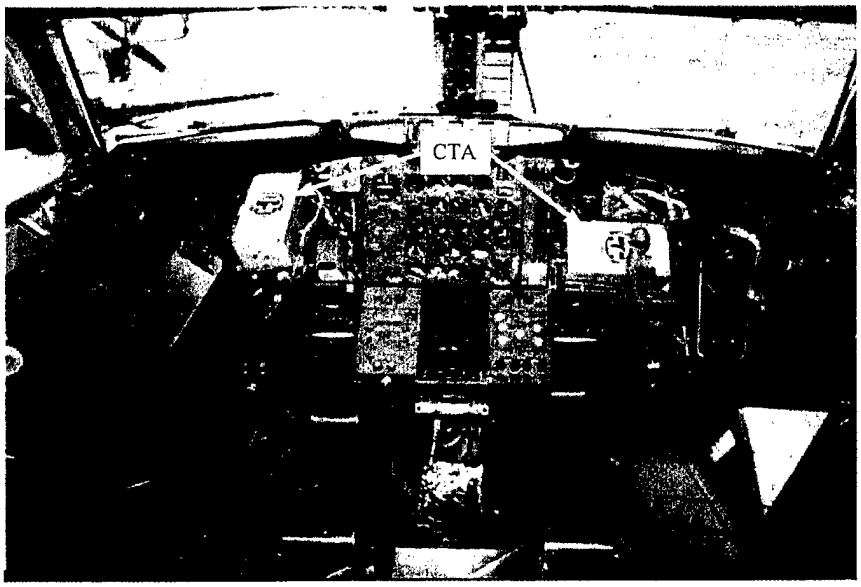

FIGURE 4-82. COMMON TEST ARTICLE IN COCKPIT

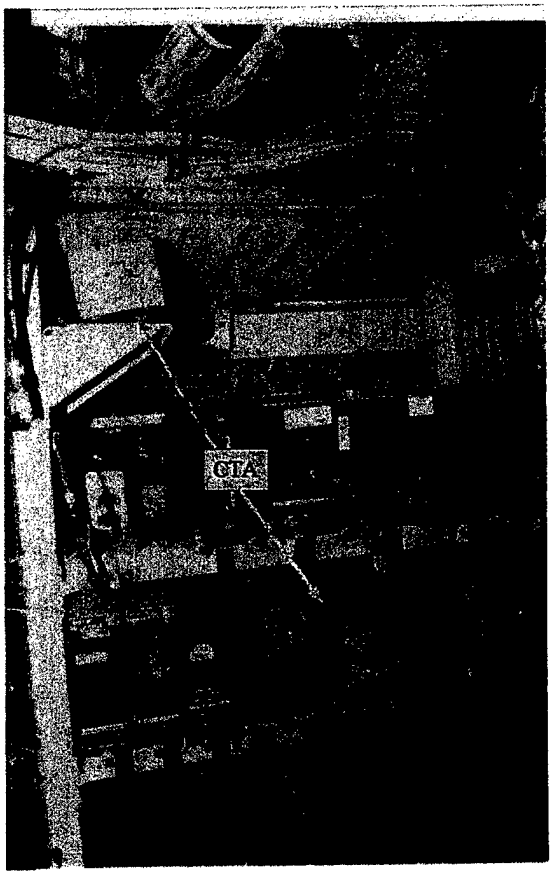

FIGURE 4-83. COMMON TEST ARTICLE IN AVIONICS BAY EQUIPMENT RACK

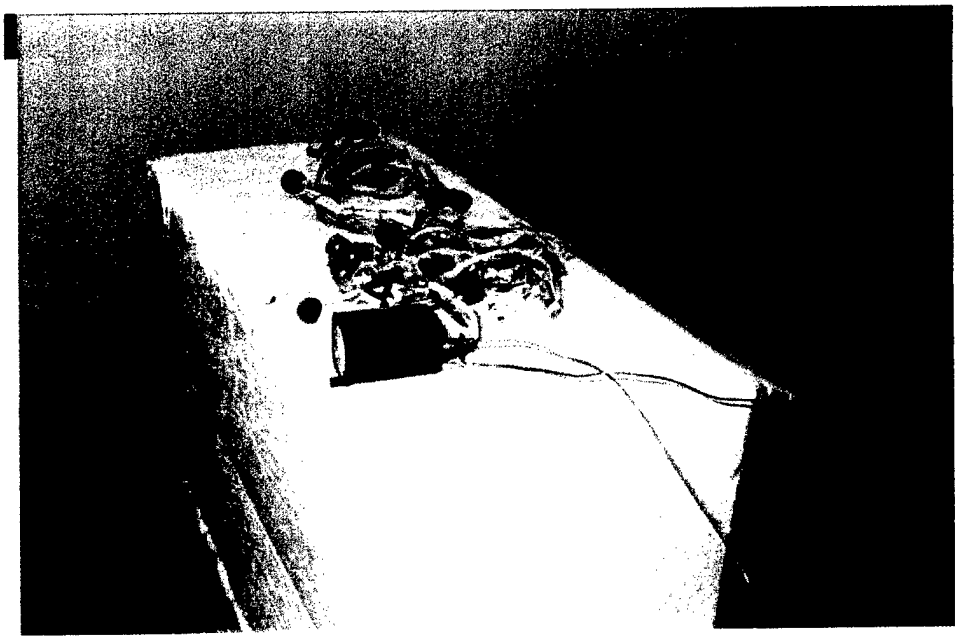

FIGURE 4-84. RADAR ALTIMETER ON DIELECTRIC BLOCK IN NSWCDD REVERBERATION CHAMBER

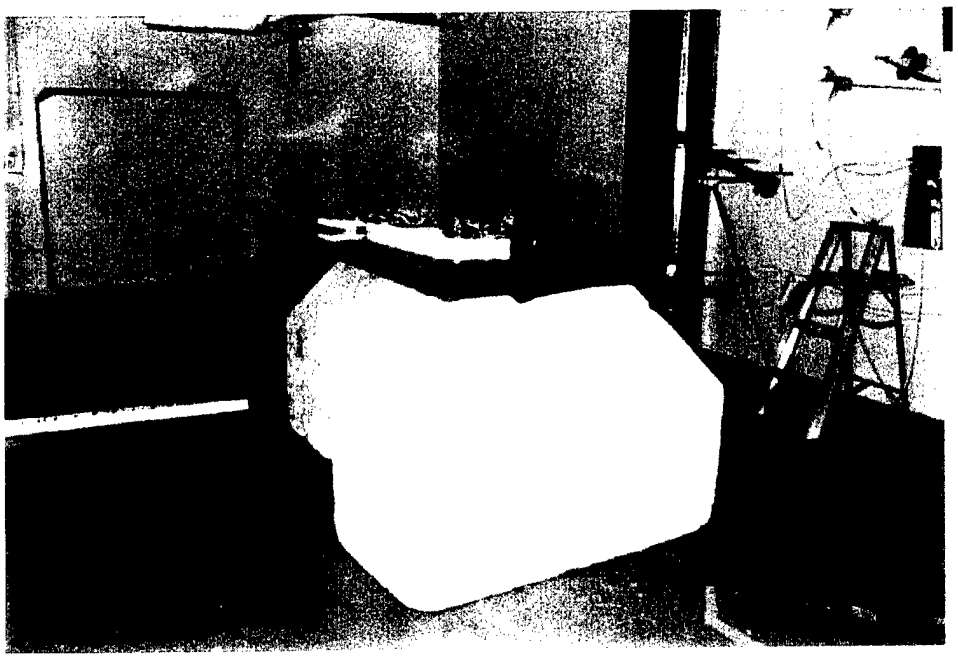

FIGURE 4-85. RADAR ALTIMETER ON METAL GROUND PLANE IN NSWCDD REVERBERATION CHAMBER

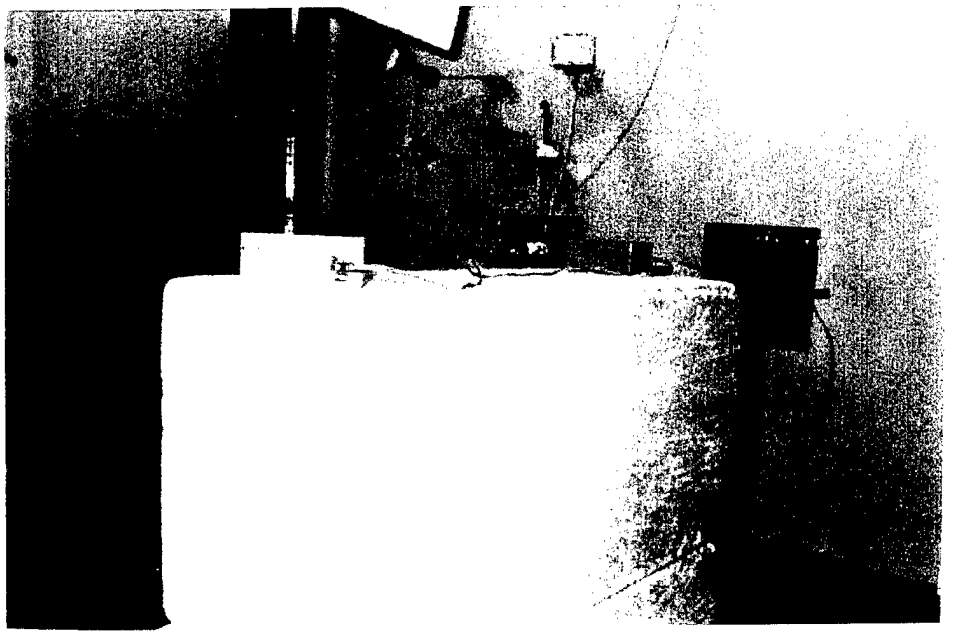

FIGURE 4-86. COMMON TEST ARTICLE ON DIELECTRIC BLOCK IN NSWCDD REVERBERATION CHAMBER

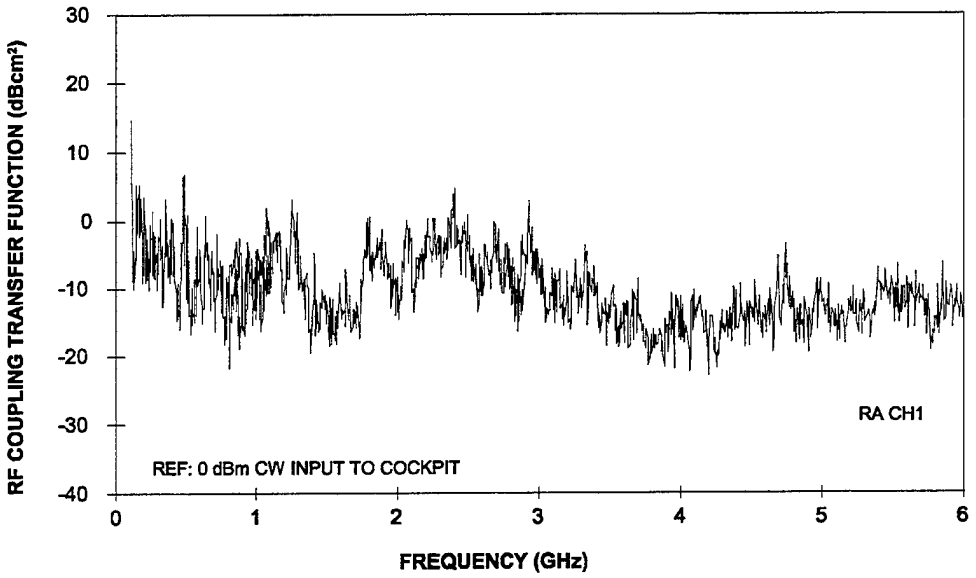

FIGURE 4-87. RADIO FREQUENCY COUPLING TRANSFER FUNCTION FOR RADAR ALTIMETER CHANNEL 1 IN AIRCRAFT FOR CW EXCITATION

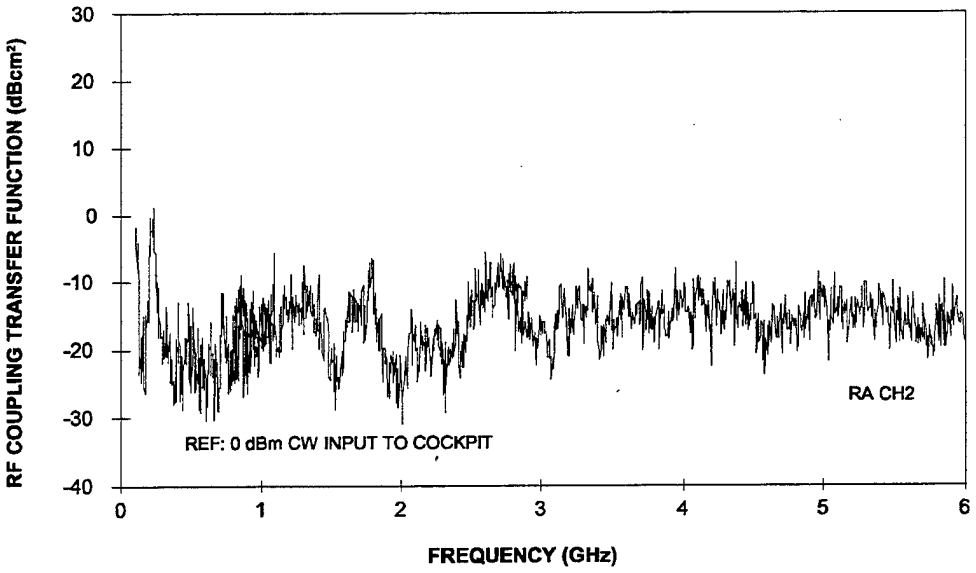

FIGURE 4-88. RADIO FREQUENCY COUPLING TRANSFER FUNCTION FOR RADAR ALTIMETER CHANNEL 2 IN AIRCRAFT FOR CW EXCITATION

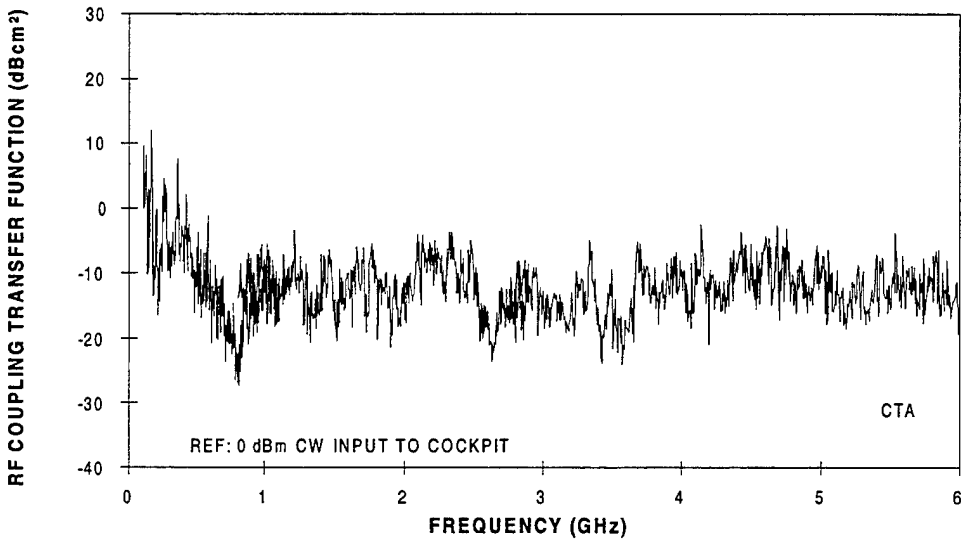

FIGURE 4-89. RADIO FREQUENCY COUPLING TRANSFER FUNCTION FOR COMMON TEST ARTICLE IN COCKPIT FOR CW EXCITATION

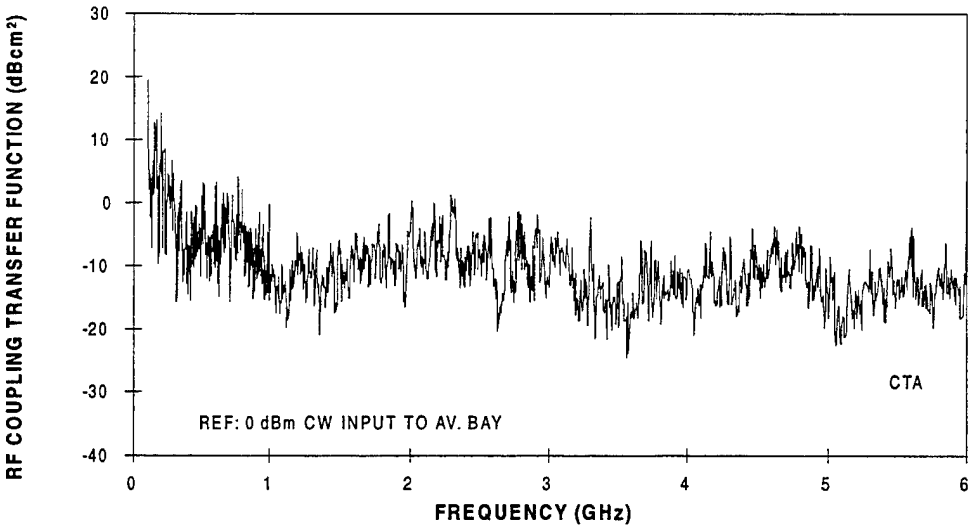

FIGURE 4-90. RADIO FREQUENCY COUPLING TRANSFER FUNCTION FOR COMMON TEST ARTICLE IN AVIONICS BAY EQUIPMENT RACK FOR CW EXCITATION

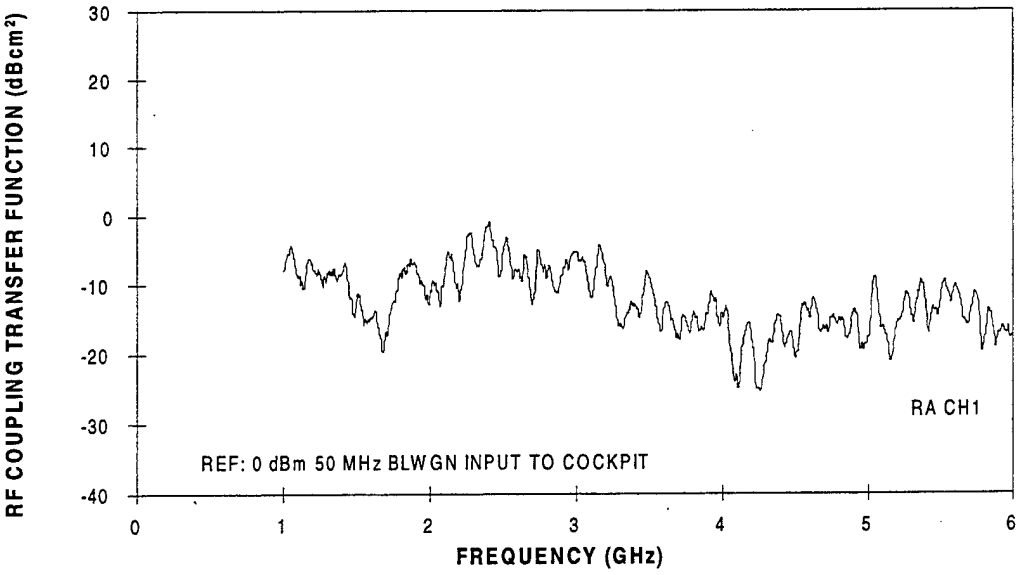

FIGURE 4-91. RADIO FREQUENCY COUPLING TRANSFER FUNCTION FOR RADAR ALTIMETER CHANNEL 1 IN AIRCRAFT FOR BLWGN EXCITATION

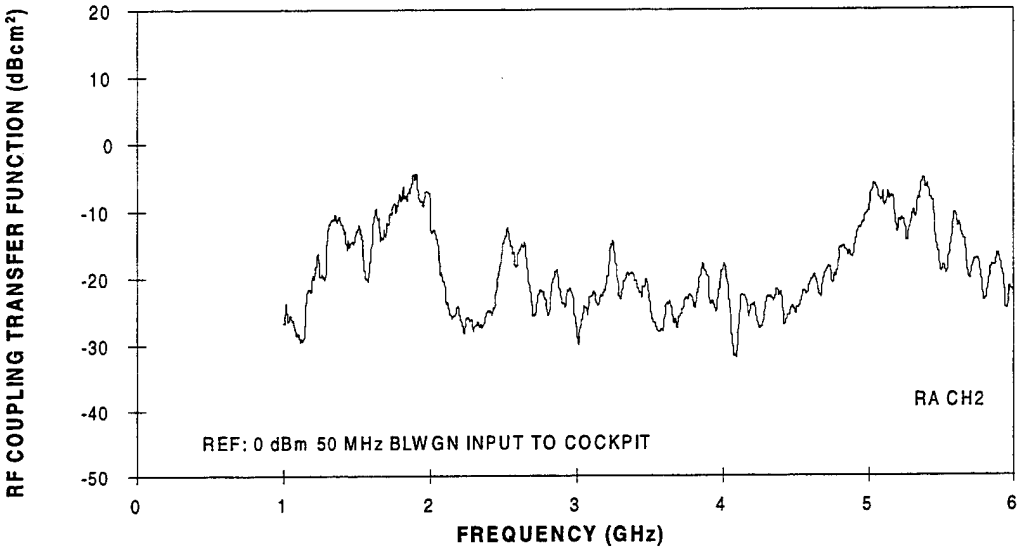

FIGURE 4-92. RADIO FREQUENCY COUPLING TRANSFER FUNCTION FOR RADAR ALTIMETER CHANNEL 2 IN AIRCRAFT FOR BLWGN EXCITATION

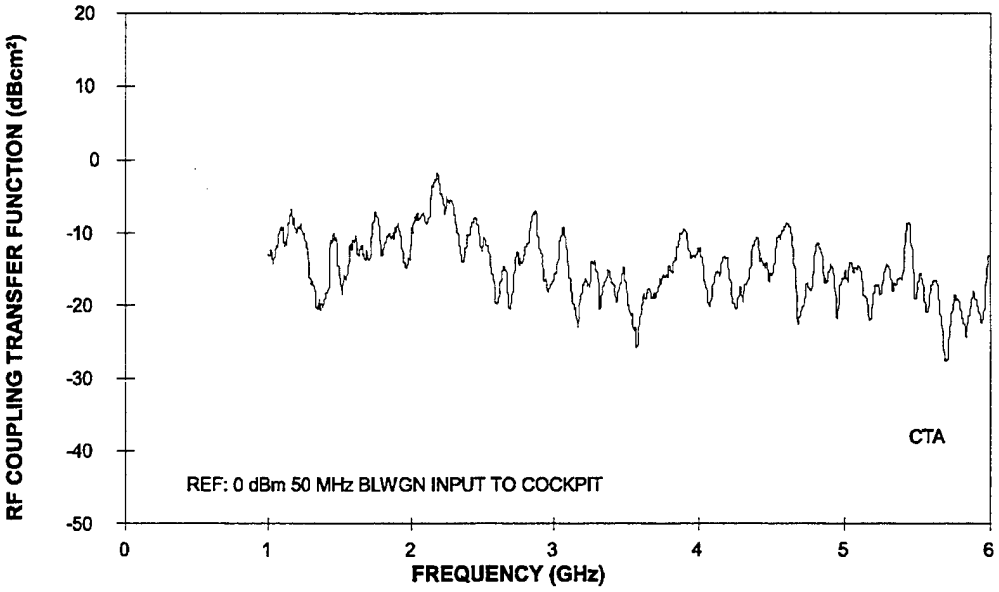

FIGURE 4-93. RADIO FREQUENCY COUPLING TRANSFER FUNCTION FOR COMMON TEST ARTICLE IN COCKPIT FOR BLWGN EXCITATION

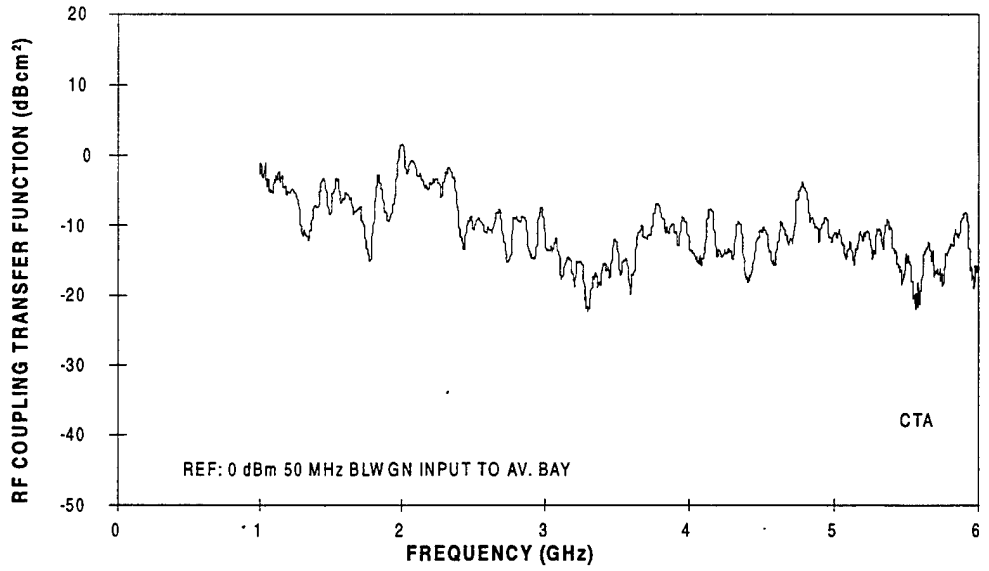

FIGURE 4-94. RADIO FREQUENCY COUPLING TRANSFER FUNCTION FOR COMMON TEST ARTICLE IN AVIONICS BAY EQUIPMENT RACK FOR BLWGN EXCITATION

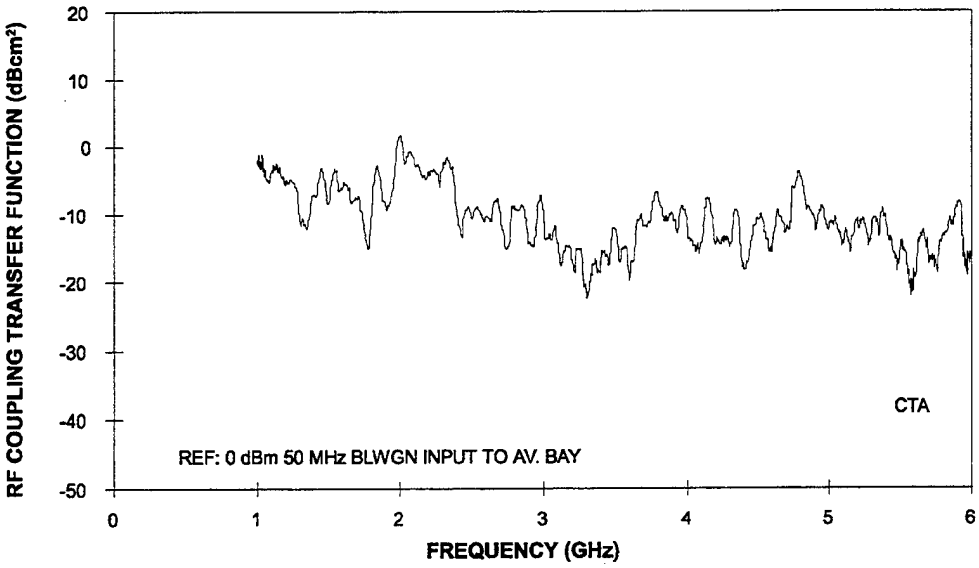

FIGURE 4-95. RADIO FREQUENCY COUPLING TRANSFER FUNCTION FOR COMMON TEST ARTICLE IN ISOLATED AVIONICS BAY LOCATION FOR BLWGN EXCITATION

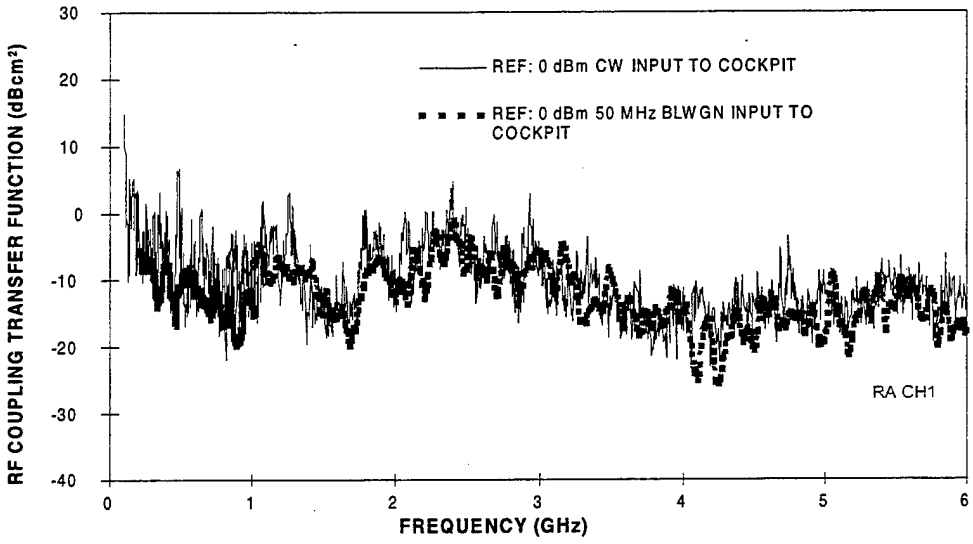

FIGURE 4-96. COMPARISON OF RADAR ALTIMETER CHANNEL 1 COUPLING TRANSFER FUNCTIONS FOR CW AND BLWGN EXCITATIONS

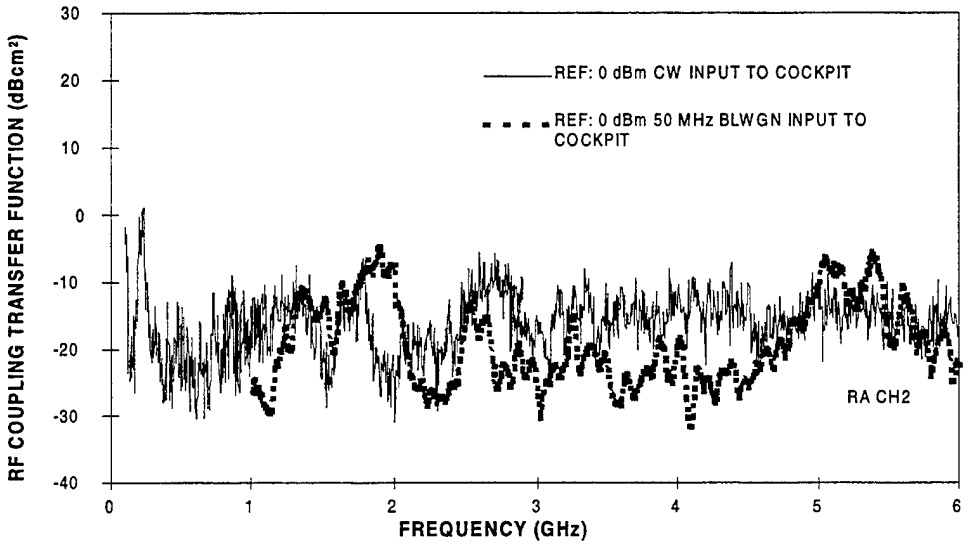

FIGURE 4-97. COMPARISON OF RADAR ALTIMETER CHANNEL 2 COUPLING TRANSFER FUNCTIONS FOR CW AND BLWGN EXCITATIONS

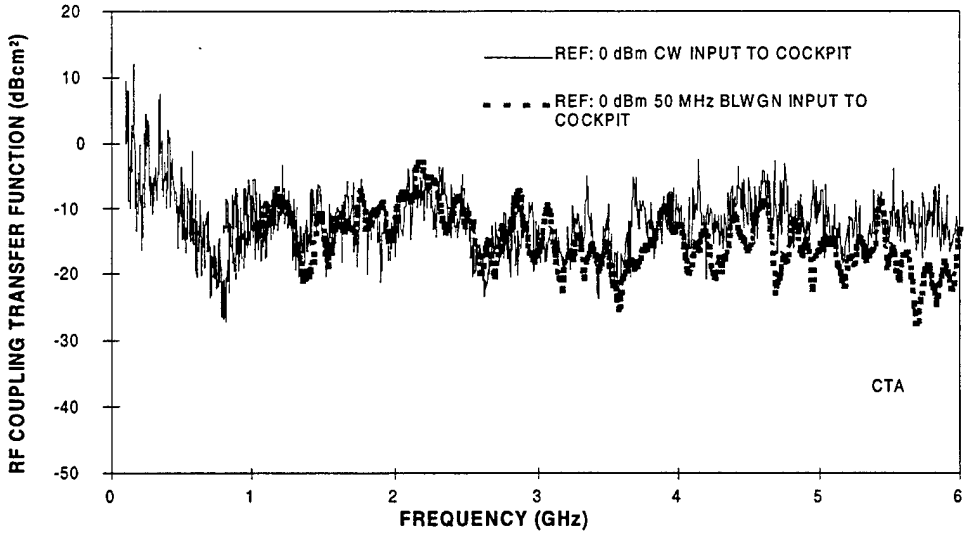

FIGURE 4-98. COMPARISON OF COMMON TEST ARTICLE COUPLING TRANSFER FUNCTIONS FOR COCKPIT LOCATION FOR CW AND BLWGN NOISE EXCITATIONS

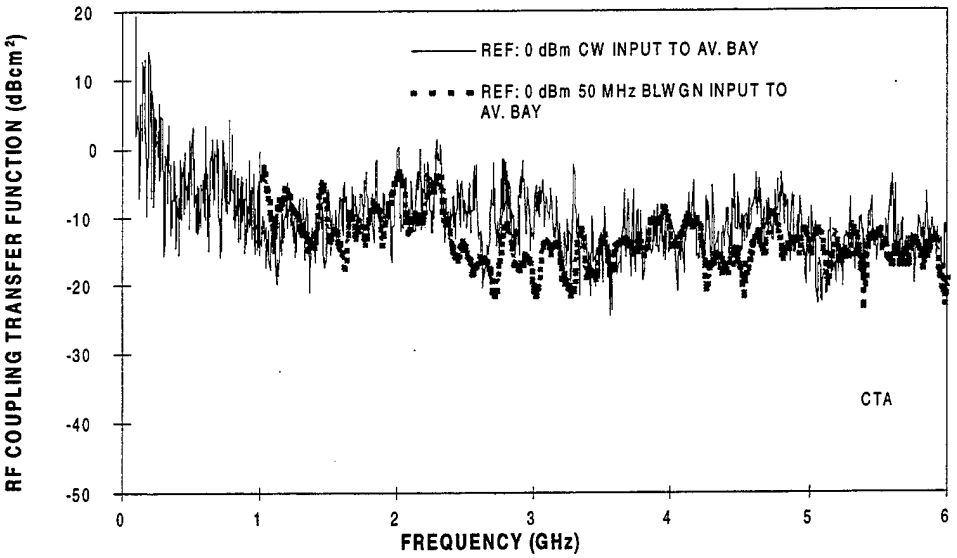

FIGURE 4-99. COMPARISON OF COMMON TEST ARTICLE COUPLING TRANSFER FUNCTIONS FOR AVIONICS BAY EQUIPMENT RACK LOCATION FOR CW AND BLWGN NOISE EXCITATIONS

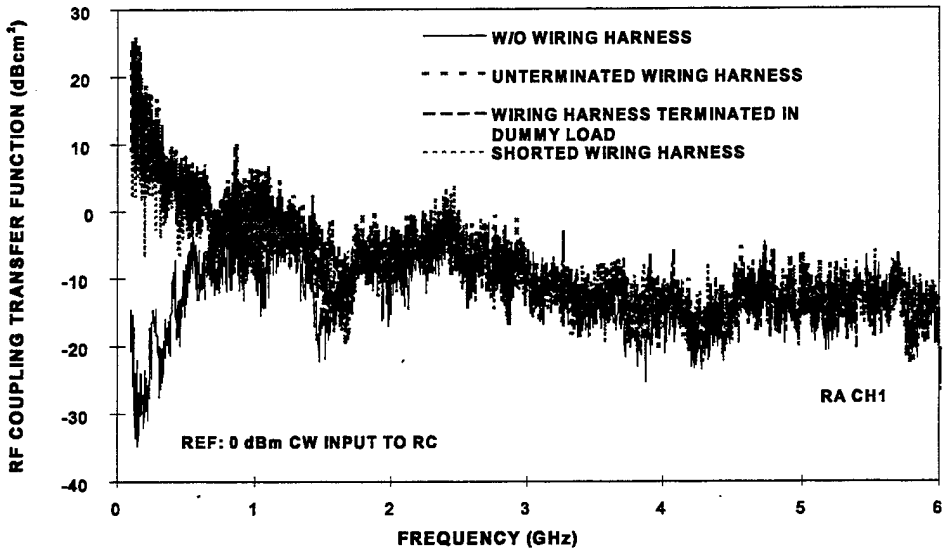

FIGURE 4-100. COMPARISON OF RADAR ALTIMETER CHANNEL 1 COUPLING TRANSFER FUNCTIONS FOR CW EXCITATION ON A DIELECTRIC BLOCK IN NSWCDD REVERBERATION CHAMBER

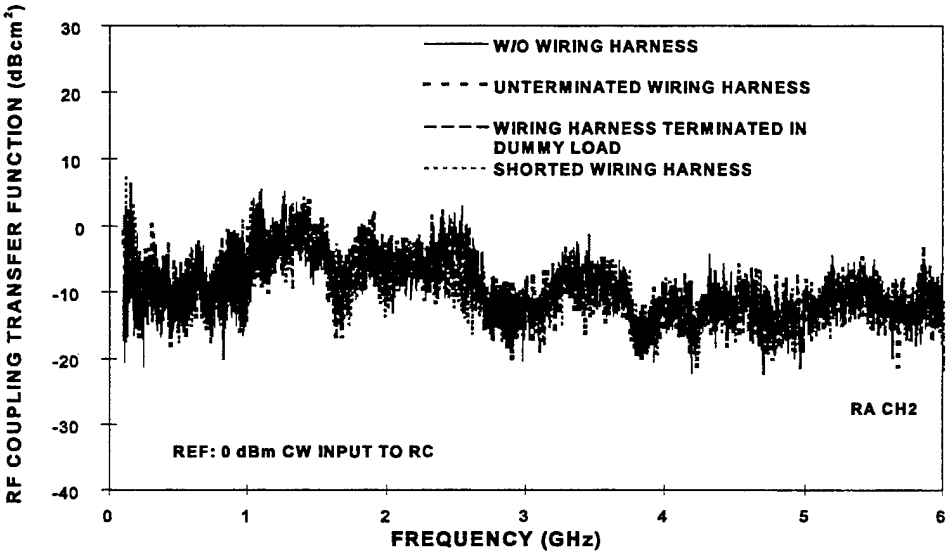

FIGURE 4-101. COMPARISON OF RADAR ALTIMETER CHANNEL 2 COUPLING TRANSFER FUNCTIONS FOR CW EXCITATION ON A DIELECTRIC BLOCK IN NSWCDD REVERBERATION CHAMBER

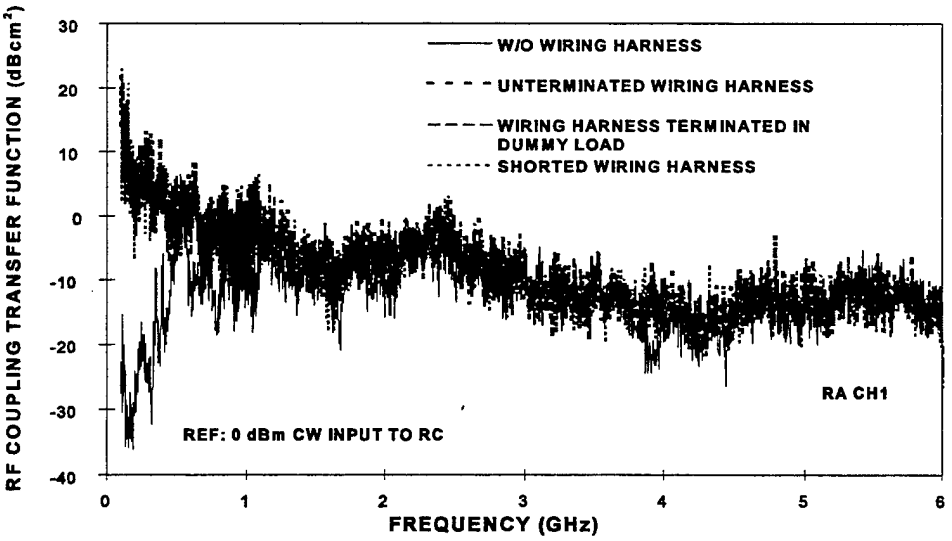

FIGURE 4-102. COMPARISON OF RADAR ALTIMETER CHANNEL 1 COUPLING TRANSFER FUNCTIONS FOR CW EXCITATION ON A METAL GROUND PLANE IN NSWCDD REVERBERATION CHAMBER

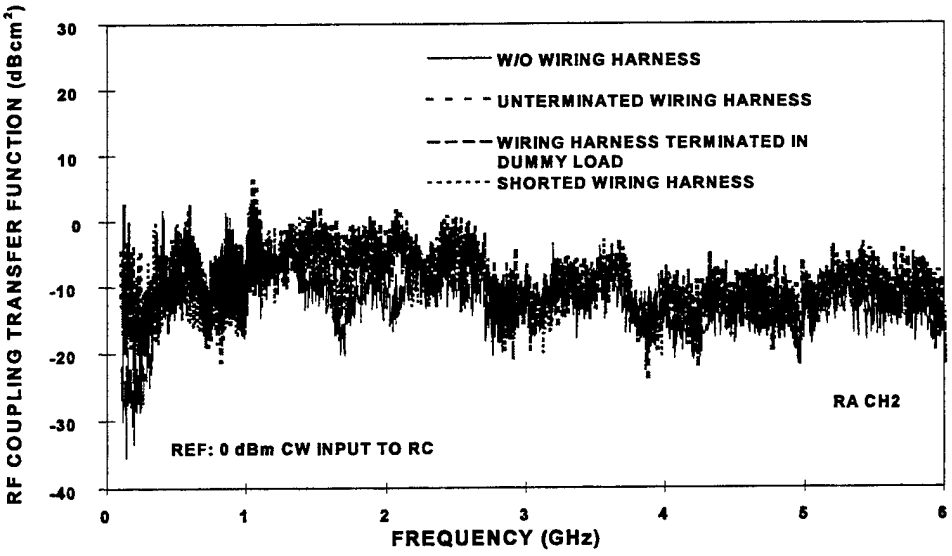

FIGURE 4-103. COMPARISON OF RADAR ALTIMETER CHANNEL 2 COUPLING TRANSFER FUNCTIONS FOR CW EXCITATION ON A METAL GROUND PLANE IN NSWCDD REVERBERATION CHAMBER

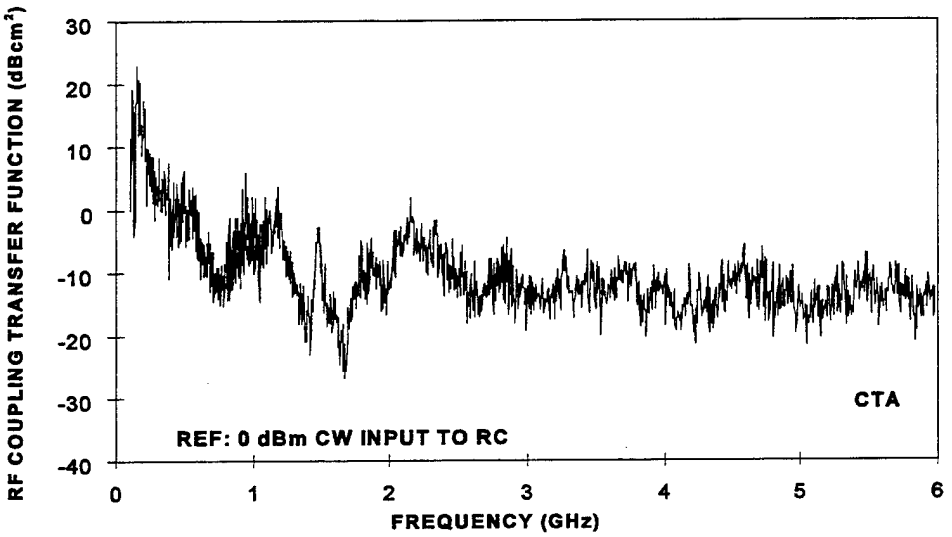

FIGURE 4-104. COMMON TEST ARTICLE COUPLING TRANSFER FUNCTION FOR CW WAVE EXCITATION ON A DIELECTRIC BLOCK IN NSWCDD REVERBERATION CHAMBER

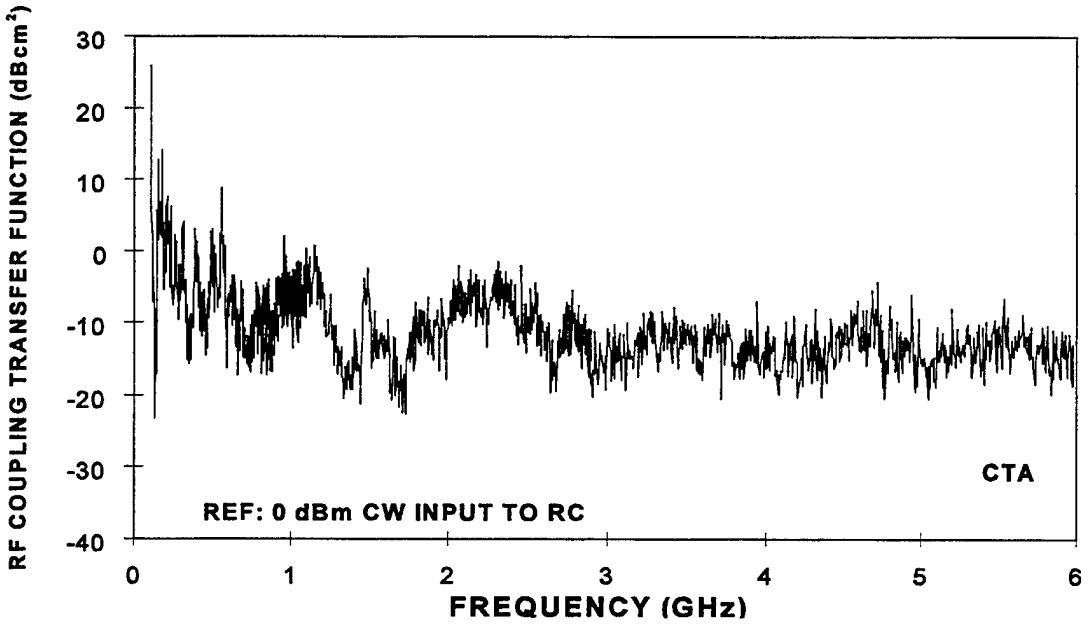

FIGURE 4-105. COMMON TEST ARTICLE COUPLING TRANSFER FUNCTION FOR CW EXCITATION ON A METAL GROUND PLANE IN NSWCDD REVERBERATION CHAMBER

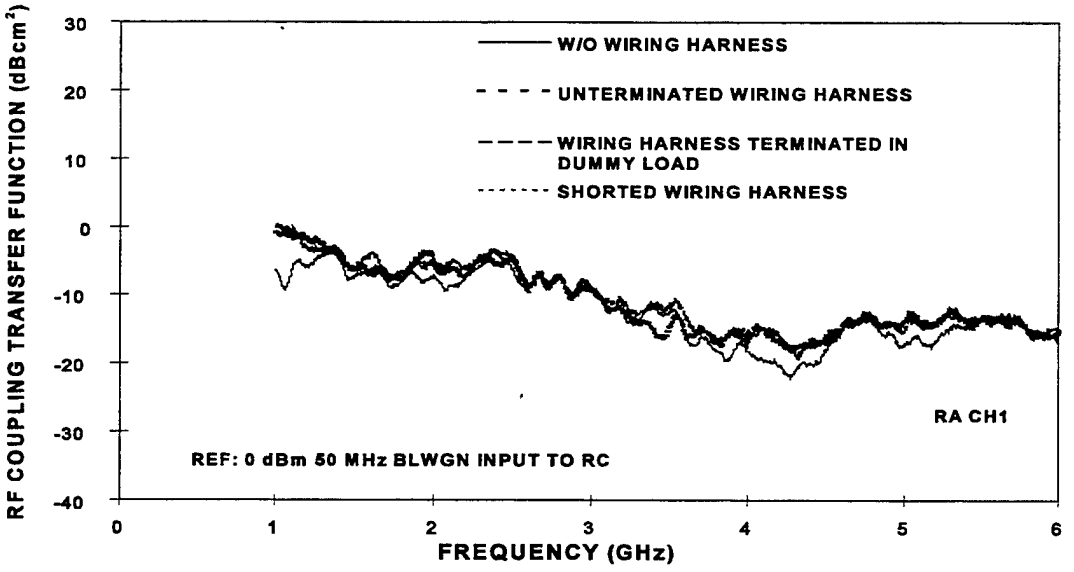

FIGURE 4-106. COMPARISON OF RADAR ALTIMETER CHANNEL 1 COUPLING TRANSFER FUNCTIONS FOR BLWGN EXCITATION ON A DIELECTRIC BLOCK IN NSWCDD REVERBERATION CHAMBER

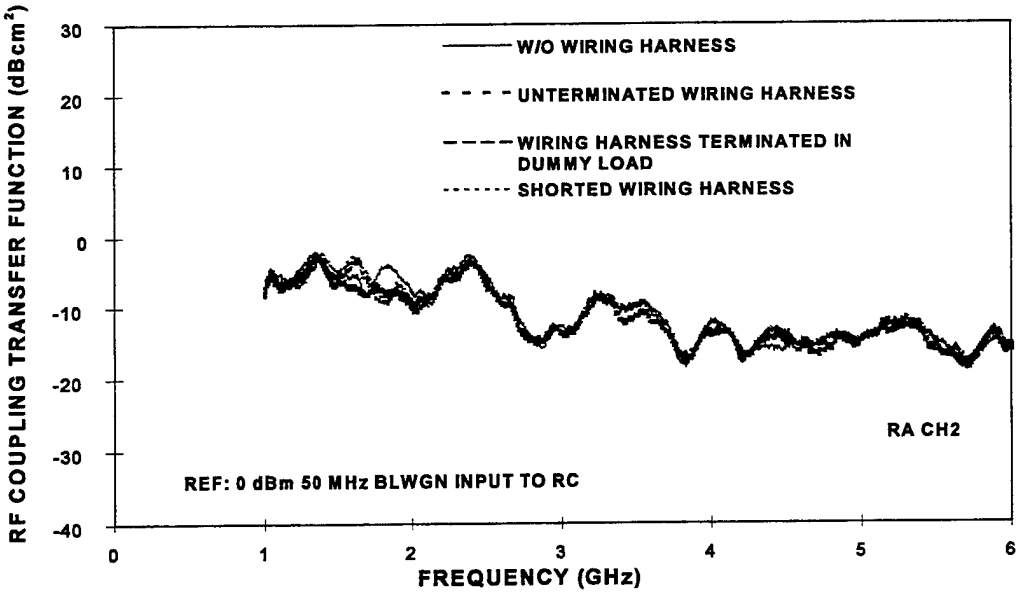

FIGURE 4-107. COMPARISON OF RADAR ALTIMETER CHANNEL 2 COUPLING TRANSFER FUNCTIONS FOR BLWGN EXCITATION ON A DIELECTRIC BLOCK IN NSWCDD REVERBERATION CHAMBER

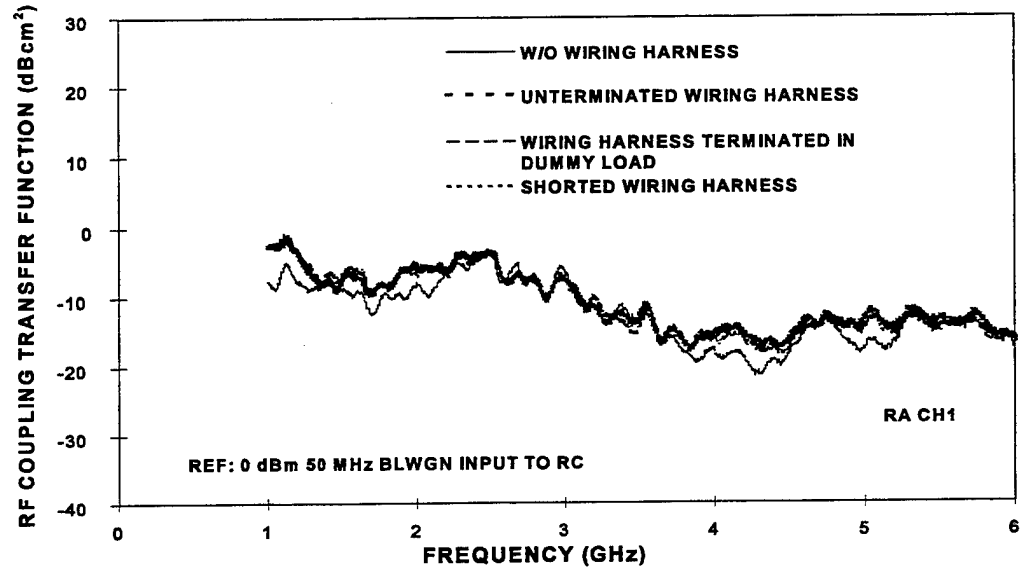

FIGURE 4-108. COMPARISON OF RADAR ALTIMETER CHANNEL 1 COUPLING TRANSFER FUNCTIONS FOR BLWGN EXCITATION ON A METAL GROUND PLANE IN NSWCDD REVERBERATION CHAMBER

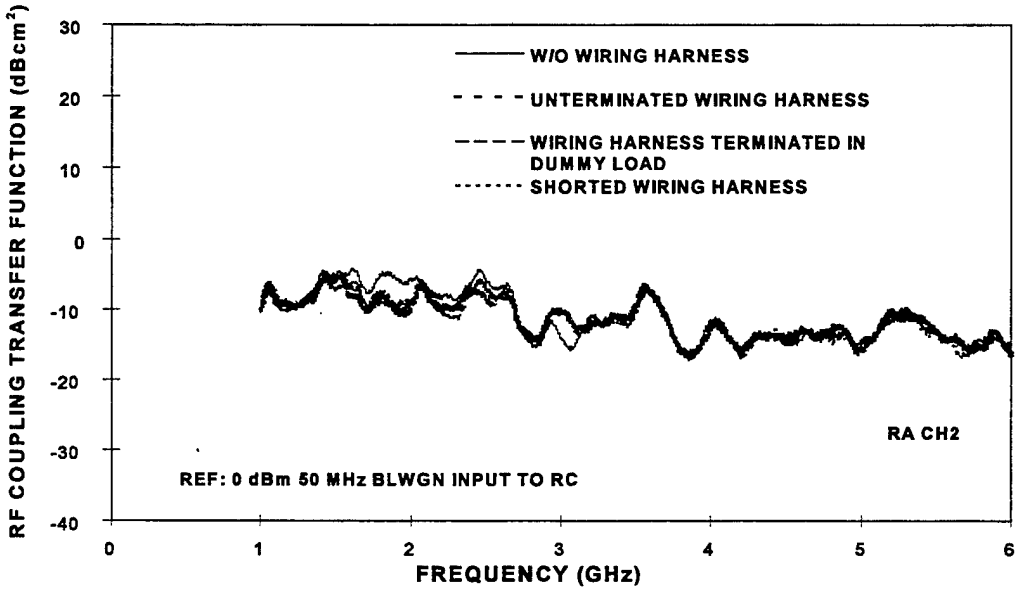

FIGURE 4-109. COMPARISON OF RADAR ALTIMETER CHANNEL 2 COUPLING TRANSFER FUNCTIONS FOR BLWGN EXCITATION ON A METAL GROUND PLANE IN NSWCDD REVERBERATION CHAMBER

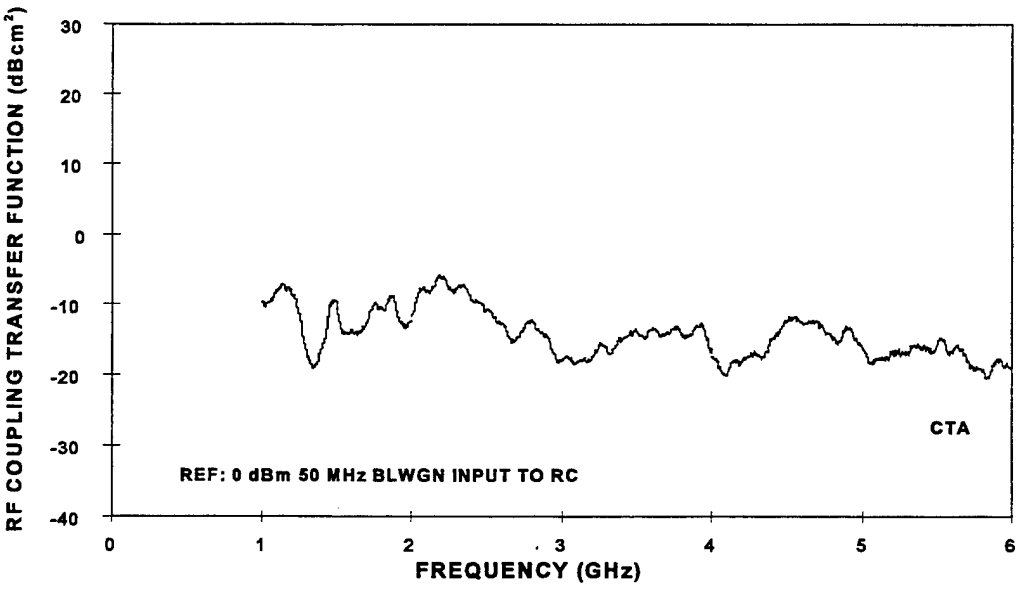

FIGURE 4-110. COMMON TEST ARTICLE COUPLING TRANSFER FUNCTION FOR BLWGN EXCITATION ON A DIELECTRIC BLOCK IN NSWCDD REVERBERATION CHAMBER

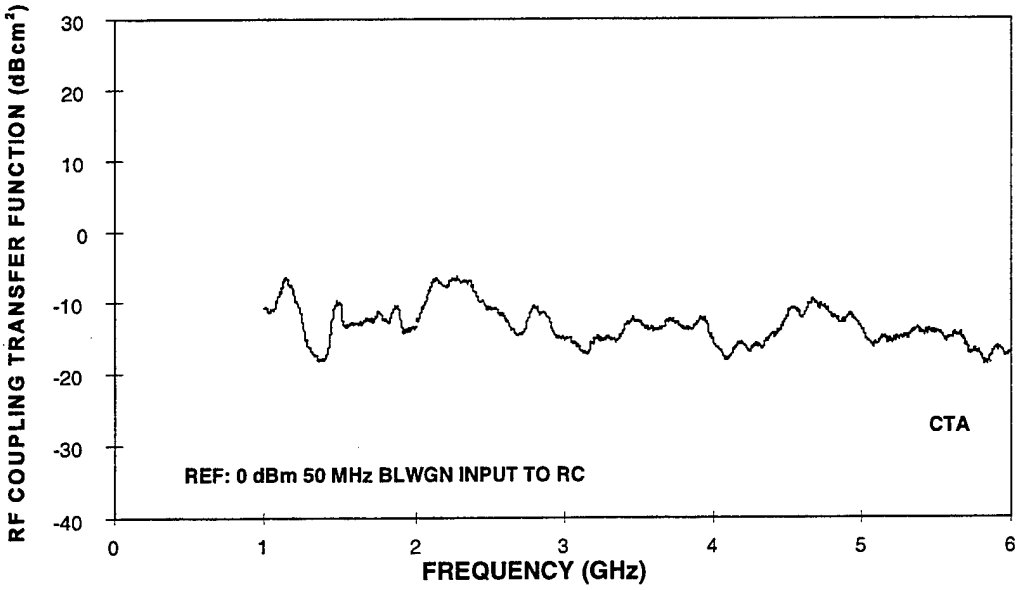

FIGURE 4-111. COMMON TEST ARTICLE COUPLING TRANSFER FUNCTION FOR BLWGN EXCITATION ON A METAL GROUND PLANE IN NSWCDD REVERBERATION CHAMBER

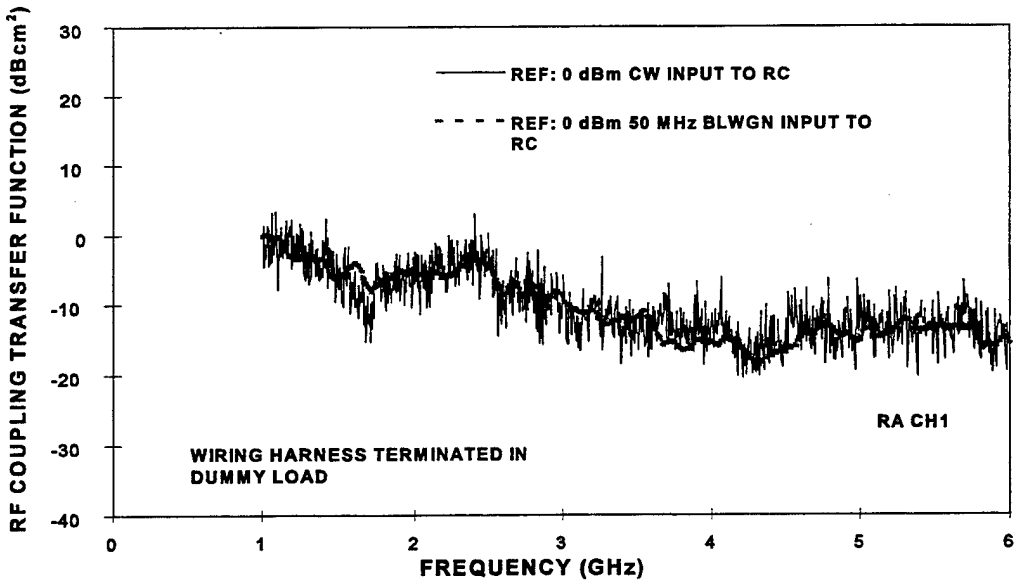

FIGURE 4-112. COMPARISON OF RADAR ALTIMETER CHANNEL 1 COUPLING TRANSFER FUNCTIONS FOR CW AND BLWGN EXCITATIONS IN NSWCDD REVERBERATION CHAMBER

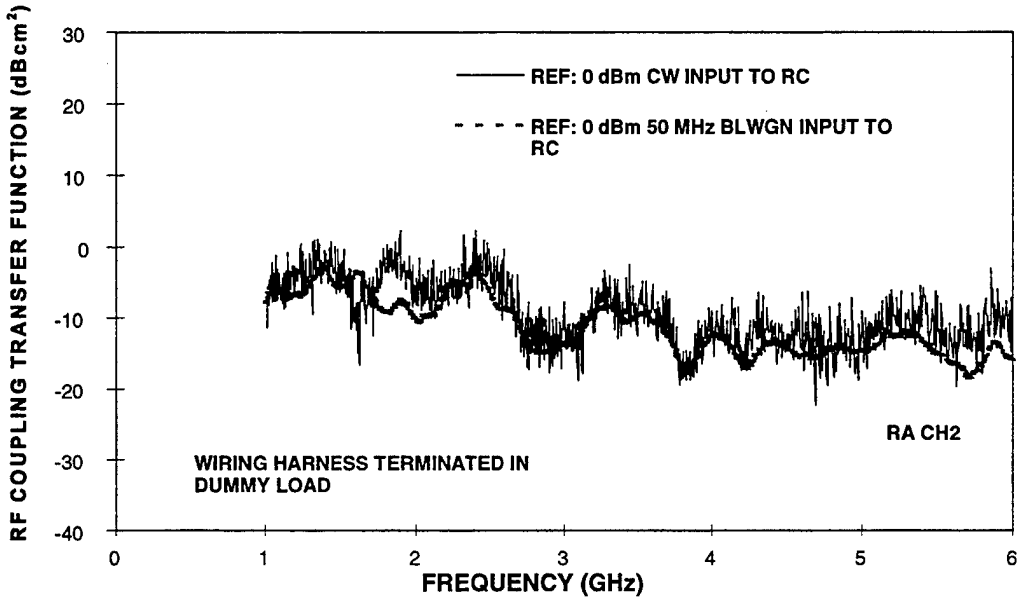

FIGURE 4-113. COMPARISON OF RADAR ALTIMETER CHANNEL 2 COUPLING TRANSFER FUNCTIONS FOR CW AND BLWGN EXCITATIONS IN NSWCDD REVERBERATION CHAMBER

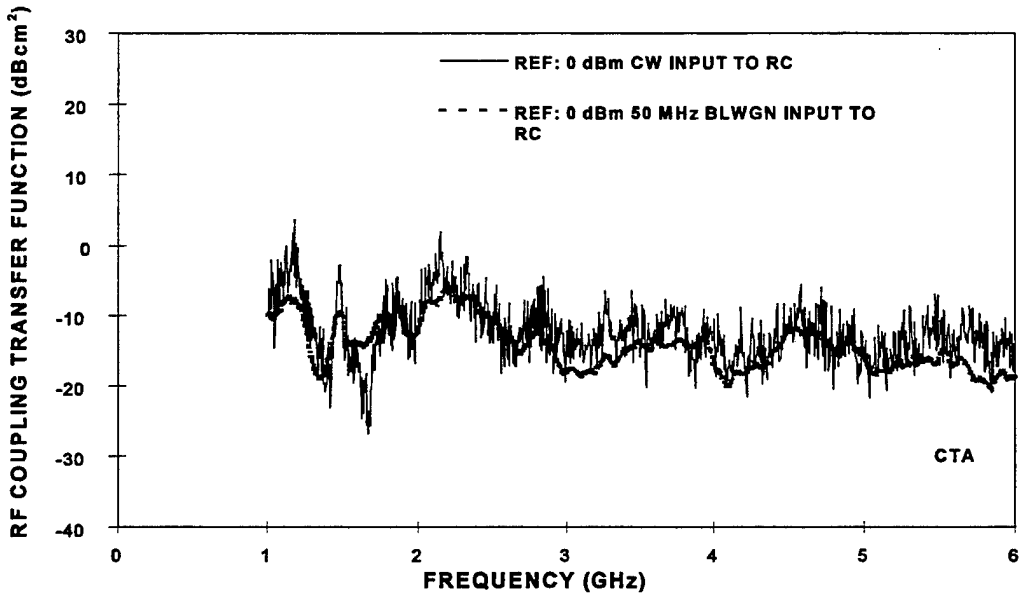

FIGURE 4-114. COMPARISON OF COMMON TEST ARTICLE COUPLING TRANSFER FUNCTIONS FOR CW AND BLWGN EXCITATIONS IN NSWCDD REVERBERATION CHAMBER

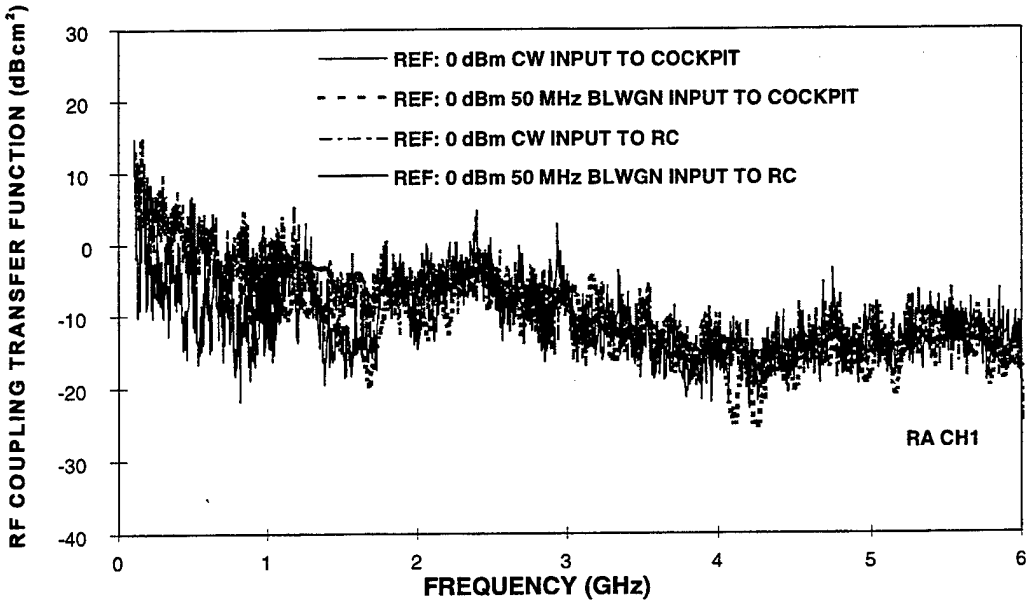

FIGURE 4-115. COMPARISON OF RADAR ALTIMETER CHANNEL 1 COUPLING TRANSFER FUNCTIONS FROM AIRCRAFT AND NSWCDD REVERBERATION CHAMBER

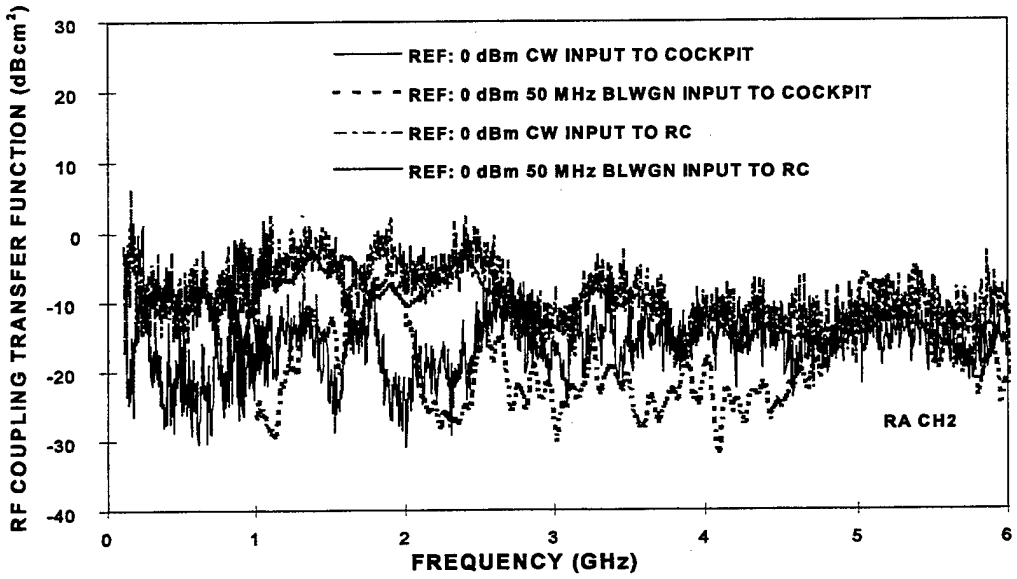

FIGURE 4-116. COMPARISON OF RADAR ALTIMETER CHANNEL 2 COUPLING TRANSFER FUNCTIONS FROM AIRCRAFT AND NSWCDD REVERBERATION CHAMBER

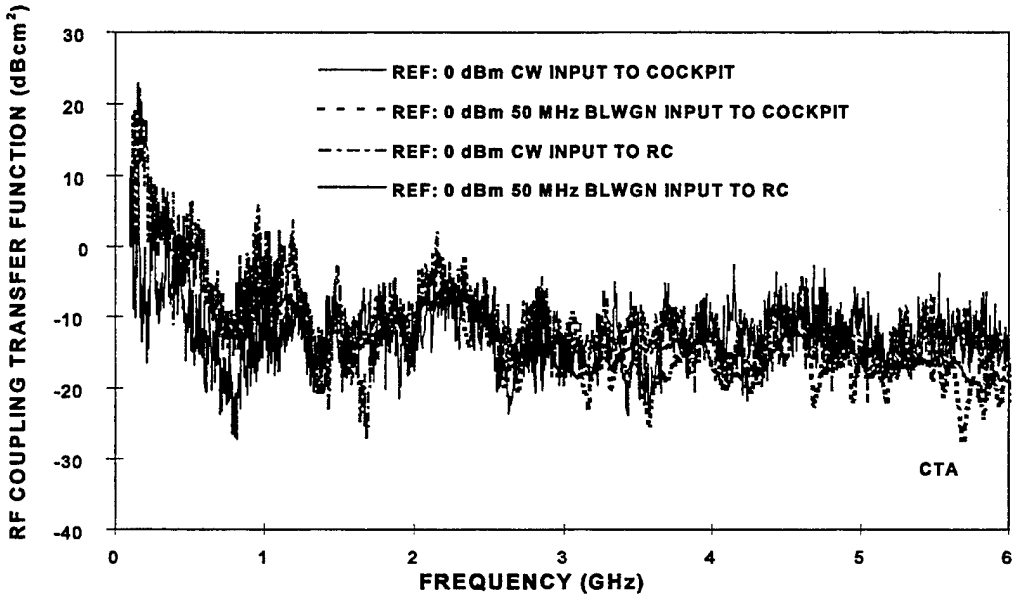

FIGURE 4-117. COMPARISON OF COMMON TEST ARTICLE COUPLING TRANSFER FUNCTIONS FROM COCKPIT LOCATION AND NSWCDD REVERBERATION CHAMBER

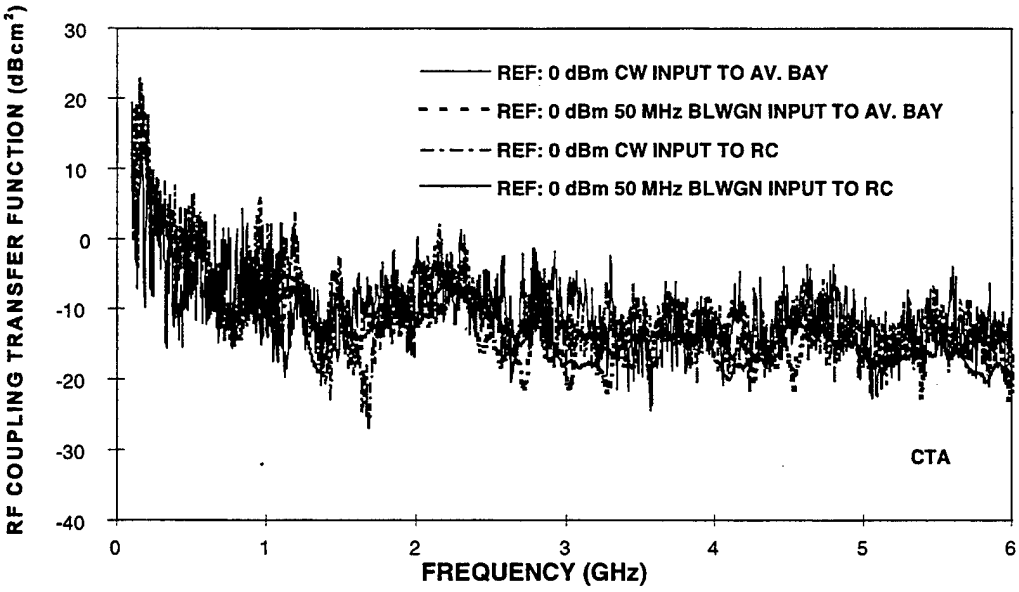

FIGURE 4-118. COMPARISON OF COMMON TEST ARTICLE COUPLING TRANSFER FUNCTIONS FROM AVIONICS BAY EQUIPMENT RACK AND NSWCDD REVERBERATION CHAMBER

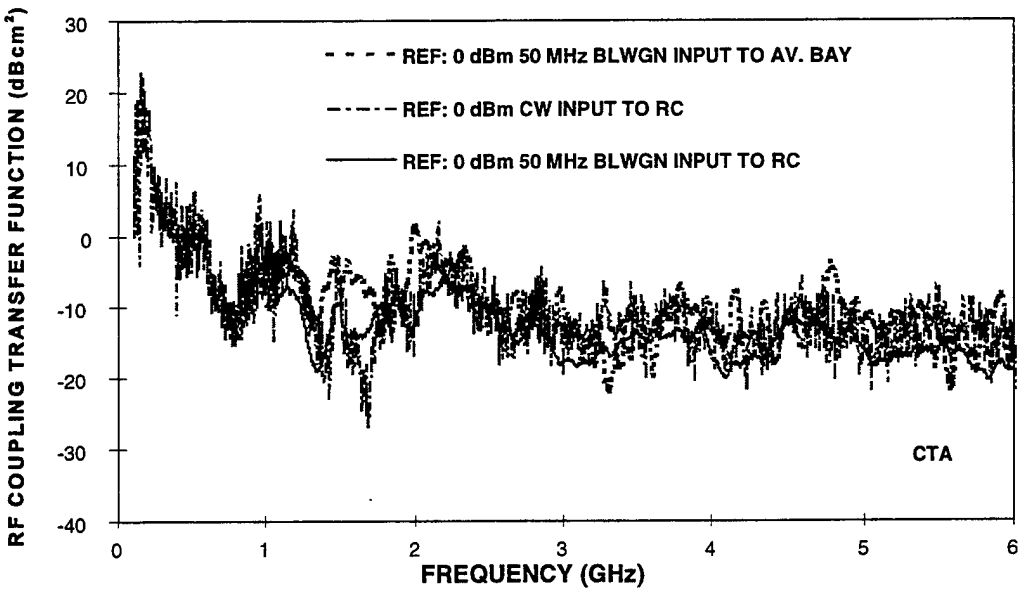

FIGURE 4-119. COMPARISON OF COMMON TEST ARTICLE COUPLING TRANSFER FUNCTIONS FROM ISOLATED AVIONICS BAY LOCATION AND NSWCDD REVERBERATION CHAMBER

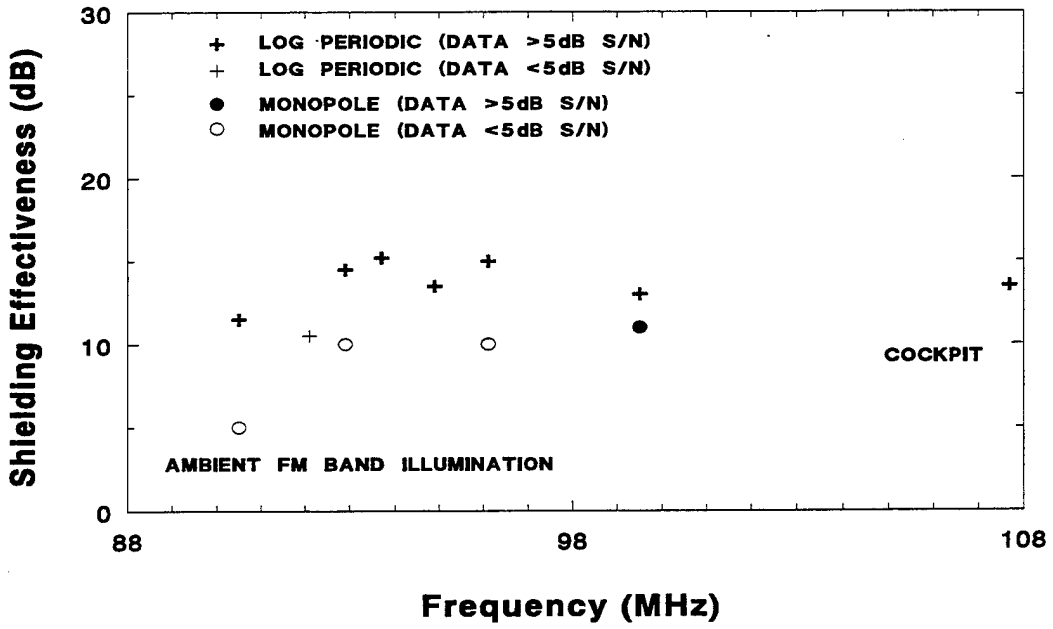

FIGURE 4-120. MINIMUM COCKPIT SHIELDING EFFECTIVENESS FOR AMBIENT FM BAND

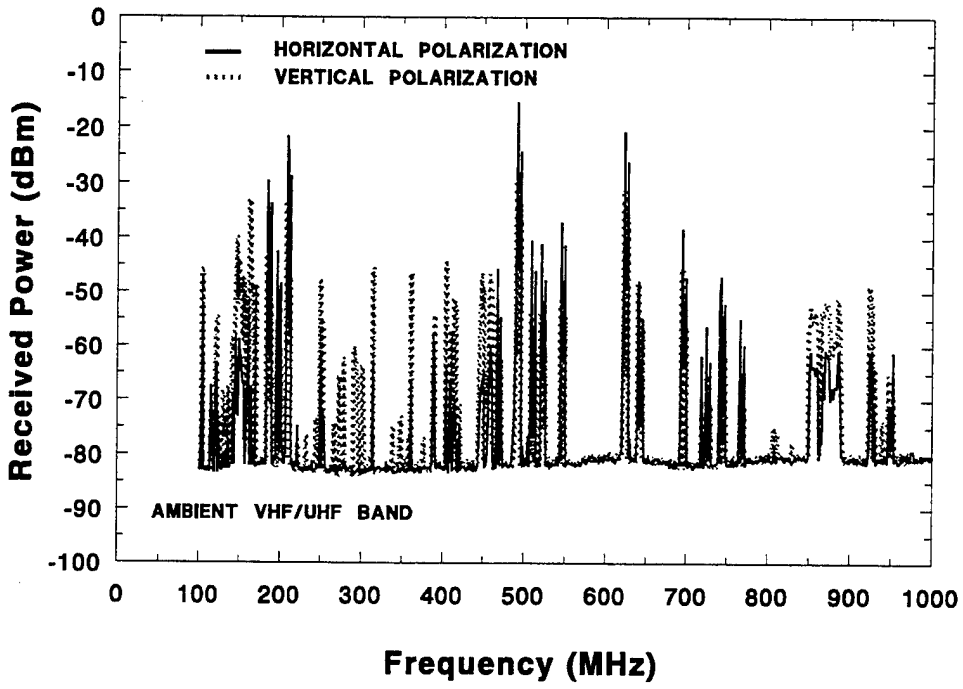

FIGURE 4-121. POLARIZATION EFFECTS FOR AMBIENT VHF/UHF BAND

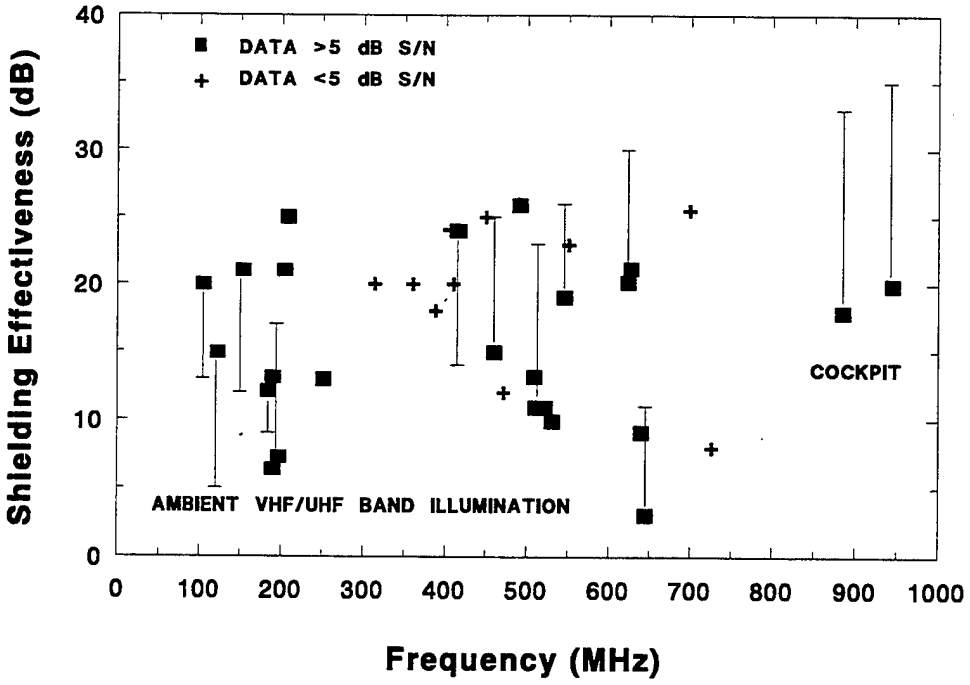

FIGURE 4-122. MINIMUM COCKPIT SHIELDING EFFECTIVENESS FOR AMBIENT VHF/UHF BAND

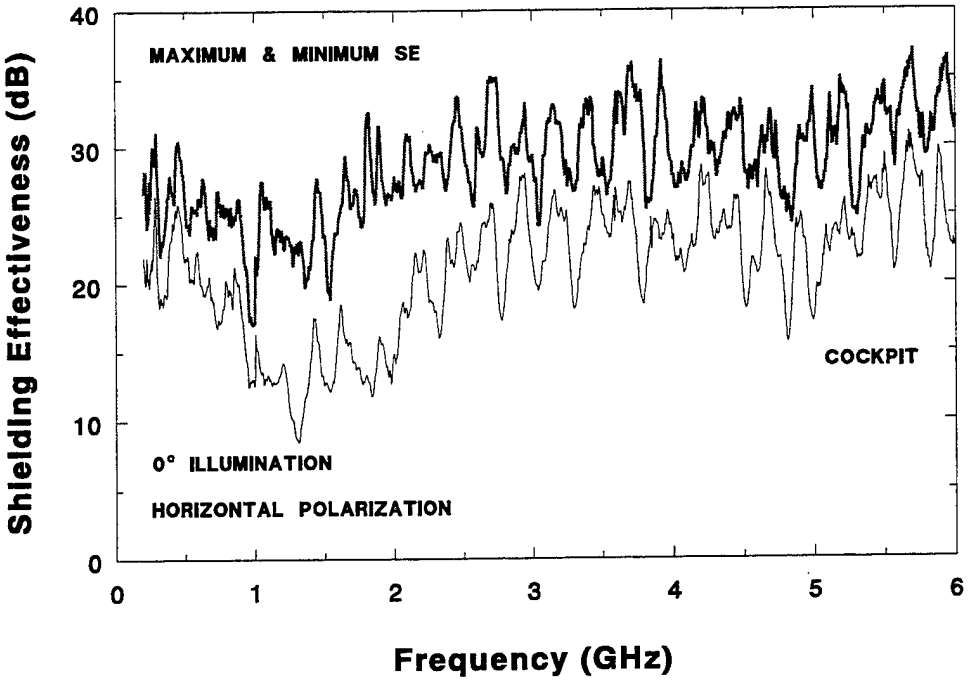

FIGURE 4-123. MAXIMUM AND MINIMUM COCKPIT SHIELDING EFFECTIVENESS FOR HORIZONTALLY POLARIZED, 0° BLGWN EXCITATION

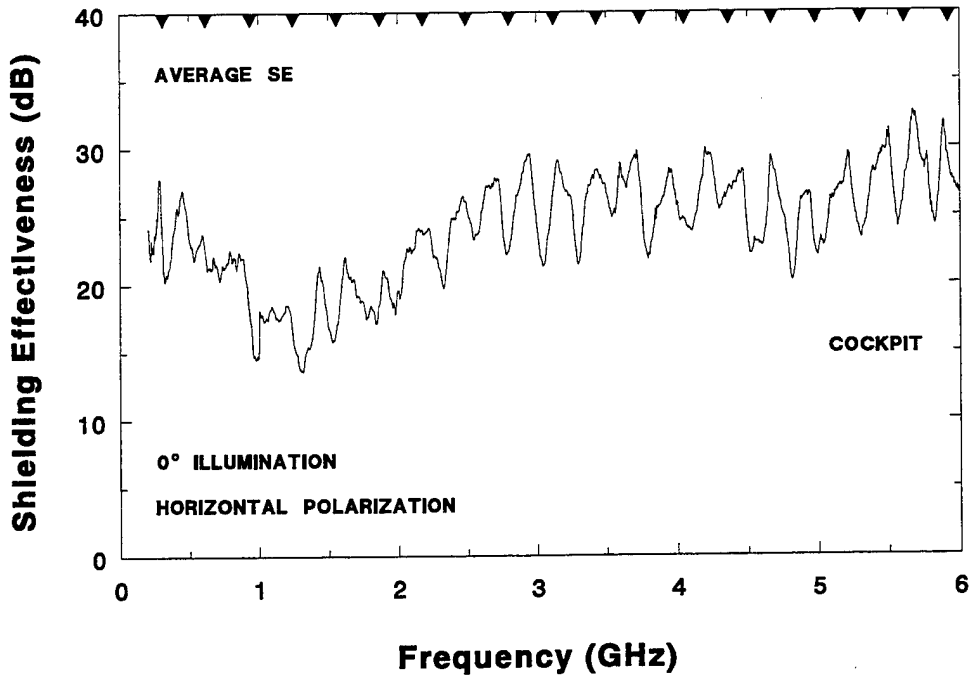

FIGURE 4-124. AVERAGE COCKPIT SHIELDING EFFECTIVENESS FOR HORIZONTALLY POLARIZED, 0° BLWGN EXCITATION

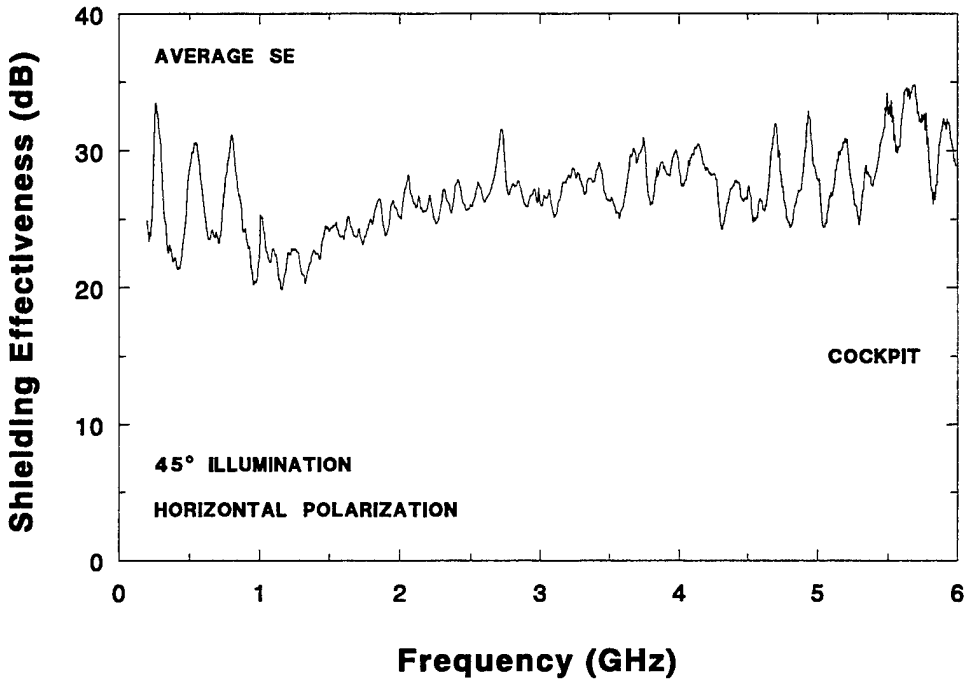

FIGURE 4-125. AVERAGE COCKPIT SHIELDING EFFECTIVENESS FOR HORIZONTALLY POLARIZED, 45° BLWGN EXCITATION

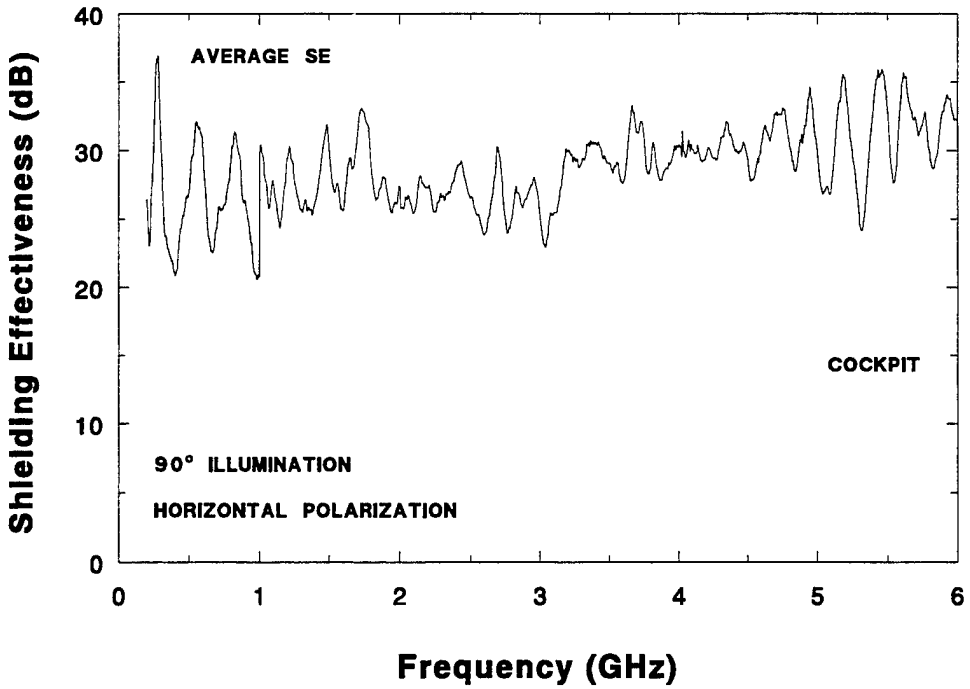

FIGURE 4-126. AVERAGE COCKPIT SHIELDING EFFECTIVENESS FOR HORIZONTALLY POLARIZED, 90° BLWGN EXCITATION

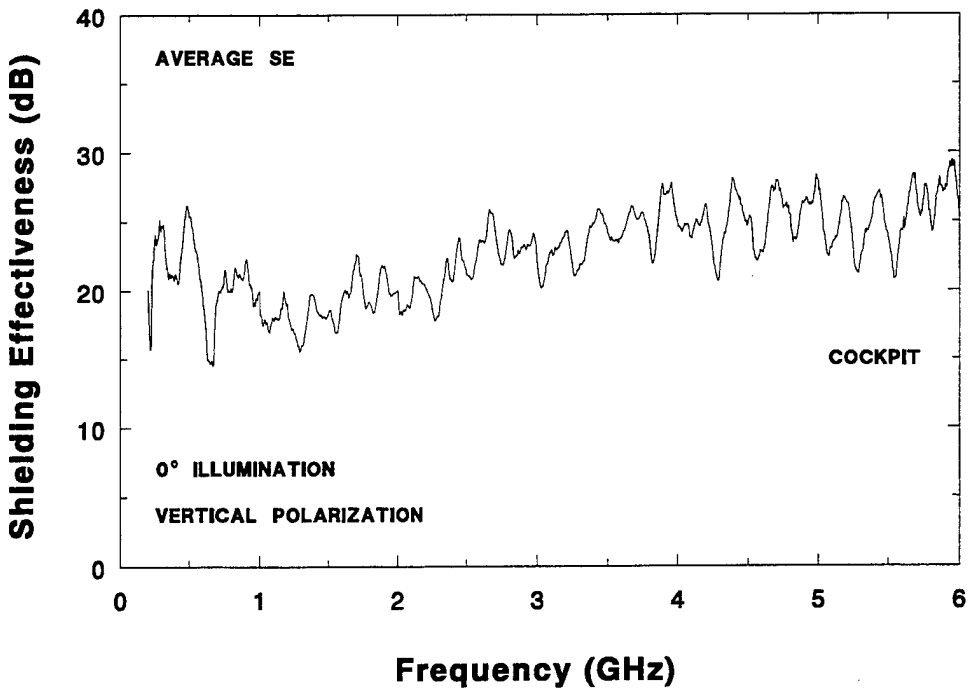

FIGURE 4-127. AVERAGE COCKPIT SHIELDING EFFECTIVENESS FOR VERTICALLY POLARIZED, 0° BLWGN EXCITATION

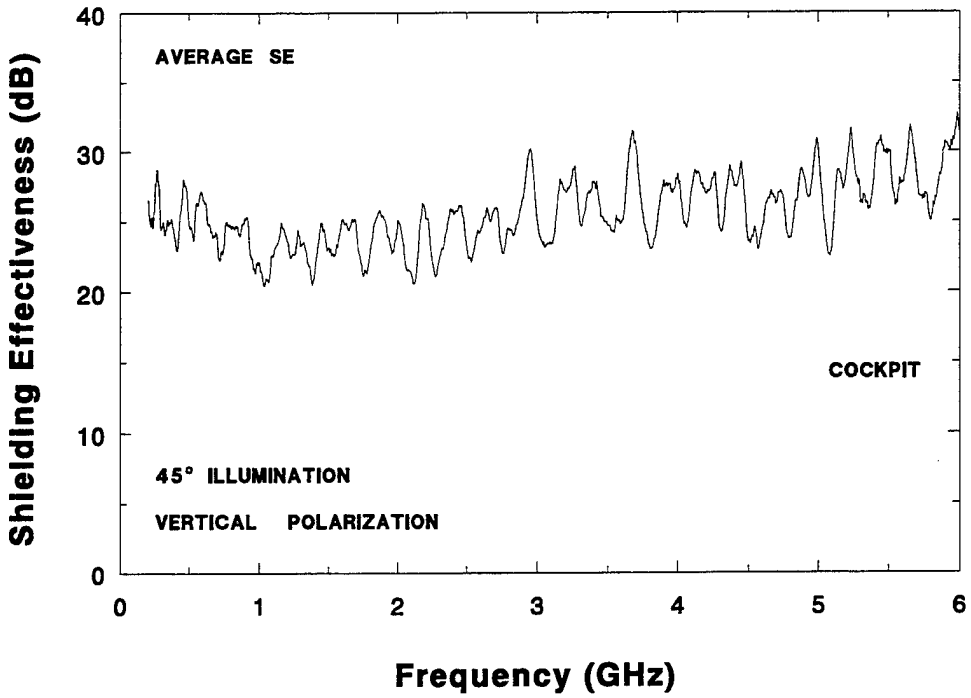

FIGURE 4-128. AVERAGE COCKPIT SHIELDING EFFECTIVENESS FOR VERTICALLY POLARIZED, 45° BLWGN EXCITATION

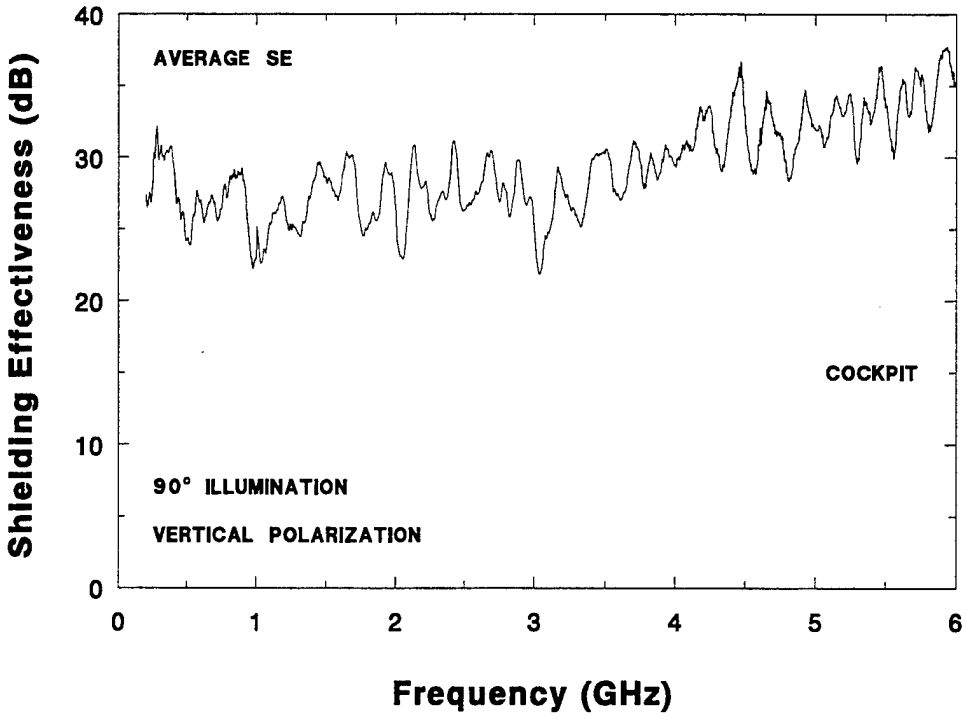

FIGURE 4-129. AVERAGE COCKPIT SHIELDING EFFECTIVESS FOR VERTICALLY POLARIZED, 90° BLGWN EXCITATION

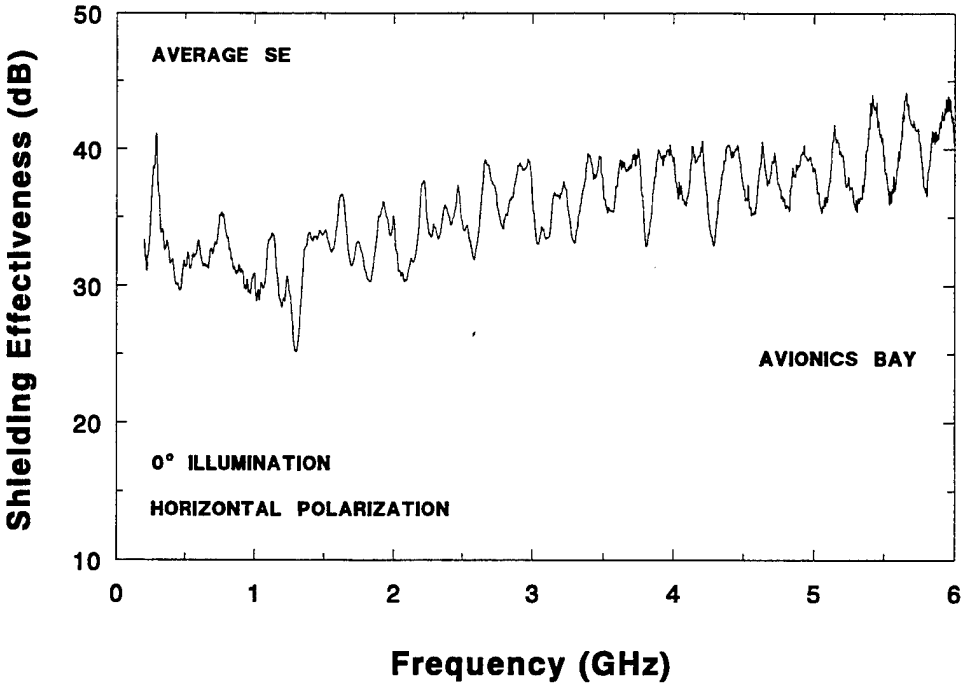

FIGURE 4-130. AVERAGE AVIONICS BAY SHIELDING EFFECTIVENESS FOR HORIZONTALLY POLARIZED, 0° BLWGN EXCITATION

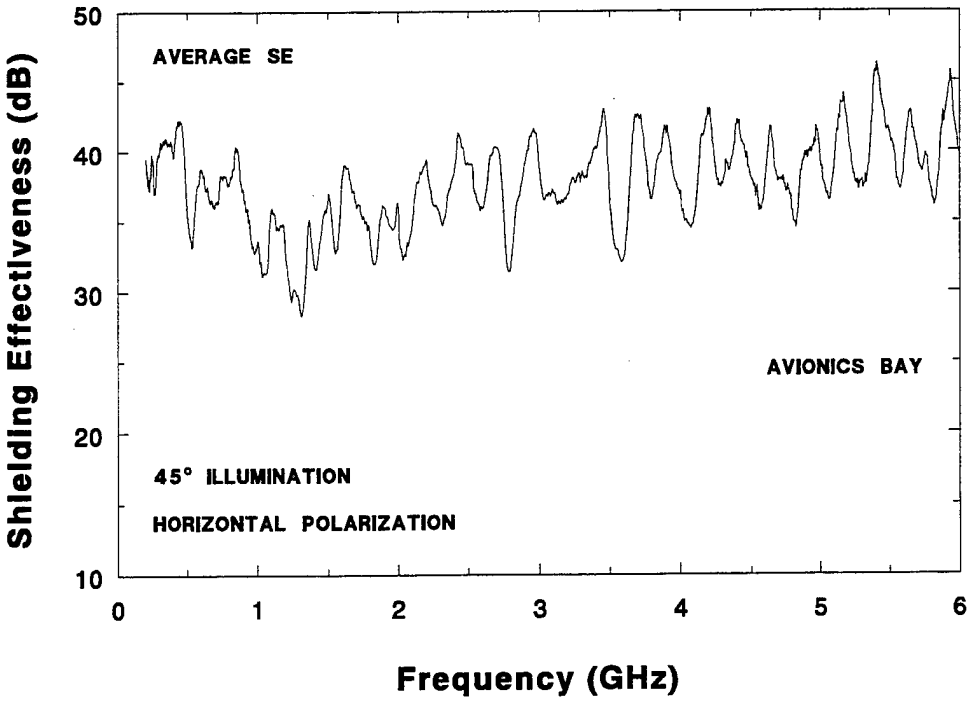

FIGURE 4-131. AVERAGE AVIONICS BAY SHIELDING EFFECTIVENESS FOR HORIZONTALLY POLARIZED, 45° BLWGN EXCITATION

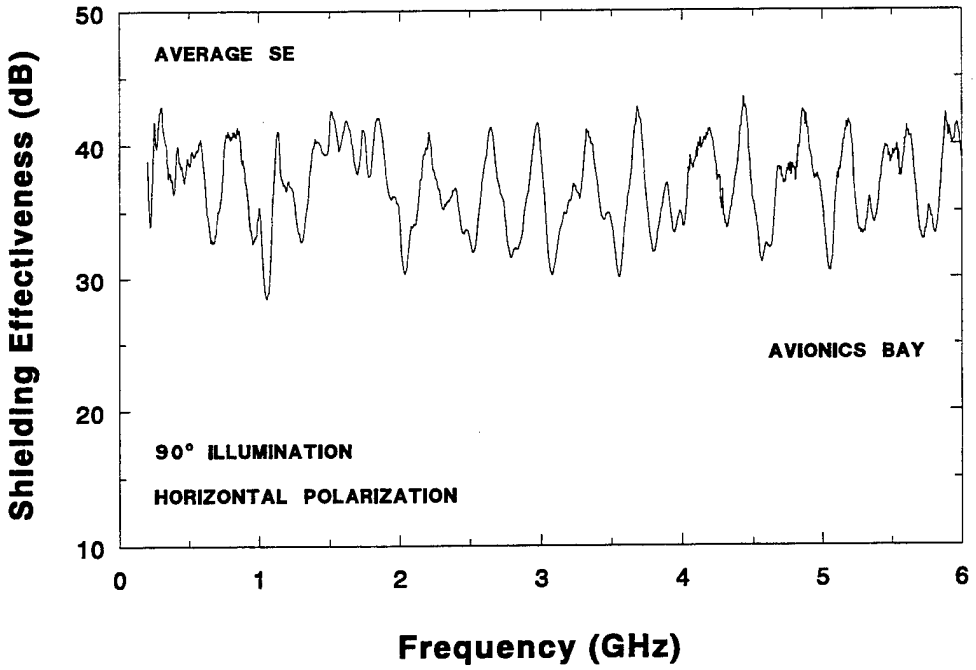

FIGURE 4-132. AVERAGE AVIONICS BAY SHIELDING EFFECTIVENESS FOR HORIZONTALLY POLARIZED, 90° BLWGN EXCITATION

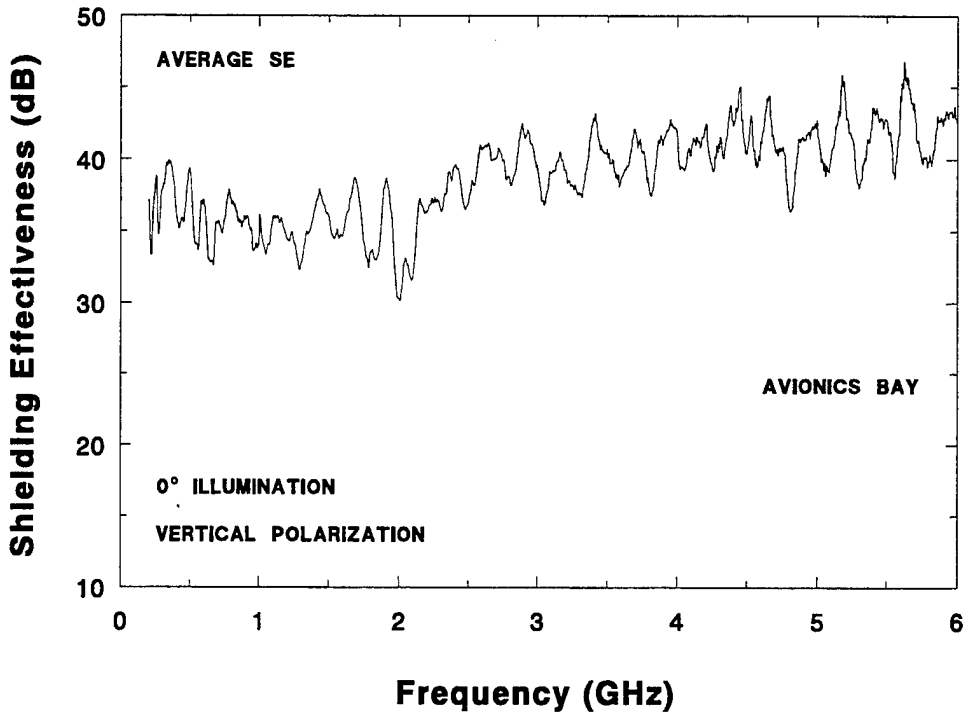

FIGURE 4-133. AVERAGE AVIONICS BAY SHIELDING EFFECTIVESS FOR VERTICALLY POLARIZED, 0° BLWGN EXCITATION

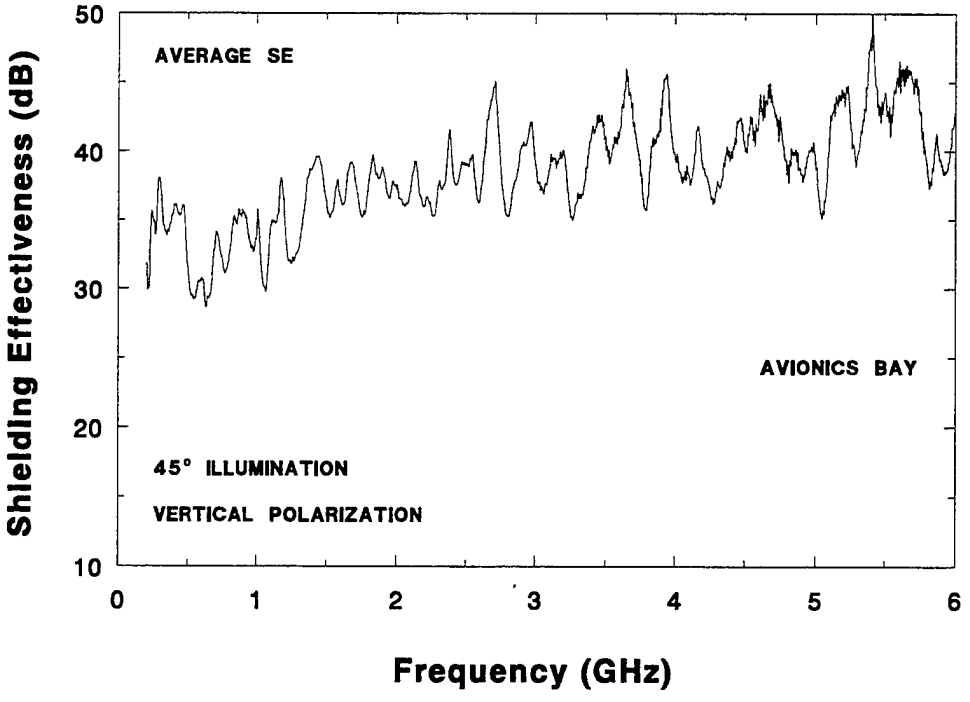

FIGURE 4-134. AVERAGE AVIONICS BAY SHIELDING EFFECTIVENESS FOR VERTICALLY POLARIZED, 45° BLWGN EXCITATION

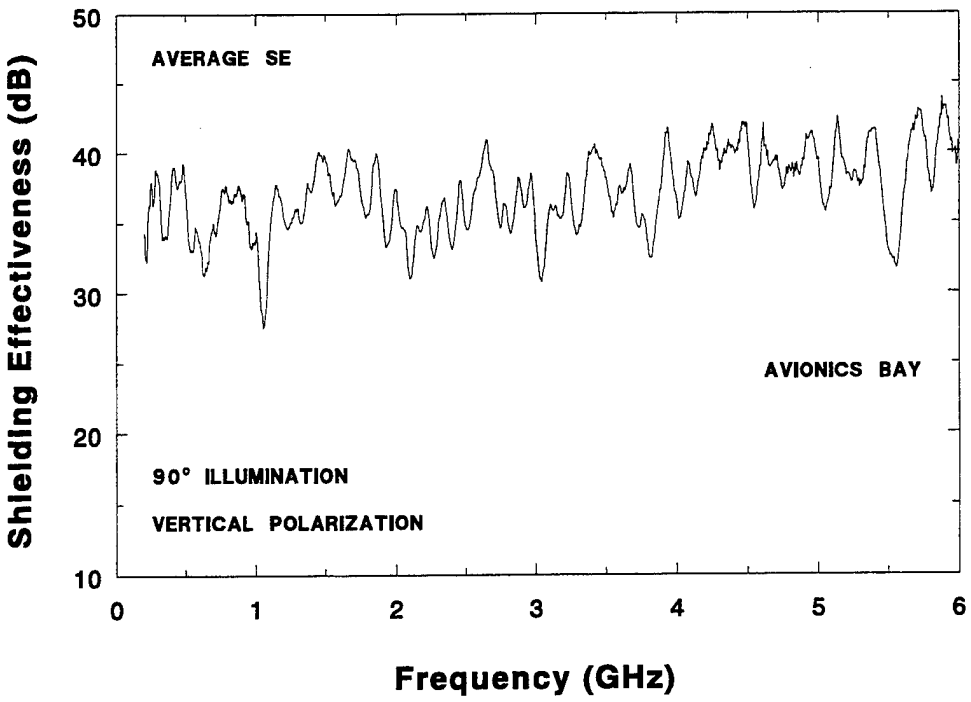

FIGURE 4-135. AVERAGE AVIONICS BAY SHIELDING EFFECTIVENESS FOR VERTICALLY POLARIZED, 90° BLWGN EXCITATION

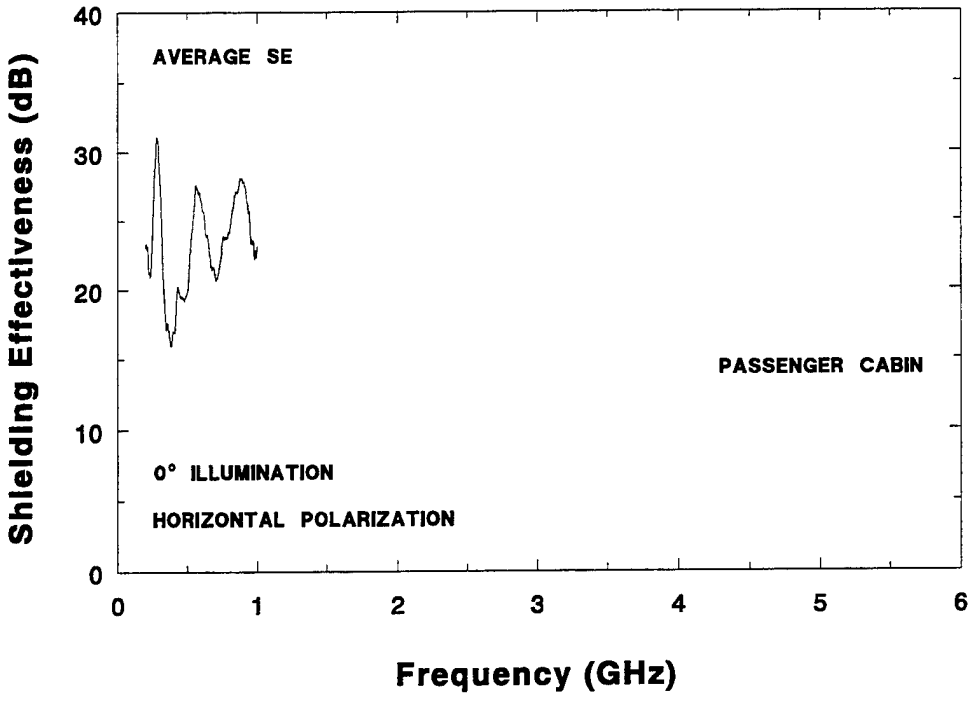

FIGURE 4-136. AVERAGE PASSENGER CABIN SHIELDING EFFECTIVENESS FOR HORIZONTALLY POLARIZED, 0° BLWGN EXCITATION

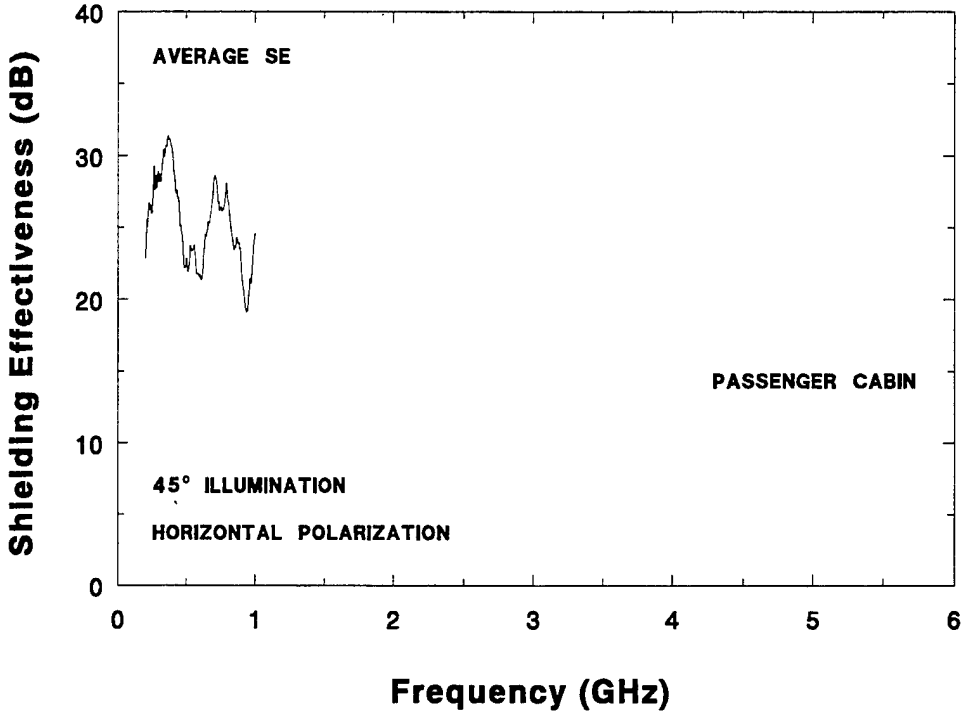

FIGURE 4-137. AVERAGE PASSENGER CABIN SHIELDING EFFECTIVENESS FOR HORIZONTALLY POLARIZED, 45° BLWGN EXCITATION

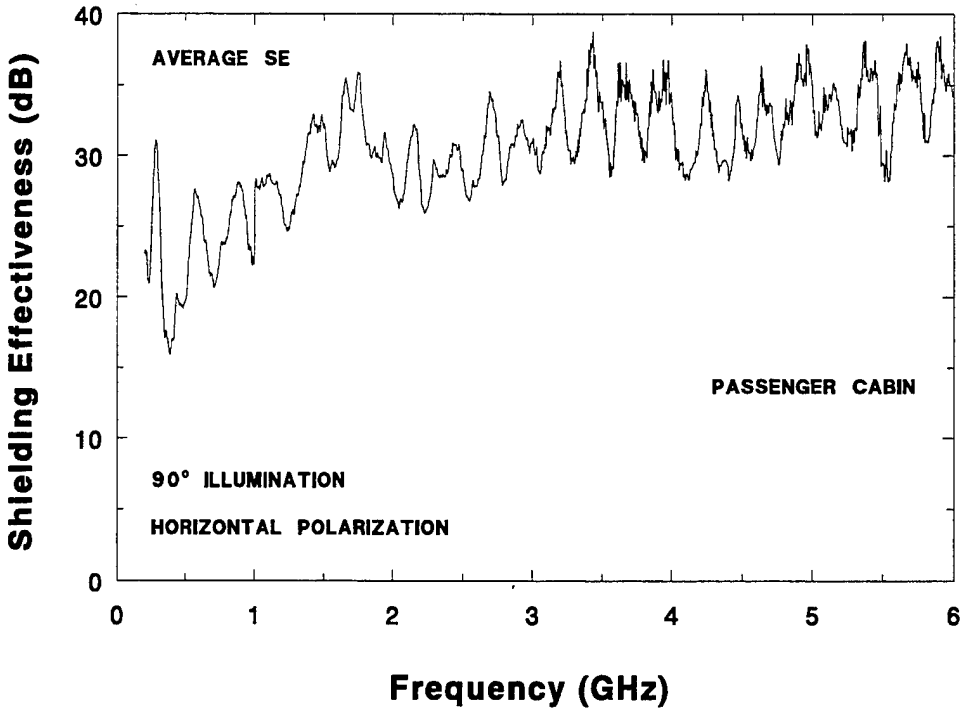

FIGURE 4-138. AVERAGE PASSENGER CABIN SHIELDING EFFECTIVENESS FOR HORIZONTALLY POLARIZED, 90° BLWGN EXCITATION

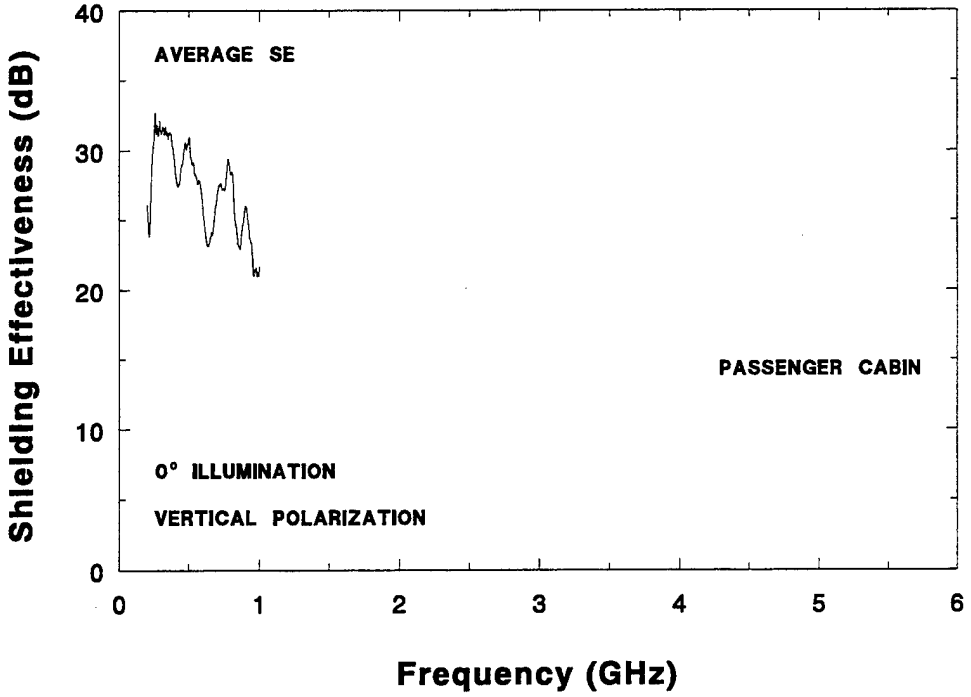

FIGURE 4-139. AVERAGE PASSENGER CABIN SHIELDING EFFECTIVENESS FOR VERTICALLY POLARIZED, 0° BLWGN EXCITATION

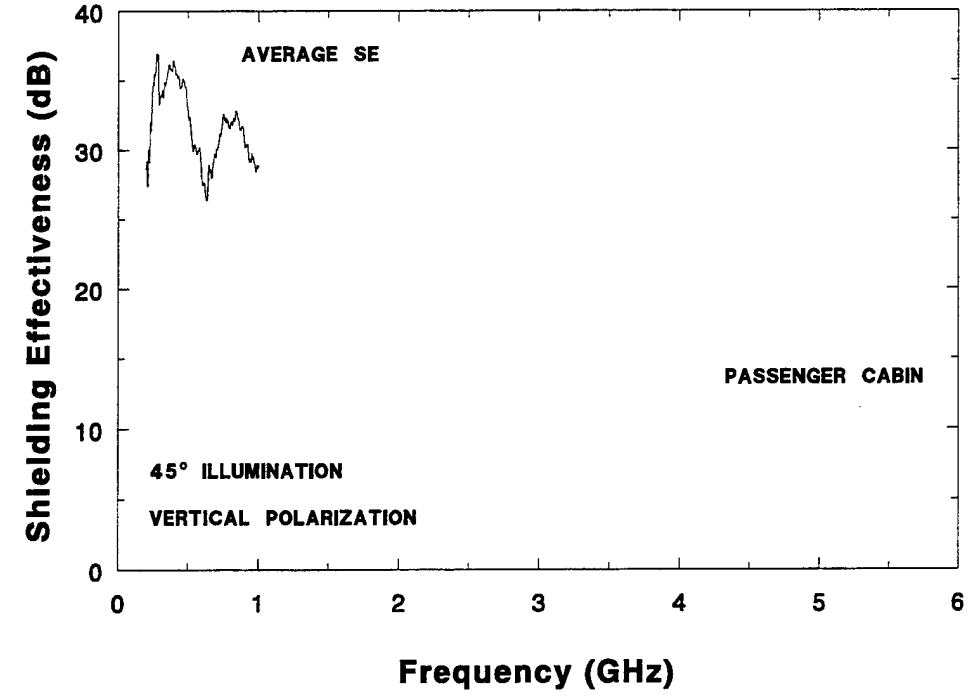

FIGURE 4-140. AVERAGE PASSENGER CABIN SHIELDING EFFECTIVENESS FOR VERTICALLY POLARIZED, 45° BLWGN EXCITATION

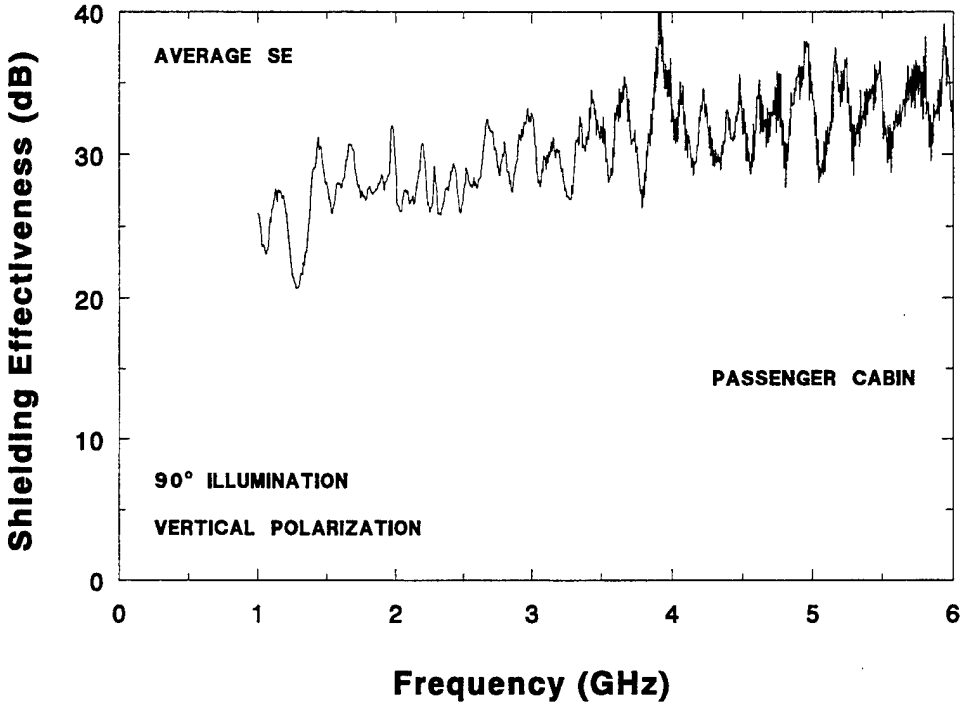

FIGURE 4-141. AVERAGE PASSENGER CABIN SHIELDING EFFECTIVENESS FOR VERTICALLY POLARIZED, 90° BLWGN EXCITATION

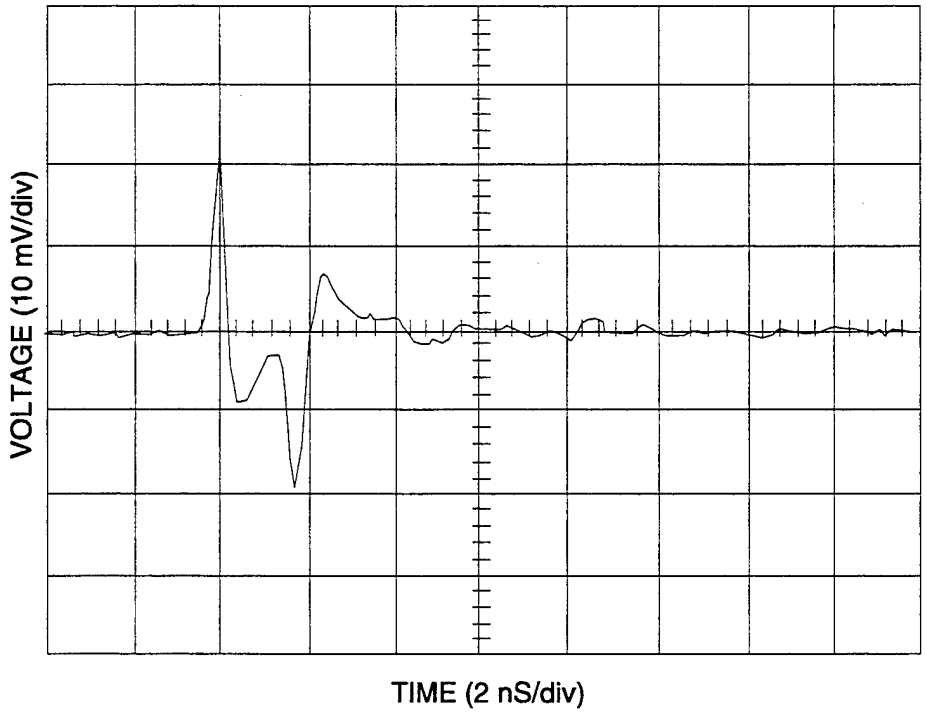

FIGURE 4-142. REFERENCE WAVEFORM FOR SHORT PULSE EXCITATION SHIELDING EFFECTIVENESS MEASUREMENT

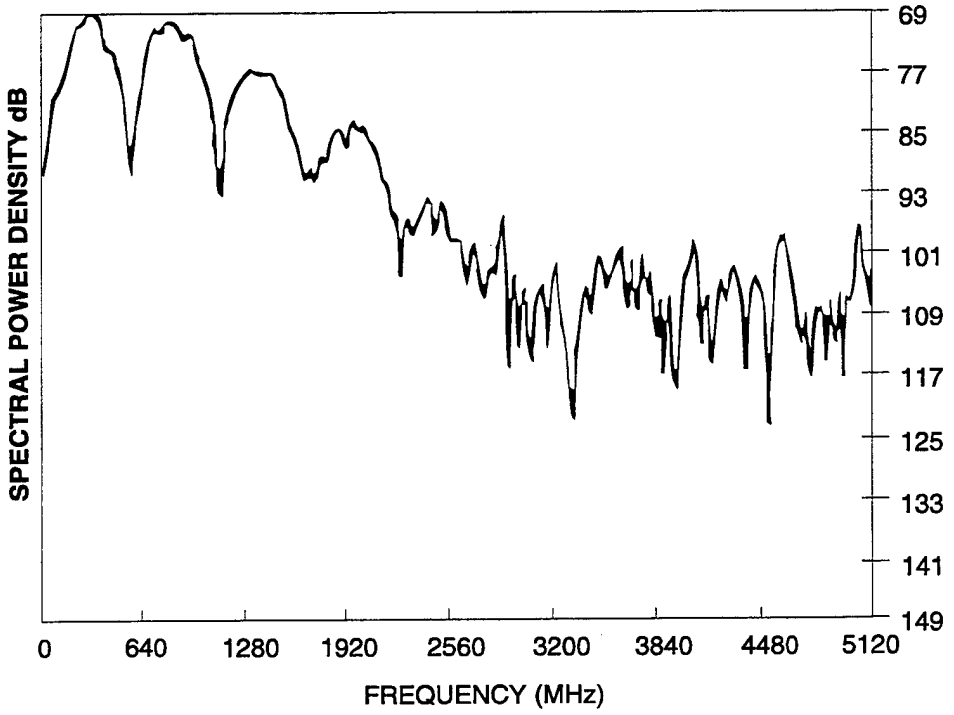

FIGURE 4-143. FREQUENCY TRANSFORM OF REFERENCE WAVEFORM FOR SHORT PULSE SHIELDING EFFECTIVENESS MEASUREMENT

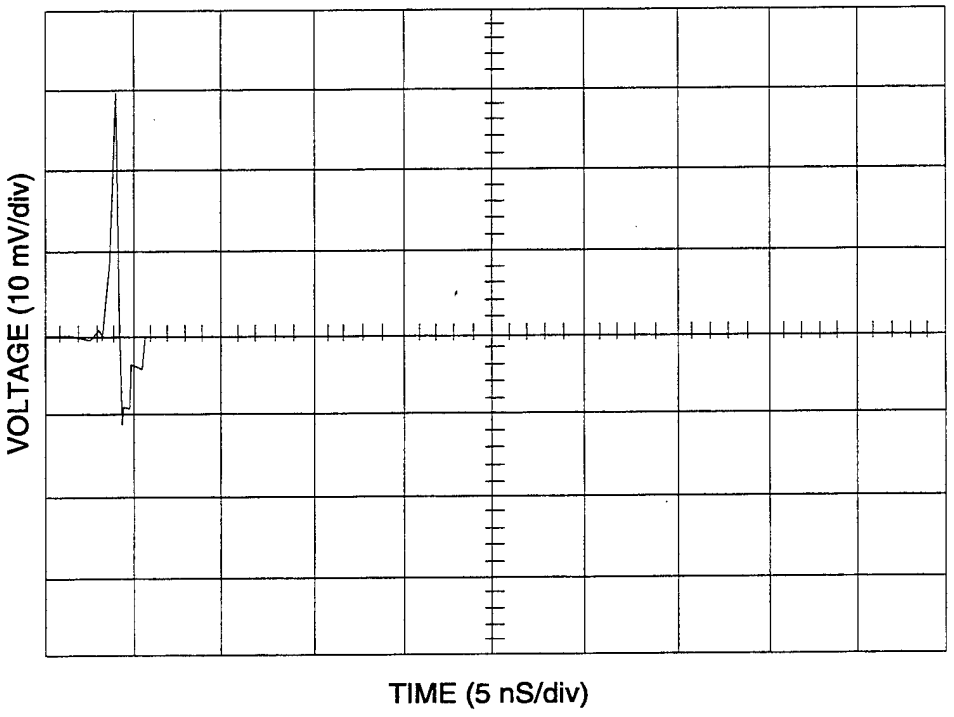

FIGURE 4-144. TIME-GATED REFERENCE WAVEFORM FOR SHORT PULSE EXCITATION SHIELDING EFFECTIVENESS MEASUREMENT

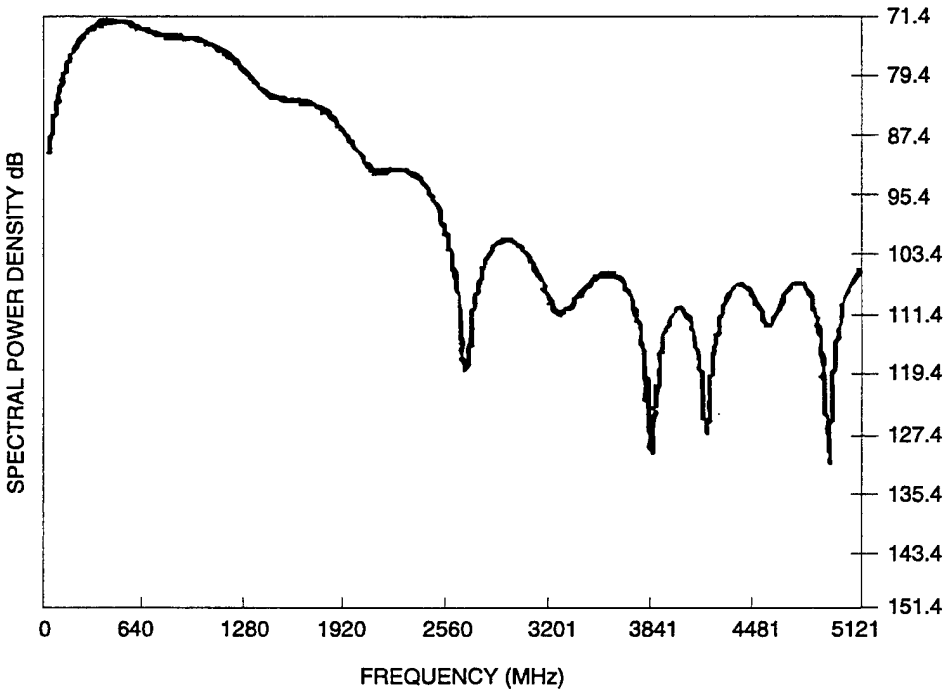

FIGURE 4-145. FREQUENCY TRANSFORM OF TIME-GATED REFERENCE WAVEFORM FOR SHORT PULSE SHIELDING EFFECTIVENESS MEASUREMENT

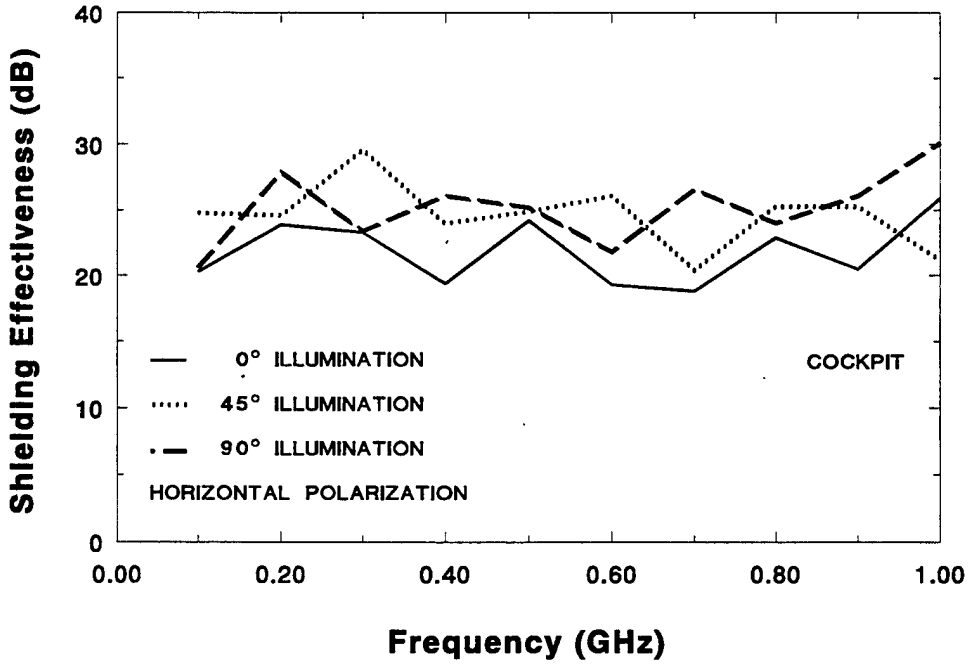

FIGURE 4-146. AVERAGE COCKPIT SHIELDING EFFECTIVENESS FOR HORIZONTALLY POLARIZED SHORT PULSE EXCITATION

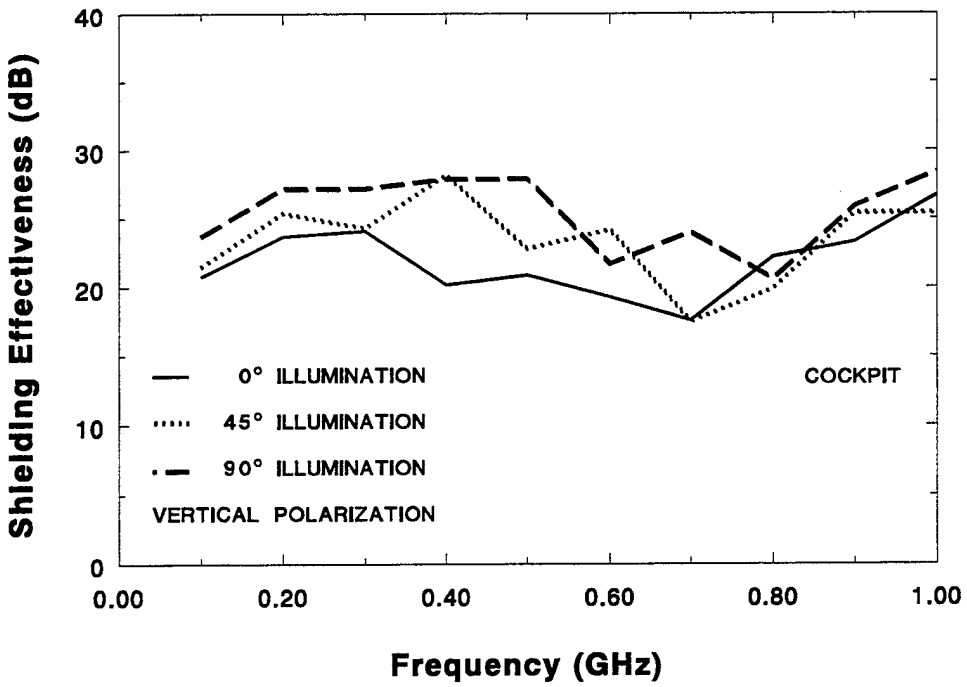

FIGURE 4-147. AVERAGE COCKPIT SHIELDING EFFECTIVENESS FOR VERTICALLY POLARIZED SHORT PULSE EXCITATION

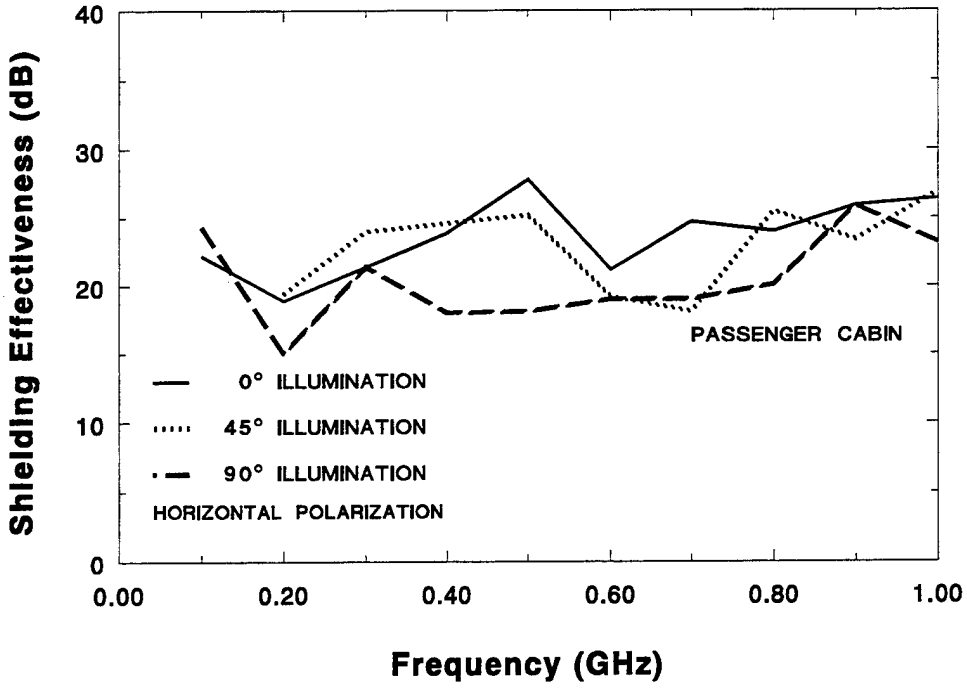

FIGURE 4-148. AVERAGE PASSENGER CABIN SHIELDING EFFECTIVENESS FOR HORIZONTALLY POLARIZED SHORT PULSE EXCITATION

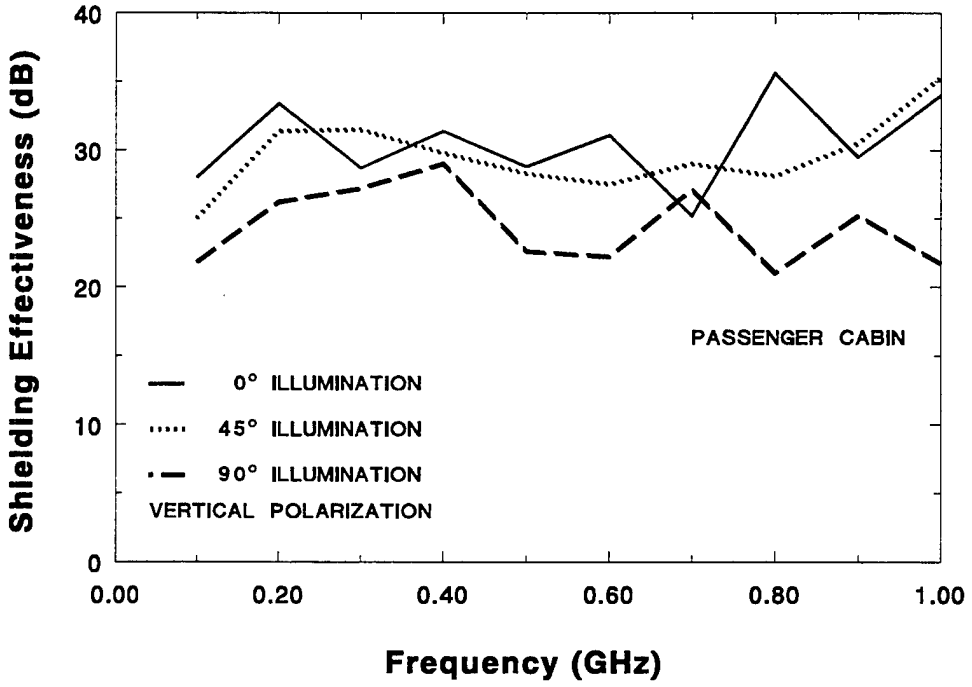

FIGURE 4-149. AVERAGE PASSENGER CABIN SHIELDING EFFECTIVENESS FOR VERTICALLY POLARIZED SHORT PULSE EXCITATION

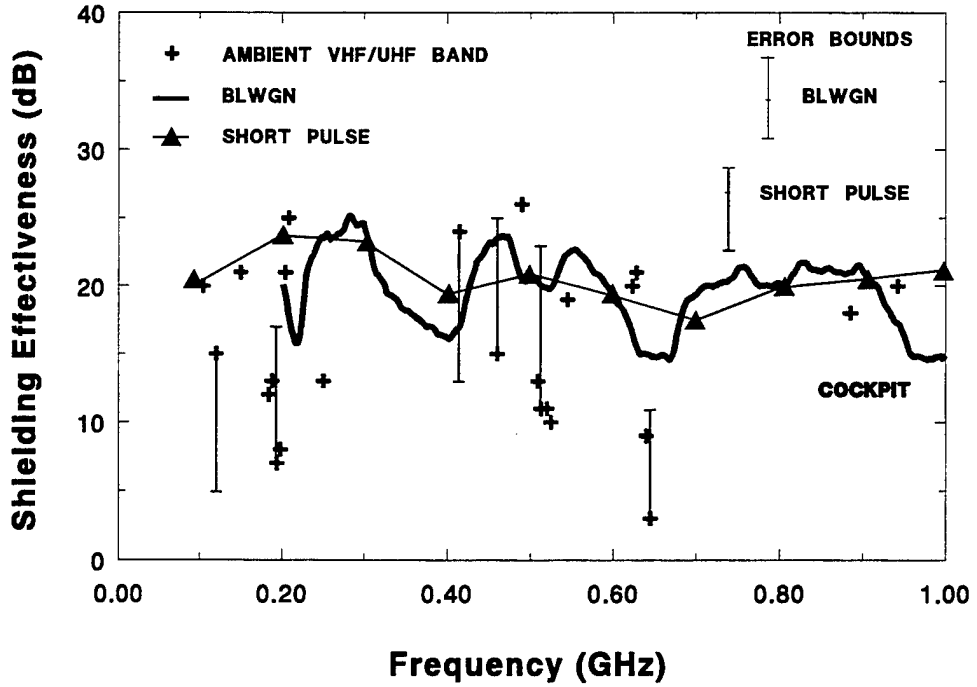

FIGURE 4-150. COMPARISON OF MINIMUM COCKPIT SHIELDING EFFECTIVENESS FOR AMBIENT VHF/UHF BAND, BLWGN, AND SHORT PULSE EXCITATION

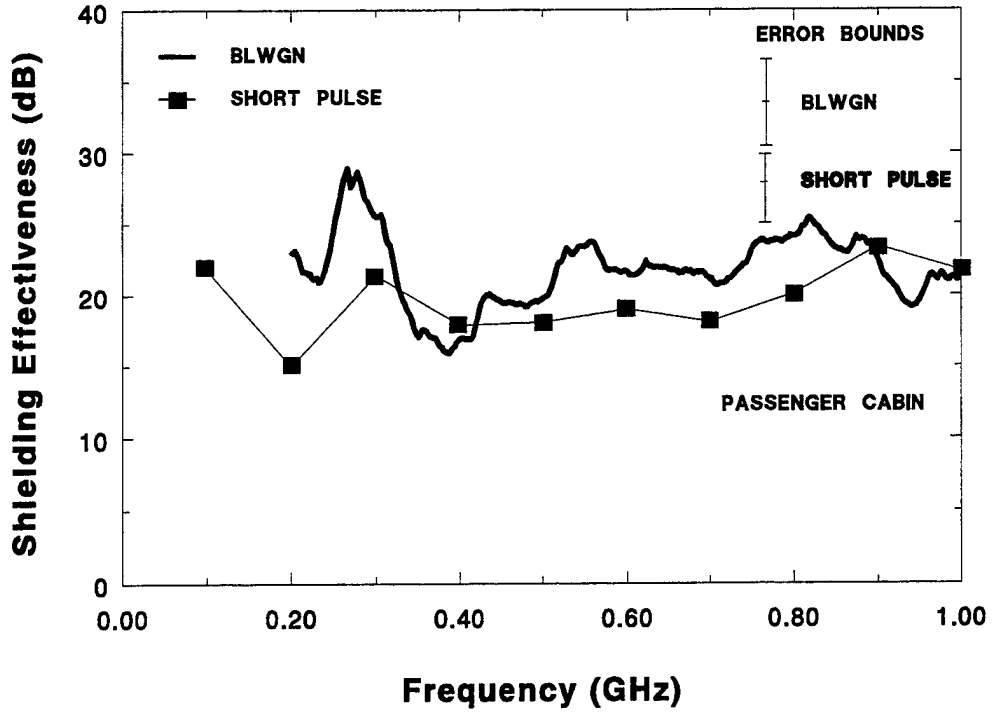

FIGURE 4-151. COMPARISON OF MINIMUM PASSENGER CABIN SHIELDING EFFECTIVENESS FOR BLWGN AND SHORT PULSE EXCITATION

TABLE 4-1. QUALITY FACTOR BANDWIDTH

	Q Bandwidth (MHz)		
Frequency (GHz)	Cockpit	Cabin	Avionics Bay
0.2	4.0	3.1	5.9
0.4	6.7	2.1	15.9
0.8	11.0	3.4	5.4
1.6	9.8	2.4	10.0
3.0	6.5	3.8	6.2
4.0	11.0	3.1	4.7
6.0	6.0	2.6	5.4

TABLE 4-2. CAVITY MODE DENSITY

	Mode Density 10/20/50 MHz BLWGN		
Frequency (GHz)	Cockpit	Cabin	Avionics Bay
0.2	2/5/12	3/6/16	1/3/8
0.4	1/3/7	5/9/24	0/1/3
0.8	1/2/5	3/6/15	2/4/9
1.6	1/2/5	4/8/21	1/2/5
3.0	1/3/8	3/5/13	2/3/8
4.0	1/2/4	3/6/16	2/4/11
6.0	2/3/8	4/8/19	2/4/9

TABLE 4-3. COMPARISON OF CAVITY-TO-CAVITY COUPLING EFFICIENCY FOR CW AND BLWGN EXCITATION

	AVERAGE COUPLING EFFICIENCY (CE)			
	EXCITATION			
	CW		BLWGN	
CAVITIES	<1 GHz	>1 GHz	<1 GHz	>1 GHz
Cockpit to Avionics Bay	-	-12 dB	-	-17 dB
Passenger Cabin to Cockpit	-5 dB	-7 dB	-3 dB	-7 dB
Passenger Cabin to Avionics Bay	-	+2 dB	-	-13 dB

TABLE 4-4. RESULTS OF COHERENCE TEST ON COCKPIT DATA

FREQUENCY	SINGLE WAVEFORM	TWO HALF WAVEFORMS	DIFFERENCE
		FIRST TIME WINDOW	
120 MHz	-18.8 dB	-19.9 dB	+1.1 dB
200 MHz	-25.2 dB	-25.3 dB	+0.1 dB
320 MHz	-22.9 dB	-22.9 dB	0.0 dB
400 MHz	-23.6 dB	-19.2 dB	-4.4 dB
520 MHz	-25.7 dB	-23.9 dB	-1.8 dB
600 MHz	-25.2 dB	-22.1 dB	-3.1 dB
720 MHz	-24.4 dB	-22.6 dB	-1.8 dB
800 MHz	-25.4 dB	-23.3 dB	-2.1 dB
920 MHz	-23.7 dB	-23.7 dB	0.0 dB
1000 MHz	-25.4 dB	-27.1 dB	+1.7 dB
		SECOND TIME WINDOW	
120 MHz	-27.0 dB	-27.9 dB	+0.9 dB
200 MHz	-34.1 dB	-31.3 dB	-2.8 dB
320 MHz	-33.7 dB	-34.0 dB	+0.3 dB
400 MHz	-33.9 dB	-31.2 dB	-2.7 dB
520 MHz	-33.3 dB	-34.3 dB	+1.0 dB
600 MHz	-32.4 dB	-29.1 dB	-3.3 dB
720 MHz	-36.3 dB	-33.7 dB	-2.6 dB
800 MHz	-32.7 dB	-33.6 dB	+0.9 dB
920 MHz	-27.9 dB	-30.2 dB	+2.3 dB
1000 MHz	-35.4 dB	-34.8 dB	-0.6 dB
		THIRD TIME WINDOW	
120 MHz	-30.7 dB	-32.8 dB	+2.1 dB
200 MHz	-39.2 dB	-40.1 dB	+0.9 dB
320 MHz	-37.0 dB	-37.1 dB	+0.1 dB
400 MHz	-36.2 dB	-36.8 dB	+0.6 dB
520 MHz	-38.2 dB	-39.8 dB	+1.6 dB
600 MHz	-39.4 dB	-39.1 dB	-0.3 dB
720 MHz	-39.3 dB	-39.5 dB	+0.2 dB
800 MHz	-37.9 dB	-39.0 dB	+1.1 dB
920 MHz	-43.0 dB	-43.7 dB	+0.7 dB
1000 MHz	-45.5 dB	-45.2 dB	-0.3 dB

TABLE 4-5. LIMITS OF ERROR FOR THE COCKPIT SHIELDING EFFECTIVENESS

FREQUENCY	SINGLE WAVEFORM	TWO HALF WAVEFORMS	DIFFERENCE
	TOTAL OF THREE WINDOWS		
120 MHz	-18.0 dB	-19.1 dB	+1.1 dB
200 MHz	-24.5 dB	-24.2 dB	-0.3 dB
320 MHz	-22.4 dB	-22.5 dB	+0.1 dB
400 MHz	-23.0 dB	-18.8 dB	-4.2 dB
520 MHz	-24.8 dB	-23.4 dB	-1.4 dB
600 MHz	-24.3 dB	-21.2 dB	-3.6 dB
720 MHz	-24.0 dB	-22.2 dB	-1.8 dB
800 MHz	-24.4 dB	-22.8 dB	-1.6 dB
920 MHz	-22.2 dB	-22.8 dB	+0.6 dB
1000 MHz	-25.0 dB	-26.4 dB	+1.4 dB

TABLE 4-6. RESULTS OF COHERENCE TEST ON PASSENGER CABIN DATA

FREQUENCY	SINGLE WAVEFORM	TWO HALF WAVEFORMS	DIFFERENCE
	FIRST TIME WINDOW		
200 MHz	-22.5 dB	-15.7 dB	-6.8 dB
400 MHz	-17.7 dB	-18.0 dB	+0.3 dB
600 MHz	-27.7 dB	-19.1 dB	-8.6 dB
800 MHz	-21.2 dB	-24.0 dB	+2.8 dB
1000 MHz	-33.5 dB	-34.2 dB	+0.7 dB
	SECOND TIME WINDOW		
200 MHz	-27.5 dB	-22.0 dB	-5.5 dB
400 MHz	-24.7 dB	-25.7 dB	+1.0 dB
600 MHz	-23.7 dB	-25.8 dB	+2.1 dB
800 MHz	-30.8 dB	-27.0 dB	-3.8 dB
1000 MHz	-32.1 dB	-31.7 dB	-0.4 dB
	THIRD TIME WINDOW		
200 MHz	-32.7 dB	-32.1 dB	-0.6 dB
400 MHz	-34.2 dB	-26.8 dB	-7.4 dB
600 MHz	-23.6 dB	-24.3 dB	+0.7 dB
800 MHz	-28.9 dB	-29.7 dB	+0.8 dB
1000 MHz	-40.0 dB	-35.6 dB	-4.4 dB

TABLE 4-7. LIMITS OF ERROR FOR PASSENGER CABIN SHIELDING EFFECTIVENESS

FREQUENCY	SINGLE WAVEFORM	TWO HALF WAVEFORMS	DIFFERENCE
200 MHz	-21.0 dB	-14.7 dB	-6.3 dB
400 MHz	-16.8 dB	-16.9 dB	+0.1 dB
600 MHz	-19.8 dB	-17.2 dB	-2.6 dB
800 MHz	-20.1 dB	-21.5 dB	+1.4 dB
1000 MHz	-29.4 dB	-28.8 dB	-0.6 dB

5.0 SUMMARY OF ANALYSIS RESULTS

The Boeing 707-720B cavities investigated had several suites of avionics equipment and most cable runs. The cables ran throughout the avionics bay and the cockpit as well as to other sections of the aircraft. Unfortunately, some of the cable bundles had been cut to facilitate equipment removal. The cavities contained insulating materials, air-conditioning ducts, etc., normally found in large transport aircraft. The hatches and doors did not have EM seals. All of the passenger cabin seats had been removed in the interval between Phase I and Phase II.

The cockpit, avionics bay, and the passenger cabin were excited from 0.2 to 6 GHz using discrete and swept frequency CW and BLWGN. Tuners provided mechanical mode-mixing for the CW excitation. The cockpit and passenger cabin were also excited using short pulses.

Data were collected to evaluate the characteristics of the cavity EME, the magnitude of the cavity-to-cavity coupling, the responses of avionics systems, and the SE of the aircraft structure.

The test results should be reasonably applicable to more modern transport aircraft. These aircraft do not, and the next generation probably will not, significantly depart from the EM topology of the Boeing 707. Factors such as weight and initial cost penalties as well as maintenance considerations mitigate against a closed EM topology for commercial aircraft. For example, various aircraft cavities will generally not have a continuous metal shield topology, and hatches and doors will not have EM seals. Except for critical systems, most cable bundles will not be shielded. Thus the EM characteristics of current and next-generation aircraft should not depart appreciably from that of the test Boeing 707. However, these tests were conducted without deliberate loading to simulate the crew and passengers. Although some data are available on minimum loading of a business/commuter type aircraft,[3,4] the full impact of passenger loading on the cavity EME remains to be investigated.

These results should also be a reasonable representation of the response of cavities of smaller business/commuter type aircraft. The cockpit/passenger cabin of these aircraft typically is a single, reasonably large cavity. The cavity will be complex and the mode density high enough at frequencies of interest to permit mode-mixing. This type aircraft often has one or more small avionics bays. The equipment layout in these bays may preclude the use of an adequately sized tuner and BLWGN or other techniques may be required for characterizing the aircraft shielding effectiveness. The results of this test, which provide comparisons of BLWGN to other excitation techniques, bear directly on that issue.

A summary of cavity characteristics developed in detail in Section 4.1 is presented in Section 5.1.

The energy coupled between aircraft cavities is an important parameter. It will be a primary factor in determining the restrictions that may have to be imposed on passenger-operated electronic devices. Cavity-to-cavity coupling is summarized in Section 5.2

The response of the RA and CTA were investigated both in the aircraft and in the NSWCDD reverberation chamber. The reverberation chamber testing investigated the importance of simulating the physical structure in the immediate vicinity of the system-under-test. A summary of these results is found in Section 5.3.

The shielding effectiveness of the aircraft structure was investigated using three different techniques, ambient EME coupling to the aircraft, excitation with BLWGN, and excitation with short pulses for time domain analysis. The results are summarized in Section 5.4.

5.1 CAVITY CHARACTERISTICS

5.1.1 Mode Density

An "effective" cavity mode density was defined as the minimum of the theoretical mode density based on cavity volume or the number of independent modes in the BW of interest. The effective mode density gives an indication of the effectiveness of various noise BWs. The effective mode density was small for all noise BWs investigated over the frequency range 0.2 to 6 GHz.

5.1.2 Mode-mixing Effectiveness

The cockpit, the smallest cavity, was sufficiently multimoded above about 0.4 GHz to satisfy the requirements of the statistical theory used in this report. The cockpit tuner used in Phase II was more effective than that used in Phase I as a result of its increased size and better orientation. Mode-mixing effects were noted at frequencies as low as 0.1 GHz. However, below about 0.7 GHz, the combination of tuner effectiveness and cavity mode density did not yield good agreement between the measured EME distribution and the theoretical distribution function.

Generally, mechanical mode-mixing in the avionics bay was disappointing. Although slightly larger than the Phase I tuner, the Phase II tuner was not significantly more effective. The internal metal structure of the avionics bay limited the tuner size and possible orientations and the placement of the antennas. The size of the log periodic antennas affected the data collected in the avionics bay. These data will require special treatment to extract useful information. As a result, data below 1 GHz obtained with the log periodic antennas in the avionics bay will not be reported.

Mechanical mode-mixing in the passenger cabin was the most effective of the three cavities. The tuner was considerably larger than the other tuners and the cabin volume provided a higher mode density. The passenger cabin EME showed good agreement with the theoretical distribution at 1 GHz. The limited data set available prevented defining the lowest frequency at which agreement with the theoretical distribution would occur.

For BLWGN, the data show that 2- or 10-MHz BWs will not provide effective mode-mixing in any of the aircraft cavities for the frequency range 0.2 to 6 GHz. However, 50-MHz BW does provide adequate mode-mixing for the three aircraft cavities.

5.1.3 Normalized Power Density

The normalized PD provides an indication of the aircraft cavity losses for a frequency-independent input power. As discussed in Section 4.1.3.3, CW excitation with mechanical mode-mixing and BLWGN excitation provide different measurements of the cavity loss. However, in most cases, the two measurements are within a nominal uncertainty band.

For the cockpit, the agreement between the CW and BLWGN is quite good. The two measurements also agree with a CW measurement from the Phase I test performed two years earlier on the same aircraft.

The passenger cabin data for the two techniques do not agree within expected uncertainty bounds and the cause needs further investigation.

The magnitude of the normalized PD is bounded by - 40, -45, and -50 dBm/cm^2 (referenced to 0 dBm input) for the cockpit, avionics bay, and passenger cabin, respectively. These data imply that the cavity losses result in a substantial reduction in the impact of any EM energy introduced into any of the cavities.

The PDs in all three cavities are independent of frequency within about 5 dB over the interval 1 to 6 GHz. This frequency-independence of the loss mechanisms was unexpected, but is common to measurements in other aircraft (U.S. Army U-21,[7] U.S. Navy C-26,[8] NASA B-757[9]).

5.1.4 Quality Factor

The cavity Q was estimated using three different techniques, time decay using BLWGN, time decay using short pulses, and normalized PD measurements.

The Q values determined from the two decay measurements are in excellent agreement for the frequency range where data from both techniques are available. The Q values derived from CW and BLWGN PD measurements are in agreement for the avionics bay and passenger cabin. However, the magnitude and frequency dependence of the Q derived from decay measurements and PD measurements substantially disagree. This discrepancy needs further investigation.

The Qs determined from decay measurements will be assumed to be of most interest. The Qs for the cockpit and avionics bay vary from less than 100 at the low frequencies to about 1000 at 6 GHz. The Q for the passenger cabin increases from less than 100 to about 2000 at 6 GHz.

5.1.5 Field Uniformity

The field uniformity in an aircraft cavity is a function of the effective mode density, the adequacy of the mode-mixing, the effect of localized absorbers, and the proximity to apertures and metal structures. Data from sufficient test configurations to permit evaluation of the field uniformity were collected only for BLWGN excitation during Phase II. However, CW excitation data from Phase I and Phase II were combined to give an estimate of the uniformity expected with mechanical mode-mixing.

The field uniformity derived from three Phase I and one Phase II CW insertion loss measurements in the cockpit show a maximum variation of less than 12 dB, with an average variation of less than 6 dB. A representative value for the standard deviation of the CW measurements over the entire frequency range is 3 dB.

For BLWGN, the field uniformity is poor for noise BWs of 2 and 10 MHz. For 50-MHz BW, the field uniformity is about ±7 dB for all three cavities, except at higher frequencies in the passenger cabin where the uniformity improves to about ±4 dB. A representative value for the standard deviation of the BLWGN measurements over the entire frequency range is 3 dB.

The field uniformity data from CW and BLWGN excitation are in good agreement.

For either excitation technique, it is important to take several measurements to determine the cavity PD within reasonable limits.

5.2 CAVITY-TO-CAVITY COUPLING/ISOLATION

The boundary between the avionics bay and the passenger cabin consisted of aluminum structural ribs interwoven with extensive cabling and covered with a Masonite or fiberglass board. Although the boundary is not continuous, the ribs and cable bundles should provide reasonable shielding up to perhaps 1 GHz where the cable spacing approaches a wavelength. The avionics bay to cockpit area has a reasonably continuous metal boundary but has many cable penetrations. The passenger cabin to cockpit area has the most continuous metal boundary but there are many cable penetrations of the boundary:

Two parameters that can be used to characterize cavity-to-cavity coupling were investigated using both CW and BLWGN excitation. The first is the coupling efficiency, which is defined as the ratio of the power density in the receive cavity to the power density in the transmit cavity. The CE is a dimensionless parameter. The second characterizing parameter is the coupling coefficient, which is the power coupled into the receive cavity for a given power density in the transmit cavity. The CC has the dimensions of area.

The coupling efficiency has nominal frequency-dependent values that vary from about −20 to about −5 dB for all cavities. The coupling coefficient has nominal frequency-dependent values that vary from −10 to about 0 dBm^2. These values indicate substantial coupling between all the aircraft cavities.

5.3 RADAR ALTIMETER/COMMON TEST ARTICLE RESPONSES

A series of measurements was obtained to investigate the relationship between the coupling of EM energy to avionics systems within aircraft cavities and in a reverberation chamber. The results for the RA indicator and the NSWCDD CTA were analyzed for this report. Both CW and BLWGN excitations were compared in the aircraft and in the reverberation chamber. Except for some limited frequency intervals over the range 1 to 6 GHz, the data were consistent with a combined measurement uncertainty with standard deviations of approximately 4 dB in the aircraft and approximately 2 dB in the reverberation chamber. The CW data tend to bound the BLWGN data.

Also investigated was the relationship between the transfer function as measured in the aircraft and in the reverberation chamber. Several different system configurations were investigated in the reverberation chamber. These included configurations with and without the cable harness tested on a dielectric block or on a ground plane. When the cable harness was connected, configuration variations included both unterminated or terminated with an appropriate load or a short. The largest coupling transfer function generally occurred with the harness connected and terminated in an appropriate load.

The transfer functions for the bounding configuration in the reverberation chamber were compared with the transfer functions in the aircraft. The comparison showed that the reverberation chamber data were within measurement uncertainty of the aircraft data and tended to bound the aircraft data.

5.4 SHIELDING EFFECTIVENESS MEASUREMENTS

For the cockpit, the SE results derived from three independent aircraft excitation techniques are in reasonably good agreement. These data indicate that a nominal value for the minimum cockpit SE over the frequency interval 0.1 to 6 GHz is 15 ± 5 dB. The SE varies by a few decibels for 45° and 90° illumination. For the cockpit, horizontal and vertical polarization yield approximately the same minimum SE.

For the avionics bay, the minimum SE is about 25 ± 5 dB at low frequencies increasing to about 30 ± 5 dB at 6 GHz. The SE varies a few decibels with aspect angle and polarization. The minimum SE occurs for a 90° aspect angle and horizontal polarization.

The minimum SE for the passenger cabin has a nominal value of 18 to 20 dB ± 5 dB over the frequency range 0.1 to 6 GHz. The data suggest no aspect-angle dependence for the passenger cabin SE. The passenger cabin SE varies a few decibels with polarization and is a minimum for horizontal polarization.

6.0 CONCLUSIONS

The Phase II test of the Boeing 707-720B aircraft at the Aerospace Maintenance and Regeneration Center, Davis Monthan AFB, Tucson, Arizona satisfied its test objectives.

The band-limited white Gaussian noise excitation technique was validated for characterizing the electromagnetic environment of an aircraft cavity as a result of the general agreement of its test results with three other independent excitation techniques.

- BLWGN may be used in cavities that may be too small or too densely packed to permit the use of a sufficiently large tuner.

- The data acquisition time for the BLWGN excitation technique can be as much as 40 times faster than acquisition of comparable data using continuous wave excitation with mechanical mode-mixing.

- The low values of the effective mode-density resulting from the low quality factor in aircraft cavities require the use of large bandwidths for the BLWGN measurements

- Bandwidth effects must be considered when interpreting data obtained with BLWGN excitation.

Shielding effectiveness data were collected for the cockpit, avionics bay, and passenger cabin over the frequency range 0.1 to 6 GHz. For two direct illumination techniques, shielding effectiveness data were obtained for three aspect angles and two polarizations.

- For the cockpit, there was general agreement in the minimum shielding effectiveness obtained from the ambient VHF/UHF electromagnetic environment, BLWGN, and short pulse excitation.

- The minimum cockpit shielding effectiveness was 15 ± 5 dB.

- The minimum shielding effectiveness for the avionics bay was 25 ± 5 dB.

- The minimum shielding effectiveness for the passenger cabin was 18 ± 5 dB.

- The above values of cavity shielding effectiveness were averaged over the substantial bandwidths associated with the BLWGN and the short pulse excitation. The results obtained from the ambient VHF/UHF electromagnetic environment suggest there may

be a fine structure in the shielding effectiveness that could reduce the indicated minimum values.

Additional characterization data on the cavity electromagnetic environment were obtained. These include new data on the effective mode density, the quality factor, and the field uniformity.

- The effective cavity mode density was shown to be substantially smaller than the theoretical mode density based on cavity dimensions.

- The quality factor for the three aircraft cavities was estimated by two different techniques referenced in the literature—time decay of the EME from a pulsed source and insertion loss. The two techniques produce quality factors in substantial disagreement.

- The quality factors determined from pulse decay times range from less than 50 at 0.1 GHz to about 1000 at 6 GHz for the cockpit and the avionics bay. For the passenger cabin, the quality factor varies from less 100 at 0.1 GHz to about 2000 at 6 GHz.

- The field uniformity in the aircraft cavities was shown to be within approximately 12 dB maximum variation and 3 dB standard deviation for sufficient mode density and mode-mixing conditions.

- The agreement between the measured and theoretical statistical distribution functions observed in the Phase I test was validated for adequate mode density and mode-mixing conditions.

- There was good agreement between similar data from Phases I and II indicating the constancy of the aircraft cavity electromagnetic conditions and the repeatability of these statistical test techniques.

The equivalence of system responses in aircraft cavities and reverberation chambers was demonstrated for five aircraft systems and the NSWCDD common test article.

- When tested on a dielectric block in the center of the NSWCDD reverberation chamber with the wire harness terminated appropriately, the system responses bounded the responses in the aircraft for the same cavity power density.

The Phase II data validated and extended the Phase I cavity-to-cavity coupling data.

- The maximum coupling occurred between the passenger cabin and avionics bay. This was expected due to the lack of a continuous metal boundary between the two cavities. The coupling efficiency was generally close to 0 dB with a few decibels of gain implied at some frequencies.

- The coupling efficiency between the passenger cabin and cockpit varied between −3 and −7 dB.

- The maximum value of the coupling efficiency between the cockpit and avionics bay was −12 dB.

7.0 RECOMMENDATIONS

The following recommendations are offered.

- Perform cavity electromagnetic environment characterization on an operational, passenger-configured, large transport aircraft using discrete and swept frequency internal excitation with mechanical mode-mixing and internal short pulse excitation. The purpose would be to validate the applicability of the Boeing 707 test results to a current operational, passenger-configured aircraft and to increase the data base on aircraft cavities. It is particularly important to clarify the variability of cavity electromagnetic-environment dependence on aircraft type.

- Perform additional shielding effectiveness measurements on an operational, passenger-configured, large transport aircraft utilizing the ambient VHF/UHF electromagnetic environment. The purpose would be to investigate the fine structure in shielding effectiveness and to obtain additional aspect angle data.

- Perform additional shielding effectiveness measurements on an operational, passenger-configured, large transport aircraft utilizing discrete and swept frequency, continuous wave excitation. The purpose would be to investigate the fine structure in shielding effectiveness and to obtain additional aspect angle data. An additional purpose would be to validate test and analysis methods to eliminate ground-reflection effects in the test results.

- Perform aircraft shielding effectiveness measurements using both plane wave and spot illumination techniques. The purpose would be to clarify the need for plane-wave illumination to determine the shielding effectiveness of aircraft. Currently, obtaining a plane-wave environment requires high transmitter powers at substantial stand-off distances.

- Perform aircraft shielding effectiveness measurements with band-limited white Gaussian noise from multiple antennas. The purpose would be to investigate the equivalence of aircraft cavity responses to BLWGN from multiple antennas and to plane-wave illumination.

- Perform cavity decay time and insertion loss measurements in a reverberation chamber. The purpose would be to investigate the apparent discrepancy between the quality factor estimates obtained with these two techniques.

- Extend the frequency range of the short pulse, time domain technique to above 1 GHz. The purpose would be to provide an independent technique for investigating aircraft electromagnetic responses at higher frequencies.

- Extend the short pulse, time domain technique to cavity power density and cavity-to-cavity coupling measurements. The purpose would be to provide data from an independent test technique to corroborate existing data.

- Perform coupling measurements on instrumented, state-of-the-art avionics systems. The measurements should be performed in one or more aircraft types and in a reverberation chamber. The avionics systems should be powered.

8.0 REFERENCES

1. Crawford, M. L. and Koepke, G. H., *Design, Evaluation and Use of a Reverberation Chamber for Performing Electromagnetic Susceptibility/Vulnerability Measurements*, NBS TN 1092, 1986.

2. Hatfield, M. O.; Freyer, G. J.; Johnson, D. M.; and Farthing, C. L., *Electromagnetic Reverberation Characteristics of a Large Transport Aircraft*, NSWCDD/TR-93/339, Jul 1994.

3. Hill, D. A.; Crawford, M. L.; Johnk, R. T.; Ondrejka, A. R.; and Camell, D. G., *Measurements of Shielding Effectiveness and Cavity Characteristics of Airplanes*, NISTIR 5023, Jul 1994.

4. Freyer, G. J. and Hatfield, M. O., "Aircraft Test Applications of Reverberation Chambers," IEEE International Symposium on Electromagnetic Compatibility, Chicago, IL, Aug 1994.

5. Loughry, T. A., *Frequency Stirring: An Alternate Approach to Mechanical Mode-Stirring for the Conduct of Electromagnetic Susceptibility Testing*, Phillips Laboratory, Kirkland AFB, NM, Report No. Pl-TR-91-1036, Nov 1991.

6. Lehman, T. H., *A Statistical Theory of Electromagnetic Fields in Complex Cavities*, Note 494, USAF Phillips Laboratory Interaction Note Series, May 1993.

7. Richardson, R. E., "Mode Stirred Chamber Calibration Factor and Relaxation Time," *IEEE Trans on Instrumentation and Measurements*, Vol. IM-34, No. 4, Dec 1985.

8. Camell, D., Personal Communication, National Institute of Standards and Technology, 1995.

9. Hatfield, M. O.; Freyer, G. J.; and Loughry, T. A., *Electromagnetic Characteristics of a Boeing 757 Aircraft*, NSWCDD/TR-96/XXX, In Process.

DISTRIBUTION

DOD ACTIVITIES (CONUS)

	Copies
ATTN CODE A76 (TECHNICAL LIBRARY) COMMANDING OFFICER CSSDD NSWC 6703 W HIGHWAY 98 PANAMA CITY FL 32407-7001	1
DEFENSE TECH INFORMATION CTR 8725 JOHN J KINGMAN RD SUITE 0944 FORT BELVOIR VA 22060-6218	2
ATTN MAJ T LOUGHRY AFRL DEPE 3550 ABERDEEN AVE SE KIRTLAND AFB NM 87117	5

NON-DOD ACTIVITIES (CONUS)

	Copies
THE CNA CORPORATION P O BOX 16268 ALEXANDRIA VA 22302-0268	1
ATTN K J MOELLER (MS 490) 8 NORTH DRYDEN ST NASA LANGLEY RESEARCH CENTER HAMPTON VA 23681-0001	5
ATTN DAVID B WALEN FAA ANM 110N 1601 LIND AVE SW RENTON WA 98055-4056	1
ATTN ROBERT JOHNK RADIO FREQUENCY TECH DIVISION ELECTRONICS AND ELECTRICAL ENGINEERING LAB NIST 325 BROADWAY BOULDER CO 80303-3328	5

INTERNAL

		Copies
B20	(STOUDT)	3
B60	(TECHNICAL LIBRARY)	3
J50	(E3 LIBRARY)	3
J52	(FREYER)	5
J52	(HATFIELD)	50
J52	(JOHNSON)	5
J52	(SLOCUM)	5